2010-5

Solar Radiation Investigations; a Foundation Study

Alanna Maguire
Technological University Dublin

Solar radiation investigations; a foundation study

Alanna Maguire BSc.

A thesis submitted for the degree of Doctor of Philosophy to the Dublin Institute of Technology

Supervisors

Dr Fiona Lyng

Dr James Walsh

Radiation and Environmental Science Centre

Focas Institute

Dublin Institute of Technology

May 2010

Abstract

Skin cancer is a global epidemic that is increasing annually. However, our knowledge of the mechanisms involved in skin carcinogenesis is relatively poor. Investigative studies to date have predominantly employed fluorescent UVA and / or UVB lamps. The information gained from such studies has pioneered this area of research effectively, however, the typical unimodal Gaussian distribution of such irradiators do not reflect that of solar radiation nor do they account for potential waveband interactions. Advancing technologies in solar simulation have opened up this field to more environmentally and biologically relevant exposures, not only in terms of distribution but also irradiance. To begin, this study addressed issues regarding the biological relevance of four different irradiators with respect to solar radiation. During this investigation the different exposure media employed (cell culture medium and PBS) were found to elicit significantly different results in terms of cell survival which were in direct conflict with the transmittance properties of the exposure media. The differential effects of the media were further investigated using endpoints that assessed the role of reactive oxygen species, mechanistic processes (caspase-3 activity, mitochondrial membrane potential) and genomic perturbations (mitotic index, comet assay) in response to solar simulated irradiation. These results prompted further investigations into the effects of solar simulated radiation on cell culture medium. Medium transfer experiments showed that cell culture medium irradiated in the absence of cells was cytotoxic to unirradiated cells. Solar simulated radiation induced bystander effects were also investigated to determine if the presence of cells during irradiation had an effect on the cytotoxicity of the irradiated medium. Thus, this study assessed the two most fundamental parameters in non-ionising radiation *in vitro* investigations in order to form

solid foundations upon which more detailed investigations into the mechanisms of skin carcinogenesis can confidently be performed.

Declaration

I certify that this thesis which I now submit for examination for the award of PhD, is entirely my own work and has not been taken from the work of others, save and to the extent that such work has been cited and acknowledged within the text of my work. This thesis was prepared according to the regulations for postgraduate study by research of the Dublin Institute of Technology and has not been submitted in whole or in part for another award in any Institute. The work reported on in this thesis conforms to the principles and requirements of the Institute's guidelines for ethics in research. The Institute has permission to keep, lend or copy this thesis in whole or in part, on condition that any such use of the material of the thesis be duly acknowledged.

Signed Maura Laguire Date 16th June 2010

For my Mum

Acknowledgements

My heartfelt thanks goes to both my supervisors Fiona Lyng and James Walsh, who have both guided and supported me and my work from day one. To all my colleagues in the Focus Institute, both past and present, for all their support whether it was a tip for an assay, teaching me something from scratch or providing the much needed, although often unintentional, comic relief on nights out through which some enduring friendships have been forged. To all my girls, for the nights of endless laughter, I could not wish for better friends. To my family, each of whom have helped me in their unique way over the years. And finally, to the person who never stopped believing in me when others did, who saw in me what I could not and whose unfaltering support helped put me back on my feet when I needed it most, to my Mum. You're forever in my heart, I love you, I thank you and I miss you.

Abbreviations

Abbreviation	Full name
8-oxoG	8-oxo-7,8-dihydroguanine
95CI	95 % confidence interval
AIF	Apoptosis inducing factor
AM	Air mass
ANOVA	statistical analyses of variance
AP	Abasic (apurine/apyrimidine) sites
Apaf-1	Apoptotic protease activating factor-1
APE-1	AP-endonuclease-1
ATP	Adenine triphosphate
BER	Base excision repair
BP	Bandpass
BSO	L-buthionine-S,R-sulfoximine
cdks	Cyclin dependent kinases
CPDs	Cyclobutane pyrimidine dimers
DD	Death domains
DED	Death effector domains
dH2O	Deionised water
DISC	Death inducing signalling complex
DMSO	Dimethyl sulfoxide
DN	Digital numbers
DNA	Deoxyribonucleic acid
DSBs	Double strand breaks
endoG	Endonuclease G
FAD	Flavin adenine dinucleotide
FMN	Flavin mononucleotide
fpg	Formamidopyrimidine-DNA glycosylase
GaAsP	Gallium arsenide phosphide
GJIC	Gap junction intercellular communication
GSH	Reduced glutathione

GSSG	Oxidised glutathione
HEPES	2-[4-(2-hydroxyethyl)piperazin-1-yl]ethanesulfonic acid
hprt	Hypoxanthine-guanine phosphoribosyltransferase
IAPs	Inhibitors of apoptosis proteins
IGF-I	Insulin like growth factor I
IGF-IR	Insulin like growth factor I receptor
IR	Infrared
LMP	Low melting point
LSM	Least square means
MMP	Mitochondrial membrane potential
MTT	Method of transcriptional and translational
NADPH	Reduced nicotinamide adenine dinucleotide phosphate
PBS	Phosphate buffered saline
PDT	Photodynamic therapy
ROS	Reactive oxygen species
SCEs	Sister chromatid exchanges
SOD	Superoxide dismutase
SSBs	Single strand breaks
tBid	Truncated form of Bcl-2 family member Bid
TGF-β1	Transforming growth factor beta
TNFR-1	Tumour necrosis factor receptor-1
UV	Ultraviolet
UVA	UV radiation with wavelengths corresponding to 315-400 nm
UVB	UV radiation with wavelengths corresponding to 280-315 nm
UVC	UV radiation with wavelengths corresponding to 100-280 nm

Table of contents

List of figures

Figure **Page**

List of tables

Chapter 1 Introduction

Solar radiation plays a vital role in the sustenance of life through processes such as photosynthesis in plants (1) and vitamin D_3 synthesis in human skin (2). However, the effects of solar radiation are not always innocuous. Our biosphere is predominantly protected from the detrimental effects of solar radiation due to the existence of the ozone layer in the stratosphere which absorbs most of the harmful radiation. However, short wavelength radiation can penetrate the atmosphere and exert detrimental effects. Radiation whose wavelengths occur from 400 nm down to 10 nm is termed ultraviolet (UV) radiation and is subdivided into three regions; UVA, UVB and UVC whose wavebands are defined as 400 – 315 nm, 315 – 280 nm and 280 – 10 nm respectively (3, 4). The shortest wavelength reported to occur at the terrestrial level is 295 nm (5). Thus, mid UVB radiation is the most energetic waveband incident at the terrestrial level. Solar UV radiation is without doubt the primary risk factor for non melanoma skin cancers (NMSC) (6). Although its involvement in malignant melanoma is less straightforward (7) epidemiological and experimental evidence clearly implicate UV radiation in malignant melanoma (8, 9). In 2005, over 76,000 cases of NMSC were registered in the UK (10) while the current incidence rate in the US is in excess of one million cases per year which equals all other malignancies combined (11, 12). It is expected that 20% and 66% of the Caucasian populations living in the US and Australia respectively will develop NMSC during their lifetime (12, 13) where the majority of NMSC cases are basal cell carcinomas (BCC) and squamous cell carcinomas (SCC) (12). The susceptibility of an individual to NMSC is influenced strongly by skin phototype where at-risk individuals are those who

burn easily and tan minimally (14). Immunosuppression also plays a significant role in skin carcinogenesis, a fact that is highlighted by the increased incidence of NMSC in organ transplant recipients on lifetime immunosuppressants and immunocompromised chronic lymphocytic leukemia patients (6). Although these potentially disfiguring carcinomas are rarely fatal, their high incidence rates have the potential to exert a substantial burden on healthcare systems, both medically and financially. However, sun protection campaigns advocating skin cancer prevention have been found to be both preventative and cost effective when modelled with melanoma incidence rates (15). The cornerstone of such campaigns is to encourage safe sun practices such as regular use of sunscreens, use of protective clothing and minimising exposures. However, such stringent recommendations have been questioned with regard to the potentially beneficial effects of solar radiation on internal cancers via vitamin D_3 synthesis (16-18). In turn, such beneficial assertions have been rebutted on the grounds that the recommended daily intake of vitamin D_3 can be adequately obtained through dietary means and supplementation thus avoiding unnecessary UV exposure and potential deoxyribonucleic acid (DNA) damage (19), where the accumulation of unrepaired DNA damage is an integral step in the carcinogenic pathway.

1.1 DNA, a brief overview

DNA is located in the nucleus of eukaryotic cells and encodes the entire genome of an individual. Genes are preferentially expressed through transcription (formation of ribonucleic acid (RNA) from DNA) and translation (formation of functional proteins from RNA) depending on the requirements of the cell. DNA consists of two polymer chains that

run anti-parallel and consist of monomeric subunits termed nucleotides. Each nucleotide consists of 3 components, a pentose sugar, a nitrogenous base and a phosphate group. Covalent phosphodiester bonds between the sugar and phosphate groups form the DNA backbone from which the bases extend. There are four bases in DNA; guanine (G), adenine (A), cytosine (C) and thymine (T) and based on their ring structure each base is termed a purine (G and A) or a pyrimidine (C and T). The two polynucleotide chains are held together via hydrogen bonding between opposing bases. Base pairing is highly conserved and non random where G always pairs with C and A always pairs with T forming three and two hydrogen bonds between each pair respectively. The abundance of conjugated bonds in the ring structures of DNA bases makes DNA an effective chromophore (20) that absorbs maximally at 260 nm (21). Although DNA does not absorb as effectively at terrestrial UV wavelengths, the efficacy of UV radiation with regard to damaging DNA increases dramatically with decreasing wavelength, particularly over the UVB region as shown in figure 1.1.

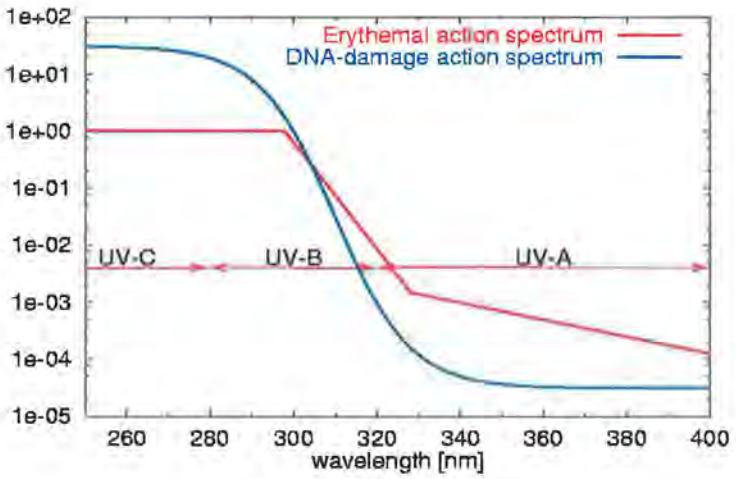

Figure 1.1 Erythemal and DNA damage action spectrum (22)

1.2 DNA and UV radiation

Absorption of UVB photons induces dimerisation of adjacent pyrimidine bases. There are 12 types of dimeric photoproducts possible including cyclobutane pyrimidine dimers (CPDs), pyrimidine 6-4 pyrimidone photoproducts (6-4PPs) and its Dewar valance isomer formed when 6-4PPs absorb radiation at 320 nm (23). All three dimeric photoproducts can be formed at the four bipyrimidine sites (TT, TC, CT and CC sequences) (24). Using high performance liquid chromatography–tandem mass spectrometry (HPLC-MS/MS), Ravanat et al (24) have shown that TT and TC sequences are 10 fold more reactive than CT and CC sequences in UVB irradiated DNA but that TT and CT favours CPD formation while TC and CC favours 6-4PP formation. Although the net amount of lesions formed at TT and TC sequences were found to be similar, CPD induction was 10 fold higher than 6-4PP induction at TT sequences while both lesions were generated in similar amounts at TC sequences. Only CPDs were produced at CT sequences while both CPDs and 6-4PP were formed at CC sequences but at low yields. The overall ratio of CDP to 6-4PP formation was 3:1, while Dewar valence isomers were barely detected at CC sequences only. These observations are supported by the work of Mouret et al (25) who observed near identical lesion distributions in normal human keratinocytes (NHK) irradiated for 1 minute in PBS at an irradiance of 3 Wm^{-2} using a UVB irradiator emitting predominantly at 312 nm but no spectral distribution was provided. These results agree with the general consensus that CPDs are the predominant dimeric lesions formed in UV irradiated cells, which may be an artefact of preferential repair. 6-4PPs are repaired more efficiently than CPDs (25, 26) which may be due to the fact that 6-4PPs are more distorting than CPDs, bending the DNA

44° and 9° respectively (27) and are thus recognised more efficiently. Furthermore, 6-4PPs have been estimated to be 3-5 times more toxic than CPDs in nucleotide excision repair (NER) deficient cells (28).

Interestingly, the work of both Ravanat et al (24) and Mouret et al (25) demonstrate that the dipyrimidine sequences at which CPDs are predominantly and least likely generated are the TT and CC sequences respectively. Furthermore, the work of Mouret et al (25) showed that CPD lesions occurring at TT sequences are the slowest lesions to be repaired while those at CC sequences are repaired far more rapidly. However, C to T and CC to TT tandem mutations are regarded as the hallmark of UV radiation (29). Mouret et al (25) infers that the lack of mutagenic potential at TT sequences is due to the A-rule. The A-rule is when the DNA repair or replication machinery does not recognise a damaged or mutated base and inserts an adenine in the opposing strand by default (30). This default mechanism maintains the base pairing rules for both bases involved in CPD mutations formed at TT but not cytosine containing sequences such as CC, CT or TC. Thus, if unrepaired, at the second round of replication post CPD induction the cytosine bases can give rise to C to T mutations. Furthermore, methylation of cytosine at C5, found exclusively at CpG dinucleotides, is thought to play an important role in UVB mutagenesis (31). A common hypothesis is that UV mutations only occur after base deamination (loss of an amino group) within the CPD (29). Deamination of cytosine and 5-methylcytosine yields uracil and thymine respectively, of which uracil is more evident for excision in DNA (32). Lee and Pfeifer (29) found methylation of cytosine at C5 promotes deamination within CPDs and

yields a corresponding increase in CC to TT and transition mutations at mutational hotspots frequently observed in the p53 gene of non melanoma skin tumours.

Although the effects of UVB radiation are predominantly executed through direct excitation of DNA bases, UVB radiation also results in oxidative damage including 8-Oxoguanine (8-oxoG) (23), where 8-oxoG is the primary DNA lesion generated under oxidative stress and thus an excellent indicator of oxidative stress (33). However, 8-oxoG DNA lesions were not detected in UVB irradiated cells unless lethal doses were employed, at which point cell death was attributed to an overwhelming production of CPDs and not an effect of oxidative damage (34). In contrast to UVB, UVA radiation is poorly absorbed by DNA (35), thus the genotoxic effects of UVA radiation have been predominantly attributed to oxidative stress via photosensitisation of, as of yet, unidentified cellular chromophore(s) (21). Photon absorption by endogenous photosensitiser(s) may react directly with DNA in an electron transfer process (type I mechanism) or by energy transfer to molecular oxygen generating reactive oxygen species (ROS, type II mechanism) which can then damage DNA (36). UVA radiation has been shown to generate intracellular ROS such as hydrogen peroxide, superoxide, singlet oxygen and the hydroxyl radical (37-40) which in turn can cause effects like protein modification (41) and lipid peroxidation (42). However, the qualitative and quantitative induction of such oxidative stressors and subsequent damage are likely to vary depending on endogenous photosensitisers present during irradiation (23).

So called UVA fingerprint mutations, namely AT-CG transversions have been found to occur more frequently in the basal layer of human squamous cell carcinomas compared to

UVB signature mutations (C-T or CC-TT transitions) (43). These findings were later confirmed using engineered human skin which also showed AT-CG transversions to be the most frequent mutational event (5/10 mutations) in the basal layer post UVA irradiation (44). Although 8-oxoG is considered the primary oxidative lesion generated by oxidative stress, its signature mutation, the GC-TA transition (33), was the least frequently observed mutation in UVA irradiated engineered human skin with only 1/10 mutations (44). However, the GC-CG transversion was the second most observed mutational event with 4/10 mutations (44), where the GC-CG transversion has been surmised to occur due to secondary oxidation of 8-oxoG which has an even lower ionisation potential than its precursor guanine (33). The prevalence of UVA mutations at the basal layer has been attributed to its increased epidermal penetration compared to UVB radiation. However, another link has been established by Javeri et al (45) who found that the abundance of human DNA glycosylase OGG1, responsible for excising 8-oxoG, decreases with increasing epidermal depth. Thus, 8-oxoG is repaired more efficiently in superficial layers which may, in part, explain the prevalence of GC-CG transversions in the basal layer of UVA irradiated human engineered skin.

Despite the fact that UVA radiation is poorly absorbed by DNA, there is a substantial amount of evidence in the literature regarding its ability to generate CPDs. Surprisingly, it has been reported that CPD lesions generated at TT sequences, not 8-oxoG lesions, are the predominant DNA lesion induced post UVA irradiation (46, 47). However, Besaratinia et al (34) found that the predominant UVA-induced DNA lesion generated was dose dependent where CPD and 8-oxoG lesions were dominant at high and low doses respectively. In

contrast, Schuch and Menck (36) found that the level of oxidative damage measured in terms of 8-oxoG exceeded that of dipyrimidine dimers in UVA irradiated DNA plasmid. Moreover, they found that the mutagenic effects of a continuous exposure to solar radiation from 10am - 2pm mid summer at a latitude of 29° south of the equator (Brazil) was similar to that observed in the UVA-irradiated DNA plasmid (36). Although these studies appear to conflict with one another, the carcinogenic potential of UVA radiation has been irrefutably demonstrated by de Laat et al (48) who observed a dose dependent induction of squamous cell carcinomas in hairless mice irradiated daily with near monochromatic radiation at 365 nm. The mutagenic potential of UVA radiation may be augmented by observations that UVA-irradiated cells display a greater affinity toward CPD production at CpG sites (49) and slower CPD repair (50) compared to UVB irradiated cells, which together increases the probability of deamination and subsequent mutagenicity if the aforementioned hypothesis is correct.

1.3 Repair mechanisms and potential targets

Although UV radiation is clearly a complete carcinogen, cells possess effective repair mechanisms capable of removing solar radiation-induced DNA lesions. The most effective repair mechanism for the removal of UV-induced lesions is photoreactivation which employs light-activated lesion specific photolyases to repair CPDs (51). However, photolyase encoding genes were not conserved in placental mammals including humans (52). Thus, the removal of pre-mutagenic lesions like CPDs in these mammals relies exclusively on nucleotide excision repair (NER) (53) that excises and removes a short

stretch of nucleotides in a 'cut and patch' type process. NER is capable of recognising a broad spectrum of DNA helix distorting lesions including UV lesions and is comprised of two sub-pathways termed global genomic repair (GGR) and transcription coupled repair (TCR) (28). GGR repairs DNA lesions throughout the entire genome whereas TCR, as the name suggests, removes transcription blocking DNA lesions on the transcribed strand, where the pathways differ in terms of activation but follow a common pathway thereafter (54). GGR is initiated by adduct recognition by the XPC-HR23B-Centrin complex (55), however, due to the mild distortions incurred to the helix by CPDs, GGR damage recognition is further assisted by XPE complexed to the UV damaged DNA binding protein (UV-DDB) which is comprised of DDB1 and DDB2 subunits (56-58). The general assumption is that TCR is activated by the physical blockage of the transcribing activities of RNA polymerase II upon which TCR-specific factors, CSA and CSB, are recruited to displace the stalled polymerase from the DNA strand in order to access the lesion for repair (57-60).

Upon recognition of the DNA lesion the transcription factor IIH (TFIIH), XPA and replication protein A (RPA) sequentially bind to the damage site. The helicases XPB and XPD are subunits of TFIIH and operate in a 3'-5' and 5'-3' direction along the damaged strand respectively opening a bubble in the double helix at the locus of the lesion. The lesion is excised by asymmetric dual incisions performed by endonucleases XPG and the XPF-ERCC1 complex which hydrolyse phosphodiester bonds on the 3' and 5' sides of the damage site respectively. XPA and RPA function to stabilise the single strand DNA sites

and the now excised region is re-synthesised by DNA polymerases using the undamaged strand as a template and the DNA fragments are ligated by DNA ligase (28, 54-60).

The importance of NER repair mechanisms in the prevention of skin carcinogenesis is highlighted by the hereditary autosomal recessive syndrome xeroderma pigmentosum (XP). There are eight complementation groups of XP (XPA-G and XPV) corresponding to different gene defects, all of which exhibit at least a 1000 fold increased susceptibility to skin carcinogenesis compared to normal individuals (60, 61). The latter complementation, XPV, is different from the former variants in that XPV cells are NER proficient and can efficiently excise DNA lesions but lack DNA polymerase η, the translesion synthesis polymerase necessary for CPD bypass (28). Cockayne syndrome (CS) and trichothiodystrophy (TDD) are two additional disorders that arise from NER defects, specifically TCR defects, that present a significantly different phenotype to XP patients including the absence of increased susceptibility to skin cancer although sun sensitivity may present (61). Using various XP cell lines (XPA, XPD, XPG and XPV) and NER proficient HeLa cells transfected with and without photolyases specific for CPD and 6-4PPs, Lima-Bessa et al (28) demonstrated that both CPDs and 6-4PPs are strong triggers for apoptosis but that CPDs, not 6-4PPs, are the major apoptotic trigger in NER proficient cell lines (both HeLa and XPV cells). Furthermore, the work of Arlett et al (62) demonstrated that transfecting immortalised XPC cell lines with full length XPC cDNA to correct the NER defect restored normal cellular sensitivity to UV radiation as measured in terms of cell survival post irradiation.

From the above studies, it is clear that both DNA repair and cell death in response to UV photoproducts are important protective mechanisms by which genomic stability is maintained. However, mutagenic lesions must be capable of evading repair and apoptotic triggering in order to initiate the carcinogenic pathway. Nijhof et al (63) found that growth-stimulated basal cells from hairless mice irradiated with repeated low doses (40 x 0.14 MED (minimal erythmal dose)) using a broadband UVA/B irradiator retained CPDs post irradiation which gradually disappeared over a period of 2 weeks during which no apoptosis was observed and thus loss was attributed to epidermal turnover. Furthermore, clusters of $p53^{+/+}$ over expressing cells were found to occur with the disappearance of CPDs in basal cells. These effects were not observed in the basal cells of mice irradiated once with a high dose of 6 MED. The authors concluded that the initial occurrence of CPD-retaining cells is a prerequisite for the eventual formation of p53 clusters, a common pre-neoplastic event in NMSC (63).

The initiating step in carcinogenesis is the preservation of unrepaired genomic damage however only mutations that provide a growth advantage play a critical role (44). For the most part, these mutations are generally found in proto-oncogenes, tumour suppressor genes and / or DNA repair genes which provides favourable conditions for neoplastic transformation (64). Of these, the tumour suppressor gene p53 is possibly the most prominent target for such mutations as evidenced by that fact that it is mutated in approximately half of all human cancers (65). p53 is a transcriptional regulator with roles in cell cycle regulation, apoptosis and autophagy (64-66) and non transcriptional apoptotic roles via interactions with Bcl-2 family members (67). Furthermore, p53 is reported to be

mutated in 50-90 % of human NMSC depending on carcinoma type and the genomic susceptibility of an individual (68, 69). Although it is clear that p53 is an important target in skin carcinogenesis where mutations in this gene has potentially far reaching effects, DNA microarray analysis demonstrate that UV radiation affects a plethora of genes. Genes that function in a variety of processes including apoptosis, cell cycle regulation, signal transduction, mRNA transcription translation and protein processing, structural, metabolism, adhesion, proteasome, and stress responses (70-73). Although all four cited studies demonstrate the complexity of the molecular response in UV irradiated cells, the studies are inconsistent with regard to the up- or down-regulating effects of UV radiation on gene expression. Although Sesto et al (73) also reported that gene expression profiling was underestimated in comparison to northern blots which may account, in part, for such discrepancies, it is highly probable that these discrepancies arise from differences in spectral irradiance, dose, cell model and time points of gene expression analysis. Despite this, such studies provide important imformation regarding gene regulation of apoptotic cells which may help identify critical targets for mutations that provide the necessary conditions for tumour progression. For example He et al (70) found that Inhibitor-of-Apoptosis (IAP) family member survivin is repressed in UVA irradiated apoptotic keratinocytes, while using immunohistochemistry, Grossman et al (74) found that survivin was expressed in 81% and 92% of human basal and squamous cell carcinomas respectively.

1.4 Rationale and objectives

It is clear from the literature reviewed above that solar radiation, more specifically UV, radiation elicits a plethora of cellular responses. However, the exact contribution of UV radiation to, and the interplay of different wavebands in, skin carcinogenesis are not fully elucidated as of yet. Of particular interest to this study are reports that the distribution of DNA lesions in UV-irradiated cells are dose dependent (24, 34). Although only the effect of dose was observed in these studies, these effects may well be applicable to the spectral irradiance of an irradiator, since it is not unfathomable that the amount of energy deposited in a cell per second ($Jm^{-2}s^{-1}$ = Wm^{-2}) may differentially affect the response and / or the ability of cells to respond to damage. Support for this conjecture is provided by the work of Hoerter et al (75) who found that increased UVA irradiances (Wm^{-2}) significantly increased oxidative stress in human fibroblasts as measured using four different indicators (protein oxidation, reduced glutathione (GSH) levels, heme oxygenase-1 (HO-1) activity and ROS). Furthermore, inconsistencies regarding UVA radiation and DNA mutagenesis have been speculated to be the result of differences in experimental systems, particularly the spectral distribution of the irradiator employed (23, 31). In addition, the photochemistry of UVA radiation has been speculated to be strongly influenced not only by the cell type but also the cellular environment (47).

These observations and concerns form the basis for this current body of research. Over the course of this PhD project, issues pertaining to the environmental relevance of both the irradiator and the exposure medium were examined with the objective of establishing both

environmentally and biologically relevant exposure parameters upon which further and more detailed future investigations into the mechanistic effects of solar radiation could be performed. As DNA damage is predominantly manifested as cell death in UV irradiated cells (21), cell death was the predominant endpoint employed in this study, as measured using the gold standard radiobiological assay, the clonogenic assay. In addition, apoptotic markers such as caspase activation and perturbations to the mitochondrial membrane potential were examined to investigate the role of programmed cell death, while the comet assay was employed to examine the ability of solar simulated radiation to incur DNA damage.

1.5 References

(1) P. Strittmatter, J. Soll & B. Bolter (2010) The chloroplast protein import machinery: A review *Methods Mol Biol* **619,** 307-21.

(2) A. R. Webb (2006) Who, what, where and when-influences on cutaneous vitamin d synthesis *Prog Biophys Mol Biol* **92,** 17-25.

(3) International Commission on Illumination (CIE) (1989) Solar spectral irradiance CIE pub. no. 85.

(4) International Commission on Illumination (CIE) (1987) International lighting vocabulary CIE pub. no. 17.4.

(5) D. B. Brown, A. E. Peritz, D. L. Mitchell, S. Chiarello, J. Uitto & F. P. Gasparro (2000) Common fluorescent sunlamps are an inappropriate substitute for sunlight *Photochemistry and Photobiology* **72,** 340-4.

(6) T. M. Oberyszyn (2008) Non-melanoma skin cancer: Importance of gender, immunosuppressive status and vitamin d *Cancer Lett* **261,** 127-36.

(7) A. K. von Thaler, Y. Kamenisch & M. Berneburg (2010) The role of ultraviolet radiation in melanomagenesis *Exp Dermatol* **19,** 81-8.

(8) C. F. Garland, F. C. Garland & E. D. Gorham (2003) Epidemiologic evidence for different roles of ultraviolet a and b radiation in melanoma mortality rates *Annals of Epidemiology* **13,** 395-404.

(9) M. R. Zaidi, C.-P. Day & G. Merlino (2008) From uvs to metastases: Modeling melanoma initiation and progression in the mouse *J Invest Dermatol* **128,** 2381-2391.

(10) S. Gandini, S. Raimondi, P. Gnagnarella, J. F. Dore, P. Maisonneuve & A. Testori (2009) Vitamin d and skin cancer: A meta-analysis *Eur J Cancer* **45,** 634-41.

(11) T. W. Ridky (2007) Nonmelanoma skin cancer *J Am Acad Dermatol* **57,** 484-501.

(12) D. S. Rigel (2008) Cutaneous ultraviolet exposure and its relationship to the development of skin cancer *Journal of the American Academy of Dermatology* **58,** S129-S132.

(13) G. M. Halliday, M. Norval, S. N. Byrne, X. X. Huang & P. Wolf (2008) The effects of sunlight on the skin *Drug Discovery Today: Disease Mechanisms* **5,** e201-e209.

(14) W. E. Roberts (2009) Skin type classification systems old and new *Dermatologic Clinics* **27,** 529-533.

(15) S. T. Shih, R. Carter, C. Sinclair, C. Mihalopoulos & T. Vos (2009) Economic evaluation of skin cancer prevention in australia *Prev Med* **49,** 449-53.

(16) H. J. van der Rhee, E. de Vries & J. W. Coebergh (2006) Does sunlight prevent cancer? A systematic review *Eur J Cancer* **42,** 2222-32.

(17) J. Reichrath (2006) The challenge resulting from positive and negative effects of sunlight: How much solar uv exposure is appropriate to balance between risks of vitamin d deficiency and skin cancer? *Progress in Biophysics and Molecular Biology* **92,** 9-16.

(18) P. Tuohimaa, E. Pukkala, G. Scélo, J. H. Olsen, D. H. Brewster, K. Hemminki, E. Tracey, E. Weiderpass, E. V. Kliewer, V. Pompe-Kirn, M. L. McBride, C. Martos, K.-S. Chia, J. M. Tonita, J. G. Jonasson, P. Boffetta & P. Brennan (2007) Does solar exposure, as indicated by the non-melanoma skin cancers, protect from solid cancers: Vitamin d as a possible explanation *European Journal of Cancer* **43,** 1701-1712.

(19) B. A. Gilchrest (2007) Sun protection and vitamin d: Three dimensions of obfuscation *The Journal of Steroid Biochemistry and Molecular Biology* **103,** 655-663.

(20) F. R. de Gruijl, H. J. van Kranen & L. H. F. Mullenders (2001) Uv-induced DNA damage, repair, mutations and oncogenic pathways in skin cancer *Journal of Photochemistry and Photobiology B: Biology* **63,** 19-27.

(21) L. F. Batista, B. Kaina, R. Meneghini & C. F. Menck (2009) How DNA lesions are turned into powerful killing structures: Insights from uv-induced apoptosis *Mutat Res* **681,** 197-208.

(22) KNMI/TEMIS (2006) Uv radiation monitoring: Uv index and uv dose http://www.temis.nl/uvradiation/info/uvaction.html April 29th 2010.

(23) J. Cadet, E. Sage & T. Douki (2005) Ultraviolet radiation-mediated damage to cellular DNA *Mutation Research/Fundamental and Molecular Mechanisms of Mutagenesis* **571,** 3-17.

(24) J.-L. Ravanat, T. Douki & J. Cadet (2001) Direct and indirect effects of uv radiation on DNA and its components *Journal of Photochemistry and Photobiology B: Biology* **63,** 88-102.

(25) S. Mouret, M. Charveron, A. Favier, J. Cadet & T. Douki (2008) Differential repair of uvb-induced cyclobutane pyrimidine dimers in cultured human skin cells and whole human skin *DNA Repair (Amst)* **7,** 704-12.

(26) L. Marrot & J. R. Meunier (2008) Skin DNA photodamage and its biological consequences *J Am Acad Dermatol* **58,** S139-48.

(27) P. C. Hanawalt (1998) Genomic instability: Environmental invasion and the enemies within *Mutat Res* **400,** 117-25.

(28) K. M. d. Lima-Bessa, M. G. Armelini, V. Chiganças, J. F. Jacysyn, G. P. Amarante-Mendes, A. Sarasin & C. F. M. Menck (2008) Cpds and 6-4pps play different roles in uv-induced cell death in normal and ner-deficient human cells *DNA Repair* **7,** 303-312.

(29) D. H. Lee & G. P. Pfeifer (2003) Deamination of 5-methylcytosines within cyclobutane pyrimidine dimers is an important component of uvb mutagenesis *J Biol Chem* **278,** 10314-21.

(30) S. Obeid, N. Blatter, R. Kranaster, A. Schnur, K. Diederichs, W. Welte & A. Marx (2010) Replication through an abasic DNA lesion: Structural basis for adenine selectivity *Embo J.*

(31) G. P. Pfeifer, Y. H. You & A. Besaratinia (2005) Mutations induced by ultraviolet light *Mutat Res* **571,** 19-31.

(32) B. Alberts, A. Johnson, J. Lewis, M. Raff, K. Roberts & P. Walter (2002) *Molecular biology of the cell* (Taylor & Francis, New York).

(33) K. Kino & H. Sugiyama (2005) Uvr-induced g-c to c-g transversions from oxidative DNA damage *Mutat Res* **571,** 33-42.

(34) A. Besaratinia, T. W. Synold, H. H. Chen, C. Chang, B. Xi, A. D. Riggs & G. P. Pfeifer (2005) DNA lesions induced by uv a1 and b radiation in human cells: Comparative analyses in the overall genome and in the p53 tumor suppressor gene *Proceedings of the National academy of Sciences* **102,** 10058-63.

(35) S. Mena, A. Ortega & J. M. Estrela (2009) Oxidative stress in environmental-induced carcinogenesis *Mutation Research/Genetic Toxicology and Environmental Mutagenesis* **674,** 36-44.

(36) A. P. Schuch & C. F. M. Menck (2010) The genotoxic effects of DNA lesions induced by artificial uv-radiation and sunlight *Journal of Photochemistry and Photobiology B: Biology* **In Press, Corrected Proof.**

(37) C. M. Chan, J. H. Huang, H. H. Lin, H. S. Chiang, B. H. Chen, J. Y. Hong & C. F. Hung (2008) Protective effects of (-)-epigallocatechin gallate on uva-induced damage in arpe19 cells *Mol Vis* **14,** 2528-34.

(38) H. Merwald, G. Klosner, C. Kokesch, M. Der-Petrossian, H. Hönigsmann & F. Trautinger (2005) Uva-induced oxidative damage and cytotoxicity depend on the mode of exposure *Journal of Photochemistry and Photobiology B: Biology* **79,** 197-207.

(39) B. Catalgol, I. Ziaja, N. Breusing, T. Jung, A. Hohn, B. Alpertunga, P. Schroeder, N. Chondrogianni, E. S. Gonos, I. Petropoulos, B. Friguet, L. O. Klotz, J. Krutmann & T. Grune (2009) The proteasome is an integral part of solar ultraviolet a radiation-induced gene expression *J Biol Chem* **284,** 30076-86.

(40) H. Wang, L. Shang & W. Hao (2003) The induction of apoptosis and reactive oxygen species in human skin fibroblast by ultraviolet a *Beijing Da Xue Xue Bao* **35,** 69-73.

(41) B. Montaner, P. O'Donovan, O. Reelfs, C. M. Perrett, X. Zhang, Y. Z. Xu, X. Ren, P. Macpherson, D. Frith & P. Karran (2007) Reactive oxygen-mediated damage to a human DNA replication and repair protein *EMBO Rep* **8,** 1074-9.

(42) Y. Yue, H. Zhou, G. Liu, Y. Li, Z. Yan & M. Duan (2010) The advantages of a novel coq10 delivery system in skin photo-protection *International Journal of Pharmaceutics* **In Press, Corrected Proof.**

(43) N. S. Agar, G. M. Halliday, R. S. Barnetson, H. N. Ananthaswamy, M. Wheeler & A. M. Jones (2004) The basal layer in human squamous tumors harbors more uva than uvb

fingerprint mutations: A role for uva in human skin carcinogenesis *Proceedings of the National academy of Sciences* **101,** 4954-9.

(44) X. X. Huang, F. Bernerd & G. M. Halliday (2009) Ultraviolet a within sunlight induces mutations in the epidermal basal layer of engineered human skin *Am J Pathol* **174,** 1534-43.

(45) A. Javeri, X. X. Huang, F. Bernerd, R. S. Mason & G. M. Halliday (2008) Human 8-oxoguanine-DNA glycosylase 1 protein and gene are expressed more abundantly in the superficial than basal layer of human epidermis *DNA Repair* **7,** 1542-1550.

(46) T. Douki, A. Reynaud-Angelin, J. Cadet & E. Sage (2003) Bipyrimidine photoproducts rather than oxidative lesions are the main type of DNA damage involved in the genotoxic effect of solar uva radiation *Biochemistry* **42,** 9221-6.

(47) S. Mouret, C. Baudouin, M. Charveron, A. Favier, J. Cadet & T. Douki (2006) Cyclobutane pyrimidine dimers are predominant DNA lesions in whole human skin exposed to uva radiation *Proc Natl Acad Sci U S A* **103,** 13765-70.

(48) A. de Laat, J. C. van der Leun & F. R. de Gruijl (1997) Carcinogenesis induced by uva (365-nm) radiation: The dose-time dependence of tumor formation in hairless mice *Carcinogenesis* **18,** 1013-20.

(49) H. Ikehata, H. Kudo, T. Masuda & T. Ono (2003) Uva induces c->t transitions at methyl-cpg-associated dipyrimidine sites in mouse skin epidermis more frequently than uvb *Mutagenesis* **18,** 511-519.

(50) S. Courdavault, C. Baudouin, M. Charveron, B. Canguilhem, A. Favier, J. Cadet & T. Douki (2005) Repair of the three main types of bipyrimidine DNA photoproducts in human keratinocytes exposed to uvb and uva radiations *DNA Repair* **4,** 836-844.

(51) S. Weber (2005) Light-driven enzymatic catalysis of DNA repair: A review of recent biophysical studies on photolyase *Biochimica et Biophysica Acta (BBA) - Bioenergetics* **1707,** 1-23.

(52) C. F. Menck (2002) Shining a light on photolyases *Nat Genet* **32,** 338-9.

(53) S. Bergink, N. G. J. Jaspers & W. Vermeulen (2007) Regulation of uv-induced DNA damage response by ubiquitylation *DNA Repair* **6,** 1231-1242.

(54) L. Maddukuri, D. Dudzinska & B. Tudek (2007) Bacterial DNA repair genes and their eukaryotic homologues: 4. The role of nucleotide excision DNA repair (ner) system in mammalian cells *Acta Biochim Pol* **54,** 469-82.

(55) P. A. Muniandy, J. Liu, A. Majumdar, S. T. Liu & M. M. Seidman (2010) DNA interstrand crosslink repair in mammalian cells: Step by step *Crit Rev Biochem Mol Biol* **45,** 23-49.

(56) J. Tang & G. Chu (2002) Xeroderma pigmentosum complementation group e and uv-damaged DNA-binding protein *DNA Repair (Amst)* **1,** 601-16.

(57) T. Nouspikel (2007) DNA repair in differentiated cells: Some new answers to old questions *Neuroscience* **145,** 1213-1221.

(58) S. Moriwaki & Y. Takahashi (2008) Photoaging and DNA repair *Journal of Dermatological Science* **50,** 169-176.

(59) M. Fousteri & L. H. Mullenders (2008) Transcription-coupled nucleotide excision repair in mammalian cells: Molecular mechanisms and biological effects *Cell Res* **18,** 73-84.

(60) J. H. Hoeijmakers (2001) Genome maintenance mechanisms for preventing cancer *Nature* **411,** 366-74.

(61) K. H. Kraemer, N. J. Patronas, R. Schiffmann, B. P. Brooks, D. Tamura & J. J. DiGiovanna (2007) Xeroderma pigmentosum, trichothiodystrophy and cockayne syndrome: A complex genotype-phenotype relationship *Neuroscience* **145,** 1388-1396.

(62) C. F. Arlett, P. N. Plowman, P. B. Rogers, C. N. Parris, F. Abbaszadeh, M. H. Green, T. J. McMillan, C. Bush, N. Foray & A. R. Lehmann (2006) Clinical and cellular ionizing radiation sensitivity in a patient with xeroderma pigmentosum *Br J Radiol* **79,** 510-7.

(63) J. G. Nijhof, A. M. Mulder, E. N. Speksnijder, E. M. Hoogervorst, L. H. Mullenders & F. R. de Gruijl (2007) Growth stimulation of uv-induced DNA damage retaining epidermal basal cells gives rise to clusters of p53 overexpressing cells *DNA Repair (Amst)* **6,** 1642-50.

(64) C. L. Benjamin & H. N. Ananthaswamy (2007) P53 and the pathogenesis of skin cancer *Toxicol Appl Pharmacol* **224,** 241-8.

(65) J.-F. Millau, N. Bastien & R. Drouin (2010) P53 transcriptional activities: A general overview and some thoughts *Mutation Research/Reviews in Mutation Research* **681,** 118-133.

(66) N. Chen & J. Debnath (2010) Autophagy and tumorigenesis *FEBS Letters* **584,** 1427-1435.

(67) D. Speidel (2010) Transcription-independent p53 apoptosis: An alternative route to death *Trends Cell Biol* **20,** 14-24.

(68) C. M. Gervin, A. McCulla, M. Williams & A. Ouhtit (2003) Dysfunction of p53 in photocarcinogenesis *Front Biosci* **8,** s715-7.

(69) P. Boukamp (2005) Non-melanoma skin cancer: What drives tumor development and progression? *Carcinogenesis* **26,** 1657-67.

(70) Y. Y. He, J. L. Huang, R. H. Sik, J. Liu, M. P. Waalkes & C. F. Chignell (2004) Expression profiling of human keratinocyte response to ultraviolet a: Implications in apoptosis *J Invest Dermatol* **122,** 533-43.

(71) C. A. Koch-Paiz, S. A. Amundson, M. L. Bittner, P. S. Meltzer & A. J. Fornace, Jr. (2004) Functional genomics of uv radiation responses in human cells *Mutat Res* **549,** 65-78.

(72) K. M. Lee, J. G. Lee, E. Y. Seo, W. H. Lee, Y. H. Nam, J. M. Yang, S. H. Kee, Y. J. Seo, J. K. Park, C. D. Kim & J. H. Lee (2005) Analysis of genes responding to ultraviolet b irradiation of hacat keratinocytes using a cdna microarray *Br J Dermatol* **152,** 52-9.

(73) A. Sesto, M. Navarro, F. Burslem & J. L. Jorcano (2002) Analysis of the ultraviolet b response in primary human keratinocytes using oligonucleotide microarrays *Proc Natl Acad Sci U S A* **99,** 2965-70.

(74) D. Grossman, J. M. McNiff, F. Li & D. C. Altieri (1999) Expression of the apoptosis inhibitor, survivin, in nonmelanoma skin cancer and gene targeting in a keratinocyte cell line *Lab Invest* **79,** 1121-6.

(75) J. D. Hoerter, C. S. Ward, K. D. Bale, A. N. Gizachew, R. Graham, J. Reynolds, M. E. Ward, C. Choi, J. L. Kagabo, M. Sauer, T. Kuipers, T. Hotchkiss, N. Banner, R. A. Chellson, T. Ohaeri, L. Gant & L. Vanderhill (2008) Effect of uva fluence rate on indicators of oxidative stress in human dermal fibroblasts *Int J Biol Sci* **4,** 63-70.

Chapter 2 Solar simulating sources - calibration and characteristics

2.1 Introduction

As outlined in chapter 1, skin cancer is a globally increasing epidemic whose incidence is known to be related to UV radiation exposure (1-5) where UV from solar radiation is known to be the main environmental factor contributing to the formation of these malignancies. The Sun approximates a blackbody irradiator at 5800 K (6, 7) and is the Earth's principal source of energy via radiation emissions from the surface of the Sun.

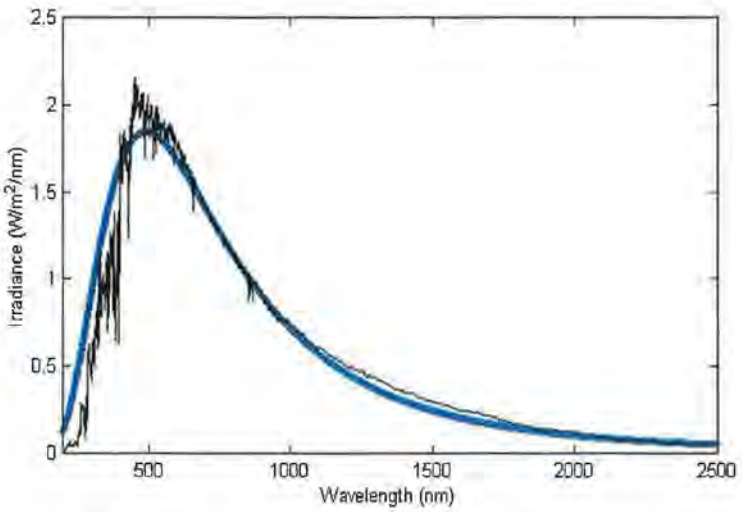

Figure 2.1 Spectral irradiance computed for a black body irradiator at a temperature of 5800 K (•) and extraterrestrial solar radiation data sampled at the top of the Earth's atmosphere (•) by Frohlich and Wehrli (8) which yields a total spectral irradiance of 1354Wm^{-2} in the solar waveband.

Figure 2.1 depicts extraterrestrial solar spectral data sampled by Frohlich and Wehrli (8) at the World Radiation Centre with the spectral irradiance for a blackbody irradiator at 5800

K overlaid. The blackbody irradiance was computed using the Planck radiation law shown in equation 2.1, which describes how the irradiance (I) at wavelength (λ) varies with temperature (T).

$$I(\lambda) = \frac{2\pi hc^2}{\lambda^5 (e^{hc/\lambda kT} - 1)} \qquad \textbf{Equation 2.1}$$

The irradiance of solar radiation at the top of the atmosphere is computed by integrating extraterrestrial solar spectral data. However, the elliptical orbit of the Earth around the Sun gives rise to variations in the Earth to Sun distance. Thus extraterrestrial irradiance is taken at the mean Earth-Sun distance giving a value of approximately 1367 Wm^{-2} known as the solar constant (9, 10). Integrating the extraterrestrial data provided by Frohlich and Wehrli (8) yields an irradiance of 1354 Wm^{-2} which compares well with the solar constant.

As radiation passes through the Earth's atmosphere, the intensity of the incident radiation is attenuated due to various processes such as Rayleigh scattering, water vapour attenuation, aerosol attenuation and most significantly for the ultraviolet region, ozone absorption (11-13). However the resulting terrestrial spectral distribution is far from a global constant since solar radiation levels fluctuate with geographical location/latitude, season, solar elevation (6) and thus relative air mass (AM). Relative AM is the atmospheric path length traversed by solar radiation (figure 2.2) and varies with solar elevation angle (e), related by equation 2.2, where a minimum AM value of 1 occurs when the Sun is directly overhead thus yielding a solar elevation angle of 90° i.e. at the equator during an equinox.

$$AM = 1/\mathrm{Sin}(e) \qquad \textbf{Equation 2.2}$$

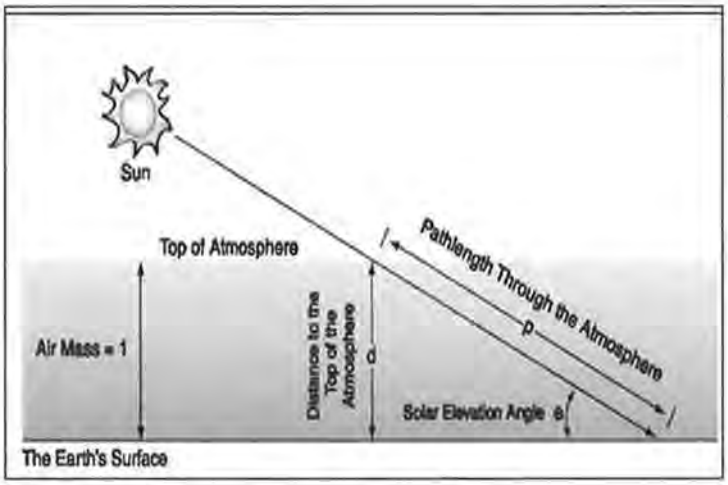

Figure 2.2 Schematic depicting how the optical path length of solar radiation through the Earth's atmosphere varies with solar elevation angle (θ) (14).

In addition to the attenuating effects of the atmosphere, the total irradiance on a horizontal surface at the terrestrial level, known as global radiation, is composed of direct and diffuse components (12, 13, 15, 16). The direct component is simply the direct beam from the sun to the point of incidence on a horizontal surface. However, diffuse radiation is complex and is comprised of forward scattered radiation from the sky and surface albedo (i.e. radiation reflected by a surface). However, in this study, only global radiation measurements are employed to ascertain simple approximations on the irradiance of a given source under investigation.

All of the above illustrates the fact that solar radiation is highly variable with no absolute standard. However, it is reasonable to assume that irradiance values approximating those at near tropic latitudes (i.e. 23° north and south of the equator) are relevant to skin carcinogenesis investigations.

Despite these difficulties, approximations on solar irradiance at the terrestrial level can be ascertained using mathematical models and / or calibrated instrumentation.

$$I_{d\lambda} = H_{o\lambda}DT_{r\lambda}T_{a\lambda}T_{w\lambda}T_{o\lambda}T_{u\lambda} \quad \textbf{Equation 2.3}$$

A typical mathematical approximation or solar irradiance model was published by Bird and Riordan (13) who used equation 2.3 to approximate global solar radiation at the terrestrial level ($I_{d\lambda}$) for given atmospheric variable values. The model applies various transmittance functions and factors to extraterrestrial irradiance data ($H_{o\lambda}$) to account for the attenuating processes that occur as radiation passes through the atmosphere. These include a correction factor for the Earth-Sun distance (D), a transmittance function at wavelength λ for Rayleigh scattering ($T_{r\lambda}$), a transmittance function at wavelength λ for aerosol attenuation ($T_{a\lambda}$), a transmittance function at wavelength λ for water vapour attenuation ($T_{w\lambda}$), ozone absorption at wavelength λ ($T_{o\lambda}$) and uniformly mixed gas absorption at wavelength λ ($T_{u\lambda}$). The extraterrestrial spectral data employed in the model was that provided by Frohlich and Wehrli (8) shown in figure 2.1.

The primary irradiator employed in this study, the Q-sun solar simulator, is designed to provide global solar irradiance typically experienced at noon mid summer in Florida in the USA i.e. at latitude 25° north of the equator. A reference spectrum for comparison would ideally consist of solar radiation measured at latitude 25° N which was not feasible due to travel requirements. This point highlights the advantage of mathematical models such as

the Bird and Riordan (13) model which allow approximations of solar irradiance at a given time and location to be computed. Thus using the mathematical model shown in equation 2.3, the global irradiance on the summer solstice (June 21st) at latitude 25°N was modelled to provide a reference spectrum for the Q-sun solar simulator and is shown in figure 2.3.

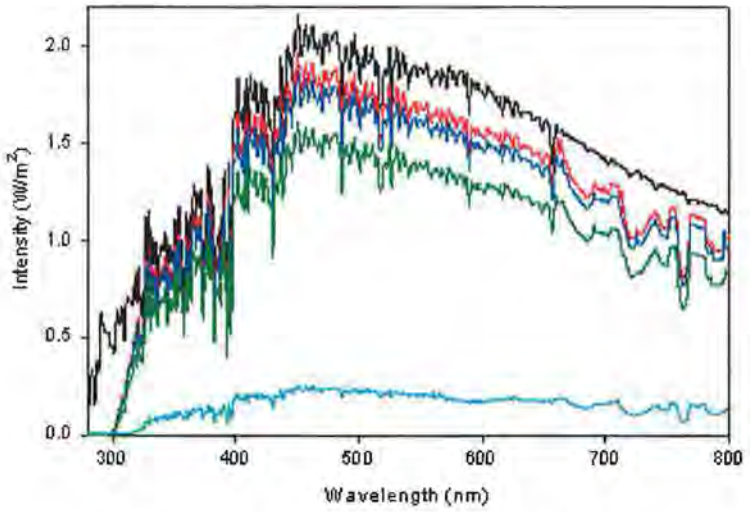

Figure 2.3 Extraterrestrial solar radiation (•) modelled using the Bird and Riordan (13) mathematical model for Florida (•) and Dublin (•) on the summer solstice, Naples (•) on July 12th and Dublin (•) on the winter solstice.

Since it was possible to measure solar radiation at various locations during the course of this project, to compare and test the model further, solar spectra were modelled for the same latitudes on the same dates. Figure 2.3 shows the spectral irradiance modelled for Naples, Italy on July 12th and Dublin, Ireland on both the winter and summer solstice (December and June 21st respectively). Integrating each of the curves over the UV region yields the UV spectral irradiance values that could be expected at these locations on the dates specified which are listed in table 2.1.

The Bird and Riordan (13) model yields a UVB irradiance of 2.86 Wm^{-2} for solar radiation on the summer solstice in Florida (25°N, solar elevation 88.5°, AM value of 1). This concurs well with a solar UVB irradiance of 2.84 Wm^{-2} modelled by Garland et al (17) for Singapore during an equinox (1°N, solar elevation of 89°, AM value of 1). The good correlation between data computed using the Bird and Riordan (13) model with data modelled in the literature for near identical solar elevation angles supports the Bird and Riordan model as a good standard against which solar simulation can be estimated.

Table 2.1 Total and individual UV irradiance values for solar radiation spectra generated using the Bird and Riordan model (13).

Location	Florida	Naples	Dublin	Dublin
Date	June 21st	July 12th	June 21st	Dec 21st
UVA & B (Wm^{-2})	75.71	66.29	61.44	7.79
UVA (Wm^{-2})	72.84	64.03	59.48	7.78
UVB (Wm^{-2})	2.86	2.26	1.96	0.01

When investigating the effects of solar radiation, the ideal situation would be to utilise solar radiation to elicit the biological response under investigation. However, this is rarely a viable option due to the stringent aseptic conditions required for cell culture and the highly variable nature of solar radiation. Since stability and reproducibility are essential to achieve trustworthy data, it is for this reason that employing an artificial irradiator is the most practical option. Although artificial irradiators are the more pragmatic alternatives to solar radiation, they are not without their challenges. There are many types of irradiator available for implementation in radiation studies. These sources vary broadly from the type of

source, wavelength range, spectral distribution, irradiance and delivery (i.e. continuous versus non-continuous), each asserting different advantages and disadvantages over one another. Since artificial irradiators provide the foundations of radiobiological investigations, the suitability or relevance of an irradiator for a given study must be determined prior to implementation. This requires prudent calibration and characterisation techniques to ensure reliable and trustworthy data can be collected. In addition, it has been shown that the irradiance of an irradiator can significantly change over the operational lifetime of a bulb (18), thus it is imperative that the temporal stability of a source be monitored to ensure the output is reproducible within a reasonable tolerance so that results collected from independent tests can be confidently associated with one another.

In turn, thorough calibration processes enable data to be confidently communicated to peers via publications in a clear and comprehensive manner. The importance of this has been voiced strongly in the literature (19, 20). However there is a lack of detail in the literature regarding the output of irradiators utilised in many studies (19). Moreover, the results of meticulously performed biological experiments can be undermined or negated by either inadequate dosimetry and / or unrealistic exposures (19, 21). Specifying a dose, the waveband, the central wavelength or even just the irradiance used in a given study does not provide enough information for inter lab comparison or replication of experimental results as it reveals insufficient information regarding the spectral distribution and / or irradiance of the irradiator employed (19, 20, 22). For example, variable responses observed using two lamps centred about the same wavelength may be the result of differences in spectral distribution and / or irradiance of the source. Furthermore, while providing two or more key

pieces of information such as the irradiance (Wm^{-2}), the total dose administered (Jm^{-2}) and / or the exposure time is sufficient for dosimetry calculations, it still confers no information regarding the spectral distribution of the irradiator thus no information concerning the output in a particular waveband can be extracted. Hence the calibrated spectral distribution of a source is the best and most efficient manner to communicate the output of an irradiator (6) with minimal ambiguity and is achieved using spectroradiometry.

The objective of this chapter is to fully characterise all artificial irradiators employed in this study and to determine the ability of each source to produce environmentally and biologically relevant exposures with respect to solar radiation. Four artificial sources were employed in this project, two high pressure xenon arc solar simulators and two low pressure mercury fluorescent UV lamps, one emitting primarily in the UVB and the other in the UVA. Information pertaining to the spectral irradiance of each source was provided by their respective manufacturers, however the quality of the information supplied was inconsistent. The spectral irradiance for each irradiator was determined using spectroradiometry and compared to the information provided by the manufacturer.

In addition to the spectral irradiance of an irradiator, the manner in which the output of an irradiator is delivered is also an integral aspect of a source. Solar radiation is a continuous source that varies in intensity but not delivery. Thus, the nature of output delivery for all four irradiators employed was investigated to determine if the output was continuous or non-continuous.

Spectroscopic analysis of the different exposure media (cell culture medium and PBS) and cell culture plasticware was also performed, to determine any possible attenuation effects they may have on the spectral irradiance administered by each irradiator. Irradiator characterisation was concluded with a temperature investigation for both solar simulators to determine if either irradiator induced any significant heating effects that may interfere with the normal function of biological samples.

2.2 Spectrometer spectral calibration

To calibrate the spectral output of each artificial irradiator and to assess the reliability of the manufacturer data each irradiator was calibrated using spectroradiometry. Calibrating artificial sources using spectroradiometry requires that the spectrometer employed be calibrated over the wavelength range of interest using a calibrated and traceable standard (21, 23). The standard employed in this study was the Bentham CL6h spectral irradiance standard (Bentham Instruments Ltd, Berkshire, UK) and is traceable to National Physical Laboratory standards (NPL, Teddington, UK).

The Bentham standard is a 150 Watt quartz halogen lamp that requires a constant DC power supply provided by the Bentham 605 power supply. Halogen lamps are incandescent tungsten filament bulbs filled with an inert gas containing a halogen, typically Bromine (Br). Incandescence is the emission of electromagnetic radiation from a hot body due to the temperature of that hot body. In the case of a tungsten filament bulb, electromagnetic radiation is produced when a potential difference (V) is applied and the filament resists the induced flow of electric current (I) which in turn causes the filament to heat and emit radiation. Eventually a temperature is reached when the resistance (R) of the filament begins to increase with increasing temperature and the filament ceases to behave linearly according to Ohm's law (V=IR). Strict regulation of the current through the filament stabilises both the temperature and resistance (R), thus preventing variations in the spectral emissions of the irradiance standard. Figure 2.4 shows the spectral irradiance of the

Bentham standard between 250 and 3000 nm, which peaks at 853 nm and according to Bentham possesses a correlated colour temperature of 3277 K.

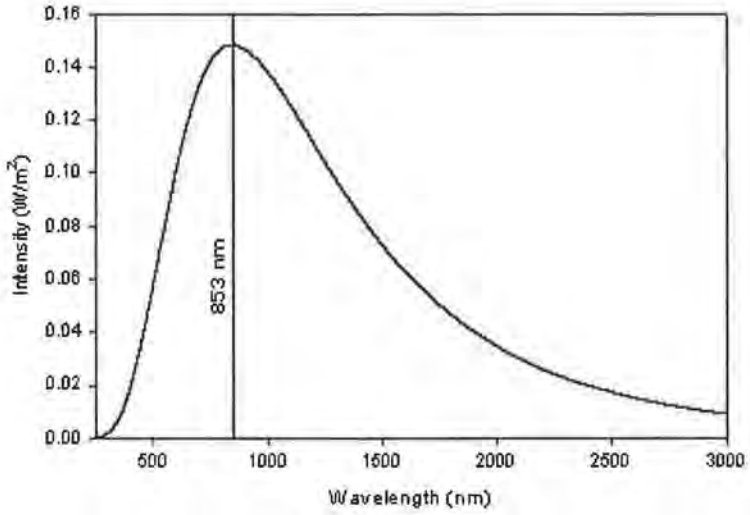

Figure 2.4 shows the spectral irradiance of the Bentham CL6h spectral irradiance standard which approximates a Blackbody irradiator at 3277 K, and is calibrated and traceable to the National Physical Laboratory, UK.

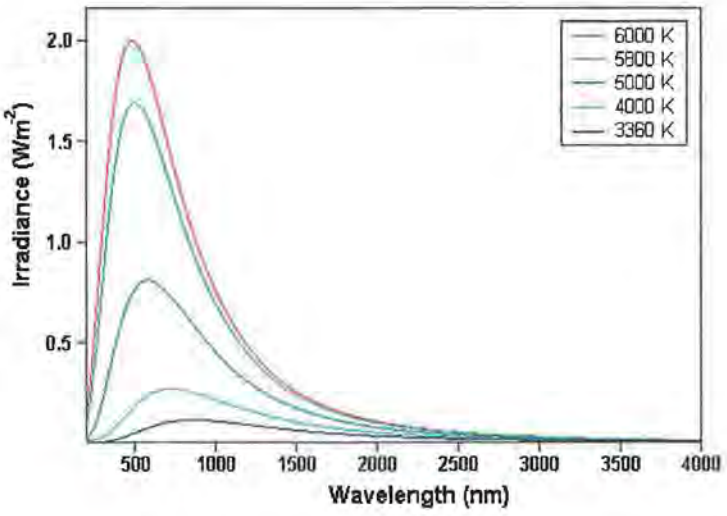

Figure 2.5 Temperature dependent spectralirradiance distribution of blackbody radiation which shows the peak intensity shift to shorter, more energetic wavelengths with increasing temperature.

The spectral distribution of the Bentham standard (figure 2.4) is similar to that of a blackbody irradiator, whose spectral distribution is temperature dependent as shown in figure 2.5. According to Weins law ($\lambda_{max}T=2.90e^{-3}$ mK) the peak wavelength (λ_{max}) of a blackbody irradiator occurs at 884 nm at a temperature (T) of 3277 K while a peak wavelength of 853 nm infers a correlated colour temperature of 4000 K. Tungsten has a melting temperature of 3690 K nor is it an ideal emitter thus differences are to be expected between ideal blackbody emission at 3277 K and that of tungsten at 3277 K.

A miniature USB2000 fibre optic spectrometer (Ocean Optics, The Netherlands) with a 200-1100 nm bandpass was used to calibrate all irradiators, where radiation is coupled to the 50 μm input slit via a 600 μm fibre optic. A cosine corrected diffuser was mounted at the front end of the input fibre to ensure all of the downwelling radiation was sampled. When sampling radiation a detector should possess a hemispherical field of view so that it samples radiation from all directions (21, 24), particularly in the case of sources with direct and diffuse components. Detector diffusers are typically cosine weighted (6, 21, 24) so that they do not underestimate radiation at large incident angles. However most sensors do not possess "ideal" cosine weighted responses but detectors employing a PTFE diffuser can achieve satisfactory responses that deviate significantly from the ideal only at angles of incidence (θ) greater than 70° (6). Thus a CC-3-UV PTFE cosine diffuser (Ocean Optics) was used in conjunction with the 600 μm fibre optic to sample over a 2π field of view to obtain a weighted response as shown in figure 2.6 over the wavelength range 200-1100 nm (25). Radiation collected by the input optics of the spectrometer is dispersed by a fixed grating across a 2048 pixel linear CCD array. Each source was sampled using the USB2000

spectrometer with an integration time of 100 ms per scan to achieve maximum signal without saturation and an average of 200 scans to increase the signal to noise ratio (26). Although the USB2000 has been reported to possess poor stray light rejection (23), it was also shown that with adequate correction the levels of stray light could be significantly reduced to less than 1% at 250 nm (23). A simple correction analogous to background subtraction was employed in this study where the difference in signal between blacked out pixels corresponding to 180 nm and at 250 nm, a wavelength at which no signal would be expected, was determined and subtracted at all wavelengths. This was performed for each independent sample due to the possibility of differing stray light profiles for each sampling. The irradiance of each source was relatively uniform, varying less then 10 % across the exposure field at which cells would be located during irradiation.

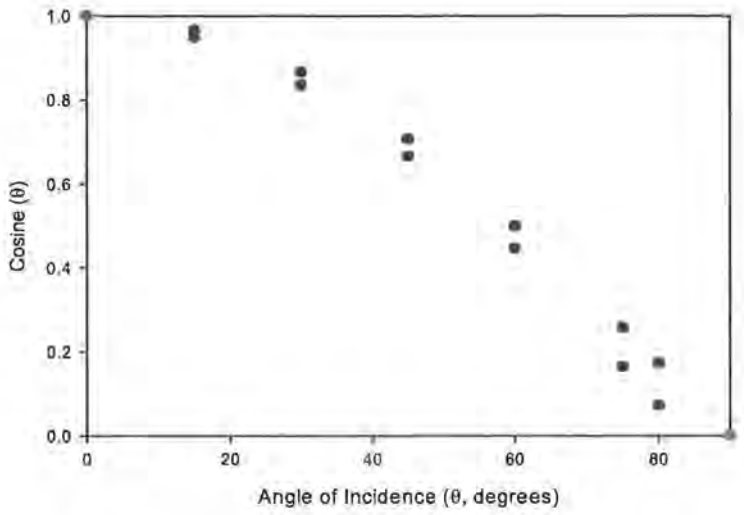

Figure 2.6 Angle of incidence dependent response of the CC-3-UV cosine diffuser (•) (25) and the ideal cosine response (•)

To calibrate the USB2000 spectrometer, the optical front end set-up described above was used to sample the calibrated Bentham standard. Figure 2.7 shows the calibrated response for the Bentham standard, extracted from the data shown in figure 2.4 in the waveband of interest to this research (i.e. 280-800 nm). The spectral distribution obtained using the USB2000 spectrometer for the Bentham in digital numbers (DN) per nanometre (nm) is shown in figure 2.8. A wavelength dependent calibration factor for the USB2000 spectrometer was computed by dividing the calibrated spectral irradiance of the Bentham standard in Wm^{-2} (figure 2.7) by the Bentham spectral distribution in DN (figure 2.8) at each wavelength. The resulting distribution is the calibration factor for the USB2000 spectrometer in Wm^{-2}/DN at each wavelength and is shown in figure 2.9. The calibration factor shown in figure 2.9 can be applied to any spectral data sampled under the same parameters in order to transform the output of the data from DN to spectral irradiance in Wm^{-2}.

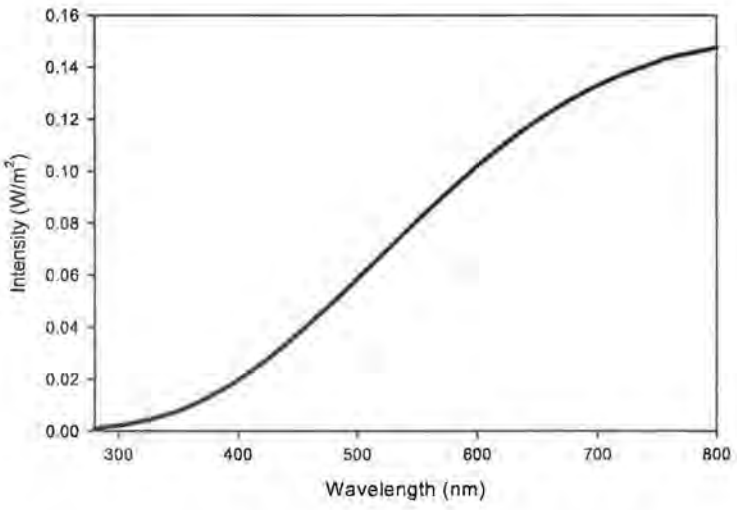

Figure 2.7 The calibrated and traceable output of the Bentham spectral irradiance standard over the waveband of interest to this research

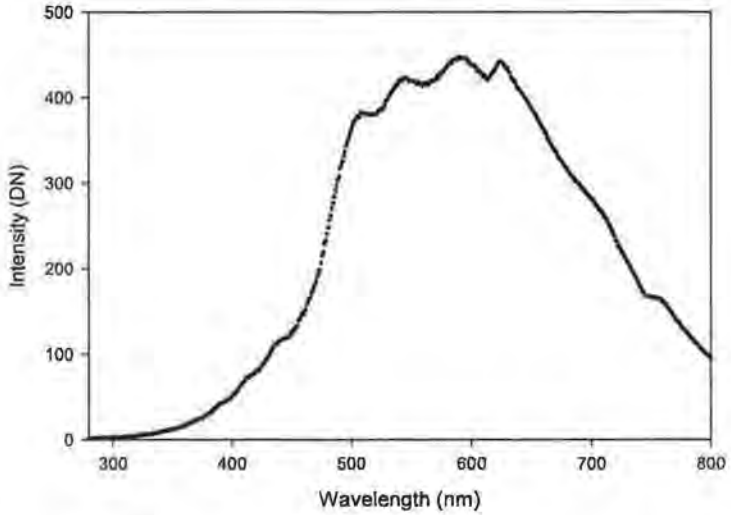

Figure 2.8 The un-calibrated spectral distribution of the Bentham standard sampled using the Ocean Optics USB S2000 spectrometer, 600m fibre optic, an integration time of 100ms and an average of 200 scans.

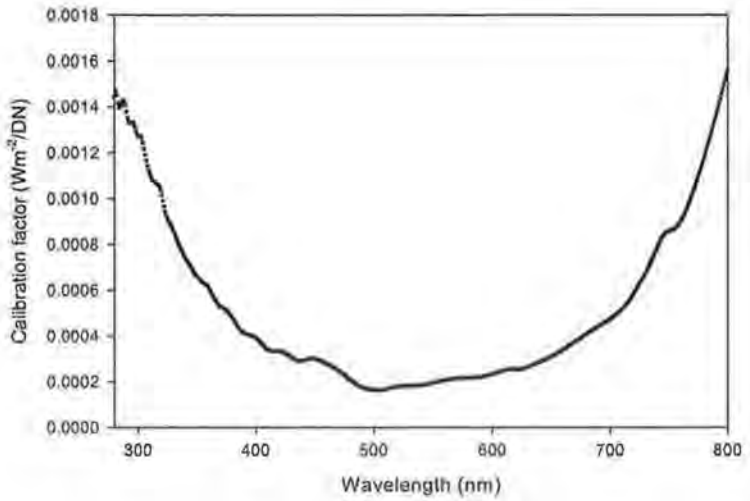

Figure 2.9 USB2000 calibration factor (Wm^{-2}/DN) for the USB2000 spectrometer computed by dividing the calibrated spectral output of the Bentham (Wm^{-2}) by the uncalibrated spectral distribution of the Bentham (DN) sampled using the USB2000 spectrometer.

2.3 Q-sun solar simulator spectral calibration

The principle irradiator in this study, the Q-sun solar simulator (Q-panel, Cleveland, USA), is a high pressure xenon arc lamp. When an electric discharge is applied to a gas, radiation is emitted as line spectra indicative of their atomic structure (27) which occur in the UV, visible and infrared (IR) regions for xenon gas. The production of continuous emission spectra are normally reserved for hot matter in condensed states i.e. liquids or solids at elevated temperatures (27). However it is possible to shift the emission of xenon from spectral to continuous by increasing both the gas pressure and the current density applied to the gas, which facilitates spectral line broadening and thus continuous emissions (28-30).

To achieve the required current density to produce a continuum emission spectrum, the Q-sun employs an external trigger system. A charged capacitor creates a high potential difference between the Q-sun bulb electrodes which is maintained by the non-ionised xenon gas which acts as an insulator. The trigger arm of the Q-sun makes contact with the centre of the quartz envelope (bulb) and applies a high voltage pulse to the envelope on ignition of the lamp. The applied voltage creates an electrostatic field that ionises xenon to the extent that it exceeds its breakdown voltage which is the point at which the gas makes the transition from electrical insulator to electrical conductor (31). When this electrical transition occurs in the vicinity of the electrodes, sparks form and propagate toward the opposite electrode. Once the length of the bulb has been traversed thus completing the 'circuit' the charged capacitor discharges. The increased current flow between the electrodes induces further ionisation of xenon, thus increasing the current density and

temperature of the gas. Hence, it is a combination of the high gas pressure, current density and elevated temperature that enables xenon to produce a continuous emission spectrum.

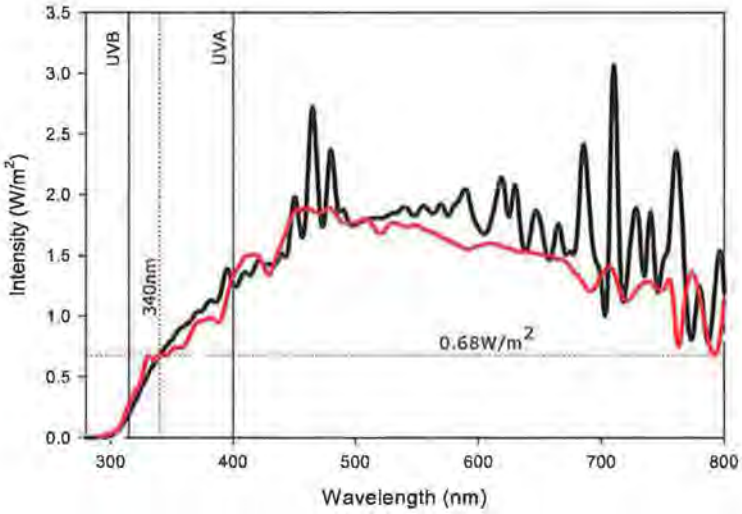

Figure 2.10 Spectral irradiance data provided by the manufacturer Q-Panel for the Q-sun solar simulator operating at 0.68 Wm^{-2} at 340 nm (•) which is designed to mimic solar radiation with an AM value of 1 at a latitude of 25° north (i.e. Florida USA) at solar noon mid summer (•), data also provided by Q-panel.

Figure 2.10 shows the spectral irradiance of the Q-sun solar simulator, as provided by the manufacturer, in $Wm^{-2}nm^{-1}$ from 280 to 800 nm. The Q-sun is designed to mimic typical solar irradiance that could be experienced under cloudless sky conditions at solar noon (sun at highest point in sky) mid summer in Florida USA i.e. at latitude 25°N. This is achieved using a Daylight-Q filter (Q-panel) that has a cut-off wavelength of 295 nm and provides an AM value of 1. An AM value of 1 is possible at latitude 25° north since on the summer solstice (i.e. mid summer, June 21st) the sun is directly above the tropic of Cancer (23.5° north). Thus the Sun is less than 2° off the overhead position at latitude 25° north, yielding a solar elevation of 88.5° and thus an AM value of 1.

The ability of an irradiator to replicate solar radiation over the entire solar spectrum is limited by the materials employed (6) thus sources tend to be calibrated in one region of their spectral distribution. As highlighted in figure 2.10, the Q-sun solar simulator is calibrated in the UV at 340 nm. The irradiance of the Q-sun output can be varied from 0.25-0.68 Wm^{-2} at 340 nm which adjusts the entire spectrum accordingly. The data presented by Q-panel corresponds to the maximum irradiance setting of 0.68 Wm^{-2} at 340 nm sampled at the calibration zone of the chamber. Integrating the Q-sun spectral distribution in figure 2.10 between 280 nm and 400 nm gives a total UV irradiance value of 74 Wm^{-2} (72.9 Wm^{-2} in the UVA and 1.5 Wm^{-2} in the UVB). Also shown in figure 2.10 is a reference spectrum, provided by Q-panel, for typical mid summer solar noon irradiance in Florida. Comparing these spectra shows the Q-sun to be an excellent approximation of solar radiation, however the reliability of the data provided was checked via in house calibration.

The irradiance at the calibration zone of the Q-sun when operating at the maximum irradiance setting of 0.68 Wm^{-2} at 340 nm was determined using the same instrumentation and parameter settings employed to yield the calibration factor in figure 2.9. Applying the calibration factor (Wm^{-2}/DN), by simple multiplication at each wavelength, to the non-calibrated Q-sun distribution (DN) (figure 2.11) transforms the data to spectral irradiance (Wm^{-2}) data as shown in figure 2.12. Also shown in figure 2.12 is the spectral data provided by the manufacturer. The spectra deviate by approximately 15 % in the visible and IR regions, however such deviations are not considered critical due to the reduced biological efficacy of these wavelengths compared to UV wavelengths where the spectra can be seen to exhibit excellent correlation.

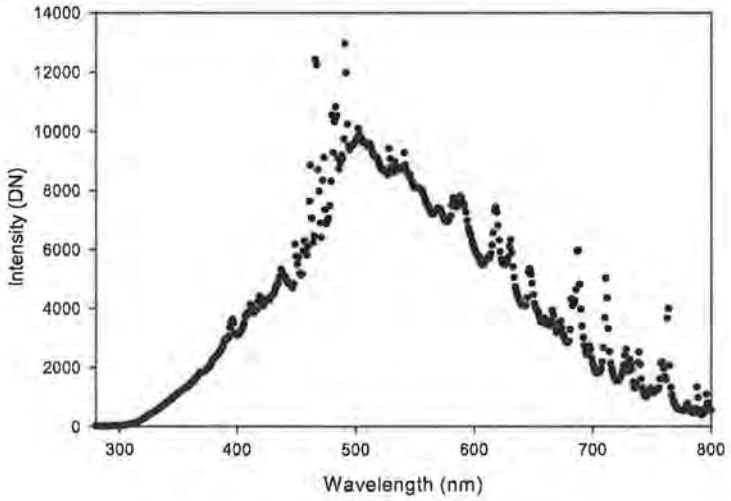

Figure 2.11 The non calibrated Q-sun distribution sampled at the calibration zone of the Q-sun chamber when operating at 0.68 Wm^{-2} at 340 nm using the USB2000 spectrometer.

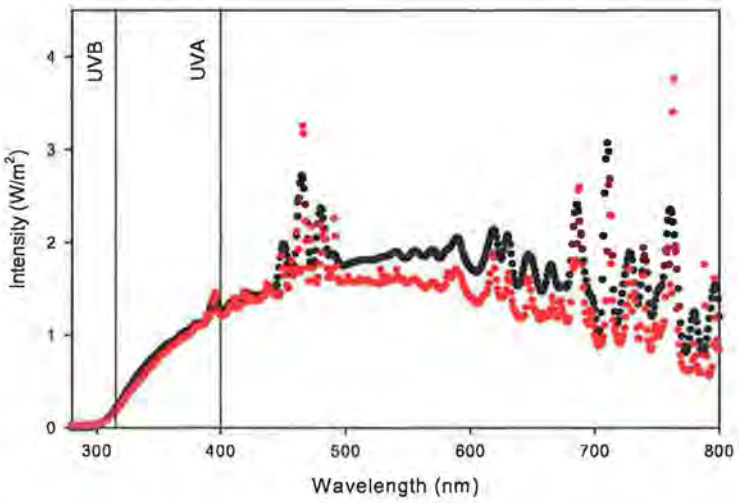

Figure 2.12 Q-sun spectral distribution when operating at 0.68 Wm^{-2} at 340 nm and sampled at the calibration zone as provided by the manufacture Q-panel (•) and sampled using the USB2000 spectrometer (•)

The stability of the Q-sun was monitored by calibrating the irradiator at regular intervals. The UV irradiance values were computed for the calibrated spectra by integrating over the

280-400 nm interval. Table 2.2 lists the spectral intensities computed for 5 independent measurements giving a mean UV irradiance and standard deviation of 68.7 ± 2.07 Wm^{-2} (67.3 ± 2 Wm^{-2} in the UVA and 1.4 ± 0.1 Wm^{-2} in the UVB), which correlates reasonably well with the manufacturer spectralirradiance of 74 Wm^{-2} (72.9 Wm^{-2} in the UVA and 1.5 Wm^{-2} in the UVB) for the calibration zone.

Table 2.2 UVA/B spectral intensities for the calibration zone of the Q-sun solar simulator computed by integrating the spectral distribution over 280–400 nm. Each replicate represents different dates on which the spectral distribution was sampled using the USB2000 spectrometer.

Replicate	UVA/B (Wm^{-2})	UVA (Wm^{-2})	UVB (Wm^{-2})
1	69.85	68.40	1.45
2	70.92	69.38	1.54
3	69.45	67.95	1.50
4	67.76	66.43	1.33
5	65.64	64.27	1.37
Mean	68.72	67.29	1.43
Std dev	2.07	1.99	0.09

The Q-sun solar simulator is a weathering chamber and was not designed with biological samples in mind. Uniform irradiance is provided across a tilted platform (platform A) as shown in figure 2.13. Photo biological experimentation required a level platform so that cells could be exposed in liquid media of uniform depth across the exposure vessel. Thus, platform A was removed and a level platform (platform B) constructed close to the calibration zone of the chamber. The Q-sun was calibrated at platform B when operating at 0.68 Wm^{-2} at 340 nm, as described for the calibration zone. The UV spectral intensities were computed and are presented in table 2.3. Figure 2.14 depicts the spectral irradiance at

both the calibration zone and the exposure level. As would be expected from the inverse square law ($I \propto 1/d^2$), a loss in irradiance at the exposure level (platform B) is observed (table 2.3). Furthermore, platform B is inclined at an angle of 10° to the Q-sun bulb thus producing non-uniform irradiance across the platform. During irradiation cells are located at the centre of the platform, at X in figure 2.13, across which the uniformity was monitored and found to be within an acceptable tolerance of 8 %.

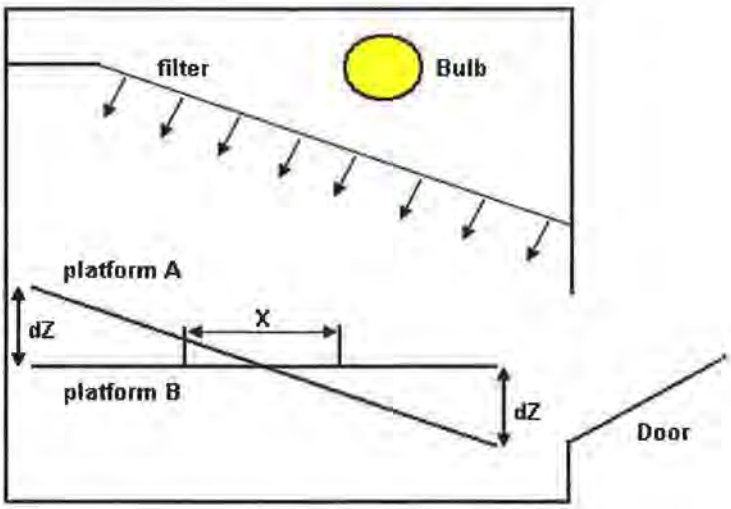

Figure 2.13 Schematic outlining the internal chamber of the Q-sun solar simulator, platform A is the removable tilted platform supplied by the manufacturer Q-panel and platform B is the constructed level platform to allow exposure of cells at uniform depths in the exposure fluid. The levelled platform results in non uniform irradiance across the platform.

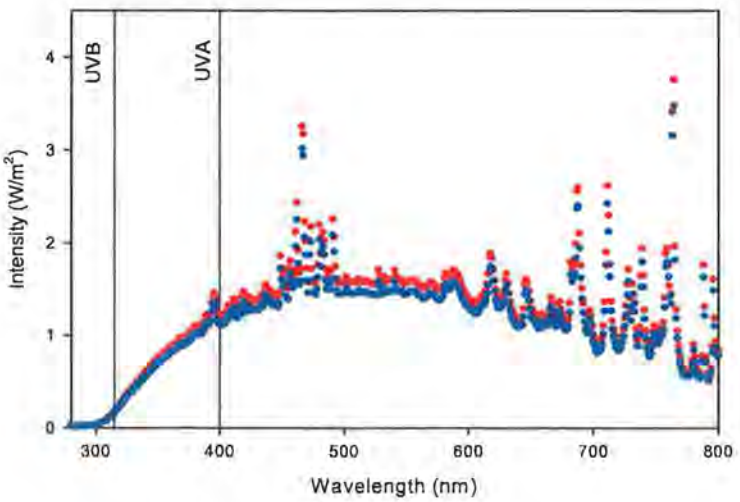

Figure 2.14 Q-sun calibrated distribution spectra sampled using the USB2000 spectrometer at the calibration zone (centre of platform A, figure 2.13) (•) and at the exposure level (centre of platform B, figure 2,13) (•).

Table 2.3 UVA/B spectral intensities at the exposure level inside Q-sun solar simulator computed by integrating the spectral distribution over 280–400 nm. Each replicate represents different dates on which the spectral distribution was sampled using the USB2000 spectrometer.

Replicate	UVA/B (Wm^{-2})	UVA (Wm^{-2})	UVB (Wm^{-2})
1	64.68	63.34	1.34
2	65.66	64.24	1.42
3	64.31	62.91	1.40
4	62.74	61.51	1.24
5	60.78	59.51	1.27
Mean	63.63	62.30	1.33
Std dev	1.91	1.85	0.08

Each Q-sun bulb was employed for a maximum of 1000 operational hours. Spectroradiometry was performed every 150-200 operational hours. The data presented here represent the data sampled over the 1000 hour lifetime of a Q-sun bulb.

2.4 Oriel solar simulator spectral calibration

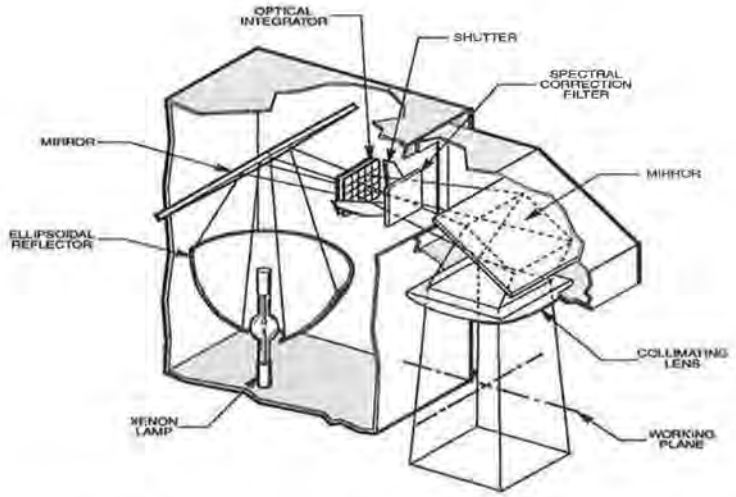

Figure 2.15 Schematic outlining the optical path through the Oriel solar simulator (32). Solar simulated radiation produced by the xenon bulb is collected by the ellipsoidal reflector which is reflected through 45° by a mirror onto the optical integrator which ensures beam uniformity prior to spectral correction by the optical filters. The beam is then reflected through another 45° onto a collimating lens to produce a parallel beam of radiation exiting the source.

The Oriel solar simulator (Oriel-Newport, California, USA) is also a xenon arc lamp ignited by an external trigger as described in section 2.3. The novel attributes of the Oriel solar simulator include not only its continuous nature, but also its variable spectral irradiance via control of the current density and the working distance from the source. Figure 2.15 is a schematic of the optical path through the instrument. Solar simulated radiation produced by the xenon bulb is collected by the ellipsoidal reflector and directed onto the first of two mirrors which reflects the radiation through 45° onto an optical integrator which ensures beam uniformity. Once transmitted though the integrator, the spectral distribution of the radiation is shaped by optical filters. The spectral distribution of the radiation exiting the Oriel is dependent on the filters employed which are

interchangeable. The filters employed in this study are designed to mimic air mass conditions when the Sun is directly overhead i.e. an AM value of 1. The beam is then reflected through another 45° onto a collimating lens at the exit of the irradiator which serves to produce a minimally diverging beam, producing uniform (± 5 %) irradiance over a 15 cm x 15 cm working plane 20 cm from the source (33).

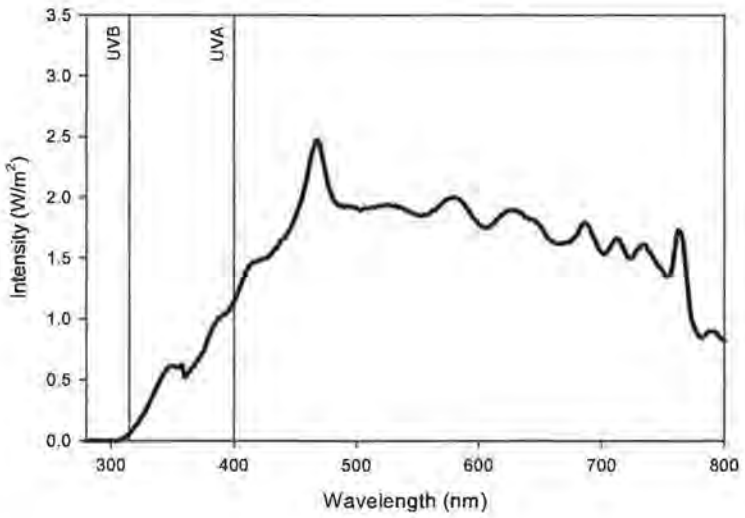

Figure 2.16 Calibrated spectral distribution of the Oriel solar simulator as provided by the manufacturer, believed to be sampled at the recommended but not specified operating parameters of 50 mA and 20 cm for the current density and working distance from the source respectively and an AM value of 1.

The Oriel spectral distribution as provided by the manufacturer, shown in figure 2.16, is believed to be sampled at the recommended working distance and current supply of 20 cm and 50 mA respectively. However, the manufacturer does not specify these details for the spectrum provided. A solar radiation reference spectrum was not provided by the manufacturer, since the irradiance of the Oriel solar simulator is variable and thus does not

reflect a particular geographic location. Integrating under the curve yields a UV spectral irradiance values of 52 Wm^{-2} (51.75 Wm^{-2} in the UVA and 0.25 Wm^{-2} in the UVB) for the manufacturer data provided.

The exposure level for irradiation experiments was set at a working distance of 25 cm from the collimating lens i.e. the distance from the lens to the bench. To determine the most suitable current setting for experimentation the Oriel was sampled using the calibrated USB2000 spectrometer. The input optics of the spectrometer were placed in the centre of the output beam at the exposure level and the current varied from 30-50 mA in 5 mA steps. By applying the calibration factor for the USB2000 spectrometer (figure 2.9), the non calibrated distribution spectra in DN were then transformed into spectral irradiance spectra in Wm^{-2} and are presented in figure 2.17.

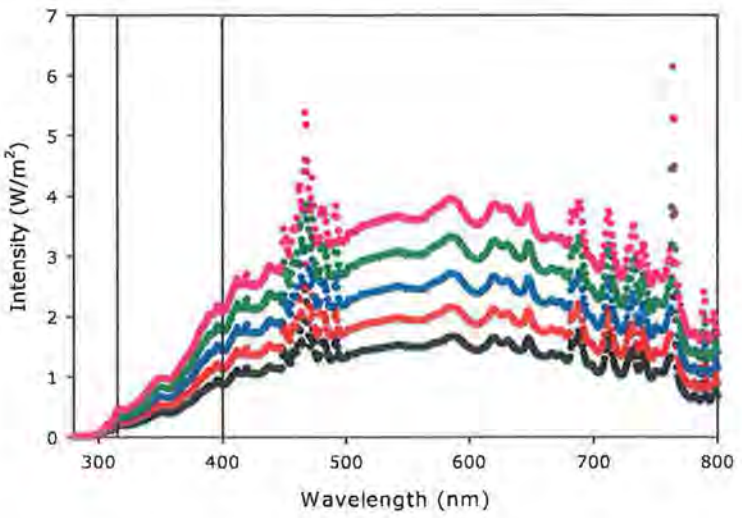

Figure 2.17 The calibrated spectra for the Oriel solar simulator sampled using the USB2000 at the exposure level 25 cm from the source when operating at current values of (•) 30 mA, (•) 35 mA, (•) 40 mA, (•) 45 mA, (•) 50 mA.

Similar to the calibration of the Q-sun, the Oriel was sampled at regular intervals to monitor the irradiance over time. Irradiance spectra (Wm^{-2}) were generated for each independent measurement of each current setting using the calibration factor (Wm^{-2}/DN) illustrated in figure 2.9. Figure 2.17 depicts the mean spectral irradiance (Wm^{-2}) of at least 4 independent measurements sampled on different days for each current setting. The UVA and B irradiance values of each independent measurement for each current setting was computed by integrating the curves from 280 nm to 400 nm and are presented in table 2.4 as the mean and standard deviation for each current setting.

Table 2.4 UVA/B spectral intensities ± standard deviation for the Oriel solar simulator operating at different current settings sampled at the exposure level (25 cm from the source), computed by integrating the spectral distribution over 280–400 nm. Data represents the mean of at least four replicates sampled on different dates.

	UVAB (Wm^{-2})	UVA (Wm^{-2})	UVB (Wm^{-2})
30mA	42.42 ± 1.44	40.46 ± 1.39	1.96 ± 0.05
35mA	54.87 ± 2.16	52.70 ± 2.70	2.17 ± 0.10
40mA	70.11 ± 3.13	66.92 ± 3.02	3.19 ± 0.10
45mA	85.80 ± 3.82	82.09 ± 3.50	3.72 ± 0.44
50mA	101.92 ± 3.70	97.52 ± 3.62	4.39 ± 0.11

The upper limit on the irradiance of solar radiation experienced at the terrestrial level would occur under cloudless sky conditions when the Sun is directly overhead which implies a solar elevation angle of 90° and corresponding AM value of 1. In section 2.1, the irradiance levels modelled for Florida on the summer solstice (25°N, solar elevation 88.5°, AM value of 1) was shown to agree with data modelled in the literature (17) for Singapore during an equinox (1°N, solar elevation of 89°, AM value of 1). The models produced UVB

irradiance values of 2.86 Wm^{-2} and 2.84 Wm^{-2} respectively for a maximum AM value of 1. Current settings exceeding 35 mA resulted in UVB irradiance values greater than those approximated by the mathematical models for optimal solar irradiation, thus a current setting of 35 mA was employed for radiobiological exposures. The spectral distribution for the Oriel when operating at 35 mA and sampled at the exposure level (25 cm from the source) is shown in figure 2.18 with the spectral irradiance data provided by the manufacturer.

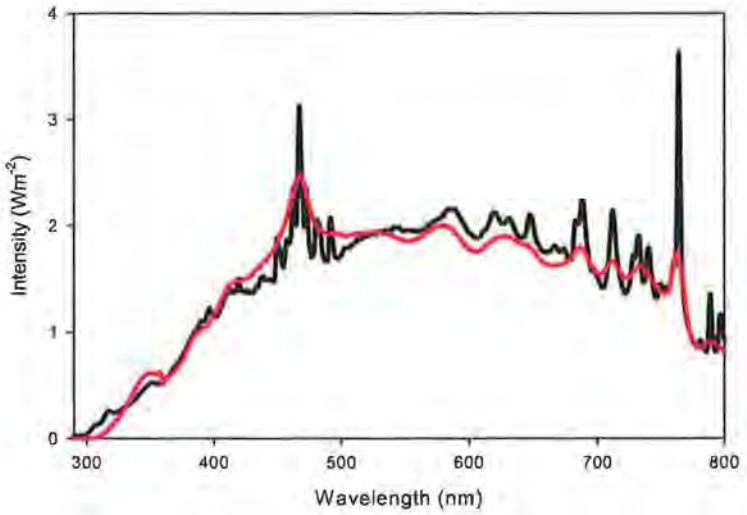

Figure 2.18 Calibrated spectral distribution for Oriel solar simulator sampled at a working distance of 25 cm for a current setting of 35 mA (•) compared with the calibrated data provided by the Oriel (•).

Once the parameter settings were determined, uniformity across the exposure level was assessed. According the manufacturer, the Oriel solar simulator possesses beam uniformity of 5 % across a 15 cm x 15 cm working plane 20 cm from the source but maintains uniformity up to 120 cm from the source (33). The collimated beam exiting the Oriel irradiates an area of 17 cm x 17 cm at the exposure level i.e. 25 cm from the source. The

uniformity of the irradiance across the footprint was measured using a UVA/B PMA2107 radiometer (Solar Light, Pennsylvania, USA) and found to be less than ± 10 %.

2.5 UV fluorescent lamps spectral calibration

Fluorescent UV lamps are commonplace in studies investigating the biological effects of solar UV radiation. Although implementation of solar simulators in biological investigations is increasing, UV lamps are the primary irradiators employed, most probably because of their ease of use, cost and availability. Thus, for comparison, two UV lamps were also examined, a fluorescent UVA lamp (Ultra Violet products Ltd Cambridge UK) and a fluorescent UVB lamp (UVItec, Cambridge UK). Neither are absolute standards for their respective wavebands but both serve as good examples to illustrate the differences between UV fluorescent lamps and solar simulators in terms of spectral distribution and irradiance.

Fluorescent UV lamps are gas discharge lamps that produce electromagnetic radiation when a current is passed through an ionised gas. In general, an evacuated bulb is filled with a low pressure inert gas and mercury atoms (figure 2.19). When the lamp is ignited, the cathode is heated and electrons are emitted by thermionic emission and accelerated through an electric field toward the anode. Collisions between electrons and the inert gas mixture ionises the gas molecules thus increasing the current flow through the bulb. If the kinetic energy of the incident electron is sufficient on collision with a mercury atom, inelastic scattering occurs resulting in the emission of a high energy UVC photon. These high

energy UVC photons initiate the fluorescence process when absorbed by the phosphor coating inside the bulb. Photons are re-radiated by the coating at longer, lower energy wavelengths, the emission spectrum of which is manipulated via the chemical content of the phosphor coating itself.

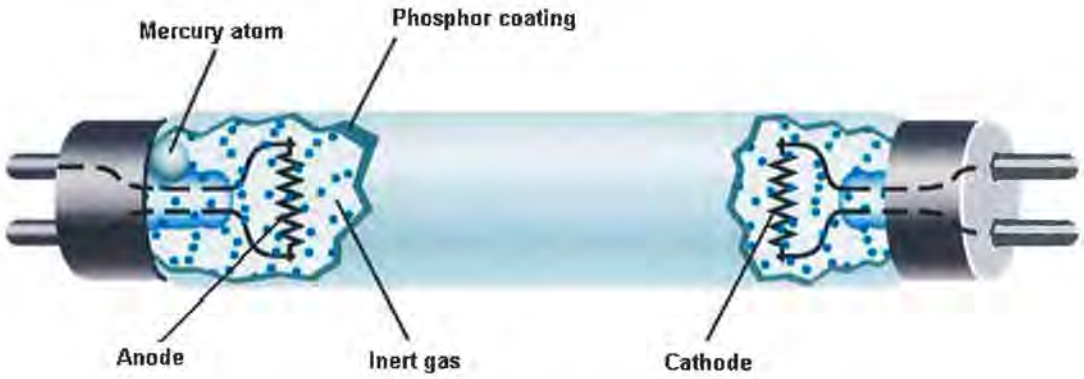

Figure 2.19 Schematic depicting a mercury vapour UV lamp

The fluorescent lamps employed for comparison are both low pressure mercury vapour lamps. Both emit photons in the UVC, primarily at 254 nm, which when incident on the phosphor coating on the inside of each bulb induces fluorescence. The distribution spectra as provided by the manufacturers of the UVA and UVB lamps are shown in figures 2.20 and 2.21. However, no information regarding the intensity of either source was available thus, the environmental relevance, in terms of irradiance, of the sources could not be assessed in the absence of in house calibration.

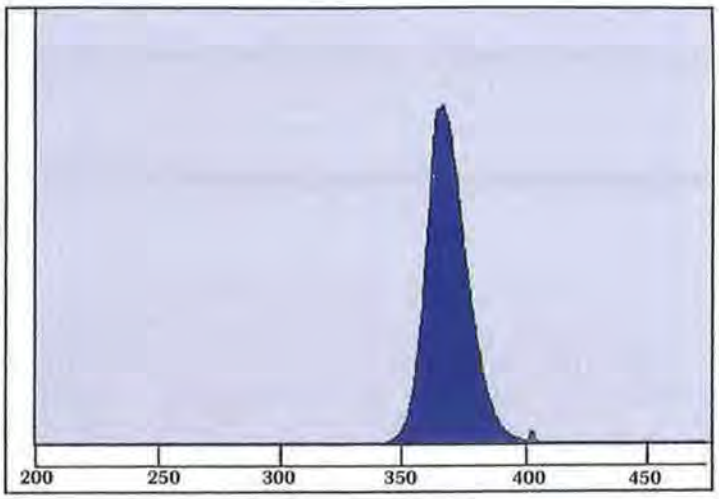

Figure 2.20 UVP manufacturer data of the spectral distribution of the UVA fluorescent lamp (34)

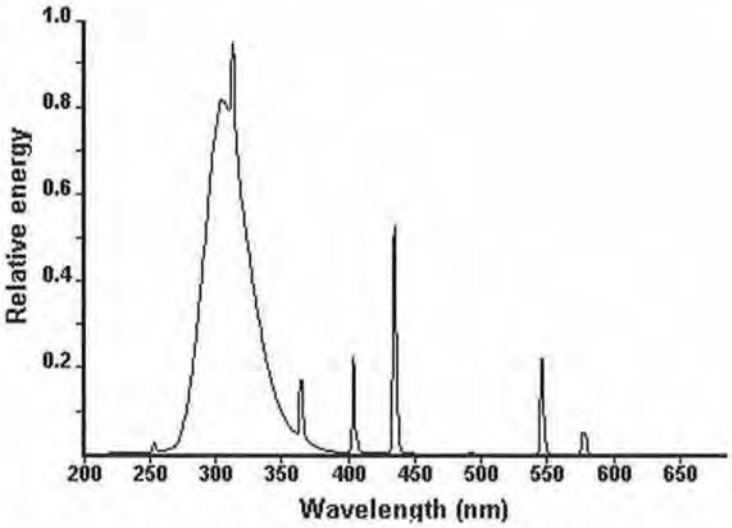

Figure 2.21 UVItec manufacturer data of the spectral distribution of the UVB fluorescent lamp(35)

Similar to the solar simulators, spectroradiometric cross calibration was employed to calibrate the UV lamps. There were no parameter settings for either lamp, just a 15 minute initialisation post ignition. A working distance of 12 cm was chosen for both UV lamps since shorter working distances did not illuminate an adequate area for sample irradiation. Both irradiators were sampled 12 cm from the source using the USB2000 spectrometer.

The non calibrated distribution spectra were transformed to irradiance spectra by applying the calibration factor (figure 2.9) and are shown in figure 2.22 and the corresponding UVA and B irradiance values computed from by integrating the irradiance spectra are shown in table 2.5.

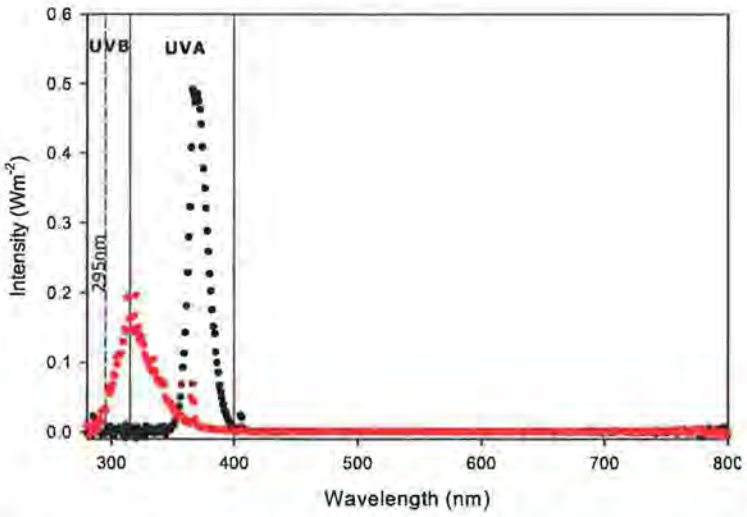

Figure 2.22 Calibrated spectral distributions for both the (•) UVA and (•) UVB fluorescent lamps

Table 2.5 Exposure level UV intensities of fluorescent lamps

Lamp	UVA/B (Wm^{-2})	UVA (Wm^{-2})	UVB (Wm^{-2})
UVA	9.5	9.49	0.01
UVB	6.39	3.96	2.43

2.6 Irradiator Calibration Discussion

The primary objective of the sections 2.2-2.5 was to calibrate each artificial irradiator employed in this study to ascertain reasonable approximations on the spectral irradiance of each source at their respective exposure levels, thus enabling the environmental and biological relevance of each source to be assessed.

The calibrated spectra for all four irradiators are shown together over 280 to 800 nm in figure 2.23 and 280 to 400 nm in figure 2.24. To demonstrate the ability of the irradiators to replicate solar radiation, the spectral distribution for solar radiation sampled in Naples, Italy (noon, July 12th 2008, 40°N, solar elevation of 63° and AM value of 1.12) is also shown in figures 2.23 and 2.24. Agreement with the literature is demonstrated in figure 2.24 where spectral data for solar UV radiation measured and published by Diffey (6) are also shown. The data obtained from the literature corresponds to Albuquerque, USA (38°N, noon, July 3rd, solar elevation of ~70°, AM value of ~1.06) and Melbourne, Australia (38°S, solar noon, January 17th 1990, solar elevation of 73°, AM value of 1.05) in their respective summer seasons. Listed in table 2.6 are the spectral intensities, solar elevation angles and AM values (where available) for the irradiators, measured solar radiation and modelled solar radiation from both this study and the literature (6, 13, 17).

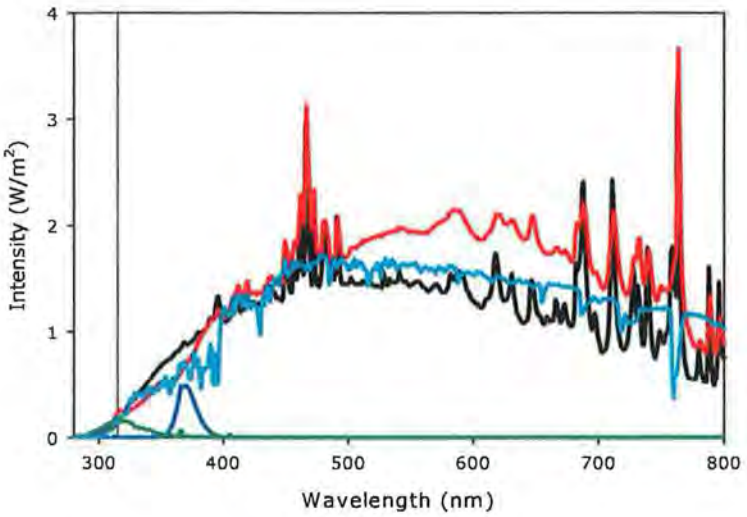

Figure 2.23 Calibrated spectra at the exposure level for (•) the Q-sun solar simulator (•) the Oriel solar simulator operating at 35 mA (•) the UVA lamp and (•) the UVB lamp and (•) solar radiation sampled midsummer in Naples, Italy 40°N

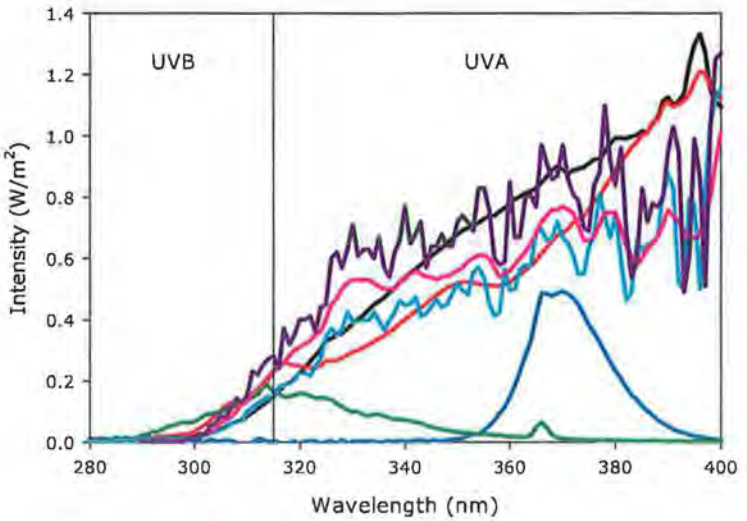

Figure 2.24 Calibrated UV spectra at the exposure level for the Q-sun solar simulator (•), the Oriel solar simulator operating at 35 mA (•), the UVA lamp (•), the UVB lamp (•), solar radiation sampled midsummer in Naples Italy 40° N (•), solar radiation sampled midsummer in Albuquerque 38°N (6) (•) and solar radiation sampled midsummer in Melbourne 38°S (6) (•).

Table 2.6 Variations in spectral distribution of all sources measured using the USB2000 spectrometer and their equivalent AM values where available compared to solar radiation spectral intensities measured or modelled at different latitudes and AM values by Bird et al (13), Diffey (6) and Garland et al (17), Equinox = March 21st and September 21st, S.Solstice = summer solstice June 21st, W.Solstice = winter solstice, December 21st.

Lamp/location	Latitude	Date	Solar elevation (e)	AM	UVA/B (W/m^2)	UVA (W/m^2)	UVB (W/m^2)
Measured using USB2000 spectrometer							
Q-sun	25°N	summer	n/a	1	63.63	62.3	1.33
Oriel	n/a	n/a	n/a	1	54.88	52.7	2.18
UVA	n/a	n/a	n/a	n/a	9.50	9.49	0.01
UVB	n/a	n/a	n/a	n/a	6.39	3.96	2.43
Naples	40°N	July 12th	63°	1.12	46.52	45.25	1.27
Bird model generated data, Bird et al (13)							
Florida	25°N	S.Solstice	88°	1	75.71	72.84	2.86
Naples	40°N	S.Solstice	72°	1.05	72.13	69.50	2.63
Naples	40°N	12th July	63°	1.12	66.29	64.03	2.26
Dublin	53°N	S.Solstice	60°	1.15	61.44	59.48	1.96
Dublin	53°N	W.Solstice	13°	4.45	7.79	7.78	0.01
Sampled by Diffey et al (6)							
Albuquerque	38°N	July 3rd	~ 70° *†	~1.06 *†	51.93	50.28	1.65
Melbourne	38°S	Jan 17th	73° *	1.05 *	62.39	60.28	2.11
Modelled by Garland et al (17)							
Singapore	1°N	Equinox	89°	1	67.54	64.7	2.84
Costa Rica	10°N	Equinox	80°	1.02	65.85	63.6	2.25
Puerto Rico	18°N	Equinox	72°	1.05	62.99	60.9	2.09
Hong Kong	22°N	Equinox	68°	1.08	61.09	59.0	2.09
Cuba	23°N	Equinox	67°	1.09	60.45	58.5	1.95
Israel	32°N	Equinox	58°	1.18	54.42	52.8	1.62
Yogoslavia	45°N	Equinox	45°	1.41	42.77	41.8	0.97
Switzerland	47°N	Equinox	43°	1.47	40.72	39.8	0.92
Iceland	68°N	Equinox	22°	2.67	18.02	17.8	0.22

* Data not directly provided by Diffey (6) but the information that was provided (time, date and location) enabled the solar elevation at solar noon to be determined using an online database (36).

† Data was sampled at 12 noon and not solar noon (6). The solar elevation listed is an approximation based on the fact that measurements taken at 11.46 am and at solar noon in Naples (40°N) on the 12th of July 2008 resulted in solar elevation angles of 63° and 71° respectively, which compares well with the online database (36). From this, it was assumed that the rate of change in solar elevation would be relatively constant and thus was estimated that there would also be an ~8° difference between solar elevation at 12 noon and solar noon for Albuquerque (38°N) on the 3rd of July.

Due to the variable nature of solar radiation there is no absolute standard for solar simulation. The objective of table 2.6 is to provide a frame of reference to support or refute, in terms of UV irradiance values, the environmental and biological relevance of an artificial irradiator in the absence of such a standard.

Mathematical models are dependent on the accuracy of the climatological data (i.e. ozone levels, pollution, aerosols and surface reflectivity) employed in the modelling process (37). Ozone is one of the primary climatological factors effecting the spectral distribution and irradiance of solar UV at the terrestrial level. The ozone data employed in the Garland et al model (17) was collected by NASA using the Total Ozone Mapping Spectrometer (TOMS) while the data computed using the Bird and Riordan model (13) employed a mean ozone thickness of 300 Dobson Units. Since the levels of ozone in the stratosphere varies with latitude (38), this may serve to explain the discrepancies observed between data computed using the Bird and Riordan model (13) and those published by Garland et al (17) for similar solar elevations and AM values. Despite this, there is reasonably good agreement between the two models which provide good approximations on the upper and lower limits of solar UV irradiance values that could be expected at the terrestrial level. Furthermore, the Garland data (17) can also be seen to be in reasonably good agreement with measured data published by Diffey (6).

Although the Oriel possess an interpretation closer to solar radiation over the UVA region, both solar simulators provide excellent approximations of solar radiation as shown in figures 2.23 and 2.24. Although neither solar simulator mimics solar radiation at a

particular geographical location when compared to the modelled and measured data in table 2.6, both administer radiant intensities that are environmentally feasible at mid to near-tropic latitudes, thus demonstrating the environmental relevance of these irradiators.

In addition to a spectral distribution that does not approach that of solar radiation as shown in figures 2.23 and 2.24, the UVA fluorescent lamp administers an irradiance of just 9.49 Wm^{-2} at the shortest working distance feasible for radiobiological exposures. This can be seen from table 2.6 to be 5-6 fold less than the UVA irradiance values administered by the Oriel and Q-sun solar simulators respectively. While the distribution of the UVA lamp is environmentally irrelevant, the magnitude of its irradiance is comparable to the UVA spectralirradiance for Dublin on the winter solstice (7.78 Wm^{-2}, e = 13°, AM value of 4.45) computed using the Bird and Riordan model (13) which would not be expected to produce any detrimental photo-biological effects.

The spectral irradiance of the UVB fluorescent lamp was computed to be 3.96 Wm^{-2} in the UVA and 2.43 Wm^{-2} in the UVB. Even though the majority of the output lies in the UVA waveband region, UVB is the more biologically active waveband, thus such an overlap is not expected to be confounding. From table 2.6, it can be seen that the spectral output of the UVB lamp exceeds the UVB irradiance measured for all artificial irradiators. However, when compared to the solar UVB radiant intensities measured and modelled data in table 2.6, it can be seen that an intensity of 2.43 Wm^{-2} in the UVB is environmentally feasible. It is the spectral distribution of the UVB lamp, however, that undermines its environmental relevance. Close examination of figure 2.24 shows that the distribution of the UVB lamp

does not reduce toward zero at 300 nm as is the case for solar radiation and both solar simulators. In fact the UVB lamp does not reduce to a minimum until ~290 nm, resulting in relatively substantial emissions below 295 nm which is reported to be the shortest wavelength found at the terrestrial level (20). Therefore, in light of the increased ability of UV radiation to elicit damage with decreasing wavelength, as demonstrated by the erythemal and DNA absorption action spectra (39, 40), these spectroradiometric results suggest that the UVB fluorescent lamp is potentially the most hazardous irradiator under investigation.

Although it is beneficial to have prior knowledge of the output emission of an irradiator before it is procured, the data provided by the manufacturer is no substitute for in house calibration prior to implementation. The primary reason for this is to monitor the temporal stability of the irradiator over its lifetime with the same instrumentation. Since comparing data collected with different instrumentation poses significant difficulties due to instrument idiosyncrasies such as sensitivity and resolution (37). Thus, irradiators must be calibrated prior to implementation with the instrument that will be employed throughout the study. The second reason is to determine the credibility of the spectral data provided. As shown above, the manufacturer of each irradiator provided information pertaining to the output of their respective source, however the quality of the information provided varied immensely.

While the data provided by the manufacturers gave some indication of the spectral distribution of each source, the fluorescent UV lamp data did not provide any usable information pertaining to the spectral irradiance as shown in figures 2.20 and 2.21.

Furthermore, it was found that emission peaks present in the UVB lamp manufacturer distribution were absent from in house calibrated spectral data, suggesting the absence of a low pass filter during manufacturer assessment of the lamp. Although visible and UVA wavelengths are less biologically effective compared to UVB, discrepancies may not always be omissions nor favourable in terms of biological effectiveness. This serves to reaffirm not only the importance of in house calibration but also spectroradiometry as the optimal technique to employ, since effects attributed to a particular waveband may in fact be due to emissions at other wavelengths, if the spectral distribution of the source is unknown.

The manufacturer data provided for the Oriel solar simulator was in spectral irradiance, however the information was incomplete. The manufacturer recommends an operational current density and working distance of 50 mA and 20 cm respectively, and although neither were specified, it is suspected that the recommended parameters were employed. Figure 2.18 shows the spectral irradiance of the Oriel solar simulator provided by the manufacturer and that obtained through in-house calibration when operating at 35 mA and sampled 25 cm from the source. The spectra exhibit excellent agreement however, the spectral line emissions of the xenon gas are more evident in the in house calibrated spectrum than the manufacturer data. The increased spectral broadening observed with the manufacturer data implies an operational current density greater than 35 mA, which concurs with the conjecture that the manufacturer data provided was sampled at the recommended but not specified 50 mA. In-house calibration of the Oriel when operating at current densities exceeding 35 mA produced UV spectral irradiance values in excess of

66.92 ± 3.02 Wm^{-2} and 3.19 ± 0.10 Wm^{-2} in the UVA and UVB respectively. These UV spectral irradiance values were obtained 25 cm from the source and would be expected to increase at shorter distances due to the inverse square law. However, the UV irradiance values computed from the manufacturer data were 51.75 Wm^{-2} and 0.25 Wm^{-2} in the UVA and UVB respectively. Thus the Oriel manufacturer data is conflicting, the increased spectral broadening suggests a current density exceeding 35 mA but the spectral intensities, the UVB in particular, suggest otherwise. Furthermore, irradiance spectra sampled 20 cm and 25 cm from the source when operating at 50 mA and 35 mA respectively would not be expected to exhibit the excellent agreement shown in figure 2.18. It is suspected that the manufacturer data was sampled using a UVB blocking filter. This provides a reasonable argument as to how a diminished UVB spectralirradiance (0.25 Wm^{-2}) is possible with a continuous emission spectrum indicative of a high current density. Furthermore, since ideal UVB blocking filters are not feasible, it is probable that the presence of a UVB blocking filter will also attenuate irradiance in the UVA region, thus producing an irradiance spectrum comparable to the in house calibrated data sampled at a lower current density and increased distance from the source.

These issues highlight the importance of thorough in-house calibration and how the problems in photobiology with regard to dosimetry lie not only with investigators but are also propagated by some manufacturers whose spectral data, if believed without investigation, could lead to erroneous conclusions arising from unaccounted spectral emissions and / or misleading irradiance spectra.

2.7 Lamp nature

In addition to the spectral distribution and irradiance of a light source, the manner in which the output of a given lamp is administered is yet another aspect of a light source that may have important implications when performing irradiations. Solar radiation is a continuous source, varying in intensity but not delivery, thus the delivery of each lamp was sampled to determine their behaviour and hence environmental relevance.

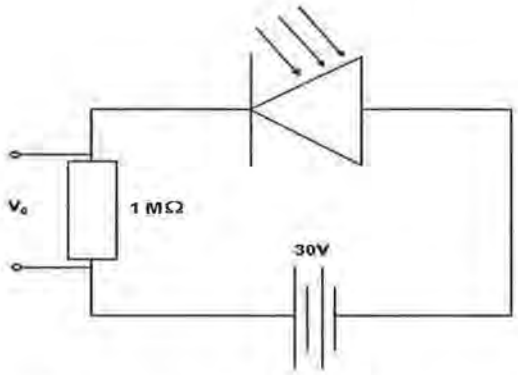

Figure 2.25 Circuit diagram of the reverse bias GaAsP photodiode in series with a 1 MΩ resistance and a 30 Volt power supply, where the behaviour of a source is measured in terms of voltage across the resistor.

All sources were sampled using a G5842 gallium arsenide phosphide (GaAsP) semiconductor photodiode (Hamamatsu photonics, Japan) with a frequency response of 3 kHz, a National Instruments DAQcard 700 and a LabVIEW™ programme designed to act as an oscilloscope so that output of a source could be viewed and recorded irrespective of its continuous or non continuous behaviour. The photodiode connected in reverse bias with a 30 Volt power supply (figure 2.25) was used to sample the outputs of the sources at a high rate of 100,000 samples per second to prevent aliasing. When connected in reverse

bias the resistance of the photodiode increases preventing the flow of current in the circuit. When irradiated, incident photons are absorbed by the photodiode material decreasing the resistance of the photodiode by increasing the number of charge carriers available to participate in current flow.

The GaAsP photodiode has a response over the UV region only as shown in figure 2.26, thus voltage measurements across the resistor (V_o) in the circuit shown in figure 2.25 are indicative of current flow through the photodiode due to incident UV photons.

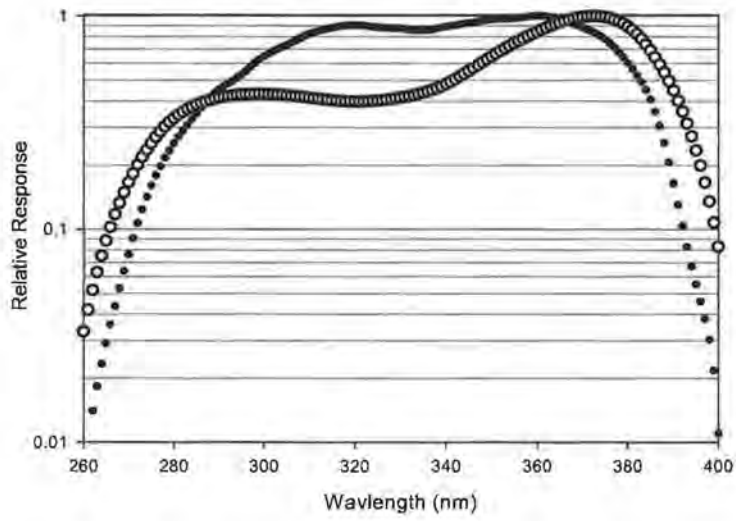

Figure 2.26 Relative response curves for the (○) Hamamatsu GaAsP photodiode G5842 and the (•) Solar Light™ UVA/B PMA2107 detector

Using a PMA2017 UVA/B radiometer (Solar Light, Pennsylvania, USA) with a response over a similar wavelength interval as the photodiode (figure 2.26), the photodiode was calibrated using solar radiation on clear cloudless sunny days mid summer in Dublin to determine the relationship between irradiance incident on the photodiode and its

corresponding voltage measurements. Figure 2.27 shows the data collected and the linear relationship between the irradiance and voltage as highlighted by the linear regression fit to the scatter.

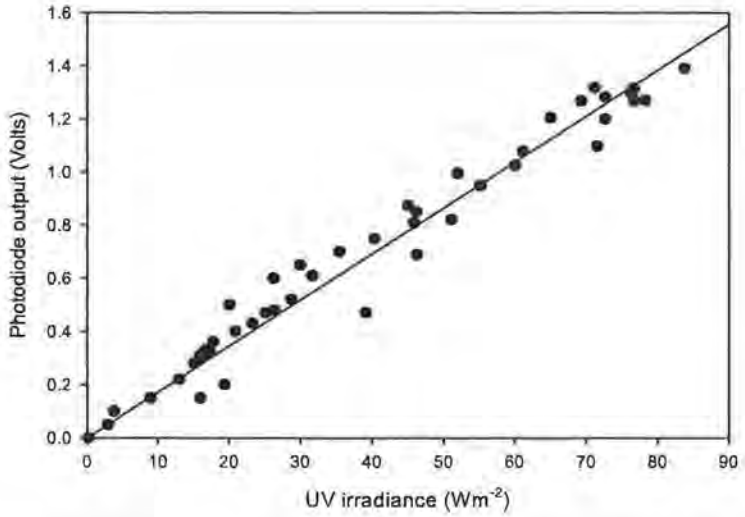

Figure 2.27 Linear relationship between voltage and solar UV irradiance on a Hamamatsu GaAsP photodiode G5842

The GaAsP photodiode was used to measure the output of each irradiator in terms of voltage. Figure 2.28 shows the nature of the solar simulators which reveals a significant difference between the behaviour of the solar simulators. The Oriel has a continuous output due its highly regulated power supply, similar to solar radiation, with a constant voltage output of 0.8 Volts as measured using the photodiode. The Q-sun is a pulsed source with a frequency of 100 Hz with a peak output of 25 Volts for each pulse. Pulsing high for approximately one tenth of its cycle, it would be expected that the Q-sun voltage output would be approximately 10 fold higher than that of the Oriel giving a voltage output of 8 Volts, however as demonstrated in figure 2.28, the Q-sun output is in excess of 30 times

that of the Oriel voltage output. The discrepancy between what would be expected and what is observed is the difference between an ideal and a real pulsed source. In the ideal, the source would pulse to 8 Volts for exactly 1 msec of its 10 msec cycle thus giving the same integral as would be expected from a constant source at 0.8 Volts over the full 10 msec as shown in figure 2.28.

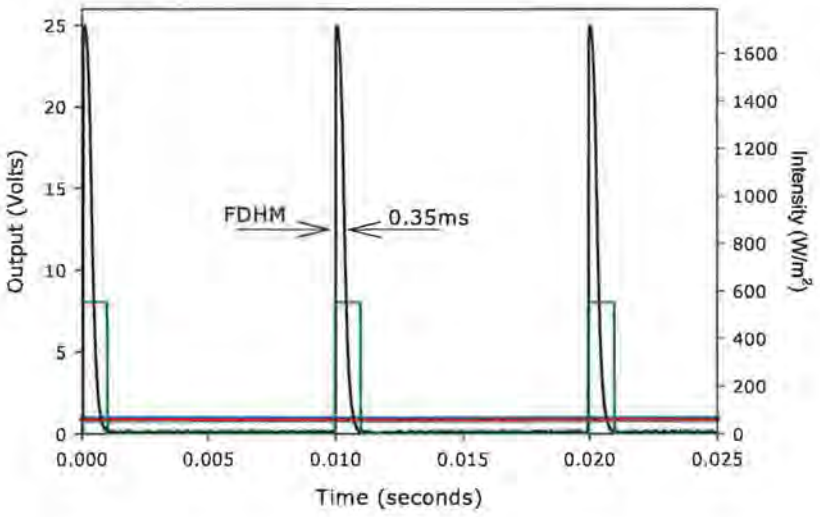

Figure 2.28 The pulsed and continuous nature of the Q-sun (•), the Oriel (•), the continuous equivalent of the Q-sun (•) and the ideal pulse (•)

However the Q-sun is not an ideal source and does not pulse to a maximum over the entire pulse duration of 1 msec thus a consideration of the full duration at half maximum (FDHM) is required. At FDHM the Q-sun pulse is approximately 1/29 of the entire 10 msec cycle (0.35 msec/10 msec). 1/29 of 25 Volts yields a continuous equivalent of 0.86 Volts for the Q-sun solar simulator, which correlates well with the continuous voltage output of 0.8 Volts for the Oriel solar simulator. The voltage difference between the Q-sun continuous equivalent and the Oriel is attributed to differences in their spectral distribution. Figure 2.29

plots the UV region for the Q-sun and Oriel solar simulators against the response curve for the GaAsP photodiode showing the Q-sun to possess an increased output compared to the Oriel over the UVA region where the response of the diode is at its maximum. Thus, it is reasonable to anticipate increased voltage output for the continuous equivalent of the Q-sun solar simulator.

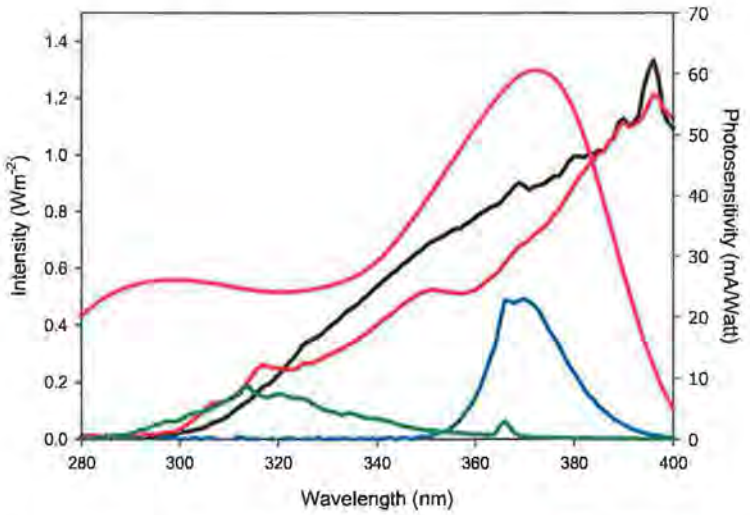

Figure 2.29 UV spectral distribution of the Q-sun (•), the Oriel (•) the UVA (•) and UVB (•) light sources and the response of the GaAsP photodiode (•)

While the GaAsP photodiode has a linear relationship between voltage and irradiance, the response of the photodiode is such that sources with different distribution spectra will incur different voltage outputs. The distribution of the Oriel and Q-sun are similar enough to allow an adjustment to determine an approximation on the irradiance delivered in a single Q-sun pulse. The simple adjustment employed was based on the fact that the Oriel UV irradiance of ~55 Wm^{-2} produced an output voltage of 0.8 Volts. From this a UV spectralirradiance in the region of 1600 Wm^{-2} is estimated to be delivered in a single pulse

from the Q-sun, an immense exposure over a brief period that may be more detrimental to biological samples than an identical exposure from a continuous source.

The UV irradiance values of the UVA and UVB lamps were found to be ~9.5 Wm^{-2} and ~6.4 Wm^{-2} respectively as shown in the previous section. With a UV irradiance of ~55 Wm^{-2}, the Oriel was found to yield a voltage output of just 0.8 Volts using the GaAsP photodiode. With spectral intensities approximately 6-9 fold smaller, it can be expected that both fluorescent lamps will yield considerably smaller voltage outputs. Furthermore, the spectral distribution of both fluorescent lamps plotted with the GaAsP photodiode response in figure 2.29 show that the maximal response of the photodiode coincides with the maximal output of the UVA fluorescent lamp. Thus, it is expected that the voltage output of the UVA lamp will exceed that of the UVB lamp, which is corroborated by the results presented in figure 2.30.

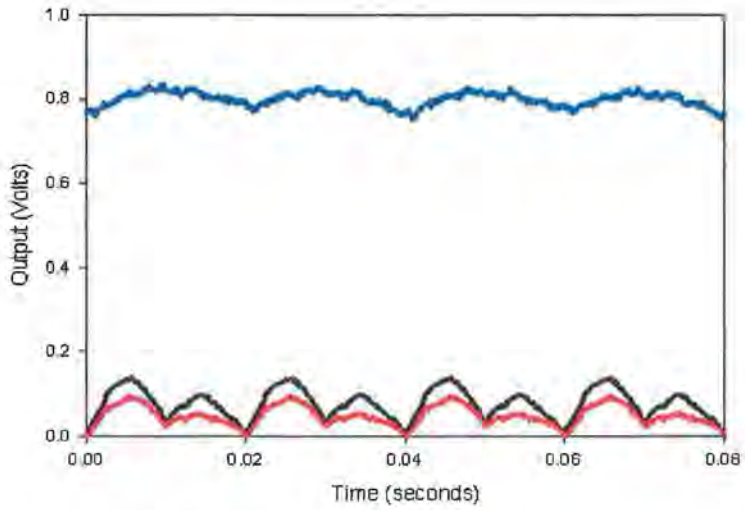

Figure 2.30 Non continuous nature of the UVA (•) and UVB (•) fluorescent lamps and the 'continuous' nature of the Oriel solar simulator (•)

2.8 Discussion of lamp nature

The behaviour of each irradiator was investigated to determine the manner in which each lamp delivered its irradiance and the degree of similarity each source exhibits with respect to the continuous delivery of solar radiation. The Oriel solar simulator was the only irradiator observed to have a continuous delivery analogous to solar radiation. Although the delivery of both UV lamps can be seen to be non continuous in figure 2.30, when compared to the Q-sun pulsed behaviour in figure 2.28, the signal variations are mild and are not believed to be a major concern with respect to the manner in which the output of the source is administered. Moreover, the output signals of the Oriel and UV fluorescent lamps appear to be altered by a 50 Hz external signal which is believed to arise from the rectified tri-phase mains voltage supply modulating the output signals of each source. However, it is the output delivery of the Q-sun solar simulator that elicits most concern. As shown in figure 2.28, the Q-sun is a non-continuous source that pulses high for approximately one tenth of its period, where each pulse is estimated to deliver a UV spectral intensity in the region of 1600 Wm^{-2}. The Bunsen Roscoe or reciprocity law states that all photochemical reactions are dependent on the total absorbed energy irrespective of the manner in which the dose is delivered (41, 42). However reservations exist regarding the applicability of this law to highly complex biological responses (43). Thus despite the Q-sun possessing an excellent representation of the solar radiation in terms of distribution and irradiance, the highly pulsed behaviour of the Q-sun incurs reservations regarding its environmental relevance which is of primary concern as the Q-sun was employed for all experimentation since the Oriel solar simulator was not procured until the latter end of the project.

2.9 Spectroscopic analysis of media and cell culturing vessels

Having characterised each irradiator in terms of spectral distribution, irradiance and output behaviour, consideration of possible attenuation processes incurred due to the vessels and media present during exposure must also be addressed to estimate the spectral irradiance incident on a sample.

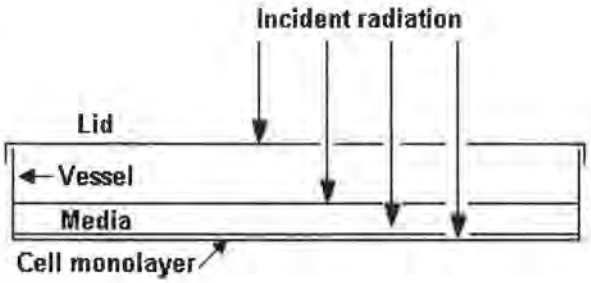

Figure 2.31 Radiation for a source must pass through the lid of the vessel, if present, and the exposure medium before interacting with cells adhered to the base of the vessel.

This study involves irradiating an immortalised keratinocyte cell line, HaCaT cells. Cell culture requires stringent aseptic conditions to ensure against contamination of cells while sterile cell culture medium provides the necessary nutrients for healthy growth. Cell cultures are maintained and passaged in sterile flasks but exposures are performed in either sterile multi-well plates or Petri dishes with removable lids in the presence of either cell culture medium or phosphate buffered saline (PBS). Radiation must therefore traverse through a lid, if present, and the exposure medium covering the cells before falling incident on the cells adhered to the base of the vessel (figure 2.31). Thus in order to assess the irradiance incident on cells being irradiated, the ability of the different vessels and media present during exposures to attenuate the irradiance of a given source must be addressed.

The transmission spectra of the media and plasticware used during sample irradiation were determined using a dual beam PerkinElmer Lambda 900 UV/Vis/NIR spectrometer. Figure 2.32 shows the transmission spectrum of a plastic lid from a Nunclon multi well plate, which can be seen to have relatively stable transmission in the IR and visible regions. However, the transmission can be seen to decrease in the UV, particularly the UVB region, which is the most energetic and biologically effective waveband in the solar spectrum. Losses in UVB irradiance levels can be expected to yield significant deviations from results generated with no UVB losses incurred.

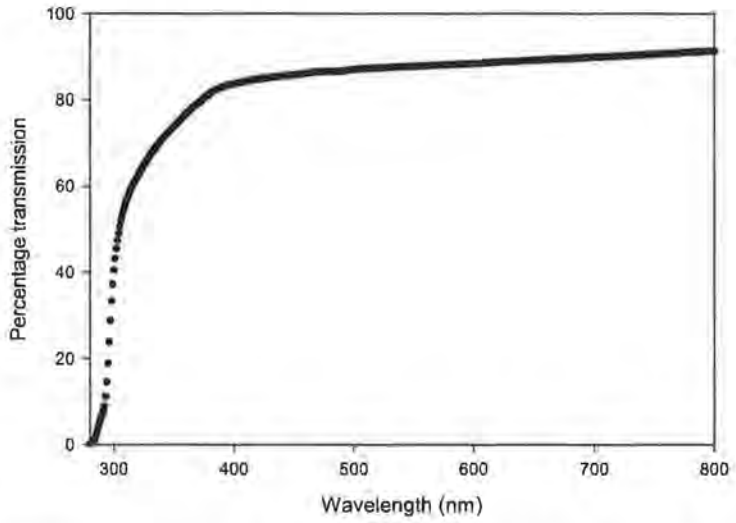

Figure 2.32 Transmission spectra of a Nunclon multi well dish plastic lid

The dimensions of both the UVA and UVB fluorescent lamps allowed irradiations to be carried out in a sterile laminar flow cabinet enabling exposures to be performed in the absence of lids, thus minimising attenuation of incident radiation. The physical dimensions of both solar simulators prevented housing in laminar flow cabinets. However there are

reports in the literature suggesting solar radiation possesses germicidal properties (44, 45). Thus, agar dishes were exposed to both solar simulators for 1 hour in order to determine the ability of the simulators to maintain a sterile environment (see appendix 1 for agar protocol). Agar dishes exposed to both solar simulators remained contamination free when incubated at 37°C for 7 days post exposure, the same time interval employed for the clonogenic assay. Thus with careful handling, all solar simulator exposures were also performed without lids and were found to be contamination free while eliminating plastic lid associated losses in radiant intensities.

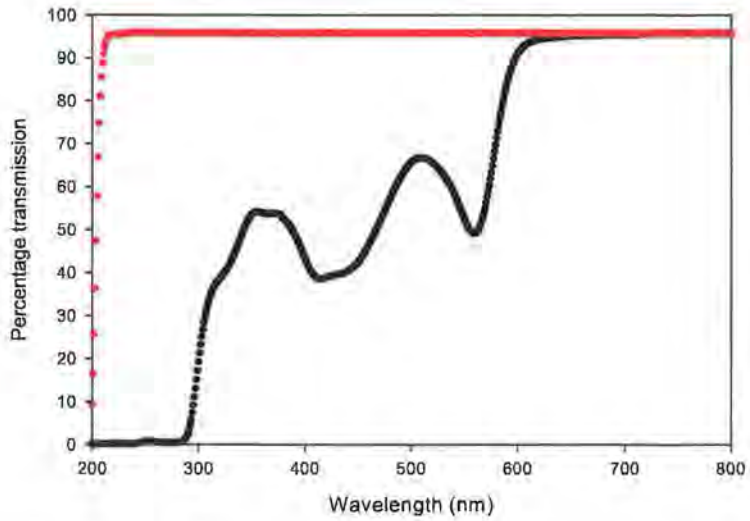

Figure 2.33 Transmission spectra of DMEM-F12 cell culture medium (•) and PBS (•)

The transmission spectra of DMEM-F12 cell culture medium (herein referred to as DMEM-F12) and PBS are shown in figure 2.33 where DMEM-F12 can be seen to absorb significant amounts of radiation below 600 nm while PBS has minimal losses in transmission right through to the UVC region. To determine the effect of transmission through PBS or DMEM-F12, the transmission spectra for both PBS and DMEM-F12 were

applied to calibrated spectral distribution (figure 2.23) for each irradiator by simple multiplication at each wavelength. Figures 2.34 and 2.35 illustrate the effect of PBS and DMEM-F12 respectively on the spectral irradiance of each source and table 2.7 lists the UV spectral intensities for each light source when transmitted or not transmitted through PBS and DMEM-F12.

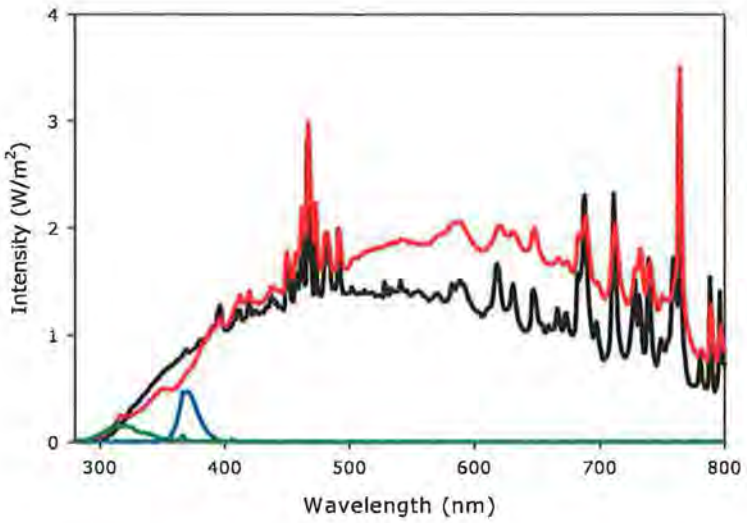

Figure 2.34 Calibrated spectra at the exposure level for (•) the Q-sun solar simulator (•) the Oriel solar simulator operating at 35 mA (•) the UVA lamp and (•) the UVB lamp transmitted through PBS.

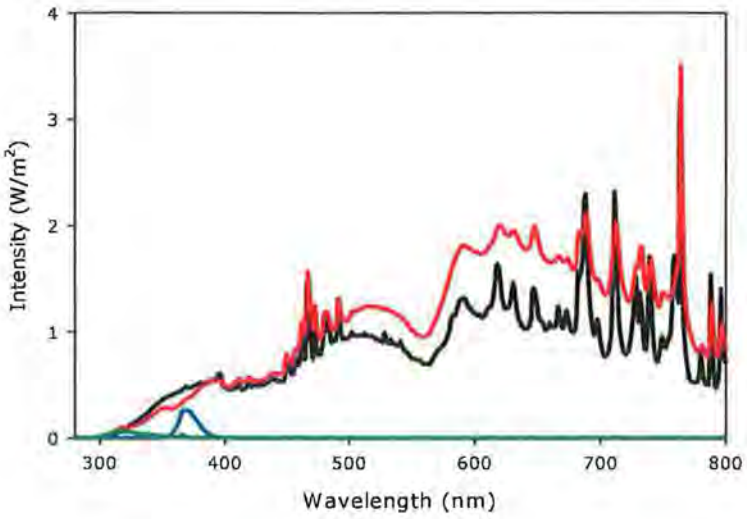

Figure 2.35 Calibrated spectra at the exposure level for (•) the Q-sun solar simulator (•) the Oriel solar simulator operating at 35 mA (•) the UVA lamp and (•) the UVB lamp transmitted through DMEM-F12.

Table 2.7 Variation in UV intensities for each light source when transmitted through PBS or DMEM-F12.

Light source	Media	UVA/B		UVA		UVB	
		(W/m^2)	% loss	(W/m^2)	% loss	(W/m^2)	% loss
Qsun	No media	63.63 W/m^2		62.30 W/m^2		1.33 W/m^2	
	PBS	60.84	- 4 %	59.57	- 4 %	1.27	- 5 %
	DMEM-F12	31.56	- 50 %	31.18	- 50 %	0.38	- 71 %
Oriel	No media	54.88 W/m^2		52.70 W/m^2		2.18 W/m^2	
	PBS	52.47	- 4 %	50.39	- 4 %	2.08	- 5 %
	DMEM-F12	26.86	- 51 %	26.21	- 50 %	0.65	- 70 %
UVA lamp	No media	9.50 W/m^2		9.49 W/m^2		0.01 W/m^2	
	PBS	9.09	- 4 %	9.08	- 4 %	0.01	- 0.00 %
	DMEM-F12	5.06	- 47 %	5.05	- 47 %	0.006	- 40 %
UVB lamp	No media	6.39 W/m^2		3.96 W/m^2		2.43 W/m^2	
	PBS	6.11	- 4 %	3.78	- 5 %	2.33	- 4 %
	DMEM-F12	2.41	- 62 %	1.75	- 56 %	0.66	- 73 %

2.10 Discussion of spectroscopic analysis

Radiation incident on a surface will undergo losses inirradiance due to reflective and transmittance processes, which are dependent on the angle of incidence and the material the radiation is incident upon. However, radiation incident perpendicular to a transmitting surface suffers minimal losses due to reflections at the surface and is transmitted into the material. When passing through the material, the intensity of the incident radiation (I_0) is attenuated (I) according to the Beer Lambert law shown in equation 2.2, where the absorbance (A) is dependent on the optical path length (l) traversed through the material and the concentration (c) of absorbing species of molar absorptivity (ε).

$$A = \varepsilon lc = -\log_{10}(I/ I_0) \qquad \textbf{Equation 2.4}$$

Thus, a dual beam spectrometer was employed to determine the loss in irradiance at each wavelength when radiation is transmitted through a cuvette of DMEM-F12 or PBS at right angles, using an optically matched cuvette containing water served as the reference. Spectroscopic analysis of the exposure media revealed immense differences in their transmission spectra, where PBS was found to have minimal losses in transmission compared to DMEM-F12 which yields significant losses inirradiance below 600 nm as was shown in figure 2.33.

Visually, transmission through PBS has virtually no effect on the spectral distribution of each source however computation of the UV irradiance values of the transmitted data show losses of 4-5 %, see table 2.7. These losses are suspected to be the result of Fresnel

reflections (R) at the different interfaces between media of different refractive indexes as illustrated by the schematic in figure 2.36.

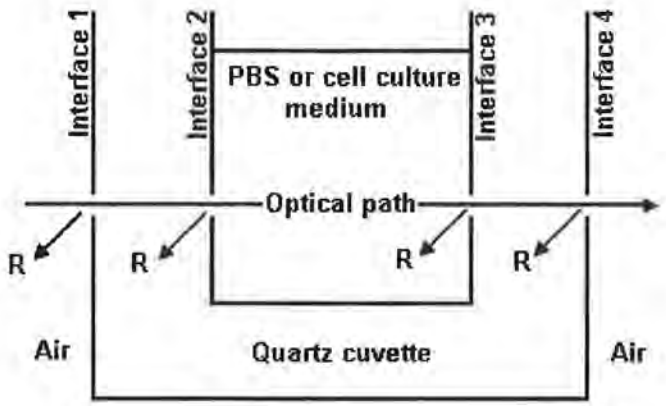

Figure 2.36 Schematic depicting the four interfaces (1 = air/quartz, 2 = quartz/media, 3 = media/quartz, and 4 = quartz/air) radiation traverses during spectroscopic analysis of PBS and DMEM-F12 and possible reflections (R) of the incident radiation if the surfaces are not optically perpendicular to the incident radiation.

Applying the transmittance spectrum of DMEM-F12 (figure 2.33) to the spectral irradiance of the irradiators revealed significant losses in irradiance when transmitted through DMEM-F12 (figure 2.35). The reduced spectral intensity experienced by each source in the UV region when transmitted though PBS or DMEM-F12 are listed in table 2.7 along with the percentage loss with respect to non transmitted spectral intensities. From table 2.7, DMEM-F12 can be seen to result in losses of up to 73 %, where the most significant losses were experienced in the UVB region of the spectra.

The results presented in this section indicate that the irradiance of an irradiator is attenuated when transmitted through DMEM-F12. Thus, cells irradiated in DMEM-F12 would receive a reduced dose compared to cells irradiated identically in PBS, which suggests that PBS exposures would have a far more detrimental effect on cell survival than DMEM-F12.

2.11 Temperature measurements

Environmental conditions are important for enzyme activity, where certain conditions favour the most active conformation of the apoenzyme, the protein moiety of a functional enzyme. Temperature is one such factor and as seen in figure 2.37, human enzymes work optimally at a temperature of 37°C (46) . Below this temperature, the kinetic energy of functional enzymes and their substrates decreases, decreasing both the frequency of collisions between molecules and the probability that the kinetic energy of the collision is sufficient to overcome the threshold energy required to initiate a reaction, thus slowing the activity of the enzyme. Increasing the temperature above 37°C causes a rapid decrease in human enzyme activity due to the increased thermal vibrations disrupting the intra molecular interactions, such as hydrogen bonding, resulting in protein denaturisation which is the loss of the protein's functional conformation (i.e. folding).

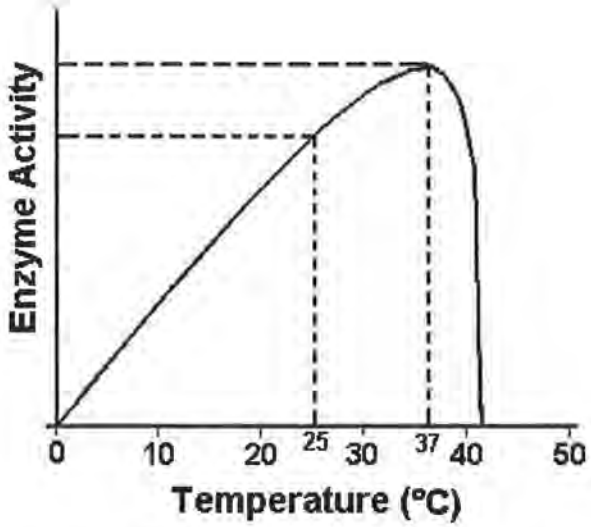

Figure 2.37 Effect of temperature on human enzyme activity, where 37°C is the optimum temperature for human enzyme activity (47)

Both the Q-sun and Oriel solar simulators have outputs in the IR region. IR radiation is primarily associated with heating effects, thus the temperature sensitivity of enzymatic activity outlined above necessitated an investigation into possible heating effects during irradiation.

The Q-sun possesses an enclosed chamber which claims a temperature controlled ambient air environment via a fan operated cooling system. The ability and reliability of the Q-sun to maintain a pre-set temperature setting of 30°C within its chamber was examined. A setting of 30°C for the Q-sun chamber was chosen to avoid overheating of the enclosed chamber and to allow for increased heat production with age since the manufacturer's manual states that "*as the lamps age, they will operate at a higher wattage and produce more heat*" (48). The Oriel solar simulator is not enclosed and thus temperature monitoring of the ambient air is not possible. However, temperature measurements of the exposure

media (DMEM-F12 and PBS) during irradiation with both the Q-sun and Oriel solar simulators were taken over a time period of 90 minutes in order to determine the heating effects, if any, that either of the simulators produces in the exposure media. All temperature measurements were carried out using a thermocouple thermometer (Fluke, model 16). Since neither of the fluorescent UV lamps employed have outputs in the infrared, neither lamp was investigated since UV radiation would have negligible heating effects compared to infrared emissions.

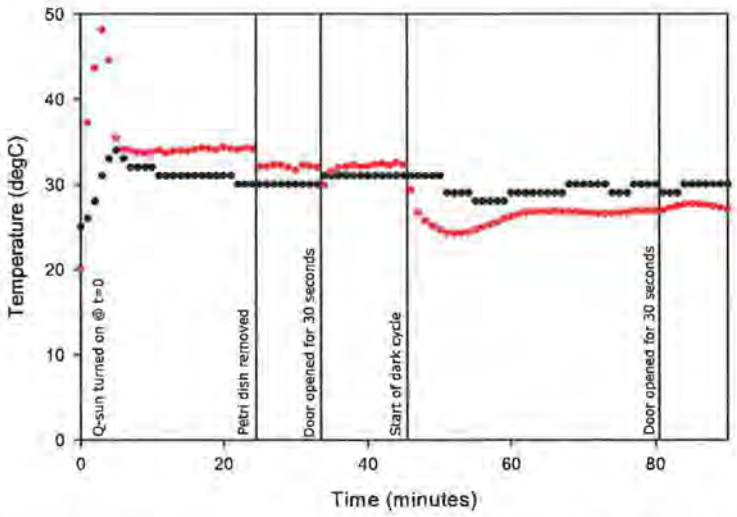

Figure 2.38 Ambient air temperature measurements within the Q-sun chamber as measured by (•) the Q-sun temperature sensor and (•) the thermocouple probe thermometer

The Q-sun has two operational modes, light and dark cycles i.e. lamp on and lamp off. Figure 2.38 shows temperature measurements of ambient air in the Q-sun chamber at the exposure level measured over a 90 minute interval to determine the effects, if any, of the initialisation process of the light cycle, commencement of the dark cycle and opening the door during both the light and dark cycles. The Q-sun ambient air temperature sensor

indicates that the temperature of the chamber increases slowly over the first 5 minutes once the light cycle has been initiated with a slight increase in temperature above the set temperature of 30°C before settling at 30±1°C within approximately 10 minutes. The thermocouple probe sensor describes a far more dramatic increase in temperature during the initialisation process. The thermocouple registered a chamber temperature of almost 50°C three minutes after ignition, the temperature then stabilised at 34°C after 6-7 minutes. The probe was situated in an empty Petri dish to determine if the enclosure formed by the Petri dish walls serves to maintain a higher temperature than would be observed in non enclosed areas of the chamber since this is where the cells and the exposure medium would be located during irradiation. The Petri dish was removed at 25 minutes which resulted in an immediate 2°C temperature drop in ambient air as measured using the thermocouple.

When irradiating samples, the chamber door is opened, the chamber sprayed with alcohol, the door closed and reopened to insert the cells for irradiation. This process takes up to a maximum of 30 seconds thus the effect of opening the chamber door for 30 seconds on ambient air temperature was evaluated. The door was opened for 30 seconds, closed and the temperature noted. The thermocouple probe registered an immediate drop in ambient air temperature which recovered and stabilised within 2-3 minutes. The Q-sun sensor measured an increase in ambient air temperature although it was still lower than that measured by the thermocouple. On initiation of the dark cycle, the thermocouple measured a sizeable drop in temperature followed by a slight recovery to 27°C where the temperature stabilised and opening the door had no effect on the ambient air temperature measurement. The Q-sun temperature sensor did not register a temperature drop for the first 5 minutes when the dark cycle commenced, after which it observed only a 3°C drop and increased variability.

Figure 2.39 shows the temperature measurements of cell culture medium DMEM-F12 and PBS during the light and dark cycle of the Q-sun solar simulator. Both the PBS and DMEM-F12 were pre warmed to 37°C, the Q-sun was set at 30°C and allowed to stabilise for 20-30 minutes. The media were transported from the incubator to the Q-sun in vials with closed lids, 6 ml of the media under test was pipetted into one well of a 6 well dish to submerge the thermocouple temperature probe. Once submerged, the initial temperature of the media was noted and the timer started. The temperature of both DMEM-F12 and PBS can be seen to decrease at first before stabilising at a temperature of approximately 25°C after about 10 minutes for both media. The temperature of both media drop quite significantly once the dark cycle is commenced, after which the rate of change in temperature decrease slows but does not stabilise over a time interval of 40 minutes. Opening the door during either the light or dark cycle had no measurable effect on the temperature of the media.

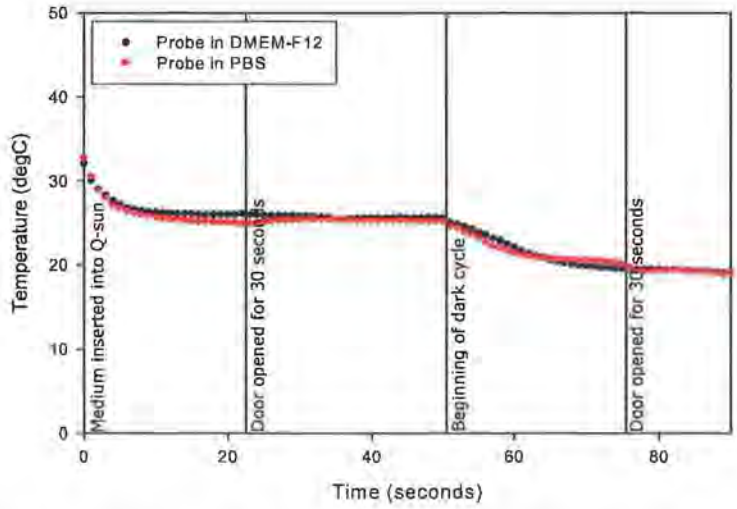

Figure 2.39 Vehicle temperature measurements during the light and dark cycles of the Q-sun solar simulator as measured by the thermocouple thermometer probe (•) in DMEM-F12 and (•) in PBS.

The Oriel solar simulator does not possess an enclosed chamber to perform exposures thus no temperature control is available with this simulator, however an initialisation time of 15 minutes for the Oriel bulb is employed as recommended by the manufacturer to allow the bulb to stabilise after ignition. Thus the Oriel was set at 35 mA, ignited and allowed to stabilise for 15 minutes. The temperature of DMEM-F12 and PBS located at the working distance of 25 cm from the source was monitored to determine any possible heating effects due to the exposure of media during irradiation with the Oriel solar simulator. Again both media were pre warmed to 37°C and transported to the Oriel in enclosed vials. The lids were removed and either 6 ml DMEM-F12 or PBS pipetted onto the thermocouple in order to submerge the probe. The temperature was noted at zero minutes immediately before exposure. Figure 2.40 shows an initial decrease in the temperature of both media which stabilised within 15 minutes, maintaining temperatures of approximately 25°C and 26°C for PBS and DMEM-F12 respectively.

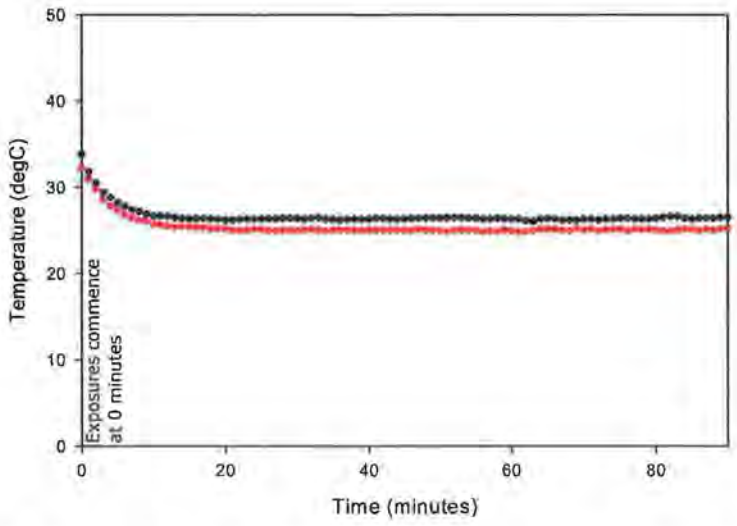

Figure 2.40 Cell culture medium (•) and PBS (•) temperature measurements during Oriel solar simulator exposures

2.12 Discussion of temperature measurements

The presence of infrared radiation in the spectra of both solar simulators in addition to potential age-related increases in bulb heat production required an investigation into possible temperature effects elicited during irradiation. The Q-sun solar simulator was of particular concern since samples are irradiated in an enclosed chamber. Upon ignition, the temperature of the chamber was found to reach almost 50°C using the thermocouple thermometer and didn't stabilise for approximately 6-7 minutes where no such temperature increase was indicated by the Q-sun temperature sensor. After the initialisation period, it was found that the Q-sun chamber is capable of maintaining a relatively stable ambient air temperature setting. However the temperature sensor employed by the Q-sun was found to be insensitive and slow to respond as highlighted by the rapid and sensitive response of the thermocouple thermometer. Based on the results obtained using the thermocouple, a period of 10-15 minutes was allowed between ignition and irradiation to avoid exposure of cells to elevated temperatures which may have detrimental effects on enzyme activity and possibly confound results.

A temperature setting of 30°C was chosen primarily to avoid detrimental effects incurred to cells due to possible overheating as was observed by Boukamp et al who reported increased tumorigenic progression in HaCaT cells maintained at 40°C (49). A reduced temperature setting also helped to minimise the rates of surface evaporation in order to avoid significant loss of exposure media depth during irradiation. Clonogenic exposures were carried out in 3ml of DMEM-F12 or PBS in 6-well multi well dishes. For 3ml of fluid, well dimensions

yield a depth of approximately 0.78 cm and a surface area of approximately 9.6 cm^2 directly exposed by an irradiator. According to the Beer-Lambert law ($A=\varepsilon cl$), shown in equation 2.2, absorbance (A) is directly proportional to the concentration (c) and the path length (l). If significant amounts of evaporation were incurred during exposures, the depth of the exposure media and hence the optical path length (l) through the fluid would decrease which in turn would affect the concentration (c) of the exposure media making inter-comparison between different exposure times difficult. However no significant losses due to evaporation were observed.

Another potential problem with regard to temperature effects is the excess production of heat as a bulb ages. As mentioned previously, the Q-sun manufacturer states that ageing bulbs will produce more heat due to increased wattage. The Q-sun is a xenon long arc lamp whose spectral emission is dependent on the current flow between the electrodes. Power (P, Watt) is the flow of current for a given potential difference ($P=IV$), thus an increase in power will correspond to an increase in the current density flowing between the electrodes of the bulb since the potential difference maintained between the electrodes is set by capacitors. In turn, alterations in the heat output may be indicative of spectral changes in the distribution of the lamp since the emission spectrum of the Q-sun is modified by the current density. However, no discernable changes in the spectral distribution of the bulb were detected with age which were only used for 1000 operational hours as recommended by the manufacturer.

Of particular interest are the possible heating effects of the exposure media when irradiated with either solar simulator since it is the exposure medium that is in direct contact with the cells during exposure and hence any temperature increases experienced by the media would be conducted to the cells. Two studies published by Aragane et al (50) and Kabsch and Alonso (51) both observed reduced rates of apoptosis in HaCaT cells in their experiments performed at 10°C and 22°C as measured by the expression of CD95 clustering and Caspase-3 cleaved substrate PARP respectively. Although the rates of apoptosis in both studies were reduced neither were completely inhibited, which considering the temperature dependent enzyme activity curve for human cells shown in figure 2.39 is unsurprising since sub optimal temperatures of 10°C and 22°C will impede but not halt enzyme activity.

Thermocouple temperature measurements of both PBS and DMEM-F12 have shown that neither solar simulator heats the exposure media, in fact the opposite holds true. The temperature of the exposed media was found to decrease from 37°C to approximately 25-26°C. Ideally a temperature of 37°C would be maintained, however, as shown in figure 2.39, a reduction of just ~ 20 % in enzyme activity would be expected at 25°C. Compared to the detrimental denaturing effects at elevated temperatures, this was considered a tolerable loss in activity.

2.13 Conclusions

The objective of this chapter was to characterise each irradiator prior to biological experimentation in order to determine their spectral distribution, spectral irradiance and behaviour and thus assess the biological relevance of each source.

It has been shown that the spectral irradiance values computed for each irradiator are environmentally feasible at the terrestrial level when compared to the highly variable solar radiation radiant intensities possible at different latitudes around the globe. However, it is the spectral distribution of the irradiators, obtained through spectroradiometry, that support or oppose the environmental relevance of a lamp. Both fluorescent UV lamps have been shown to possess distribution spectra that do not replicate solar radiation. The UVA lamp has a Gaussian distribution centred on 365 nm whose irradiance is possible at high latitudes during winter months and thus would not be expected to induce detrimental photo biological effects. The UVB lamp when plotted alongside the spectral distribution for both solar radiation and the solar simulators appears to give an excellent representation of UVB as implied by the UVB spectral irradiance of the lamp. However on closer inspection, the UVB lamp can be seen can be seen to have an output at wavelengths below 295 nm, the lowest terrestrial wavelength, while the spectral distribution of both solar simulators have been shown to give excellent approximations on the spectral distribution of solar radiation.

Analysis of the exposure media have shown both to maintain temperatures of approximately 25°C which may impede enzyme activity but will not result in temperature

related damage possible at elevated temperatures. Spectroscopic analysis of the media revealed DMEM-F12 to be highly absorbing while PBS is highly transmitting, suggesting that PBS exposures would be far more detrimental than DMEM-F12 exposures. However, it is the pulsed behaviour of the Q-sun solar simulator that incurs most concerns, since approximations regarding the spectral irradiance administered per pulse shows the UV irradiance to be in excess of 1600 Wm^{-2} which irrespective of exposure medium employed is a massive insult. Based on the results presented in this chapter, the abilities of each irradiator to induce cell death in both DMEM-F12 and PBS are examined in chapter 3.

2.14 References

(1) R. P. Gallagher & T. K. Lee (2006) Adverse effects of ultraviolet radiation: A brief review *Progress in Biophysics and Molecular Biology* **92,** 119-131.

(2) J. Reichrath (2006) The challenge resulting from positive and negative effects of sunlight: How much solar uv exposure is appropriate to balance between risks of vitamin d deficiency and skin cancer? *Progress in Biophysics and Molecular Biology* **92,** 9-16.

(3) Y. Matsumura & H. N. Ananthaswamy (2004) Toxic effects of ultraviolet radiation on the skin *Toxicol Appl Pharmacol* **195,** 298-308.

(4) D. Goukassian, F. Gad, M. Yaar, M. S. Eller, U. S. Nehal & B. A. Gilchrest (2000) Mechanisms and implications of the age-associated decrease in DNA repair capacity *Faseb J* **14,** 1325-34.

(5) F. R. de Gruijl, H. J. Sterenborg, P. D. Forbes, R. E. Davies, C. Cole, G. Kelfkens, H. van Weelden, H. Slaper & J. C. van der Leun (1993) Wavelength dependence of skin cancer induction by ultraviolet irradiation of albino hairless mice *Cancer Res* **53,** 53-60.

(6) B. L. Diffey (2002) Sources and measurement of ultraviolet radiation *Methods* **28,** 4-13.

(7) N. P. Lavery (2007) Mathematical framework for predicting solar thermal build-up of spectrally selective coatings at the earth's surface *Applied Mathematical Modelling* **31,** 1635-1651.

(8) C. Frohlich & C. Wehrli (1985) Extraterrestrial solar spectrum

(9) S. Darula, R. Kittler & C. A. Gueymard (2005) Reference luminous solar constant and solar luminance for illuminance calculations *Solar Energy* **79,** 559-565.

(10) C. A. Gueymard (2006) Reference solar spectra: Their evolution, standardization issues, and comparison to recent measurements *Advances in Space Research* **37,** 323-340.

(11) M. A. Case, Y. A. Owusu, H. Chapman, T. Dargan & P. Ruscher (2008) On the matter of proposed new low-latitude solar reference spectra *Renewable Energy* **33,** 2645-2652.

(12) C. A. Gueymard (2001) Parameterized transmittance model for direct beam and circumsolar spectral irradiance *Solar Energy* **71,** 325-346.

(13) R. E. Bird & C. Riordan (1986) Simple solar spectral model for direct and diffuse irradiance on horizontal and tilted planes at the earth's surface for cloudless atmospheres *Journal of Applied Meteorology* **25,** 87-97.

(14) Globe (2002) Calculating relative air mass http://www.globe.gov/sda/tg/airmass.pdf 13 October 2009.

(15) S. X. Chu & L. H. Liu (2009) Analysis of terrestrial solar radiation exergy *Solar Energy* **In Press, Corrected Proof**.

(16) R. S. W. Ireland (1996) The angular distribution of solar ultraviolet, visible and near-infrared radiation from cloudless skies *Photochemistry and Photobiology* **63,** 483-486.

(17) C. F. Garland, F. C. Garland & E. D. Gorham (2003) Epidemiologic evidence for different roles of ultraviolet a and b radiation in melanoma mortality rates *Annals of Epidemiology* **13,** 395-404.

(18) A. Heikkilä, P. Kärhä, A. Tanskanen, M. Kaunismaa, T. Koskela, J. Kaurola, T. Ture & S. Syrjälä (2009) Characterizing a uv chamber with mercury lamps for assessment of comparability to natural uv conditions *Polymer Testing* **28,** 57-65.

(19) F. P. Gasparro & D. B. Brown (2000) Photobiology 102: Uv sources and dosimetry - the proper use and measurement of "Photons as a reagent" *Journal of Investigative Dermatology* **114,** 613-5.

(20) D. B. Brown, A. E. Peritz, D. L. Mitchell, S. Chiarello, J. Uitto & F. P. Gasparro (2000) Common fluorescent sunlamps are an inappropriate substitute for sunlight *Photochemistry and Photobiology* **72,** 340-4.

(21) A. R. Webb (2003) Uv instrumentation for field and forest research *Agricultural and Forest Meteorology* **120,** 27-38.

(22) CIE, B. L. Diffey, C. T. Jansen, F. Urbach & H. C. Wulf (2007) Erythema reference action spectrum and standard erythema dose *ISO/CIE 17166:1999*, 1-14.

(23) H. Oliver & H. Moseley (2002) The use of diode array spectroradiometers for dosimetry in phototherapy *Physics in Medicine and Biology* **47,** 4411.

(24) C. M. H. Driscoll (1997) Dosimetry methods for uv radiation *Radiat Prot Dosimetry* **72,** 217-222.

(25) Ocean-Optics (2008) Cosine-corrected irradiance probes http://www.oceanoptics.com/Products/irradianceprobes.asp 12 October 2009.

(26) J. E. Walsh, K. Y. Kavanagh, S. Fennell, J. Murphy & M. Harmey (2000) Fibre-optic micro-spectrometers for biomedical sensing *Transactions of the Institute of Measurement and Control* **22,** 355-369.

(27) H. D. Young & R. A. Freedman (1996) *University physics* (Addison-Wesley, Reading, Mass.).

(28) Kawanaka, Ogata, Kubodera, Sasaki & Kurosawa (1997) Improved output characteristics of a vacuum ultraviolet xenon gas jet discharge lamp with a magnetic field *Applied Physics B: Lasers and Optics* **65,** 609-612.

(29) U. Hällsten & O. Solin (2002) A method for the recording of density reduction in proton beam irradiated high pressure xenon *Nuclear Instruments and Methods in Physics Research Section B: Beam Interactions with Materials and Atoms* **187,** 275-280.

(30) R. K. H. Gebel, H. R. Mestwerdt & R. R. Hayslett (1971) Near infrared sensitized photocathodes and film sensitivities for typical xenon-lamp radiation and related subjects *Ohio Journal of Science* **71,** 343-357.

(31) F. Ghaleb, W. Benstâali & A. Belasri (2008) Calculation of breakdown voltage in plasma display panels *Materials Science and Engineering: C* **28,** 791-794.

(32) Oriel-Newport (2003) Simulation of solar irradiation http://www.newport.com/Simulation-of-Solar-Irradiation/411986/1033/catalog.aspx 13th October 2009.

(33) Oriel-Newport (2007) Sun 2000 solar simulators manual data sheet.

(34) UVP-products (2009) Spectral chart http://www.uvp.com/pdf/365wf.pdf 13th October 2009.

(35) UVitec (2009) Personal communication via email 18th Feburary 2009

(36) Time-and-Date (2009) Sunrise and sunset calculator http://www.timeanddate.com/ 19 November 2009.

(37) E. C. Weatherhead & A. R. Webb (1997) International response to the challenge of measuring solar ultra-violet radiation *Radiat Prot Dosimetry* **72,** 223-229.

(38) A. R. Webb (1997) Changes in stratospheric ozone concentrations and solar uv levels *Radiat Prot Dosimetry* **72,** 207-216.

(39) A. F. McKinlay & B. L. Diffey (1987) Reference action spectrum for ultraviolet induced erythema in human skin *CIE Journal* **6,** Pages 17-22

(40) R. B. Setlow (1974) The wavelengths in sunlight effective in producing skin cancer: A theoretical analysis *Proceedings of the National academy of Sciences of the United States of America* **71,** 3363-6.

(41) R. Bunsen & H. Roscoe (1859) Photochemische untersuchungen. *Ann Phys.* **108,** 193.

(42) J. W. Martin, J. W. Chin & T. Nguyen (2003) Reciprocity law experiments in polymeric photodegradation: A critical review *Progress in Organic Coatings* **47,** 292-311.

(43) A. Schindl, B. Rosado-Schlosser & F. Trautinger (2001) Reciprocity regulation in photobiology. An overview *Hautarzt* **52,** 779-85.

(44) D. H. Sliney & S. Wengraitis (2006) Is a differentiated advice by season and region necessary? *Prog Biophys Mol Biol* **92,** 150-60.

(45) Y. Tong & B. Lighthart (1997) Solar radiation has a lethal effect on natural populations of culturable outdoor atmospheric bacteria *Atmospheric Environment* **31,** 897-900.

(46) Campbell (1996) *Biology* (The Benjamin/Cummings Publishing Company, California).

(47) B. Brochez (2006) Enzymes http://www.ischool.zm/bio/Ch.%203%20Enzymes.htm 13 October 2009.

(48) Q-Panel (2003) Weathering and light stability Manual.

(49) P. Boukamp, S. Popp, K. Bleuel, E. Tomakidi, A. Burkle & N. E. Fusenig (1999) Tumorigenic conversion of immortal human skin keratinocytes (hacat) by elevated temperature *Oncogene* **18,** 5638-45.

(50) Y. Aragane, D. Kulms, D. Metze, G. Wilkes, B. Poppelmann, T. A. Luger & T. Schwarz (1998) Ultraviolet light induces apoptosis via direct activation of cd95 (fas/apo-1) independently of its ligand cd95l *Journal of Cell Biology* **140,** 171-82.

(51) K. Kabsch & A. Alonso (2002) The human papillomavirus type 16 (hpv-16) e5 protein sensitizes human keratinocytes to apoptosis induced by osmotic stress *Oncogene* **21,** 947-53.

Chapter 3 Spectral dependant cell survival

3.1 Introduction

A plethora of studies exists in the literature looking at the biological effects of UV radiation where the type of source employed in such studies can vary immensely in spectral distribution and irradiance (1, 2). The majority of the work to date that has provided vital information regarding the ability of UV radiation to elicit both detrimental (erythma, mutagenesis, immunosuppression, oxidative stress and skin cancer initiation (3-9)) and positive (vitamin D synthesis, skin disorder treatment (10, 11)) effects have been determined through the use of fluorescent sunlamps. The information obtained from such irradiators has provided the foundations for solar radiation investigations. However, as the necessity for more detailed information regarding radiation-induced impairment of cellular function grows, attention must turn to the instrumentation employed and their relevance to the study at hand. Wavelength and energy are inversely proportional where the increasing efficacy of radiation to elicit damage with decreasing wavelength is demonstrated by the relative spectral effectiveness of radiation (12) and biological action spectra (13, 14). This combined with the ability of a source to administer environmentally relevant emissions as would be experienced at the terrestrial level stresses the importance of spectral distribution and irradiance of a given source when attempting to elucidate the mechanisms involved in skin carcinogenesis.

In the previous chapter, four artificial irradiators (Q-sun, Oriel, UVA lamp and UVB lamp) were thoroughly calibrated using spectroradiometry and their output behaviour was characterised. While it was found that the irradiators varied significantly in terms of spectral irradiance, it was the non-continuous behaviour of the Q-sun solar simulator that evoked most concern since the Q-sun was found to administer its output in a pulsed manner delivering an exaggerated UV spectral irradiance of approximately 1600 Wm^{-2} per pulse.

The objective of this chapter is to perform radiobiological experiments on a human keratinocyte cell line, HaCaT cells, to determine the ability of each irradiator to elicit cell death as measured using the clonogenic assay. However, particular emphasis is placed on the ability of the non-continuous Q-sun compared to the continuous Oriel in order to determine if the Q-sun is in fact environmentally relevant despite its excellent approximation of solar radiation in terms of spectral distribution.

3.2 Methods

3.2.1 Cell culturing procedures

A human keratinocyte cell line, HaCaT cells, originally obtained as a kind gift from Dr. Petra Boukamp, DKFZ, Germany, was used for this study. HaCaT cells are immortal but non-malignant with a doubling time of 21 hours (15) and mutations in both p53 alleles (16). HaCaT cells were cultured in Dulbecco's MEM-F12 (1:1) medium (DMEM-F12) (Cambrex, U.K.) containing 10% fetal calf serum (Gibco, Irvine, U.K.), 1% penicillin-streptomycin solution 1000IU (Gibco) and 1 μg/ml hydrocortisone (Sigma, Dorset, U.K.). Cells were incubated under humid conditions at 37°C, with 5% CO_2 in air. Subculture was routinely performed when cells were 80-90% confluent, using a 1:1 solution of 0.2% trypsin and 1 mM versene at 37°C. Cells from flasks with sub-confluent cultures were removed using the 1:1 trypsin/versene solution. Once the cells detached, the trypsin/versene solution was neutralised using DMEM-F12. After centrifugation, the supernatant was decanted off and the pellet re-suspended in fresh DMEM-F12. Single cell suspensions were obtained using a pipette or vortex and cell counts were determined using a haemocytometer (see appendix 1).

3.2.2 Clonogenic Assay

Clonogenic expansion of single cells was determined using the method devised by Puck and Marcus (17) which allows survival of single cells to be quantified post exposure to

some toxic event. Survival is determined by the ability of single cells to form macroscopic colonies distinguishable from one another (figure 3.1) after a predetermined incubation period for a given cell line, where a colony is said to be a group of approximately 50 or more cells which should arise from a single cell.

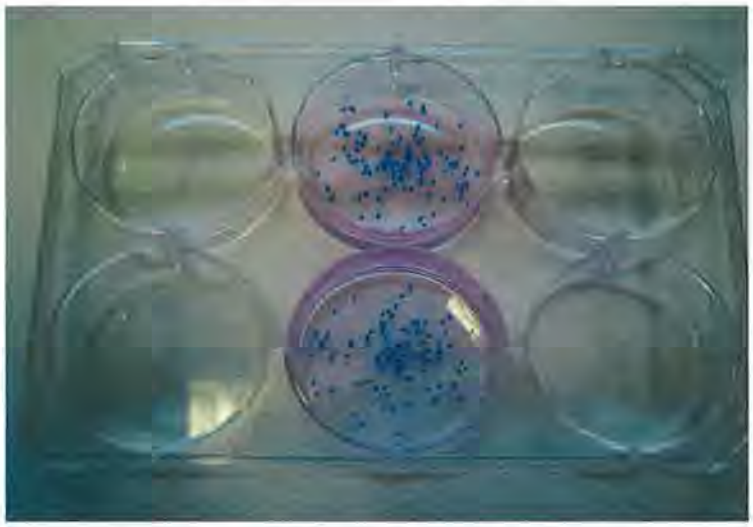

Figure 3.1 Colonies stained using carbol fuchsin in a 6 well plate (Nunc). As the colonies were counted they were marked with a blue dot to ensure the colony was counted once only.

The HaCaT cell line has a plating efficiency of 27.2 ± 3.6% determined using equation 3.1. In order to obtain a reasonable number of colonies, cells were seeded at 400 cells in 3 ml DMEM-F12 per well in Nunclon 6 well plates (figure 3.1) and incubated (conditions as above) overnight for 16 hours prior to irradiation. The extended incubation period between seeding and irradiation was employed for all experiments since exposures that required cell washes resulted in reduced and irregular control colony numbers compared to non-washed secondary controls, termed incubator controls, when insufficient time for attachment was

allowed. However, dishes were checked prior to irradiation to confirm that the plated cells were still predominantly single cells.

$$\text{Plating Efficiency (PE)} = \frac{\text{Number of colonies obtained} * 100}{\text{Number of cells seeded}} \qquad \text{Equation 3.1}$$

With a doubling time of 21 hours, a 7 day incubation period is sufficient for HaCaT cells to form macroscopic colonies. Thus post exposure, cells were incubated for 7 days, after which cells were stained using a 20% carbol fuchsin solution for 5 minutes and scored.

3.2.3 Cell exposures

Cells were directly irradiated in either 3 ml DMEM-F12 or 3 ml PBS without lids using the Q-sun, the Oriel, the UVA or UVB lamp. Cells exposed in DMEM-F12 were removed from the incubator, exposed and returned to the incubator immediately post exposure with no medium change.

For PBS exposures, the DMEM-F12 cell culture medium was harvested from cells, filtered and stored in the incubator during irradiation. The cells were washed once with 1ml PBS and the wash discarded, 3 ml fresh PBS was added and the cells exposed. Post exposure, the exposed PBS was discarded and cells received 3 ml per well of the stored DMEM-F12 immediately post exposure and returned to the incubator. All samples were re-incubated for 7 days post exposure prior to clonogenic staining.

3.2.4 Statistics

The type and number of factors contributing to a response under investigation dictate the statistical model required. In all analyses performed throughout this study, there are 3-4 treatment variables (exposure medium (M), exposure duration (t), replicate (E) and Irradiator employed (I)) contributing to the effect under investigation (cellular response (Y)). Thus, the analysis required is a factorial statistical analyses of variance (ANOVA), which assumes the data under analysis are normally distributed, independent and possess equal variance (homoscedasticity) (18). Transforming data using logarithms is a method of reducing possible violations of the above assumptions by making the distribution more normal, eliminating multiplicative effects (dependence) and reducing the variance within data populations to acceptable limits (19). Thus, the response data (Y) was Log transformed to ensure the model complies with the requirements of ANOVA as shown in equation 3.4. Once the raw data was Log transformed, ANOVA was performed on the data from which the Least Square Means (LSM) ± 95% confidence interval (95CI) of at least 3 independent replicates (unless otherwise stated) and pair-wise data using the Bonferroni adjustment were computed. All analyses were done using statistical software package SAS 9.1 and SAS enterprise guide 3.0. Significance was taken at a level of $p \leq 0.05$.

$$Y = M \times t \times E \times I \qquad \text{Equation 3.2}$$

$$Log(Y) = Log(M \times t \times E \times I) \qquad \text{Equation 3.3}$$

$$Log(Y) = Log(M) + Log(t) + Log(E) + Log(I) \qquad \text{Equation 3.4}$$

3.3 Results and discussion

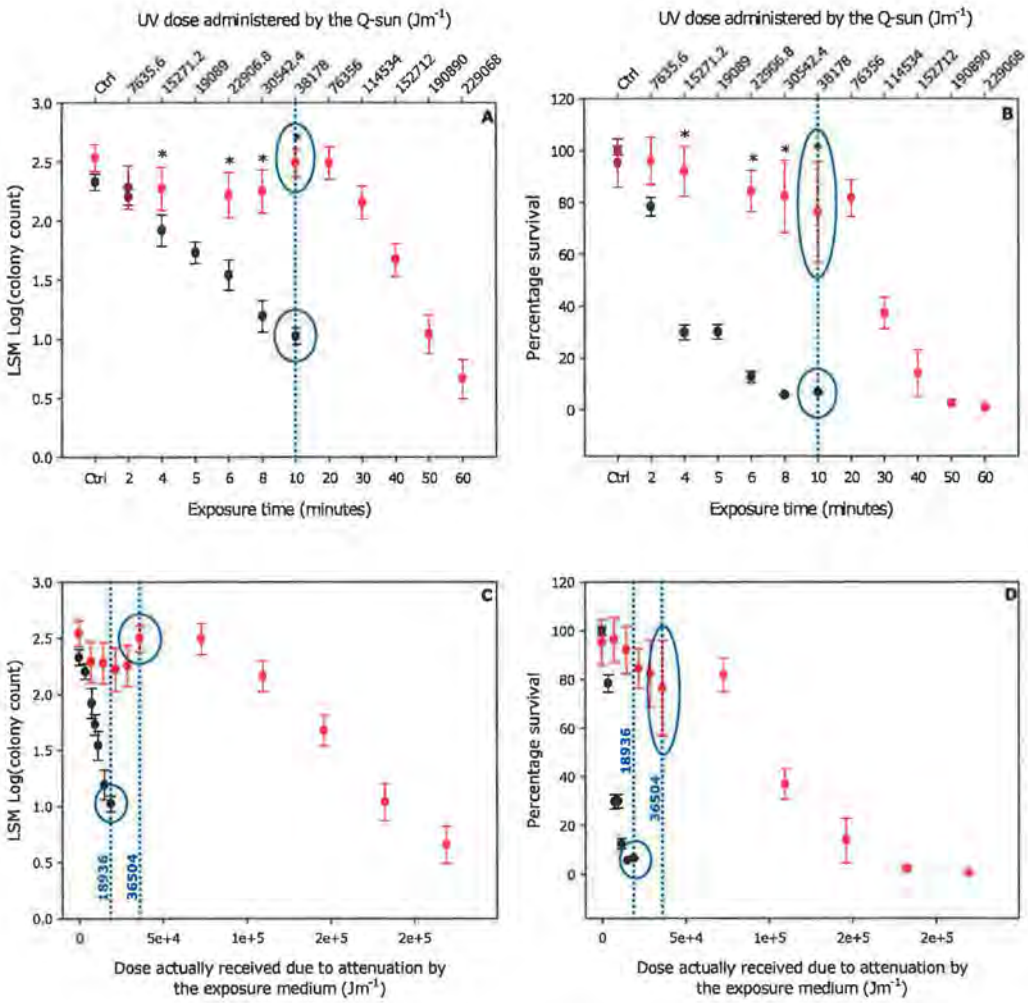

Figure 3.2 Direct exposure of HaCaT cells in DMEM-F12 (•) and PBS (•) using the Q-sun solar simulator with an irradiance of ~64 Wm^{-2} ; data are presented as the LSM ± 95CI in (A) and (C) or normalised to their respective controls ± the standard deviation in (B) and (D). (A) and (B) show the data plotted against the exposure time in minutes and the corresponding UV dose administered by the Q-sun for a given exposure duration. (C) and (D) account for the attenuating effects of the exposure medium and show the survival data plotted against the actual dose received. The 10 minute exposures are highlighted by the blue circles and dotted lines. ∗ represents significant difference between different exposure media for a given exposure time.

Once fully characterised, each irradiator was employed to perform radiobiological experiments, as described in the methods section above. The survival of HaCaT cells irradiated in either DMEM-F12 or PBS using the Q-sun and Oriel are shown in figures 3.2 and 3.3 respectively. As shown in figure 3.2 A and B, minimal survival is achieved after a 10 and 50 minute exposure in DMEM-F12 and PBS respectively using the Q-sun. Although both the LSM and normalised data (percentage survival) clearly demonstrate the dose response of irradiated cells, the normalised data can be seen to violate the ANOVA assumption of homoscedasticity as demonstrated by the high degree of variance in the data, which demonstrates the validity of log transformation prior to statistical analysis. Similarly for the Oriel, exposures of 10 and 30 minutes in DMEM-F12 and PBS respectively produced minimal cell survival as shown in figure 3.3.

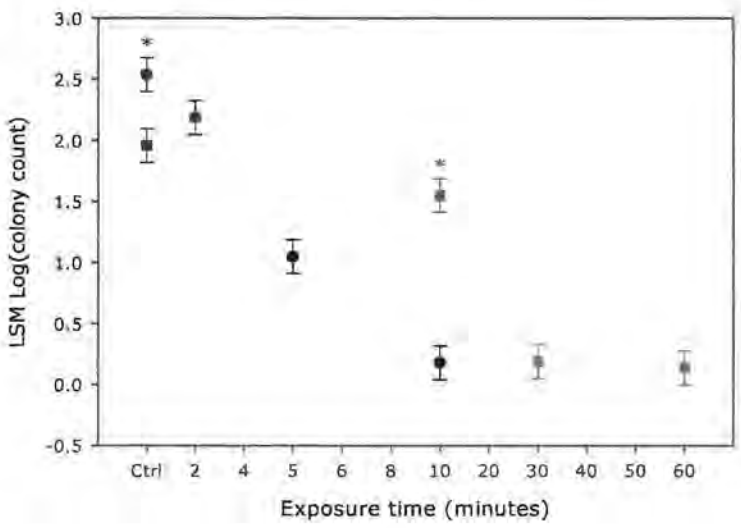

Figure 3.3 Direct exposure of HaCaT cells in DMEM-F12 (•) and PBS (■) to the Oriel operating at 35mA;* represents significant difference between different exposure media for a given exposure time.

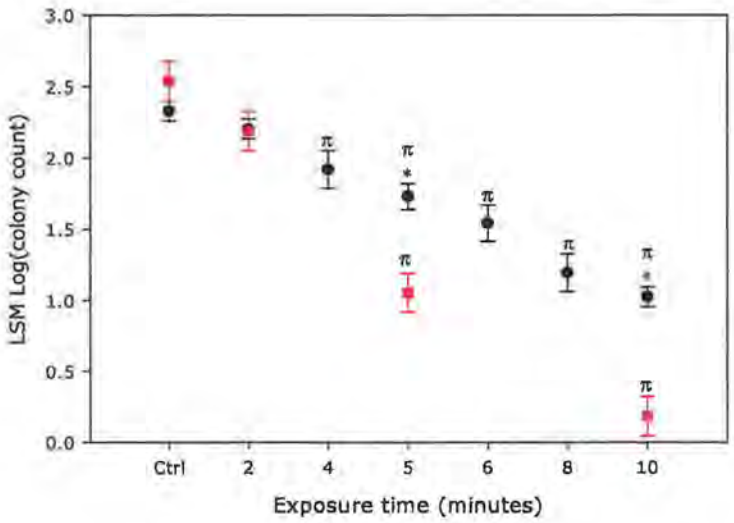

Figure 3.4 Direct exposure of HaCaT cells in DMEM-F12 using the Q-sun (●) and the Oriel (■) solar simulators; ∗ represents significant difference between different exposure media for a given exposure time and π represents significant difference between a dose and its respective control.

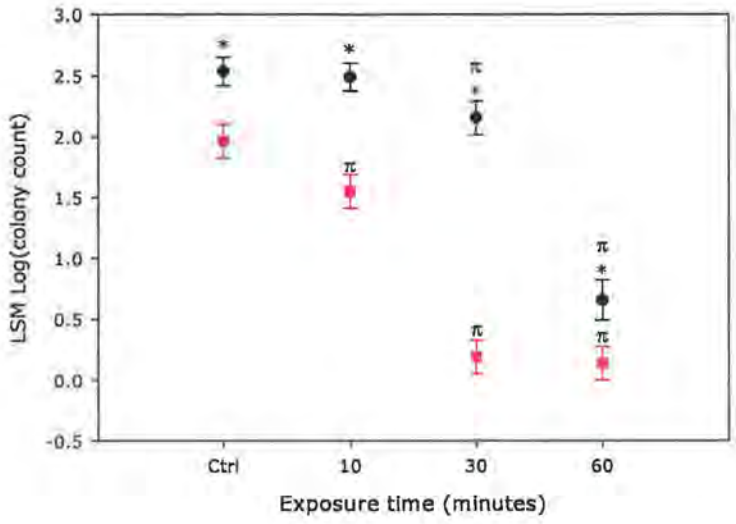

Figure 3.5 Direct exposure of HaCaT cells in PBS using the Q-sun (●) and the Oriel (■) solar simulators; ∗ represents significant difference between different exposure media for a given exposure time and π represents significant difference between a dose and its respective control.

A direct comparison of the DMEM-F12 and PBS dose response curves for each simulator shows the Oriel solar simulator to elicit increased cell killing, irrespective of exposure media, compared to exposures performed under identical conditions using the Q-sun solar simulator as shown in figures 3.4 and 3.5.

Exposures performed using the Q-sun solar simulator fall under the heading of flash photolysis due to the high frequency at which the lamp pulses (20). An initial concern using the Q-sun solar simulator was the possibility that the response of HaCaT cells would be rapid enough to discern the pulsed nature of the Q-sun and / or that the exaggerated dose administered during the duty cycle of the Q-sun would elicit responses different to those incurred by a continuous source. The Bunsen-Roscoe or reciprocity law states that all photochemical reactions are dependent on the total absorbed energy irrespective of the factors that determine the total dose i.e. irradiance and exposure time (20, 21). Although there are some reservations on the applicability of this law to biological systems due to the complex cellular responses to damage (22, 23), if the reciprocity law is obeyed then the same photo-response should be observed when the integral of the total dose administered is the same regardless of how the dose is delivered (20). Comparisons of the dose response for HaCaT cells exposed using the Q-sun and Oriel show that the survival of cells exposed using the Q-sun is consistently and significantly elevated compared to cells exposed under identical conditions using the Oriel regardless of exposure medium. These data show that the Q-sun flash photolysis nature does in fact obey the reciprocity law, abating concerns regarding the environmental relevance of the Q-sun output delivery. The difference in cell survival observed between the two solar simulators is attributed to differences in their

spectral irradiances, specifically the UVB region where the Oriel solar simulator provides an output of 2.18 Wm^{-2} compared to the Q-sun UVB output of 1.33 Wm^{-2}, and not behavioural differences. However, it is suspected that a critical or threshold frequency for biological irradiations exists, since a decrease in frequency would require an increase in irradiance delivered per pulse in order to achieve the same integral exposure. Thus it is not unreasonable to believe that if the frequency of delivery is sufficiently reduced, an irradiance value would be reached where the response of cells would begin to deviate significantly from those elicited under continuous irradiation conditions due to the immense insult administered per pulse and / or the response of the cells irradiated.

A reciprocity study performed by Miyamoto et al (24) found that pulsed wave laser photodynamic therapy (PDT) and continuous wave PDT elicited apoptotic and necrotic deaths respectively. Based on the hypothesis that increased cytotoxicity is required to incur necrosis, Miyamoto et al (24) concluded that pulsed exposures are less cytotoxic than continuous exposures.

Similar to the work done by Miyamoto et al (24), the results presented here show non continuous exposures to be less detrimental than continuous exposures. Although the differences observed in survival have been surmised to arise from differences in spectral output, there is the possibility that simulators elicit different mechanisms of cell death. The clonogenic assay measures cell death where little information regarding the modes of cell death incurred (apoptosis or necrosis) can be extracted from the dose response curves. However comparisons of the cell survival curves exposed in DMEM-F12 for both solar

simulators (figure 3.4) and similarly for cells exposed in PBS (figure 3.5) show that the dose response incurred for a given exposure medium to either solar simulator are comparable, particularly for DMEM-F12. These results suggest that the solar simulators do not differ significantly, if at all, in their modes of cell death induced for a given exposure medium, however the possibility cannot be ruled out without further investigation.

Irradiation of HaCaT cells using the UVA lamp resulted in no cell death even with an exposure of 20 minutes regardless of the exposure media (figure 3.6). However, cells irradiated using the UVB fluorescent lamp produced the most dramatic dose response curves (figure 3.7) of all irradiators under investigation. Cells irradiated in DMEM-F12 and PBS resulted in minimal survival after 7 and 3 minute exposures respectively.

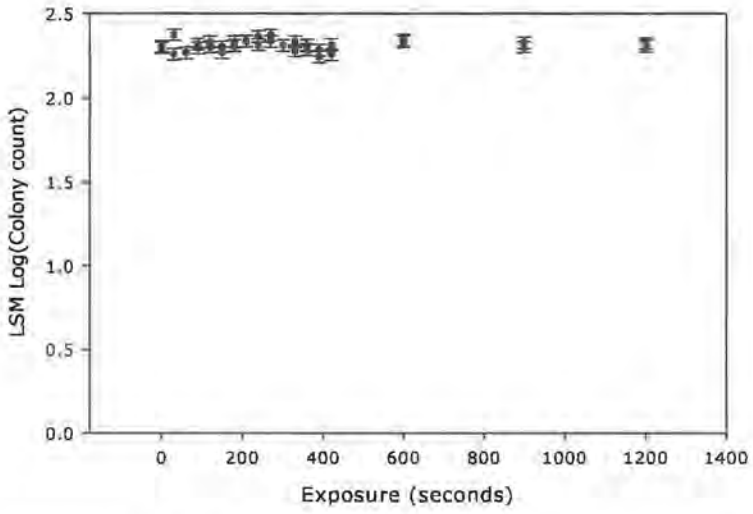

Figure 3.6 Direct exposure of HaCaT cells in DMEM-F12 (•) and PBS (■) to the UVA fluorescent lamp

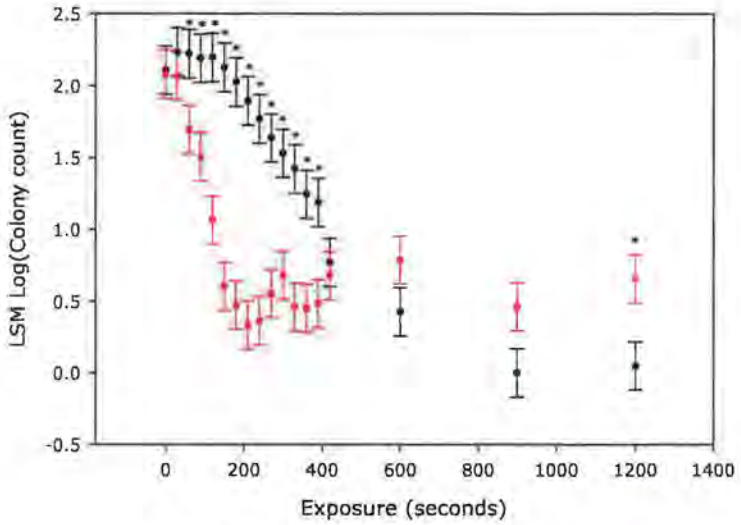

Figure 3.7 Direct exposure of HaCaT cells in DMEM-F12 (•) and PBS (■) to the UVB fluorescent lamp; ∗ represents significant difference between different exposure media for a given exposure time

In contrast to the solar simulator results, the UVB lamp exposures performed in PBS and DMEM-F12 produced results that concur with the transmittance functions presented in figure 2.36, where PBS exposures resulted in increased cell killing compared to DMEM-F12 exposures. The UVB lamp has an intensity of 2.43 Wm^{-2} in the UVB region which is not exceptionally different to the UVB output of the Oriel at 2.18 Wm^{-2}. However, Oriel PBS exposures resulted in minimum survival after a 30 minute exposure whereas UVB lamp PBS exposures resulted in maximal cell killing within 3 minutes, a 10 fold difference in the tolerable exposure duration despite the lamps administering similar radiant intensities. Revisiting the UV spectral distribution of both the Oriel and the UVB lamp in figure 2.27, it can be seen that the radiobiological results for the UVB lamp confirm the conjecture proposed in chapter 2 that the UVB lamp is the most hazardous irradiator under investigation, owing to the sizeable and environmentally irrelevant emissions at wavelengths below 300 nm. Thus, due to the increasing efficacy of radiation with

decreasing wavelength, it is clear that the UVB lamp provides a far greater biologically effective, yet environmentally irrelevant irradiance.

An intriguing effect regarding the exposure medium was revealed as a by-product of the study presented in this chapter. The spectroscopic results presented in figure 2.36 showed that the irradiance and thus the dose received by a cell is greatly reduced for DMEM-F12 exposures compared to an identical exposure in PBS. Radiobiological experiments performed using the UVB lamp concur with the spectroscopic results in figure 2.36. However, exposures carried out with both the Q-sun and Oriel solar simulators yield contradictory results since DMEM-F12 exposures were found to be far more effective than PBS exposures with regard to cell killing (figures 3.2 and 3.3). The ability of the exposure medium to attenuate the dose received is demonstrated in figures 3.2 C and D where the UV dose administered by the Q-sun (38178 Jm^{-1}) in 10 minutes is attenuated to 18936 Jm^{-1} and 36504 Jm^{-1} by DMEM-F12 and PBS respectively. Despite this, maximal cell killing is achieved with a 10 minute DMEM-F12 exposure whilst cells irradiated in PBS for the same duration and receiving nearly twice the dose as their DMEM-F12 counterparts yield survival not significantly different from their respective controls. A possible explanation for these conflicting results could be photosensitiser(s) present in DMEM-F12 cell culture medium whose absorption spectra may occur at longer less energetic wavelengths than those present in the spectral output of the UVB lamp. It is suspected that these hypothetically photosensitising wavelengths fall in the UVA waveband, although the possibility of visible and infrared radiation effects, synergistic or otherwise, cannot be disregarded since the UVA lamp elicits no cell death. However, this may be due to

insufficient irradiance at, or omission of, said hypothetically photosensitising wavelengths in the spectral distribution of the UVA lamp. The results presented here support both the importance of spectral distribution and reciprocity law compliance of the Q-sun solar simulator. It can also be concluded that DMEM-F12 medium augments the effects of solar simulated irradiation via some medium-mediated effect.

3.4 Conclusions

The importance of instrumentation calibration, spectral distribution and irradiance cannot be emphasised enough when attempting to discern the ability of solar radiation to elicit biological effects, as illustrated by the results presented in this chapter. Of particular interest with respect to spectral distribution, are the results obtained using the UVB lamp. The deleterious spectral distribution of the UVB irradiator is not obtrusively evident when compared to solar radiation, artificial and natural, yet its effect on survival was far more devastating than that elicited using solar simulated radiation. These results demonstrate how even an apparently low output at sub terrestrial level wavelengths can significantly alter cellular responses. Furthermore, without comprehensive knowledge of the UVB lamp spectral distribution, it may have been erroneously concluded that the augmented cell killing ability of the UVB irradiator was merely due to increased irradiance and not the presence of environmentally irrelevant wavelengths with enhanced biological efficacy.

The unforeseen effects due to the exposure media not only demonstrate the importance of initial experimental parameters, but also highlight the implications of full spectrum

irradiation. Although it is desirable to know the contributions of individual wavebands, the possibility of interactions between different wavelengths present in solar radiation, whether the effects are synergistic, antagonistic, or purely additive, cannot be neglected and may yield significantly different results from individual waveband analysis. Although full spectrum irradiators can provide excellent approximations of solar radiation, it is not only the spectral distribution and irradiance that determines the environmental relevance of an irradiator but also the nature of their output delivery. The comparative study performed here using the Oriel and Q-sun solar simulators demonstrated that the pulsed nature of the Q-sun complies with the reciprocity law despite the exaggerated manner in which the Q-sun output is delivered. However, this may not hold true for all irradiators and is most probably frequency dependent and thus is yet another aspect of an artificial irradiator that may potentially confound radiobiological experiments.

Although the modes of cell death for given exposure medium were surmised to not different significantly, if at all, from one another, the same supposition cannot be extended to the different exposure medium where DMEM-F12 can be seen to be significantly more cytotoxic than PBS. Thus, the next chapter investigates the role of ROS in DMEM-F12 mediated cell death.

3.5 References

(1) D. B. Brown, A. E. Peritz, D. L. Mitchell, S. Chiarello, J. Uitto & F. P. Gasparro (2000) Common fluorescent sunlamps are an inappropriate substitute for sunlight *Photochemistry and Photobiology* **72,** 340-4.

(2) P. Gróf, G. Rontó & E. Sage (2002) A computational study of physical and biological characterization of common uv sources and filters, and their relevance for substituting sunlight *Journal of Photochemistry and Photobiology B: Biology* **68,** 53-59.

(3) K. Hanada (2000) Photoprotective role of metallothionein in uv-injury -- metallothionein-null mouse exhibits reduced tolerance against ultraviolet-b *Journal of Dermatological Science* **23,** S51-S56.

(4) H. Ikehata, H. Kudo, T. Masuda & T. Ono (2003) Uva induces c->t transitions at methyl-cpg-associated dipyrimidine sites in mouse skin epidermis more frequently than uvb *Mutagenesis* **18,** 511-519.

(5) H. Ikehata, T. Masuda, H. Sakata & T. Ono (2003) Analysis of mutation spectra in uvb-exposed mouse skin epidermis and dermis: Frequent occurrence of c-t transition at methylated cpg-associated dipyrimidine sites *Environmental and Molecular Mutagenesis* **41,** 280-292.

(6) A. A. Vink, A. M. Moodycliffe, V. Shreedhar, S. E. Ullrich, L. Roza, D. B. Yarosh & M. L. Kripke (1997) The inhibition of antigen-presenting activity of dendritic cells resulting from uv irradiation of murine skin is restored by in vitro photorepair of cyclobutane pyrimidine dimers *Proc Natl Acad Sci U S A* **94,** 5255-60.

(7) S. K. Katiyar (2007) Interleukin-12 and photocarcinogenesis *Toxicology and Applied Pharmacology* **224,** 220-227.

(8) C. Nishigori (2006) Cellular aspects of photocarcinogenesis *Photochem Photobiol Sci* **5,** 208-14.

(9) V. O. Melnikova & H. N. Ananthaswamy (2005) Cellular and molecular events leading to the development of skin cancer *Mutation Research/Fundamental and Molecular Mechanisms of Mutagenesis* **571,** 91-106.

(10) I. Terenetskaya (2000) Spectral monitoring of biologically active solar uvb radiation using an in vitro model of vitamin d synthesis *Talanta* **53,** 195-203.

(11) Y. Matsumura & H. N. Ananthaswamy (2004) Toxic effects of ultraviolet radiation on the skin *Toxicol Appl Pharmacol* **195,** 298-308.

(12) IRPA (1989) Proposed change to the irpa 1985 guidelines on limits of exposure to ultraviolet radiation. International non-ionizing radiation committee of the international radiation protection association *Health Physics* **56,** 971-2.

(13) A. F. McKinlay & B. L. Diffey (1987) Reference action spectrum for ultraviolet induced erythema in human skin *CIE Journal* **6,** Pages 17-22

(14) R. B. Setlow (1974) The wavelengths in sunlight effective in producing skin cancer: A theoretical analysis *Proceedings of the National academy of Sciences of the United States of America* **71,** 3363-6.

(15) P. Boukamp, R. T. Petrussevska, D. Breitkreutz, J. Hornung, A. Markham & N. E. Fusenig (1988) Normal keratinization in a spontaneously immortalized aneuploid human keratinocyte cell line *Journal of Cell Biology* **106,** 761-71.

(16) T. A. Lehman, R. Modali, P. Boukamp, J. Stanek, W. P. Bennett, J. A. Welsh, R. A. Metcalf, M. R. Stampfer, N. Fusenig, E. M. Rogan & et al. (1993) P53 mutations in human immortalized epithelial cell lines *Carcinogenesis* **14,** 833-9.

(17) T. T. Puck & P. I. Marcus (1956) Action of x-rays on mammalian cells *Journal of Experimental Medicine* **103,** 653-66.

(18) Statistical-solutions (2009) Assumptions of the factorial anova http://www.statisticssolutions.com/methods-chapter/statistical-tests/assumptions-of-the-factorial-anova/ April 6th 2010.

(19) B. Thiessen (2009) Assumptions of anova http://homepage.mac.com/bradthiessen/stats/m301/4a.pdf April 6th 2010.

(20) J. W. Martin, J. W. Chin & T. Nguyen (2003) Reciprocity law experiments in polymeric photodegradation: A critical review *Progress in Organic Coatings* **47,** 292-311.

(21) R. Bunsen & H. Roscoe (1859) Photochemische untersuchungen. *Ann Phys.* **108,** 193.

(22) H. Merwald, G. Klosner, C. Kokesch, M. Der-Petrossian, H. Hönigsmann & F. Trautinger (2005) Uva-induced oxidative damage and cytotoxicity depend on the mode of exposure *Journal of Photochemistry and Photobiology B: Biology* **79,** 197-207.

(23) A. Schindl, B. Rosado-Schlosser & F. Trautinger (2001) Reciprocity regulation in photobiology. An overview *Hautarzt* **52,** 779-85.

(24) Y. Miyamoto, Y. Umebayashi & T. Nishisaka (1999) Comparison of phototoxicity mechanism between pulsed and continuous wave irradiation in photodynamic therapy *Journal of Photochemistry and Photobiology B: Biology* **53,** 53-59.

Chapter 4 Investigating the role of reactive oxygen species in medium-mediated cell death

4,1 Introduction

While investigating the abilities of different irradiators to incur cell death in HaCaT cells in chapter 3, an unexpected effect due to the exposure medium was observed. It was found that cells irradiated in DMEM-F12 cell culture medium with solar simulated radiation produced increased cell death compared to identical exposures performed in PBS. These results contradict the spectroscopic results in chapter 2 which imply that irradiation in PBS would incur greater levels of cell death due to increased transmittance of incident radiation compared to DMEM-F12. The unexpected ability of DMEM-F12 to yield such a dramatic dose response is further investigated in this chapter. As previously mentioned, UVA radiation is thought to elicit its effects primarily through oxidative processes involving as of yet unidentified non-DNA chromophore(s). Since UVA radiation is the predominant UV waveband in the spectral irradiance of the Q-sun solar simulator and cell culture medium provides the nutrients readily available *in vivo* to *in vitro* cultures, it is possible that the enhanced cell death observed in cells irradiated in DMEM-F12 is due to the production of ROS in DMEM-F12 itself. Thus different antioxidants were employed to examine the potential role of ROS in the extensive cell killing observed when cells are irradiated with solar simulated radiation in DMEM-F12.

4.2 Methods

4.2.1 Cell culturing, seeding and the clonogenic assay

HaCaT cells were cultured, seeded and the clonogenic assay performed as outlined in chapter 2, sections 3.2.1 and 3.2.2. Briefly, HaCaT cells were cultured in DMEM-F12 cell culture medium containing 10% FBS, 1% penicillin-streptomycin and 1 μg/ml hydrocortisone. Cells were incubated under humid conditions at 37°C, with 5% CO_2 in air and subcultured when cells were 80-90% confluent. Cells for direct and indirect (unexposed recipient cell) exposures were seeded at a density of 400 cells in 3 ml DMEM-F12 per well 16 hours before irradiation or treatment. For the clonogenic assay, cells were exposed or treated and then incubated for 7 days after which they were stained using carbol fuchsin for 5 minutes and scored.

4.2.2 Concentrations and dose responses of antioxidants and inhibitors

Dimethyl sulfoxide (DMSO) has been reported to exhibit both therapeutic and toxic abilities (1-3) thus a dose response to determine a non toxic concentration for HaCaT cells was performed over the range 0-5% (v/v).

Cells are reported to contain endogenous reduced glutathione (GSH) at a concentration between 3-5 mM (4). Although supplementation of GSH at a concentration of 5 mM has been used in the literature (5), a dose response study over the range $5x10^{-3} - 5x10^{3}$ μM was performed to determine the effect, if any, that exogenous supplementation of GSH would have on HaCaT cells under normal redox conditions.

L-buthionine-*S,R*-sulfoximine (BSO) prevents de novo synthesis of GSH (6, 7) by inhibiting the enzyme γ-glutamylcysteine synthetase involved in GSH biosynthesis (7). To determine a non toxic BSO concentration for HaCaT cells under normal redox status, a dose response was performed over the range 0-10^6 ng/ml.

Direct and indirect exposures were then performed with and without the presence of antioxidants at concentrations of 0.5% (v/v) DMSO, 0.1 mg/ml superoxide dismutase (SOD, EC 1.15.1.1) (8), 5 mM GSH (EC 200-725-4) (5) and 20 µg/ml Catalase (EC 1.11.1.6) (8) as found via dose response experiments and/or concentrations used in literature.

4.2.3 Direct exposures in cell culture medium ± antioxidants

All exposures were performed 16 hours post cell seeding in the pre sterilised Q-sun solar simulator chamber without lids. Prior to exposure, antioxidants were added directly to the 3 ml DMEM-F12 covering cells to give final concentrations of 0.1 mg/ml SOD, 0.5% (v/v) DMSO, 20 µg/ml catalase or 5 mM GSH and allowed to incubate for 30 minutes. Cells were directly exposed in DMEM-F12 with or without antioxidants with no medium change post exposure. Immediately post exposure cells were returned to the incubator for 7 days before survival was assayed using the clonogenic assay. Controls were handled identically but received sham irradiations i.e. 'irradiated' in the dark with the bulb off.

4.2.4 Indirect blank medium exposures ± antioxidants

Blank (no cells) DMEM-F12 cell culture medium with and without antioxidants at final concentrations of 0.1 mg/ml SOD, 0.5% (v/v) DMSO, 20 μg/ml catalase or 5 mM GSH was irradiated in the pre sterilised Q-sun solar simulator chamber. Immediately, 1 hour, 24 hours and 48 hours post exposure the blank medium ± antioxidants was harvested, filtered and transferred to unirradiated recipient cells seeded 16 hours prior to treatment. Recipient cells were then incubated for 7 days with no further medium changes before survival was assayed using the clonogenic assay. Irradiated DMEM-F12 earmarked for the later times of transfer was stored in the incubator post exposure until the time of transfer occurred. Controls were handled identically but received sham irradiations.

4.2.5 Statistics

Results represent a minimum of 3 independent tests unless otherwise stated, with a minimum of 2 replicates per independent test. The data was log transformed and ANOVA was performed on the linear regressions and pair-wise data were computed using the Bonferroni adjustment. Data are presented as the LSM of the log transformed colony counts ± 95CI. All analyses were done using statistical software package SAS 9.1 and SAS enterprise guide 3.0. Significance was taken at a level of $p \leq 0.05$.

4.3 Results and discussion

The role of ROS in the propagation of DMEM-F12 cell killing was investigated using various antioxidants. Prior to irradiation with and without antioxidants, suitable antioxidant concentrations were determined. SOD and catalase at concentrations of 0.1 mg/ml and 20 µg/ml respectively, which were found effective for HaCaT cells in previous studies performed in our laboratory, were employed to determine the role of superoxide and hydrogen peroxide respectively. In order to determine a suitable non-toxic concentration of DMSO for HaCaT cells, a dose response was performed, the results of which are shown in figure 4.1. Based on these results a non-toxic concentration of 0.5% (v/v) DMSO was chosen to determine the role of the hydroxyl radical.

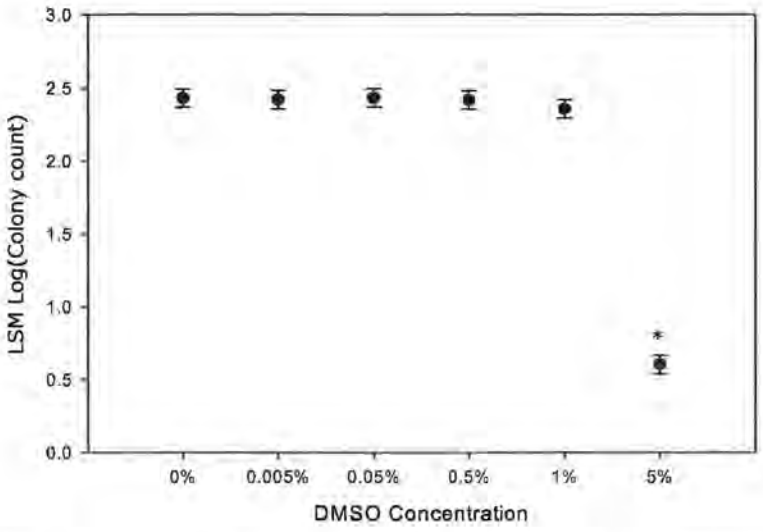

Figure 4.1 DMSO dose response, cells exposed to varying concentrations of DMSO in DMEM-F12, data presented as LSM ± 95CI for n =3 independent tests, * indicates significant difference compared to untreated control ($p \leq 0.05$).

The dose response of HaCaT cells treated with varying concentrations of GSH shows that GSH supplementation up to 5 mM has no effect on survival or plating efficiency (figure 4.2). A concentration of 5 mM GSH was chosen to investigate the role of hydrogen peroxide which is consistent with concentrations used in the literature (5).

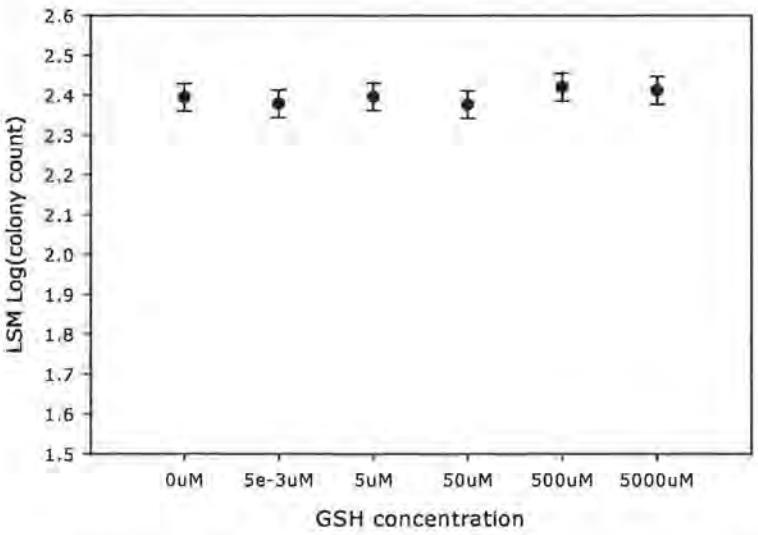

Figure 4.2 Effect of GSH supplementation on the colony forming ability of HaCaT cells, data presented as LSM ± 95CI for n =3 independent tests, * indicates significant difference compared to untreated control ($p \leq 0.05$).

The results for direct exposure of cells in DMEM-F12 with and without antioxidants (0.1 mg/ml SOD, 0.5% v/v DMSO, 5 mM GSH or 20 μg/ml catalase) are shown in figure 4.3. Antioxidants were added directly to DMEM-F12 covering cells and allowed to incubate for 30 minutes prior to irradiation in the Q-sun solar simulator. The results presented in figure 4.3 show that SOD had a slightly negative but not significant effect on cell survival. Edwards and Silva (9) investigated the source of photoinactivation of the enzyme lysosome and found that inclusion of SOD resulted in increased photoinactivation. This finding was attributed to increased levels of hydrogen peroxide produced during the dismutation process ($O_2^{\cdot-} + O_2^{\cdot-} \rightarrow H_2O_2 + O_2$). Thus, it is possible

that the superoxide radical does play a small but negligible role in the cell killing abilities of DMEM-F12 that gives way to slight but not significant increases in cell death due to the production of hydrogen peroxide in the dismutation process when SOD is present during irradiation. Due to the low permeability of SOD (10), the production of superoxide and thus hydrogen peroxide is believed to be extracellular. DMSO, which is membrane permeable (11), had no effect on survival implying that the hydroxyl radical does not play a measureable role in the propagation of medium mediated cell death when irradiated with solar simulated radiation.

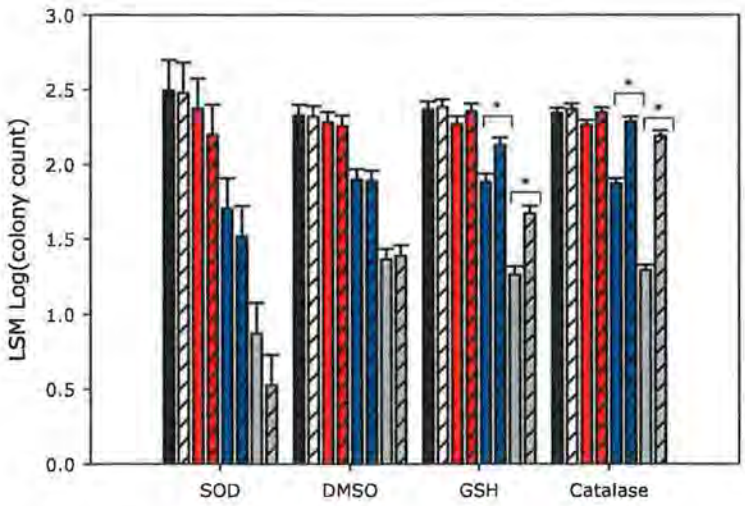

Figure 4.3 Direct exposure dose response plots; HaCaT cells irradiated in DMEM-F12 with and without the presence of SOD (0.1 mg/ml), DMSO (0.5% v/v), GSH (5 mM) or catalase (20 µg/ml): (■) sham irradiated controls, (■) 2 minutes, (■) 5 minutes, (■) 10 minutes. Solid and thatched bars indicate the absence and presence of antioxidants respectively. Data are presented as the LSM ± 95CI for n =3 independent tests, * indicates significant difference between time matched exposures between antioxidant treated and untreated cells.

Both GSH and catalase convert hydrogen peroxide to water (12). Survival of cells exposed directly in DMEM-F12 supplemented with GSH and catalase both yield significant increases in survival compared to cells directly exposed for the same

duration in DMEM-F12 without antioxidant supplementation. This suggests a significant role for hydrogen peroxide mediating solar simulated radiation induced cell death in DMEM-F12. Although both antioxidants yield significant increases in cell survival, catalase appears to be the most effective. The difference in efficacy of GSH and catalase may result from differences in activity and / or that GSH is cell membrane permeable whereas catalase is not (5). If the latter is the predominant effect then this would suggest the difference between GSH and catalase survival is due to diminished GSH concentrations at the time of exposure due to cellular uptake which in turn suggests that the production of hydrogen peroxide is predominantly extracellular. Thus, the effects, if any, that irradiation may have on DMEM-F12 cell culture medium itself and consequently on cell survival was investigated.

Pre-warmed (37°C) blank DMEM-F12 was irradiated for 2, 5 and 10 minutes and transferred to unexposed recipient cells immediately, 1 hour, 24 hours and 48 hours post exposure. Control recipient cells were treated with sham irradiated blank DMEM-F12 transferred immediately, 1 hour, 24 hours and 48 hours post sham irradiation. Figure 4.4 shows the survival of unexposed recipient cells treated with blank irradiated DMEM-F12 at all times of transfer. A dose response with increasing exposure time of blank DMEM-F12 was observed. This effect was observed at all times of transfer but only blank DMEM-F12 irradiated for 10 minutes produced a significant decrease in recipient cell survival compared to their respective controls at all transfer times.

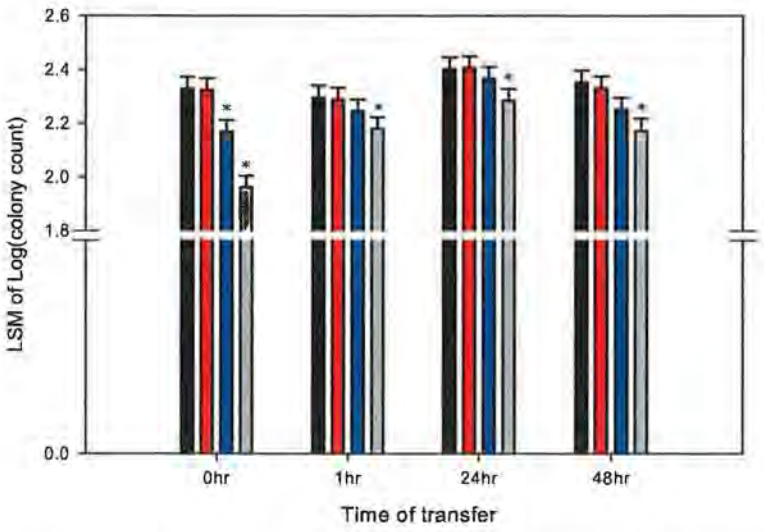

Figure 4.4 Survival curves for unexposed recipient cells treated with blank DMEM-F12 irradiated and transferred immediately, 1 hour, 24 hours and 48 hours post exposure; (■) sham irradiated controls, (■) 2 minutes, (■) 5 minutes, (■) 10 minutes; data presented as the LSM ± 95CI for n =3 independent tests, * indicates significant difference between dose and its respective control.

Blank DMEM-F12 transfer experiments were repeated with and without the presence of antioxidants to establish whether or not ROS contribute to the decrease in recipient cell survival observed in figure 4.4. Pre-warmed blank DMEM-F12 supplemented or not with 0.5% v/v DMSO, 5 mM GSH or 20 μg/ml catalase was irradiated for 2, 5 and 10 minutes and controls were sham irradiated. At the appropriate time post exposure the medium with and without antioxidants was harvested, filtered and transferred to unexposed recipient cells. Figure 4.5 illustrates the survival of unexposed recipient cells treated with irradiated or sham irradiated blank DMEM-F12 with and without antioxidants immediately post exposure.

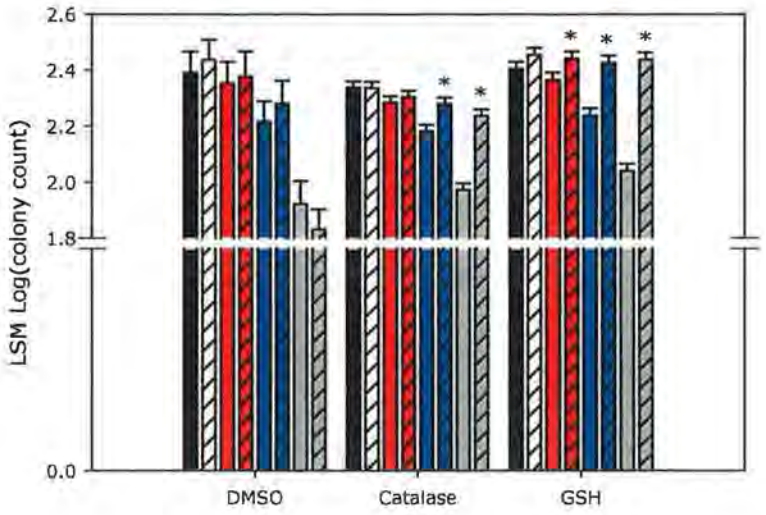

Figure 4.5 Cell survival for unexposed recipient cells treated with irradiated blank DMEM-F12 with and without DMSO (0.5% v/v), catalase (20 μg/ml) or GSH (5 mM) transferred to unexposed recipient cells immediately post exposure: (■) sham irradiated controls, (■) 2 minutes, (■) 5 minutes, (▒) 10 minutes. Solid and thatched bars indicate the absence and presence of antioxidants respectively. Data are presented as the LSM ± 95CI for n=3 independent tests, * indicates significant difference between time matched exposures with and without antioxidants.

As expected, the presence of DMSO confers no protection against possible ROS formation. However, the presence of GSH or catalase in blank DMEM-F12 produced significant increases in recipient cell survival. Interestingly, the increase in recipient cell survival due to the presence of catalase in indirect exposures (figure 4.5) produced a similar response to that observed when cells were directly irradiated in DMEM-F12 supplemented with catalase (figure 4.3). However, the differential effects of GSH supplementation of DMEM-F12 in direct and indirect irradiation of cells (figures 4.3 and 4.5) are most intriguing. Although the increase in survival due to the presence of GSH in both direct and indirect exposures are significant, direct exposure survival still exhibits a dose response, while recipient cells treated with blank DMEM-F12 supplemented with GSH produced survival not significantly different from controls at all exposure times (i.e. 2, 5, and 10 minute exposures). These results support the

hypothesis that the production of hydrogen peroxide is predominantly extracellular and that the difference in cell survival due to the presence of GSH and catalase during direct exposures is due to cellular uptake.

Although generation of ROS is known to be rapid and short lived, irradiated blank DMEM-F12 transfers with and without antioxidants were also performed 1, 24 and 48 hours post exposure as shown in figures 4.6, 4.7 and 4.8 respectively. The rationale for carrying out blank irradiated DMEM-F12 transfers in the presence of antioxidants at the later time intervals was based on the supposition that the reduced survival observed at the later times of transfer in figure 4.4 may be due to ROS-induced damage of one or more of the components of DMEM-F12.

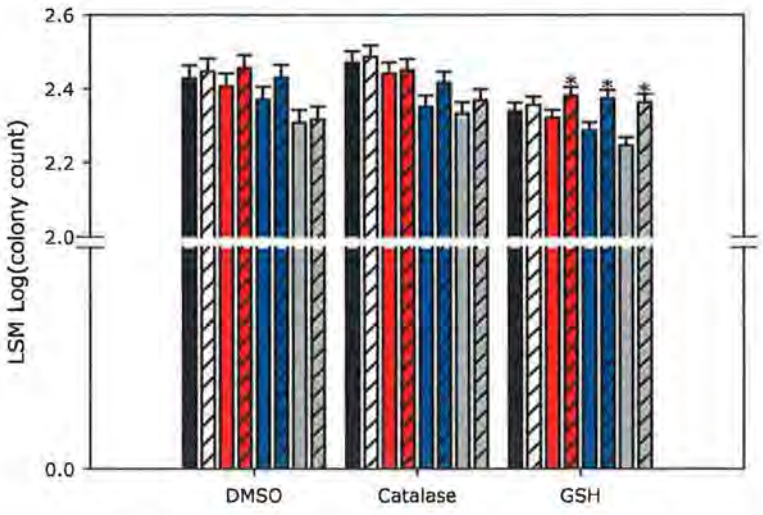

Figure 4.6 Cell survival for unexposed recipient cells treated with irradiated blank DMEM-F12 with and without DMSO (0.5% v/v), catalase (20 μg/ml) or GSH (5 mM) 1 hour post exposure: (■) sham irradiated controls, (■) 2 minutes, (■) 5 minutes, (≈) 10 minutes. Solid and thatched bars indicate the absence and presence of antioxidants respectively. Data are presented as the LSM ± 95CI for n=3 independent tests, * indicates significant difference between time matched exposures with and without antioxidants.

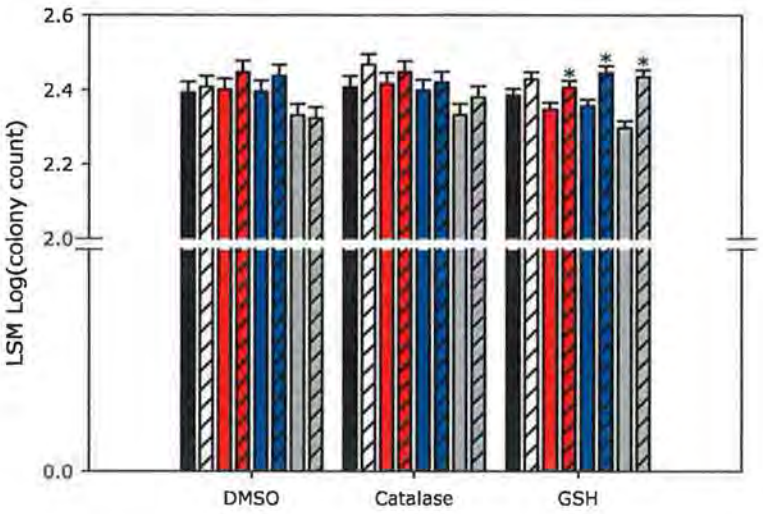

Figure 4.7 Survival for unexposed recipient cells treated with irradiated blank DMEM-F12 with and without DMSO (0.5% v/v), catalase (20 μg/ml) or GSH (5 mM) 24 hours post exposure: (■) sham irradiated controls, (■) 2 minutes, (■) 5 minutes, (■) 10 minutes. Solid and thatched bars indicate the absence and presence of antioxidants respectively. Data are presented as the LSM ± 95CI for n=3 independent tests, * indicates significant difference between time matched exposures with and without antioxidants.

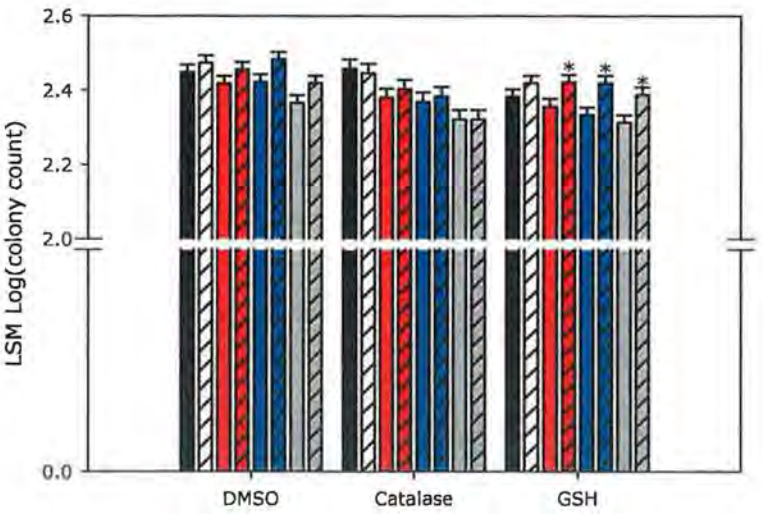

Figure 4.8 Cell survival for unexposed recipient cells treated with irradiated blank DMEM-F12 with and without DMSO (0.5% v/v), catalase (20 μg/ml) or GSH (5 mM) 48 hours post exposure: (■) sham irradiated controls, (■) 2 minutes, (■) 5 minutes, (■) 10 minutes. Solid and thatched bars indicate the absence and presence of antioxidants respectively. Data are presented as the LSM ± 95CI for n=3 independent tests, * indicates significant difference between time matched exposures with and without antioxidants.

The results show that the presence of DMSO or catalase has no effect on cell survival. Although a significant difference was observed at the DMSO 48 hour time of transfer, the difference is not thought to be due to pro-survival properties of DMSO since there was no evidence in either the direct or earlier indirect exposure results of any such processes within this system. GSH supplementation yielded increases in survival for all exposure times (2, 5 and 10 minutes) at all times of transfer (1, 24 and 48 hours). This increase in survival is believed to arise from the ability of GSH to permeate the cell membrane causing the intracellular ratio of reduced to oxidised glutathione (GSH:GSSG) to increase thus providing improved defences against the production of endogenous ROS. The possibility that GSH provides a protective effect against damage incurred to the cell culture medium by hydrogen peroxide at the time of irradiation is undermined since catalase confers no such protective effect.

These improved defences against the production of endogenous ROS is also a more reasonable hypothesis then the possibility that GSH exerts a

To determine whether 5 mM GSH was an excessive supplementation concentration for indirect exposures, the ability of lower concentrations of GSH to overcome reduced survival incurred when blank DMEM-F12 was irradiated for 10 minutes and transferred immediately post exposure to unexposed recipient cells was investigated. Although figure 4.9 shows that a concentration of 0.5 mM significantly increases survival ($p < 0.05$) above that experienced in the absence of GSH, only 5 mM GSH was found to increase survival to a level that was found to be not significantly different from controls, thus validating the use of GSH at a concentration of 5 mM for indirect exposures.

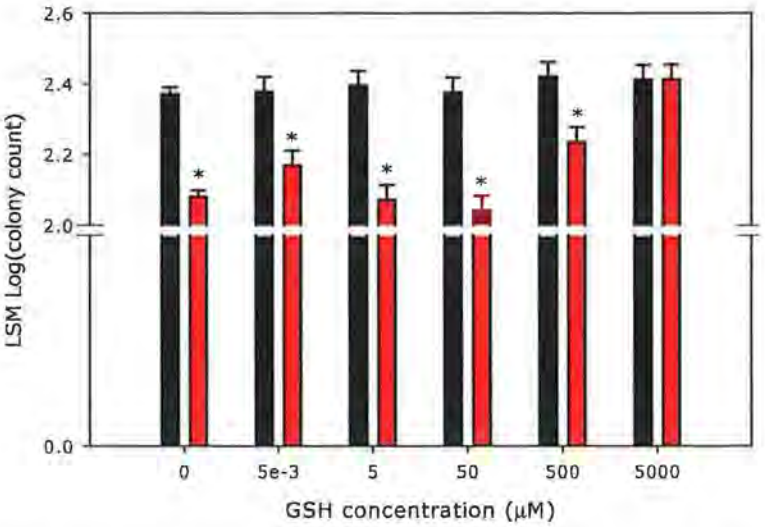

Figure 4.9 Survival of unexposed recipient cells treated with blank DMEM-F12 supplemented with GSH and irradiated for 10 minutes (■) or sham irradiated (■) and transferred immediately post exposure to unexposed recipient cells. Data are presented as the LSM ± 95CI for n=3 independent tests, * indicates significant difference between irradiated and sham irradiated survival for a given GSH concentration.

Although GSH is taken up by cells, it is not done so directly. GSH is hydrolysed into its constituent amino acids (L-glutamate, L-cysteine and L-glycine) which are transported into the cell (13). De novo synthesis of intracellular GSH is carried out via two sequential ATP dependent enzymatic reactions, the first of which is catalysed by γ–glutamylcysteine synthase which binds L-glutamate and L-cysteine (12). The ability of HaCaT cells to synthesise GSH was determined using BSO, an inhibitor of γ–glutamylcysteine synthase. Figure 4.10 shows the survival of HaCaT cells treated with increasing concentrations of BSO under normal redox conditions where a reduction in survival is observed at concentrations greater than 10^4 ng/ml (10 μg/ml). These results demonstrate that HaCaT cells do synthesise GSH, thus it is possible that exogenous supplementation does contribute to the reducing potential of HaCaT cells by increasing the GSH:GSSG ratio.

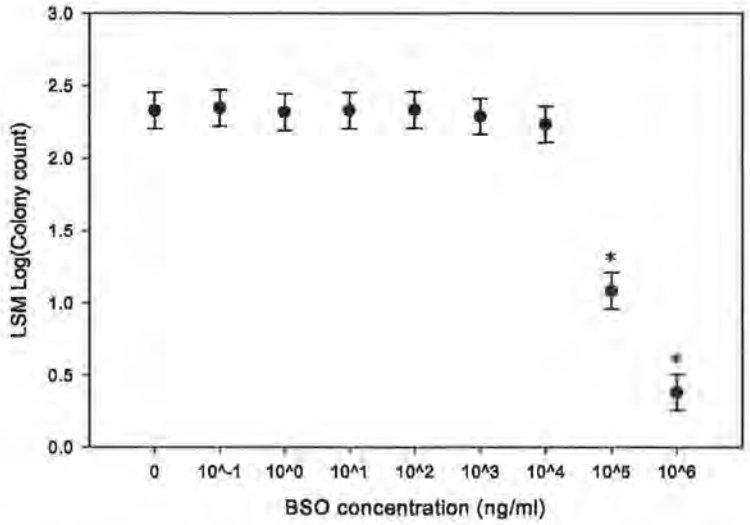

Figure 4.10 Dose response for cells exposed to varying concentrations of BSO in DMEM-F12. Data are presented as LSM ± 95CI for n=3 independent tests, * indicates significant difference between BSO treated and untreated cells.

Whether or not GSH supplementation elicits its pro survival effects by increasing the reducing potential of HaCaT cells was investigated in both direct and indirect exposures. Exposures were performed using a non-lethal concentration of BSO (10 ng/ml) with and without the presence of 5 mM GSH, and compared to cell survival results obtained from exposures performed with and without 5 mM GSH, the results for which are presented in figures 4.11 and 4.12.

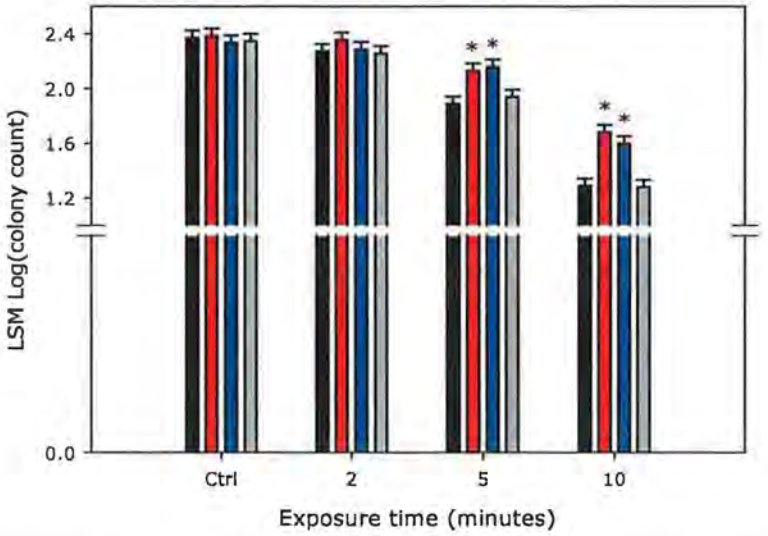

Figure 4.11 Direct exposure of cells in DMEM-F12 supplemented with (■) nothing , (■) 5 mM GSH, (■) 5 mM GSH and 10 ng/ml BSO or (■) 10 ng/ml BSO. Data are presented as the LSM ± 95CI for n=3 independent tests, * indicates significant difference between time matched supplemented and unsupplemented exposures.

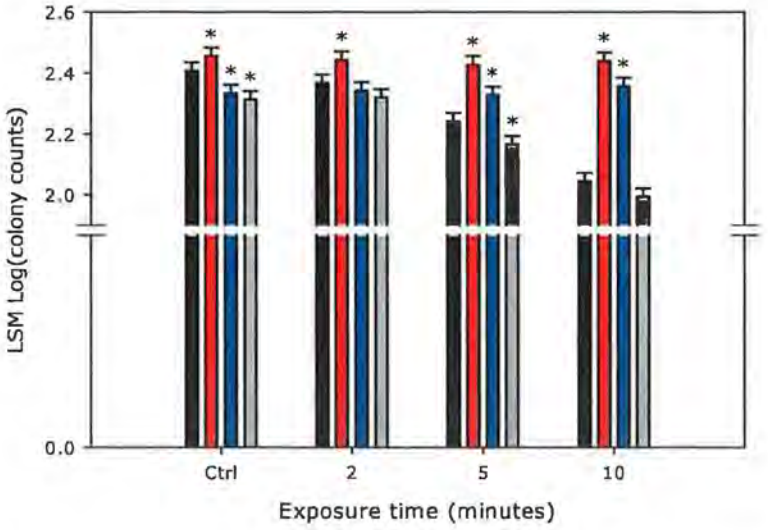

Figure 4.12 Indirect exposure of cells in DMEM-F12 supplemented with (■) nothing , (■) 5 mM GSH, (■) 5 mM GSH and 10 ng/ml BSO or (■) 10 ng/ml BSO. Data presented as the LSM ± 95CI for n=3 independent experiments, * indicates significant difference between time matched supplemented and unsupplemented exposures.

The presence of BSO during direct exposures had no effect on cell survival compared to unsupplemented exposures (figure 4.11). Furthermore, the increased survival of cells

directly irradiated in the presence of GSH was not abrogated due to the presence of BSO (figure 4.11). As expected, the presence of GSH in the indirect exposures eliminated the dose response observed with unsupplemented indirect exposures (figure 4.12). Although the presence of BSO with GSH significantly diminished the effectiveness of GSH in the indirect exposures, its presence did not inhibit GSH from abrogating this dose response (figure 4.12). However, it is suspected that the significant reduction in the effectiveness of GSH is an artefact of plating efficiency and not a detrimental effect due to the presence of BSO. This is suspected because indirect exposures performed with DMEM-F12 supplemented with GSH alone or GSH and BSO together are not significantly different to their respective controls for all exposure times. However, the GSH control and the GSH and BSO control are significantly different not only from one another, but also to the unsupplemented control. Figures 4.9 and 4.10 both show that the presence of 5 mM GSH and 10 ng/ml BSO respectively does not yield significant differences in survival. The plating effect is thought to arise due to the low precision in cells counts. Cells plated for the clonogenic assay are of the order of 10^2 (i.e. 400 cells per well) but are calculated from a volume of fluid normally containing 10^5 cells precise to one decimal place (i.e. 5.5×10^5 cells ml^{-1}). Thus, calculating low seeding densities from high density stock solutions with low precision can result in a high probability of variation between seeding densities computed from independent stock solutions. To minimise this variation/effect, one independent test for each supplementation should ideally be generated from one independent cell stock solution and this repeated for further independent tests. This will ensure that the variance between independent tests is the same for each supplementation. However, only the BSO exposures with and without GSH were performed in this manner which is

reflected in the lack of significant difference between their controls as shown in figure 4.12.

Although both the direct and indirect BSO results suggest that GSH does not exact its pro survival effects by increasing the reducing capacity of HaCaT cells, it is believed that the non-toxic concentration of BSO chosen was too low. Since BSO binds to the active site of γ–glutamylcysteine synthase irreversibly (14-17), it is consumed in the process. The concentration of BSO employed was chosen due to its lack of toxicity under normal redox conditions but was thought that under oxidative stress, this concentration would become toxic to cells due to a potentially higher demand for GSH. Thus, although a BSO concentration of 10 ng/ml will inhibit a portion of the γ–glutamylcysteine synthase population, its effect on cell survival can be seen to be undetectable. Thus, it is probable that the BSO concentration used was ineffective despite increased demands on the reducing capacity of cells due to radiation induced toxic conditions.

4.4 Conclusions

Both direct and indirect DMEM-F12 antioxidant exposure results show that reduced survival of cells irradiated in DMEM-F12 is mediated predominantly by the production of extracellular hydrogen peroxide. However, the indirect results also showed that blank DMEM-F12 irradiated and transferred to unexposed recipient cells 1 hour or more post exposure resulted in significantly reduced survival that cannot be overcome with the inclusion of antioxidants except GSH. Although the ability of GSH to increase survival at the late times of transfer was surmised to be the result of increased reducing

capabilities of supplemented cells, it is possible that the presence of GSH at the later time points enabled cells to overcome possible deleterious photo degradation effects of DMEM-F12.

4.5 References

(1) C. Brayton (1986) Dimethyl sulfoxide (dmso): A review *Cornell Vet.* **76,** 61-90.

(2) G. Cavaletti, N. Oggioni, F. Sala, G. Pezzoni, E. Cavalletti, P. Marmiroli, M. G. Petruccioli, L. Frattola & G. Tredici (2000) Effect on the peripheral nervous system of systemically administered dimethylsulfoxide in the rat: A neurophysiological and pathological study *Toxicology Letters* **118,** 103-107.

(3) J. Chen, M. Chopp & Y. Li (1999) Neuroprotective effects of progesterone after transient middle cerebral artery occlusion in rat *Journal of the Neurological Sciences* **171,** 24-30.

(4) R. M. Tyrrell & V. E. Reeve (2006) Potential protection of skin by acute uva irradiation--from cellular to animal models *Progress in Biophysics and Molecular Biology* **92,** 86-91.

(5) J. Dahle, E. Kvam & T. Stokke (2005) Bystander effects in uv-induced genomic instability: Antioxidants inhibit delayed mutagenesis induced by ultraviolet a and b radiation *Journal of Carcinogenesis* **4,** 11.

(6) T. M. Donohue, T. V. Curry-McCoy, S. L. Todero, R. L. White, K. K. Kharbanda, A. A. Nanji & N. A. Osna (2007) L-buthionine (s,r) sulfoximine depletes hepatic glutathione but protects against ethanol-induced liver injury *Alcoholism Clinical and Experimental Research* **31,** 1053-1060.

(7) M. Thomas, T. Nicklee & D. W. Hedley (1995) Differential effects of depleting agents on cytoplasmic and nuclear non-protein sulphydryls: A fluorescence image cytometry study *Br J Cancer* **72,** 45-50.

(8) F. M. Lyng, P. Maguire, B. McClean, C. Seymour & C. Mothersill (2006) The involvement of calcium and map kinase signaling pathways in the production of radiation-induced bystander effects *Radiation Research* **165,** 400-9.

(9) A. M. Edwards & E. Silva (2001) Effect of visible light on selected enzymes, vitamins and amino acids *Journal of Photochemistry and Photobiology B: Biology* **63,** 126-31.

(10) P. Duann, P. K. Datta, C. Pan, J. B. Blumberg, M. Sharma & E. A. Lianos (2006) Superoxide dismutase mimetic preserves the glomerular capillary permeability barrier to protein *Journal of Pharmacology and Experimental Therapeutics* **316,** 1249-1254.

(11) M. S. Lustgarten, Y. C. Jang, Y. Liu, F. L. Muller, W. Qi, M. Steinhelper, S. V. Brooks, L. Larkin, T. Shimizu, T. Shirasawa, L. M. McManus, A. Bhattacharya, A. Richardson & H. Van Remmen (2009) Conditional knockout of mn-sod targeted to type iib skeletal muscle fibers increases oxidative stress and is sufficient to alter aerobic exercise capacity *Am J Physiol Cell Physiol* **297,** C1520-1532.

(12) S. I. Baskin & H. Salem (1997) *Oxidants, antioxidants and free radicals* (Taylor & Francis, Washington DC).

(13) M. H. Hanigan (1998) [gamma]-glutamyl transpeptidase, a glutathionase: Its expression and function in carcinogenesis *Chemico-Biological Interactions* **111-112,** 333-342.

(14) O. W. Griffith & A. Meister (1979) Potent and specific inhibition of glutathione synthesis by buthionine sulfoximine (s-n-butyl homocysteine sulfoximine) *J Biol Chem* **254,** 7558-60.

(15) O. W. Griffith, M. E. Anderson & A. Meister (1979) Inhibition of glutathione biosynthesis by prothionine sulfoximine (s-n-propyl homocysteine sulfoximine), a selective inhibitor of gamma-glutamylcysteine synthetase *J Biol Chem* **254,** 1205-10.

(16) H. H. Bailey (1998) -s,r-buthionine sulfoximine: Historical development and clinical issues *Chemico-Biological Interactions* **111-112,** 239-254.

(17) R. Reliene & R. H. Schiestl (2006) Glutathione depletion by buthionine sulfoximine induces DNA deletions in mice *Carcinogenesis* **27,** 240-4.

Chapter 5 Mechanistic effects

5.1 Introduction

When performing non-ionising radiation investigations, the exposure media in which biological samples are maintained during irradiation is a fundamental parameter to consider prior to experimentation, however the reasoning behind the choice of exposure medium is rarely specified. Cell culture medium and PBS appear to be primary exposure media employed, with a possible bias toward PBS (1-11). The results presented in the previous chapters have demonstrated a significant difference in the capabilities of the different exposure media to elicit cell death when irradiated with solar simulated radiation. This was shown in chapter 4 to be primarily attributed to the extracellular production of hydrogen peroxide in DMEM-F12 medium. Cell death was measured using the clonogenic assay which is generally considered the gold standard in radiobiological studies for determining radio-sensitivity. However, the clonogenic assay does not provide information regarding the events leading to and the mechanism(s) by which cell death is incurred.

Cell death is a normal component of the health and development of multicellular organisms and is conventionally subdivided into regulated and unregulated mechanisms known as apoptosis and necrosis respectively (12). Although evidence is emerging that necrosis is in fact a regulated event (13), it is primarily associated with extensive damage leading to uncontrolled cell degradation and localised inflammation (12) while apoptosis is an energy dependent systematic degradation of the cell (14) from which pre-committed cells are capable of withdrawing (15). Thus, this chapter investigates

whether apoptosis plays a role in solar simulated radiation induced cell death enabling further investigation into the differential effects of irradiating cells in DMEM-F12 and PBS in terms of apoptotic activity.

Apoptosis is a highly complex and tightly regulated form of programmed cell death in which cells actively participate in their own demise. Apoptosis can be triggered by both external and internal stimuli. Consequently, the two predominant pathways by which apoptosis can be executed are aptly termed the extrinsic and intrinsic pathways. The extrinsic pathway is triggered when trans membrane death receptors of the tumour necrosis factor receptor-1 (TNFR-1) superfamily are activated by their respective ligand(s) while the intrinsic pathway is triggered in response to internal signals such as DNA damage (16, 17). Both pathways are dependent on the activity of a family of proteins, termed caspases that are one of the main effectors of apoptosis. Caspases are a group of cysteine proteases that exist within the cell as inactive pro-forms or zymogens that require cleavage for activation, and are divided into two groups, initiator (-2, -8, -9 and -10) and effector (-3, -6, -7) caspases (16, 17). Although the initiator caspases primarily associated with the extrinsic and intrinsic pathways differ, these pathways converge at effector caspase activation since both caspase-8 and -9 of the extrinsic and intrinsic pathways respectively activate caspase-3 (14), a critical death effector in caspase mediated cell death (18).

In the extrinsic pathway, ligation of the appropriate extracellular signalling molecules triggers transmembrane death receptor trimerisation. The intracellular death domains (DD) of the now trimeric receptor recruit adaptor molecules that possess death effector domains (DED) which in turn recruits inactive procaspase-8, see figure 5.1. Together,

these proteins form the death inducing signalling complex (DISC). Procaspase-8 is cleaved at its DED releasing activated caspase-8, which is believed to occur by autoproteolysis due to the clustering of procaspase-8 at the DISC (19, 20).

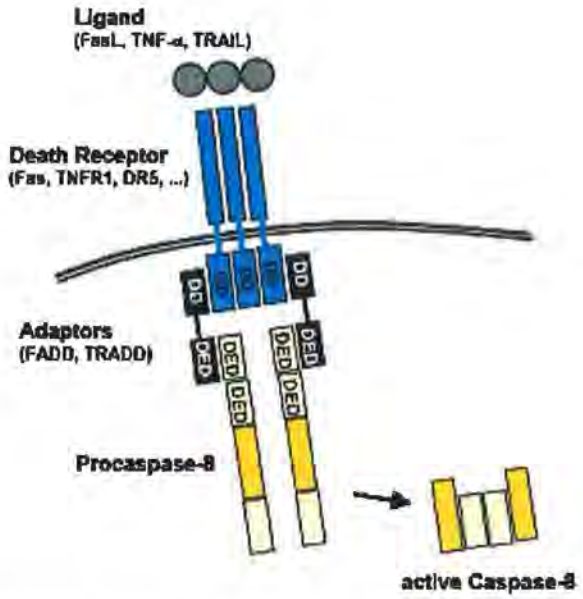

Figure 5.1 Receptor mediated activation of caspase-8 at the death inducing signalling complex (DISC) (21)

Activation of the intrinsic pathway is dependent on the release of a mitochondrial intra-membrane space protein, cytochrome c. The release of cytochrome c is tightly regulated by the Bcl-2 family of proteins (22). This family consists of pro and anti apoptotic proteins that actively participate in the demise (Bid, Bax, Bak) or maintenance (Bcl-2, Bcl-$_{xL}$) of the mitochondrial membrane integrity, the functions of which are reviewed elsewhere (23-26). In response to death inducing stimuli, the pro-apoptotic proteins (Bid, Bax, Bak) are up-regulated, overcoming the inhibiting effects of the anti-apoptotic proteins (Bcl-2, Bcl-$_{xL}$), thus resulting in mitochondrial membrane permeablisation and cytochrome c release. When released, cytochrome c binds to the cytosolic protein

apoptotic protease activating factor-1 (Apaf-1) (16). This interaction results in an adenine triphosphate (ATP)-dependent conformational change in Apaf-1 which, allows 7 molecules of Apaf-1 to associate with each other forming a multi-protein complex known as the apoptosome (27, 28), see figure 5.2. This wheel-like structure recruits inactive procaspase-9 which is then cleaved to form activated caspase-9. Thus, once activated, initiator caspases proteolytically activate effector caspases, such as caspase-3, which serve to mediate and amplify the death signal that ultimately results in the demise of the cell (16, 17).

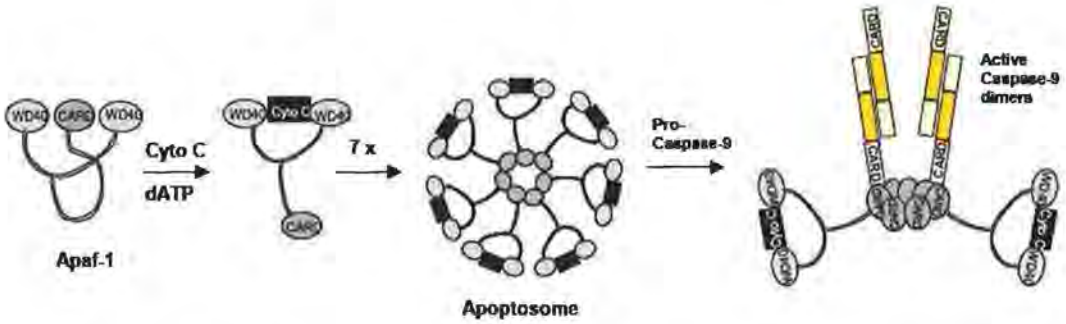

Figure 5.2 Formation of the apoptosome and activation caspase-9 (21)

In this study, apoptotic induction was measured in terms of caspase-3/7 activity since both the intrinsic and extrinsic pathways converge at caspase-3 activation (14). The assay employed measures the activity of both effector caspases-3 and -7 (29) since there is a high level of functional redundancy between these two effector caspases (20). Although mitochondrial membrane permeablisation is largely associated with the intrinsic pathway, the ability of solar simulated radiation to incur losses in mitochondrial membrane potential (MMP) was investigated since UVB radiation has been predominantly associated with the intrinsic pathway (30).

5.2 Methods

5.2.1 alamarBlue™ cell viability assay

Cells were seeded in clear plastic 96 well dishes at densities of 10,000 and 5,000 cells per well for the 24 and 48 hour post exposure analysis respectively. Cells were exposed without lids in the Q-sun solar simulator in either 200 µl DMEM-F12 or 200 µl PBS. Prior to PBS exposures, the medium covering cells was discarded, the cells washed twice with 100 µl PBS per well, the washes discarded and 200 µl fresh PBS per well added prior to exposure. Post irradiation, the exposed PBS was discarded and 200µl fresh cell culture medium re-added. All samples were re-incubated post exposure. At 21 and 45 hours post exposure, samples were washed twice with 100 µl PBS per well and treated with 100 µl 5% v/v alamarBlue™ solution (1/20 dilution of alamarBlue™ solution (Biosource, Camarillo CA, USA) in phenol free DMEM-F12 cell culture medium, see appendix 2 for reconstitution procedure) per well and incubated for 3 hours. Using a Tecan GENios plate reader, the fluorescence was measured using excitation and emission wavelengths of 540 nm and 595 nm respectively.

5.2.2 Caspase-3/7 activity

Promega multiplexing CellTiter-Blue® and Caspase-Glo® 3/7 assay kits were employed. These assays permit cell viability and caspase 3/7 activity to be determined in the same cell populations post treatment. Cells were seeded at 10,000 cells per well in opaque white walled 96 well plates 16 hours prior to irradiation. Cells were irradiated in either DMEM-F12 or PBS.

The assay protocols recommend adding the CellTiter-Blue® and Caspase-Glo® reagents to the medium covering cells at ratios of 1:5 and 1:1 respectively for maximum sensitivity. Thus, the volume of medium covering cells post irradiation is an important parameter to consider for the DMEM-F12 exposures. Based on the number of independent tests and replicates per independent test using the recommended 100 µl Caspase-Glo® reagent per well, a volume of 84 µl of DMEM-F12 post exposure was desirable. Prior to experimentation, it was found that 90, 95 and 105 µl DMEM-F12 per well resulted in, on average, 84 µl DMEM-F12 post exposure when irradiated for 2, 5 and 10 minutes respectively due to radiation induced evaporation. Thus, prior to both PBS and DMEM-F12 exposures, the medium covering cells during the 16 hour incubation was discarded. For DMEM-F12 exposures, the cells were not washed and either 84, 90, 95 or 105 µl DMEM-F12 per well was added to plates denoted for sham, 2 minute, 5 minute or 10 minute irradiations respectively. Immediately post exposure, 16.8 µl (16.8:84 = 1:5) CellTiter-Blue® reagent per well was added to cells giving a final volume of 100.8 µl. For PBS exposures, cells were washed twice in 100 µl PBS, the washes discarded and the cells irradiated in 200 µl fresh PBS. Immediately post exposure, the PBS was discarded and 84 µl DMEM-F12 and 16.8 µl CellTiter-Blue® reagent per well was added to cells also giving a final volume of 100.8 µl. Cells were incubated with the CellTiter-Blue® reagent for 1 hour. After 1 hour, the fluorescence was read using the Tecan GENios plate-reader with excitation and emission filters peaking at 540 nm and 595 nm respectively. Immediately after the fluorescence was read, 100.8 µl ((84 + 16.8):100.8 = 1:1) Caspase-Glo® reagent was added per well and incubated for 1 hour after which the luminescence was read using the Tecan GENios plate-reader with an integration time of 1 second.

The time at which the Caspase-Glo® reagent was added to cells post irradiation was optimised using a 5 minute exposure in DMEM-F12 since this was the minimum exposure duration at which cell death was observed. The manufacturers (Promega) recommend allowing an incubation time of 1-2 hours with the CellTiter-Blue® reagent, the fluorescence of which is measured before caspase activity dependent luminescence. Thus, the earliest point at which the Caspase-Glo® reagent could be added was 1 hour post irradiation which allows a 1 hour CellTiter-Blue® incubation when added immediately post exposure. Luminescence increases with caspase activity, table 5.1 shows the fold increase over controls in luminescence at different times post irradiation for cells exposed for 5 minutes in DMEM-F12 and the corresponding cell viability. Based on these results, cells were assayed for viability and caspase activity 1 and 2 hours post exposure respectively for all exposures in both DMEM-F12 and PBS.

Table 5.1 Kinetics study results to optimise the time post irradiation at which caspase-3/7 would be measured

Time point	Cell viability fluorescence			Caspase 3/7 activity luminescence		
(Fl & Lum)	Ctrl	5min	Ratio (5min/Ctrl)	Ctrl	5min	Ratio (5min/Ctrl)
1 & 2hr	38853.8	31902.2	0.82	100.3	240.5	2.4
3 & 4hr	42608.0	32364.7	0.76	104.8	187.8	1.8
5 & 6hr	58426.2	43088.8	0.74	153.2	261.3	1.7

5.2.3 Mitochondrial membrane potential

Cells were seeded on glass bottomed Petri dishes at a density of 20,000 cells per dish, cells were plated on the glass inserts at a volume of 150-220 µl and allowed to adhere for 2-3 hours before 3 ml of cell culture medium was added and samples incubated overnight. Samples were exposed in the Q-sun solar simulator in either 3 ml cell culture medium or 3 ml PBS without lids. For samples exposed in PBS, cell culture medium was removed prior to exposure, filtered and stored. Samples were washed once in 1 ml PBS, the wash discarded and 3 ml fresh PBS added to the samples. Immediately post exposure, the exposed PBS was discarded and 3 ml stored cell culture medium re-added to samples. All samples were incubated at 37°C post exposure until their respective time points. Twenty minutes prior to each time point, samples were washed twice in 0.5 ml PBS with 1mM $CaCl_2$ / $MgCl_2$ (see appendix 2), washes discarded and incubated with 1 ml 5 µM rhodamine 123 (Sigma) for 20 minutes. After dye incubation, samples were washed three times with 0.5 ml PBS with 1mM $CaCl_2$ / $MgCl_2$, washes discarded and 1ml fresh PBS with 1mM $CaCl_2$ / $MgCl_2$ added to each sample. Confocal microscopy was employed to measure the fluorescence of rhodamine 123 in conjunction with LSM510 software. The dye was excited at 488 nm with an argon ion laser and using an emission filter, fluorescent emissions were recorded at 520 nm.

5.2.4 Statistics

Results represent a minimum of 3 independent tests unless otherwise stated, with a minimum of 2 replicates per independent test. Data was log transformed and ANOVA was performed on the linear regressions and pair-wise data were computed using the

Bonferroni adjustment. Data are presented as the LSM ± 95CI. All analyses were done using statistical software package SAS 9.1 and SAS enterprise guide 3.0. Significance was taken at a level of $p \leq 0.05$.

5.3 Results and discussion

Resazurin is a non-fluorescent blue indicator dye that is reduced by metabolically active cells to the highly fluorescent pink compound, Resorufin (31). Both the alamarBlue™ and CellTiter-Blue® assays are commercial preparations of Resazurin which allows the innate metabolic activity of viable cells to be monitored through their capacity to reduce resazurin to resorufin. Although the capacity of cells to reduce resazurin has been linked to electron transport chain modifications (32), Gonzalez et al (33) found cytosolic and microsomal enzymes, as well as mitochondrial enzymes, capable of catalysing the reduction of resazurin and thus, advise against interpreting losses in viability solely as mitochondrial damage.

Figures 5.3 and 5.4 illustrate the viability of cells irradiated in DMEM-F12 and PBS respectively as measured using the alamarBlue™ viability assay. Cell viability was assessed 24 and 48 hours post exposure for both exposure media. Both the DMEM-F12 and PBS results exhibit a dose-dependent loss in viability 24 hours post exposure, with further losses experienced 48 hours post exposure. Examining the 10 minute exposure point for both PBS and DMEM-F12 shows that a 10 minute exposure in PBS is not significantly different to controls 24 or 48 hours post exposure, while a 10 minute exposure in DMEM-F12 can be seen to be significantly reduced with respect to controls at 48 hours post exposure. This concurs with the dose response data shown in figure 3.2 in chapter 3.

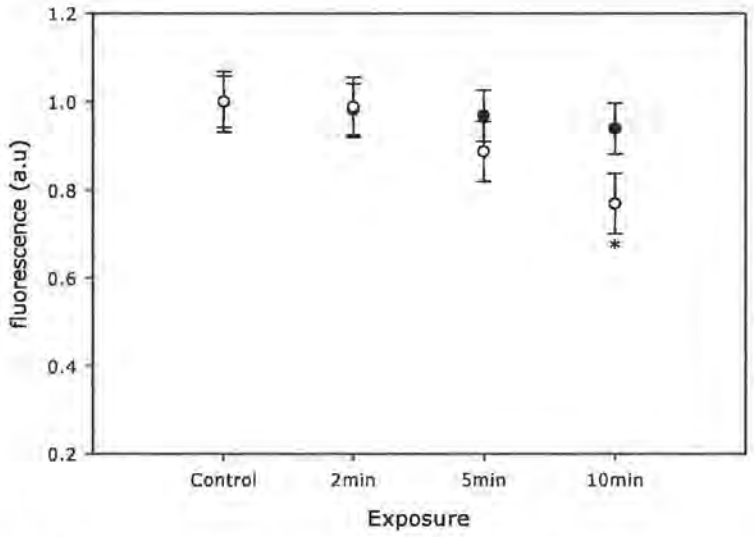

Figure 5.3 HaCaT cells irradiated in DMEM-F12 using the Q-sun solar simulator and cell viability measured 24 hours (●) and 48 hours (○) post exposure using the alamarBlue™ cell viability assay, data is presented as the LSM ± 95CI computed using ANOVA on the log transformed data, * significantly different to control ($p \leq 0.05$).

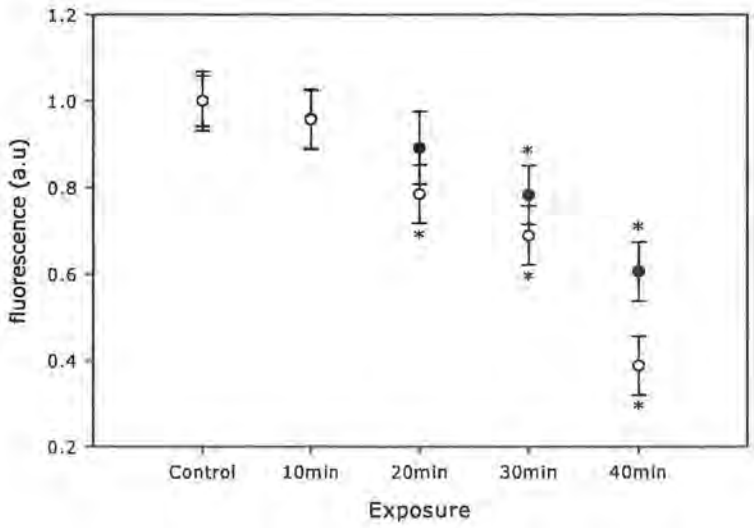

Figure 5.4 HaCaT cells irradiated in PBS using the Q-sun solar simulator and cell viability measured 24 hours (●) and 48 hours (○) post exposure using the alamarBlue™ cell viability assay, data is presented as the LSM ± 95CI computed using ANOVA on the log transformed data, * significantly different to control ($p \leq 0.05$).

The CellTiter-Blue® viability assay was multiplexed with the Caspase-Glo® 3/7 assay 1 and 2 hours post irradiation respectively, thus enabling cell viability and caspase-3/7 activity to be monitored in the same cell populations. Figures 5.5 and 5.6 show the viability and caspase activity for cells irradiated in DMEM-F12 and PBS respectively. Cells irradiated in DMEM-F12 clearly demonstrate a dose dependent increase in caspase-3/7 activity with a corresponding decrease in cell viability as would be expected in a population of cells undergoing apoptosis. Interestingly, cells irradiated in PBS do not exhibit any changes in viability or caspase-3/7 activity with respect to controls, even when irradiated for 60 minutes.

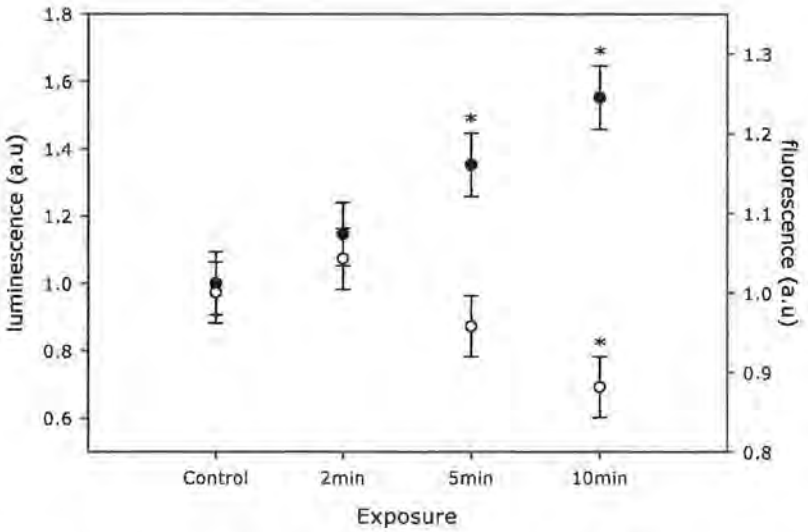

Figure 5.5 Multiplexed assay data showing caspase-3/7 activity (●) and cell viability (○) measured as luminescence and fluorescence in the same cell populations 1 and 2 hours post Q-sun irradiation in DMEM-F12 respectively, data is presented as the LSM ± 95CI computed using ANOVA on the log transformed data, * significantly different to control ($p \leq 0.05$).

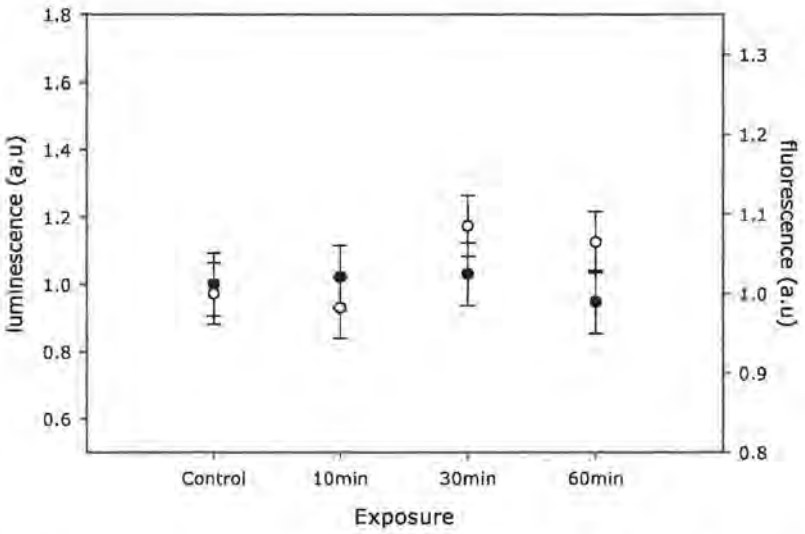

Figure 5.6 Multiplexed assay data showing caspase-3/7 activity (●) and cell viability (○) measured as luminescence and fluorescence in the same cell populations 1 and 2 hours post Q-sun irradiation in PBS respectively, data is presented as the LSM ± 95CI computed using ANOVA on the log transformed data, * significantly different to control ($p \leq 0.05$).

UVB radiation has been surmised to induce apoptosis predominately through the intrinsic pathway (30). A key event in the intrinsic pathway is MMP depolarisation (34). The fluorescent probe rhodamine 123 was employed to determine the effect(s), if any, that solar simulated radiation may have on MMP, since rhodamine 123 has long been known to specifically stain intact mitochondrial membranes (35). If the integrity of the mitochondrial membrane is compromised, then rhodamine 123 will fail to stain the damaged mitochondria which will be reflected as a loss in fluorescence with respect to unirradiated controls.

Figure 5.5A, B and C show the MMP results when cells are irradiated for 2, 5 and 10 minutes in DMEM-F12 respectively, and analysed at various times post exposure. Time-matched sham irradiated controls were included for each exposure duration where all time-matched controls were found to be not significantly different to one another.

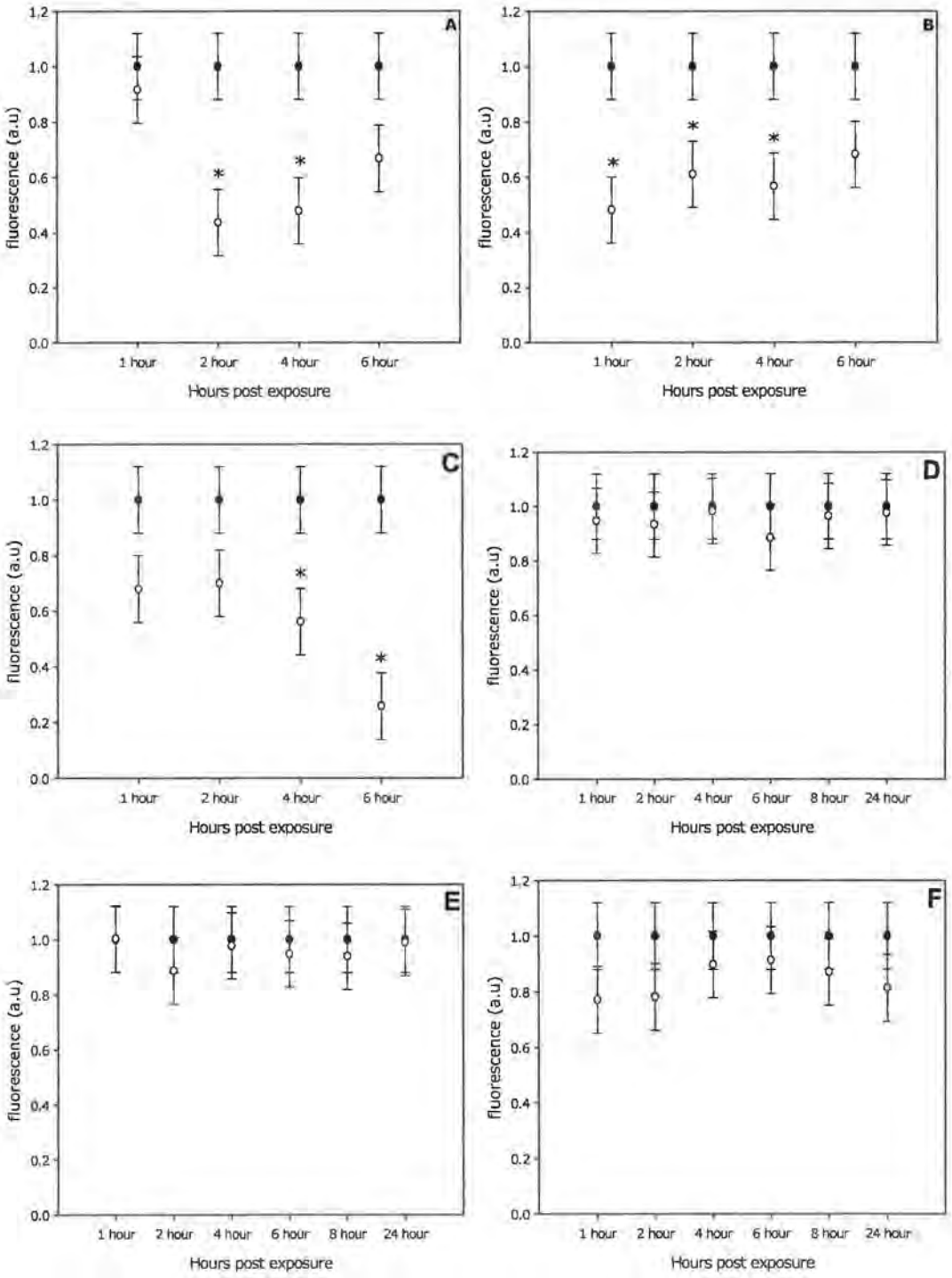

Figure 5.7 HaCaT cells irradiated for 2 (A), 5 (B) and 10 (C) minutes in DMEM-F12 or for 10 (D), 30 (E) and 60 (F) minutes in PBS using the Q-sun solar simulator. The mitochondrial membrane potential was measured at different time points post exposure, time matched controls (●) were run simultaneously with irradiated samples (○). Data is presented as the LSM ± 95CI computed using ANOVA on the log transformed fluorescence data, * significantly different to time matched control ($p \leq 0.05$).

With the exception of the 2 minute DMEM-F12 exposure analysed 1 hour post exposure (figure 5.5A), irradiating HaCaT cells in DMEM-F12 for 2 and 5 minutes resulted in a significant loss in MMP post exposure with respect to time matched controls. This significant loss in MMP was found to be transient since the loss in MMP 6 hours post irradiation for both the 2 and 5 minute exposures were found to be not significantly different to their respective time matched controls. Conversely, the MMP of cells irradiated for 10 minutes in DMEM-F12 was found to decrease in a time dependent manner over the 6 hour interval analysed post exposure. In stark contrast to the DMEM-F12 results, analysis of the MMP in cells irradiated in PBS show that these cells, irrespective of the exposure duration, do not experience a loss in MMP with respect to controls for at least 24 hours post irradiation, (figure 5.5D-F).

The DMEM-F12 results suggest that cells irradiated in DMEM-F12 with solar simulated radiation experience a loss in MMP within the first 2 hours post exposure, irrespective of the exposure duration. After this, depending on the extent of the insult, the MMP either recovers or further losses are incurred. These events may, in part, be related to the association between cytochrome c and cardiolipin, a membrane lipid predominantly found in the mitochondria (36, 37). An electrostatic attractive force exists between cytochrome c and cardiolipin which must be disrupted in order for cytochrome c to be released (38, 39). Oxidative stress has been shown to be capable of mediating this dissociation (40) where both UVA and UVB radiation have been shown to increase oxidative stress in human keratinocytes (41, 42). In chapter 4, evidence that strongly implicates hydrogen peroxide in DMEM-F12 mediated cell death was presented. The ability of catalase to inhibit cell death implies that the hydrogen peroxide generated is predominantly extracellular. However, the smaller yet still significant

increases in survival observed with GSH, which is readily taken up by cells (8), may be indicative of intracellular ROS quenching. Thus, it is possible that solar simulated radiation generates intracellular ROS in a dose dependent manner which in turn regulates the dissociation of cytochrome c from cardiolipin. Although the release of cytochrome c has been shown to be a complete, enzyme-independent and rapid event occurring within 5 minutes of initiation irrespective of the type or strength of apoptotic stimulus, the time elapsed between apoptotic stimulation and cytochrome c release was found to vary (43). While such temporal discrepancies have recently been reported to be a complex balance between caspase-3 initiators and inhibitors (15), it could be reasoned that a threshold level of damaging agents, such as ROS, is required to tip the balance in favour of apoptotic induction including cardiolipin dissociation and the subsequent release of cytochrome c. Thus, it could be that all three DMEM-F12 exposures (2, 5 and 10 minutes) generate sufficient damage to compromise the integrity of the MMP but only the 5 and 10 minute exposures attain the threshold level required to initiate the demise of the cardiolipin-cytochrome c association. The work of Garg and Chang (44) supports this hypothesis. They observed that the level of intracellular ROS generated in cells treated with hydrogen peroxide saturated at a concentration of 0.5 mM hydrogen peroxide where further increases in the concentration of hydrogen peroxide did not result in further increases in the level of intracellular ROS generated. However, cell death was not observed unless a concentration of $\geq$ 1 mM hydrogen peroxide was employed. They also observed that cells degrade hydrogen peroxide at a constant rate, reducing the concentration of hydrogen peroxide by 50% within one hour. Thus, they concluded that the discrepancy between the concentrations of hydrogen peroxide required to incur cell death and saturation of intracellular ROS generated was due to the fact that at a fixed cell density higher concentrations of hydrogen peroxide were better

maintained due to fixed degradation rates in cultures (44). Furthermore, this conjecture compliments both the caspase-3/7 activity in figure 5.5 and the cell survival results presented in figure 3.4, where both the 5 and 10 but not the 2 minute exposures were found to be significantly different to controls.

Although this model agrees with the review by Assefa et al (30), who found that the literature strongly implicates the intrinsic pathway in UVB mediated apoptosis, the predominant UV waveband in solar simulated radiation is UVA which is believed to elicit its effects predominantly through oxidative stress (45). Thus, due to the production of extracellular hydrogen peroxide in DMEM-F12 upon irradiation and the strong presence of UVA radiation in solar simulated radiation, it is possible that apoptosis is concurrently or predominantly induced via the death receptor mediated extrinsic pathway.

The extrinsic pathway can also incur losses in MMP via caspase-8 mediated activation of the pro-apoptotic Bcl-2 family member Bid (46, 47). Once cleaved, the truncated form of Bid (tBid) relocates to the mitochondria (48) where it facilitates outer membrane pore formation via Bax/Bak oligomerisation (49). In addition, tBid has also been reported to facilitate cytochrome c release by direct binding to cardiolipin at mitochondrial contact sites (50). Although it has been reported that tBid is not required for Bax translocation during UV induced apoptosis, the irradiator employed in these studies was a UVC lamp emitting at 254 nm (51, 52). As discussed in chapter 1, the absorption spectrum of DNA peaks at ~ 260 nm (53). Thus, DNA is a potent chromophore for this environmentally irrelevant wavelength (254 nm) and as such, it would not be unreasonable to expect significantly different responses to that which

would be incurred by environmentally relevant wavelengths which are poorly absorbed by DNA in comparison to 254 nm.

Alternatively, it could be that mitochondrial membrane permeablisation facilitates the efflux of intra-membrane space proteins other than cytochrome c, such as Smac/Diablo, apoptosis inducing factor (AIF) and endonuclease G (endoG), whose function(s) may be integral to the initiated response. For example, Smac/Diablo functions by binding to the inhibitors of apoptosis proteins (IAPs), which in the absence of Smac/Diablo inhibit caspases-3, -7 and -9 (54) while AIF and endoG function to induce caspase-independent cell death (55).

Mitochondrial membrane permeablisation, which is associated with the dissipation of MMP, is considered the point at which a cell irreversibly commits to apoptosis (56). Thus, the apparent recovery of MMP post irradiation in cells irradiated in DMEM-F12 may be an artefact of an insufficient number of replicates. The statistical data presented was derived from just 2 independent tests from which 3 different areas were imaged per independent experiment, and the fluorescence intensity of 10 individual cells per image was measured. Although further replicates would be desirable to increase the power of these observations, it is unlikely that the Bonferroni statistical adjustment resulted in false positives in the significance between groups since its conservative corrections has been reported to lead to the opposite problem, increasing false negative rates, but only when the number of tests exceeds a few hundred (57). Although cytochrome c has been speculated to re-enter the inter membrane space after it has exited (43) which may serve to prevent mitochondrial dysfunction by enabling oxidative phosphorylation to continue, it was also speculated that maintenance of this metabolic pathway is done so

primarily to fuel the ATP dependent processes involved in apoptosis (43). Furthermore, once the mitochondrial outer membrane is permeablised, proteins involved in caspase-independent cell death pathways are also released and should, in the absence of caspase activity, ensure the demise of the cell. However, in a study examining the effects of hydrogen peroxide on cardiac myocytes, Cook et al (58) found that treated cell populations experienced an early loss in MMP which was restored but then subsequently lost again. Cook et al (58) speculated that this effect is due to two distinct cell death events. They proposed that the initial loss and subsequent recovery in MMP may be indicative of a subpopulation of cells undergoing rapid cell death. Such cells would not be present in the cell populations examined at the later time points due to loss of adhesion and cell washes which could present as a recovery in MMP if the remaining cells are less damaged than the initial subpopulation. Although, the time interval (3 hours) over which Cook et al (58) observed these effects is substantially different to the time interval examined here, it is possible that if the MMP analysis for cells irradiated in DMEM-F12 was extended to later time points, that further reductions in MMP would be observed.

Most of the conjectures presented above, however, do not appear to be applicable to cells irradiated in PBS. The absence of caspase activity in PBS irradiated cells implicates necrosis and / or caspase-independent cell death pathways. However, the alamarBlue™ results undermine the possibility that necrosis is the predominant form of cell death since cells irradiated in PBS were found to be viable 24 and 48 hours post irradiation. Furthermore, MMP dissipation has been observed in necrotic cells (59). Mitochondrial membrane permeablisation is essential for the release of proteins involved in caspase-independent cell death (55) and since the alamarBlue™ results

indicate that cell death does occur within 24 hours, this eliminates caspase-independent cell death pathways.

Caspase-3 activation in human keratinocytes has been reported to occur from 4 to as much as 12 hours post UV irradiation (60-62). Thus, the apparent lack of caspase-3/7 activation in cells irradiated in PBS may merely be a temporal issue. Caspase-3/7 activity was measured 2 hours post irradiation in this study. This time point was based on the optimal activity observed in a kinetics study of caspase-3/7 activity in cells irradiated for 5 minutes in DMEM-F12. The kinetics of caspase-3/7 activity was optimised using a 5 minute DMEM-F12 exposure because this was found to be the shortest exposure duration at which cell death was observed to be significantly different to controls. However, it appears as though optimising caspase activity based on the minimum exposure duration required to elicit cell death and not the exposure medium fails to account for potentially different induction mechanisms or at least temporal differences in capase-3/7 activation. Since cytochrome c release has been observed in UV irradiated human keratinocytes in the absence of MMP dissipation (4), it is quite possible that caspase-3 is activated in PBS irradiated cells later than 2 hours post exposure. Alternatively, caspase-12 has been shown to be a direct activator of caspase-9 in the absence of cytochrome c release (63) where activation of caspase-9 has been shown to be necessary for UVB radiation induced apoptosis in human keratinocytes (64).

5.4 Conclusions

While the results presented in this chapter do not clarify which pathway(s) are triggered in response to solar simulated radiation, they clearly demonstrate that under identical exposure parameters, the response of cells irradiated in DMEM-F12 and PBS are significantly different. Whether the differences observed are merely temporal differences in the same pathway(s) or that different pathways are triggered that are dependent on the exposure media employed is unknown at present and requires further investigation.

5.5 References

(1) K. M. d. Lima-Bessa, M. G. Armelini, V. Chigançcas, J. F. Jacysyn, G. P. Amarante-Mendes, A. Sarasin & C. F. M. Menck (2008) Cpds and 6-4pps play different roles in uv-induced cell death in normal and ner-deficient human cells *DNA Repair* **7,** 303-312.

(2) J.-Y. Bae, J.-S. Choi, Y.-J. Choi, S.-Y. Shin, S.-W. Kang, S. J. Han & Y.-H. Kang (2008) (-)epigallocatechin gallate hampers collagen destruction and collagenase activation in ultraviolet-b-irradiated human dermal fibroblasts: Involvement of mitogen-activated protein kinase *Food and Chemical Toxicology* **46,** 1298-1307.

(3) Y.-T. Han, Z.-W. Han, G.-Y. Yu, Y.-J. Wang, R.-Y. Cui & C.-B. Wang (2004) Inhibitory effect of polypeptide from chlamys farreri on ultraviolet a-induced oxidative damage on human skin fibroblasts in vitro *Pharmacological Research* **49,** 265-274.

(4) M. F. Denning, Y. Wang, S. Tibudan, S. Alkan, B. J. Nickoloff & J. Z. Qin (2002) Caspase activation and disruption of mitochondrial membrane potential during uv radiation-induced apoptosis of human keratinocytes requires activation of protein kinase c *Cell Death Differentation* **9,** 40-52.

(5) L. C. DeVeaux, L. S. Durtschi, J. G. Case & D. P. Wells (2006) Bystander effects in unicellular organisms *Mutation Research/Fundamental and Molecular Mechanisms of Mutagenesis* **597,** 78-86.

(6) J. D. Stoien & R. J. Wang (1974) Effect of near-ultraviolet and visible light on mammalian cells in culture ii. Formation of toxic photoproducts in tissue culture medium by blacklight *Proceedings of the National academy of Sciences* **71,** 3961-5.

(7) G. Banerjee, N. Gupta, A. Kapoor & G. Raman (2005) Uv induced bystander signaling leading to apoptosis *Cancer Letters* **223,** 275-84.

(8) J. Dahle, E. Kvam & T. Stokke (2005) Bystander effects in uv-induced genomic instability: Antioxidants inhibit delayed mutagenesis induced by ultraviolet a and b radiation *Journal of Carcinogenesis* **4,** 11.

(9) H. Yamada, M. Murata, K. Suzuki & S. Koizumi (2004) Ultraviolet irradiation increases the sensitivity of cultured human skin cells to cadmium probably through the inhibition of metallothionein gene expression *Toxicology and Applied Pharmacology* **200,** 251-257.

(10) J. P. O'Reilly & C. Mothersill (1997) Comparative effects of uv a and uv b on clonogenic survival and delayed cell death in skin cell lines from humans and fish *International Journal of Radiation Biology* **72,** 111-119.

(11) N. Azzam & A. Dovrat (2004) Long-term lens organ culture system to determine age-related effects of uv irradiation on the eye lens *Experimental Eye Research* **79,** 903-911.

(12) A. Degterev & J. Yuan (2008) Expansion and evolution of cell death programmes *Nat Rev Mol Cell Biol* **9,** 378-390.

(13) M. Henriquez, R. Armisen, A. Stutzin & A. F. Quest (2008) Cell death by necrosis, a regulated way to go *Curr Mol Med* **8,** 187-206.

(14) S. Elmore (2007) Apoptosis: A review of programmed cell death *Toxicol Pathol* **35,** 495-516.

(15) J. G. Albeck, J. M. Burke, B. B. Aldridge, M. Zhang, D. A. Lauffenburger & P. K. Sorger (2008) Quantitative analysis of pathways controlling extrinsic apoptosis in single cells *Mol Cell* **30,** 11-25.

(16) K. M. Boatright & G. S. Salvesen (2003) Mechanisms of caspase activation *Curr Opin Cell Biol* **15,** 725-31.

(17) K. C. Zimmermann, C. Bonzon & D. R. Green (2001) The machinery of programmed cell death *Pharmacol Ther* **92,** 57-70.

(18) M. E. Wright, D. K. Han & D. M. Hockenbery (2000) Caspase-3 and inhibitor of apoptosis protein(s) interactions in saccharomyces cerevisiae and mammalian cells *FEBS Letters* **481,** 13-18.

(19) J. B. Denault & G. S. Salvesen (2002) Caspases: Keys in the ignition of cell death *Chem Rev* **102,** 4489-500.

(20) M. Lamkanfi & T.-D. Kanneganti (2010) Caspase-7: A protease involved in apoptosis and inflammation *The International Journal of Biochemistry & Cell Biology* **42,** 21-24.

(21) A. Gewies (2003) Introduction to apoptosis http://www.celldeath.de/encyclo/aporev/aporev.htm March 12th 2010.

(22) D. G. Breckenridge & D. Xue (2004) Regulation of mitochondrial membrane permeabilization by bcl-2 family proteins and caspases *Curr Opin Cell Biol* **16,** 647-52.

(23) E. Er, L. Oliver, P. F. Cartron, P. Juin, S. Manon & F. M. Vallette (2006) Mitochondria as the target of the pro-apoptotic protein bax *Biochim Biophys Acta* **1757,** 1301-11.

(24) M. Certo, V. Del Gaizo Moore, M. Nishino, G. Wei, S. Korsmeyer, S. A. Armstrong & A. Letai (2006) Mitochondria primed by death signals determine cellular addiction to antiapoptotic bcl-2 family members *Cancer Cell* **9,** 351-65.

(25) T. Kuwana & D. D. Newmeyer (2003) Bcl-2-family proteins and the role of mitochondria in apoptosis *Curr Opin Cell Biol* **15,** 691-9.

(26) S. Desagher & J. C. Martinou (2000) Mitochondria as the central control point of apoptosis *Trends Cell Biol* **10,** 369-77.

(27) C. Pop, J. Timmer, S. Sperandio & G. S. Salvesen (2006) The apoptosome activates caspase-9 by dimerization *Molecular Cell* **22,** 269-275.

(28) Z. T. Schafer & S. Kornbluth (2006) The apoptosome: Physiological, developmental, and pathological modes of regulation *Developmental Cell* **10,** 549-561.

(29) Promega (2009), pp. 1-18.

(30) Z. Assefa, A. Van Laethem, M. Garmyn & P. Agostinis (2005) Ultraviolet radiation-induced apoptosis in keratinocytes: On the role of cytosolic factors *Biochimica et Biophysica Acta - Reviews on Cancer* **1755,** 90-106.

(31) S. Anoopkumar-Dukie, J. B. Carey, T. Conere, E. O'Sullivan, F. N. van Pelt & A. Allshire (2005) Resazurin assay of radiation response in cultured cells *Br J Radiol* **78,** 945-7.

(32) K. Schirmer, J.-A. Herbrick, S. , B. Greenberg, M. , G. Dixon, D. & N. Bols, C. (1999) Use of fish gill cells in culture to evaluate the cytotoxicity and photocytotoxicity of intact and photomodified creosote *Environmental Toxicology and Chemistry* **18,** 1277-1288.

(33) R. J. Gonzalez & J. B. Tarloff (2001) Evaluation of hepatic subcellular fractions for alamar blue and mtt reductase activity *Toxicol In Vitro* **15,** 257-9.

(34) O. T. Hermida, K. W. Kinnally & L. M. Dejean (2009) Bcl-2 does not inhibit bax insertion during intrinsic apoptosis *Biophysical Journal* **96,** 530a-530a.

(35) L. V. Johnson, M. L. Walsh & L. B. Chen (1980) Localization of mitochondria in living cells with rhodamine 123 *Proceedings of the National Academy of Sciences of the United States of America* **77,** 990-994.

(36) R. F. Epand, U. Schlattner, T. Wallimann, M.-L. Lacombe & R. M. Epand (2007) Novel lipid transfer property of two mitochondrial proteins that bridge the inner and outer membranes *Biophysical Journal* **92,** 126-137.

(37) Z. T. Schug & E. Gottlieb (2009) Cardiolipin acts as a mitochondrial signalling platform to launch apoptosis *Biochimica et Biophysica Acta (BBA) - Biomembranes* **1788,** 2022-2031.

(38) S. L. Iverson & S. Orrenius (2004) The cardiolipin-cytochrome c interaction and the mitochondrial regulation of apoptosis *Archives of Biochemistry and Biophysics* **423,** 37-46.

(39) G. Perkins, E. Bossy-Wetzel & M. H. Ellisman (2009) New insights into mitochondrial structure during cell death *Experimental Neurology* **218,** 183-192.

(40) G. Petrosillo, F. M. Ruggiero, M. Pistolese & G. Paradies (2001) Reactive oxygen species generated from the mitochondrial electron transport chain induce cytochrome c dissociation from beef-heart submitochondrial particles via cardiolipin peroxidation. Possible role in the apoptosis *FEBS Letters* **509,** 435-438.

(41) A. Svobodová, A. Zdarilová, D. Walterová & J. Vostálová (2007) Flavonolignans from silybum marianum moderate uva-induced oxidative damage to hacat keratinocytes *Journal of Dermatological Science* **48,** 213-224.

(42) D. Kovacs, S. Raffa, E. Flori, N. Aspite, S. Briganti, G. Cardinali, M. R. Torrisi & M. Picardo (2009) Keratinocyte growth factor down-regulates intracellular ros production induced by uvb *Journal of Dermatological Science* **54,** 106-113.

(43) J. C. Goldstein, N. J. Waterhouse, P. Juin, G. I. Evan & D. R. Green (2000) The coordinate release of cytochrome c during apoptosis is rapid, complete and kinetically invariant *Nat Cell Biol* **2,** 156-62.

(44) T. K. Garg & J. Y. Chang (2004) 15-deoxy-delta 12, 14-prostaglandin j2 prevents reactive oxygen species generation and mitochondrial membrane depolarization induced by oxidative stress *BMC Pharmacol* **4,** 6.

(45) M. Schauen, H.-T. Hornig-Do, S. Schomberg, G. Herrmann & R. J. Wiesner (2007) Mitochondrial electron transport chain activity is not involved in ultraviolet a (uva)-induced cell death *Free Radical Biology and Medicine* **42,** 499-509.

(46) J. Skommer, D. Wlodkowic & A. Deptala (2007) Larger than life: Mitochondria and the bcl-2 family *Leukemia Research* **31,** 277-286.

(47) H. Li, H. Zhu, C.-j. Xu & J. Yuan (1998) Cleavage of bid by caspase 8 mediates the mitochondrial damage in the fas pathway of apoptosis *Cell* **94,** 491-501.

(48) J. F. Lovell, L. P. Billen, S. Bindner, A. Shamas-Din, C. Fradin, B. Leber & D. W. Andrews (2008) Membrane binding by tbid initiates an ordered series of events culminating in membrane permeabilization by bax *Cell* **135,** 1074-1084.

(49) A. V. Vaseva & U. M. Moll (2009) The mitochondrial p53 pathway *Biochimica et Biophysica Acta (BBA) - Bioenergetics* **1787,** 414-420.

(50) T.-H. Kim, Y. Zhao, W.-X. Ding, J. N. Shin, X. He, Y.-W. Seo, J. Chen, H. Rabinowich, A. A. Amoscato & X.-M. Yin (2004) Bid-cardiolipin interaction at mitochondrial contact site contributes to mitochondrial cristae reorganization and cytochrome c release *Mol. Biol. Cell* **15,** 3061-3072.

(51) Y. Wu, D. Xing, W. R. Chen & X. Wang (2007) Bid is not required for bax translocation during uv-induced apoptosis *Cell Signal* **19,** 2468-78.

(52) Y. Wu, D. Xing, L. Liu & B. Gao (2008) Regulation of bax activation and apoptotic response to uv irradiation by p53 transcription-dependent and -independent pathways *Cancer Letters* **271,** 231-239.

(53) I. Atsushi & I. Takashi (1986) Absorption spectra of deoxyribose, ribosephosphate, atp and DNA by direct transmission measurements in the vacuum-uv (150—190 nm) and far-uv (190—260 nm) regions using synchrotron radiation as a light source *Photochemistry and Photobiology* **44,** 355-358.

(54) B. A. Abhari & J. Davoodi (2008) A mechanistic insight into smac peptide interference with xiap-bir2 inhibition of executioner caspases *Journal of Molecular Biology* **381,** 645-654.

(55) M. Donovan & T. G. Cotter (2004) Control of mitochondrial integrity by bcl-2 family members and caspase-independent cell death *Biochimica et Biophysica Acta (BBA) - Molecular Cell Research* **1644,** 133-147.

(56) D. R. Green & G. Kroemer (2005) Pharmacological manipulation of cell death: Clinical applications in sight? *The Journal of Clinical Investigation* **115,** 2610-2617.

(57) T. K. Rice, N. J. Schork, D. C. Rao & D. C. R. a. C. C. Gu (2008) in *Advances in genetics* (Academic Press, Vol. Volume 60, pp. 293-308.

(58) S. A. Cook, P. H. Sugden & A. Clerk (1999) Regulation of bcl-2 family proteins during development and in response to oxidative stress in cardiac myocytes : Association with changes in mitochondrial membrane potential *Circ Res* **85,** 940-949.

(59) A. Szigeti, S. Bellyei, B. Gasz, A. Boronkai, E. Hocsak, O. Minik, Z. Bognar, G. Varbiro, B. Sumegi & F. Gallyas Jr (2006) Induction of necrotic cell death and mitochondrial permeabilization by heme binding protein 2/soul *FEBS Letters* **580,** 6447-6454.

(60) H. Shimizu, Y. Banno, N. Sumi, T. Naganawa, Y. Kitajima & Y. Nozawa (1999) Activation of p38 mitogen-activated protein kinase and caspases in uvb-induced apoptosis of human keratinocyte hacat cells *J Invest Dermatol* **112,** 769-74.

(61) H. Takahashi, N. Komatsu, M. Ibe, A. Ishida-Yamamoto, Y. Hashimoto & H. Iizuka (2007) Cystatin a suppresses ultraviolet b-induced apoptosis of keratinocytes *J Dermatol Sci* **46,** 179-87.

(62) M. Kurita, T. Shimauchi, M. Kobayashi, K. Atarashi, K. Mori & Y. Tokura (2007) Induction of keratinocyte apoptosis by photosensitizing chemicals plus uva *J Dermatol Sci* **45,** 105-12.

(63) N. Morishima, K. Nakanishi, H. Takenouchi, T. Shibata & Y. Yasuhiko (2002) An endoplasmic reticulum stress-specific caspase cascade in apoptosis *Journal of Biological Chemistry* **277,** 34287-34294.

(64) L. A. Sitailo, S. S. Tibudan & M. F. Denning (2002) Activation of caspase-9 is required for uv-induced apoptosis of human keratinocytes *J Biol Chem* **277,** 19346-52.

Chapter 6 Solar radiation induced DNA damage

6.1 Introduction

Using the Q-sun solar simulator, chapters 3-5 have shown that the response of cells is dependent on the exposure medium employed during irradiation which is primarily attributed to the extracellular generation of hydrogen peroxide in the cell culture medium DMEM-F12. This chapter further investigates the differential effects of the exposure medium in terms of DNA damage.

DNA is the fundamental building block of life (1) from which the phenotype of all living organisms is derived. The importance of DNA is reflected in genetic disorders, particularly single gene disorders where just a single gene defect can give rise to diseases such as cystic fibrosis, sickle cell anemia and achondroplasia dwarfism (2-4). Although in recent years, the significance of non-nuclear targets have come to the forefront in radiation biology, direct interactions between the genome and incident radiation are still vitally important. This point may be of particular relevance for skin carcinogenesis, since melanin, the innate UV filter in skin, forms nuclear caps covering the 'sunny-side' of proliferating cells in the basal layer (5) which may be an intrinsic mechanism by which the skin naturally protects the genomic material of a cell from a phototoxic insult.

This chapter specifically addresses the ability of solar simulated radiation to elicit genomic perturbations in directly irradiated kertinocytes, and if the exposure medium potentiates any such effects. Mitotic inhibition and the comet or single cell gel

electrophoresis assay were employed as markers of checkpoint efficiency and DNA damage respectively. Mitotic inhibition is a measure of how a cell is prevented, or not, from progressing through the cell cycle (6), while the comet assay measures damage in the form of single strand breaks (SSBs), double strand breaks (DSBs), alkali-labile sites i.e. nucleotides that have lost their purine (apurinic) or pyrimidine (apyrimidinic) base and are collectively termed abasic (AP) sites (7).

6.2 Methods

6.2.1 Cytogenetics / mitotic inhibition

Cells were grown to approximately 70-80% confluence and irradiated or sham irradiated using the Q-sun solar simulator, as outlined in chapter 2, in either cell culture medium or PBS. In the case of PBS exposures, immediately before irradiation the cell culture medium was removed and stored, the cells washed once in 1 ml PBS and 3 ml fresh PBS added and the cells were irradiated. Immediately post exposure, the PBS was discarded and replaced with 3 ml of the stored cell culture medium. All cells were incubated for 30 minutes to post exposure to re-acclimatise to 37°C prior to adding the pre-warmed (37°C) spindle inhibitor Colcemid (Gibco). Colcemid was added to each sample at a concentration of 10 µl per ml of cell culture medium and the cells incubated for a further 2 hours, after which the cells were trypsinised. Once trypsinised, the cells were stored on ice to prevent DNA repair until they were centrifuged at 1200 rpm for 10 minutes at 4°C. After centrifuging, the supernatant was decanted and 5 ml KCl (0.075 M at 4°C) hypotonic was added to lyse the cell membrane and swell the chromosomes and incubated on ice for 20 minutes. The cells were then centrifuged at 1200 rpm for 10 minutes at 4°C. The supernatant was decanted and 10 ml of Carnoy's fixative (methanol to acetic acid ratio 3:1 at 4°C) was added and centrifuged at 1200 rpm for 10 minutes at 4°C, the supernatant decanted and 10 ml fresh Carnoy's fixative added before refrigerating overnight.

Samples were removed from the refrigerator and allowed to reach room temperature. The samples were then centrifuged for 10 minutes at 1200 rpm and the supernatant

decanted. 10 ml fresh fixative was added, the samples aspirated and centrifuged for 10 minutes at 1200 rpm. The fixative was removed leaving an approximate volume ratio of 1 part cell pellet and 2 parts fixative. Using slides pre cleaned in methanol, the cell samples were dropcast onto the slides from a height (10-15 cm) to ensure the cell membrane broke and released intact metaphases which were fixed to the slide using a Bunsen flame. Once cooled the slides were stained in a 3% Giemsa solution (Gibco) prepared in pH 8.0 buffer (BDH) for 10 minutes and washed twice in the same buffer and allowed to dry standing at room temperature overnight. The slides were then mounted with coverslips using DPX and allowed to dry overnight before scoring the mitotic index. Mitotic index was calculated as the percentage of cells in mitosis in a count of 2000 cells and mitotic inhibition was calculated as the percentage reduction in mitotic index in irradiated cells compared to unirradiated cells using equation 6.1 as described in the literature (6, 8)

$$\text{Mitotic Inhibition (\%)} = \frac{\text{(Control Mitotic Index – Irradiated Mitotic Index)} \times 100}{\text{Control Mtotic Index}}$$

Equation 6.1

5.2.2 FPG modified comet assay

Cells were grown to ~80% confluence in 85 mm Petri dishes and exposed without lids in either cell culture medium or PBS using the Q-sun solar simulator. Cells were trypsinised immediately post exposure and then centrifuged at 1200 rpm for 10 minutes at room temperature. The supernatant was discarded and the cells re-suspended in 1 ml of medium. A 10% cell suspension in Trypan Blue was used to perform cell counts and determine cell viability using a haemocytometer (see appendix 2). One millilitre

aliquots containing 2 x 10^5 cells was generated for each dose point. The negative and positive control aliquots were produced using sham irradiated and untreated cells respectively.

6.2.2.1 Generating positive controls

The untreated control aliquot was centrifuged at 1200 rpm for 10 minutes at 4°C. Once centrifuged, the supernatant was discarded and the cells re-suspended in 1 ml of a chilled (4°C) 100 μM hydrogen peroxide solution (diluted in PBS) and treated on ice for 5 minutes, after which 2 ml cell culture medium was added to dilute the hydrogen peroxide.

For the hydrogen peroxide dose response, nine untreated control cell aliquots were generated, centrifuged and treated with varying concentrations of hydrogen peroxide (0-100mM, see appendix 6) for 5 minutes on ice and subsequently diluted with cell culture medium.

6.2.2.2 Slide generation

Once the positive controls were produced, all aliquots were centrifuged at 1200 rpm for 10 minutes. Dealing with each pellet sequentially, the supernatant was removed and the cell pellet re-suspended in 400 μl of 0.8% low melting point (LMP) agarose at 37°C. 60 μl of each LMP agarose cell suspension was dropcast onto four pre-coated slides (see appendix 3), covered with cover-slips and placed on an ice block for 1 minute to set the agarose. Slides were removed from the ice block and the coverslips removed from each

slide. This was repeated for each pellet, where each aliquot gave rise to four slides as shown in figure 6.1.

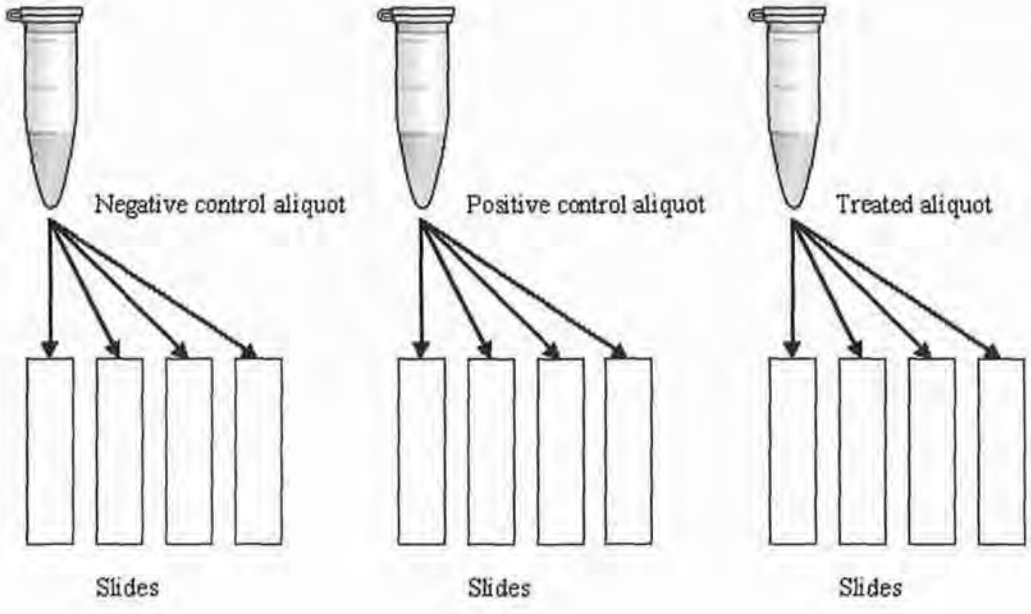

Figure 6.1 Schematic depicting how each aliquot gives rise to four slides. Each independent experiment had a positive control, a negative control and 3 treated aliquots; 2, 5 and 10 minutes for cells irradiated in DMEM-F12 medium and 10, 30 and 60 minutes for cells irradiated in PBS.

6.2.2.3 Lysis

Once the slides were prepared and coverslips removed, slides were racked and transferred into light tight box. The slides were then immersed in chilled (4°C) lysis solution (see appendix 3) and refrigerated for 1 hour at 4°C.

6.2.2.4 Enzyme incubation

After lysis, the solution was discarded and the slides washed three times in chilled (4°C) enzyme buffer (see appendix 3) for 5 minutes each at 4°C.

After the enzyme buffer washes, two slides from each dose were treated with either 50 µl of fpg enzyme (0.16 µg/ml) (see appendix 3) in enzyme buffer or 50 µl of enzyme buffer only, see figure 6.2. Coverslips were placed on all slides and the slides transferred to a moistened light tight box and incubated for 30 minutes at 37°C.

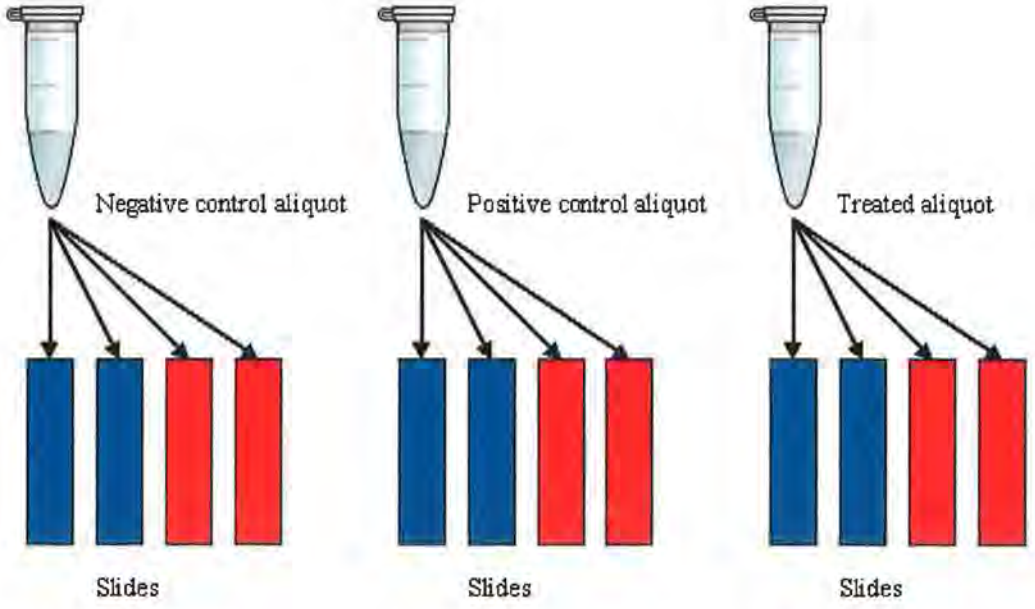

Figure 6.2 Schematic illustrating that two slides from each aliquot was treated with 50 µl of fpg (0.16 µg/ml) in enzyme buffer (blue slides) or 50 µl of enzyme buffer only (red slides)

6.2.2.5 DNA unwinding

After the enzyme incubation, the coverslips were removed from the slides, the slides were re-racked and transferred into clean light tight boxes. The slides were immersed in

electrophoresis buffer at room temperature (see appendix 3). Slides were treated at room temperature for 40 minutes to facilitate DNA unwinding.

6.2.2.6 Electrophoresis

After the DNA unwinding step, the slides were removed from the electrophoresis buffer and randomly distributed in the electrophoresis tank (figure 6.3). The tank was filled with fresh electrophoresis buffer at room temperature until the buffer covered the slides. The tank was closed and connected to a voltage supply set at 23 Volts and current ≤300 mA for 20 minutes.

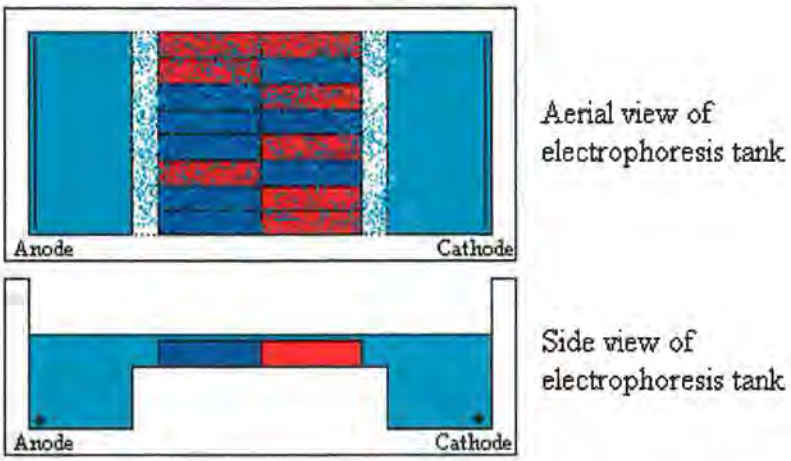

Figure 6.3 Schematic depicting how slides (red and blue) are randomly arranged and submerged in buffer (cyan) in the electrophoresis tank

6.2.2.7 Neutralisation

Once electrophoresis was complete, the slides were transferred to clean racks and light tight boxes, immersed in chilled (4°C) neutralisation buffer (see appendix 3) and refrigerated for 5 minutes 4°C.

6.2.2.8 Staining and scoring

Once neutralised, each slide was treated with 50 µl of ethidium bromide (25 µg/ml in dH_2O) and covered with a coverslip. Using an excitation wavelength of 525 nm, the fluorescence of fifty cells per slide were scored within 24 hours using a Nikon Eclipse E600 fluorescence microscope equipped with a filter cube consisting of a 540/25 nm bandpass (BP) excitation filter, a 565 nm dichroic mirror and 605/55 nm BP emission filter, and an Andor Luca camera (model no DL-658M-TIL) in conjunction with Komet 5.5 software. The software employs an adjustable reading frame, the size of which is set prior to the scoring session, which is overlaid on the comet as shown in figure 6.4. Once scored, indicators known as callipers appear in the reading frame denoting the head and tail regions of the comet, also shown in figure 6.4. Based on the DNA content in the head and tail regions as denoted by the callipers, the software determines various parameters including percentage head DNA content, percentage tail DNA content, tail length, olive and extent tail moments and the tail length to head diameter ratio using the fluorescence emissions within the reading frame. The parameter used in this study is the percentage tail DNA content, which is a ratio of the DNA detected in the tail region with respect to the total DNA content detected in both the head and tail regions.

Figure 6.4 Image of a comet captured using the Komet 5.5 software and illustrating both the reading frame and the callipers used to detect and the different regions of the comet.

5.2.3 Statistics

Results represent a minimum of 3 independent tests with 2 replicate slides per dose / treatment in each independent test from which 50 cells were scored per replicate slide. The percentage tail DNA was log transformed and ANOVA performed. Pair-wise data were computed using the Bonferroni adjustment. All analyses were done using statistical software package SAS 9.1 and SAS enterprise guide 3.0. Significance was taken at a level of $p \leq 0.05$. Data are presented as the LSM ± 95CI derived from the statistical model.

6.3 Results and discussion

The ability of solar radiation to induce chromosome breaks was investigated using cytogenetics. However, after one independent test it was clear that HaCaT cells were intrinsically aneuploid which agrees with the characterisation of HaCaT cells by Boukamp et al (9). Although the cytogenetics study was not pursued any further, the data collected does provide useful information regarding the mitotic index and the ability of solar simulated radiation to inhibit mitotic processes in irradiated cells. Mitotic inhibition is considered an indicator of G_2 checkpoint efficiency where high mitotic inhibition is considered indicative of longer cell cycle delays so that cells can execute the appropriate response (6) whether that be repair or apoptosis.

Table 6.1 Mitotic index and mitotic inhibition for HaCaT cells exposed in DMEM-F12 cell culture medium. Mitotic index results were based on a minimum count of 2000 cells per dose.

Medium exposures	Mitotic index %	Mitotic inhibition %
Control	6.36	
2 minutes	3.91	2.45
5 minutes	1.28	5.08
10 minutes	1.58	4.78

The mitotic index results in table 6.1 show that cells irradiated in DMEM-F12 medium are inhibited in a dose dependent manner that appears to saturate when cells are irradiated for 5 minutes or more. Although the mitotic inhibition data was computed from counts of at least 2000 cells for each exposure time, additional independent tests would be desirable before this saturation effect can be conclusively confirmed. Interestingly though, the saturation of mitotic inhibition concurs with the oxidation-

mediated dissociation of cardiolipin and cytochrome c theory presented in the previous chapter. Nonetheless, mitotic inhibition, as observed, is indicative of cell cycle arrest. Cell cycle arrest facilitates DNA repair or apoptosis which prevents potentially mutagenic cells from passing damaged genomes to future progeny. One of the principle regulators of cell cycle arrest is p53 (10). In response to cell damage, this transcription protein up-regulates p21 expression (10) which through its ability to inhibit cyclin dependent kinases (cdks) is an important mediator of cell cycle arrest (11). HaCaT cells are p53 null ($p53^{-/-}$) and thus do not possess functional p53 protein (12). However, the mitotic index results demonstrate that HaCaT cells retain the ability to arrest when irradiated in DMEM-F12 and, to a lesser extent, in PBS. Cells were not cell cycle synchronised prior to irradiation thus, it is unlikely that cells arrested in the same phase of the cell cycle. From this, it is clear that HaCaT cells must retain one or more p53 independent cell cycle arrest pathways that possess the ability to arrest cells in different cell cycle phases. One possible candidate is the INK4 family protein member $p16^{INK4a}$ which inhibits cdk4 and cdk6 from phosphorylating the protein product of the retinoblastoma gene known as Rb (13). Rb is normally conjugated to E2F transcription factors but upon phosphorylation, Rb dissociates from its E2F conjugate (14), freeing it to transcribe genes necessary to progress from G_1 to S-phase. Thus, expression of p16 causes cells to arrest in G_1. Furthermore, p16 has been demonstrated to play a role in both G_1 and G_2 cell cycle arrest following UV irradiation (15-17). Alternatively, the protein responsible could be p33, a tumour suppressor that shares many biological functions with p53 and has been shown to be upregulated in UVA irradiated apoptotic HaCaT cells (18).

Table 6.2 presents the mitotic index and mitotic inhibition results for cells irradiated and sham irradiated in PBS. The mitotic index for sham irradiated PBS controls can be seen to be substantially different to that observed for cells sham irradiated in DMEM-F12, 1.46% versus 6.36% respectively. The sham irradiated controls were treated identically, in that both were transported to the Q-sun and sham irradiated for 30 seconds using the dark cycle of the Q-sun and returned to the incubator immediately post sham irradiation. Cells were 70-80% confluent in 90 mm Petri dishes at the time of (sham) irradiation thus cell washing when replacing the culture medium prior to PBS exposures would not be expected to significantly reduce the number of cells present during (sham) irradiation. Thus, the drop in mitotic index between the sham irradiated controls is attributed to the absence of nutrients in PBS sham irradiated. However, as mentioned, the mitotic data presented are the result of one independent test where additional independent tests would be desirable in order to statistically confirm any effects.

Table 6.2 Mitotic index and mitotic inhibition for HaCaT cells exposed in PBS. Mitotic index results based on a minimum count of 2000 cells per dose point

PBS exposures	Mitotic index %	Mitotic inhibition %
Control	1.46	
10 minutes	1.17	0.29
30 minutes	2.10	-0.64
60 minutes	2.29	-0.83

In contrast to the mitotic inhibition observed in cells irradiated in DMEM-F12, the percentage of cells entering M-phase post irradiation in PBS can be seen to increase at the longer exposure times as shown in table 6.2. It is possible that the increased mitotic index observed in cells irradiated for extended durations in PBS is due to poor G_2

checkpoint efficacy and / or premature exit of G_2 arrest resulting in increased cell populations progressing to, but unable to exit M-phase due to treatment with the spindle inhibitor Colcemid 30 minutes post exposure. From the dose response of cells irradiated in PBS (figure 3.2), it is known that the survival of cells irradiated for 30 and 60 minutes in PBS is significantly reduced with respect to controls, p-values of 0.0012 and < 0.0001 respectively. This suggests that cells extensively irradiated in PBS may become endocyclic. Endocycling (endoreplicating / endoreduplicating) cells possess alternating S and Gap phases but no cell divison (19). DNA damage has been suggested to provide a molecular environment conducive to endocycle entry at the G_2 checkpoint to which $p53^{-/-}$ cells are particularly susceptible since most checkpoints in the cell cycle are regulated by p53 (20). After a small number of cycles it is postulated that endocycling cells can undergo mitotic cell death rather than apoptosis (6). Interestingly, Mehrotra et al (21) found that apoptosis is repressed in endocycling cells due to, in part, silencing of proapoptotic gene promoters which could serve to explain the absence of proapoptotic events in PBS irradiated cells presented in chapter 5. Thus, to establish the ability of solar simulated radiation to induce DNA damage, the comet assay was employed.

As shown in chapter 4, the cellular response of cells irradiated in DMEM-F12 is more representative of medium photosensitisation than of solar simulated radiation induced damage where exposures performed in the presence of catalase and GSH show that hydrogen peroxide is the predominant oxidant generated. Of the four DNA nucleotides, guanine is the most susceptible to oxidation (22) due to its low ionisation energy (23). In the presence of an oxidant, guanine readily oxidises to form 8-oxoG (24). The DNA repair mechanism primarily responsible for the repair of oxidative lesions such as 8-

oxoG is base excision repair (BER) (25). BER is initiated by a DNA glycosylase which excises the damaged base (26). The resulting AP site(s) are then cleaved by AP-endonuclease-1 (APE-1) to facilitate repair (27). Although there are an array of DNA glycosylases that respond to different types of base damage, there also exists a degree of functional redundancy between glycosylases due to partial overlapping of initiating lesions (28). Formamidopyrimidine-DNA glycosylase (fpg) used in this assay is the bacterial homolog of the human DNA repair glycosylase hOGG1, both of which excise 8-oxoG (29). Thus, if the treatment under analysis promotes oxidative lesions in the form of 8-oxoG, incorporating an fpg incubation step in the comet assay will either equal or exceed the amount of DNA damage detected in fpg untreated cells. This was found to be true for all durations of exposure to solar simulated radiation in both PBS and DMEM-F12.

Prior to assessing the level of DNA damage incurred due to solar simulated irradiation, HaCaT cells were treated with various concentrations of hydrogen peroxide in order to establish a suitable concentration to employ as the positive control in solar simulated irradiation experiments. Figure 6.5 illustrates the dose response obtained when HaCaT cells were treated with various concentrations of hydrogen peroxide for 5 minutes on ice. Maximal damage was achieved with 0.1 mM and reached a plateau with increasing concentration thereafter. A concentration of 0.01 mM was found to be not significantly different to untreated control cells, irrespective of the presence of fpg, thus indicating a steep gradient over which hydrogen peroxide switches from being relatively benign to cytotoxic. Based on the results presented in figure 6.5, a concentration of 0.1 mM hydrogen peroxide was employed as the positive control for all irradiation experiments.

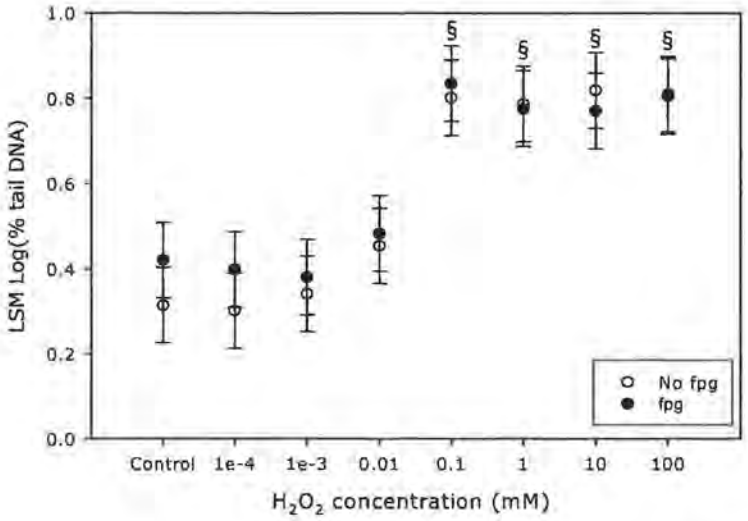

Figure 6.5 Comet assay results for the hydrogen peroxide dose response for HaCaT cells. Cells were treated with various concentrations of hydrogen peroxide and treated with (●) or without (O) fpg. The data is presented as the LSM ± 95CI for n = 4 independent experiments, consisting of 2 replicates per independent from which 50 cells were scored per replicate, § indicates significant difference between both fpg treated and untreated cells and their respective controls (p≤ 0.05).

Figure 6.6 shows the comet assay results for cells irradiated in DMEM-F12. Interestingly, no significant difference was found between fpg treated and untreated cells irradiated in DMEM-F12 for 5 or 10 minutes despite the production of extracellular of hydrogen peroxide in DMEM-F12 which was established in chapter 4 to be responsible for the dramatic dose response observed in figure 3.2. Limitations on the sensitivity of the Komet software employed appear to impair its ability to detect tail DNA content in excess of 80%. When such highly damaged cells were scored, the software failed to differentiate between the head and tail regions of the comet. Although it is possible to manually score comets, this was not done in order to avoid possible bias associated with manual scoring. Thus, these comets were excluded from the scoring process. Although omitting highly damaged cells may yield underestimations of the actual damage incurred, particularly for fpg treated cells, it is possible that lack of

significance between fpg treated and fpg untreated cells is in fact due to enhanced single and /or double strand break detection in fpg untreated cells.

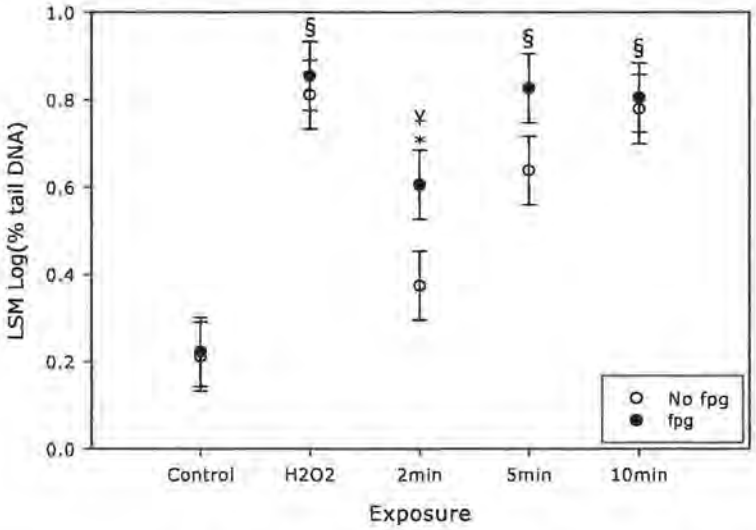

Figure 6.6 Comet assay results for HaCaT cells irradiated or sham irradiated in DMEM-F12 using the Q-sun solar simulator and 0.1 mM hydrogen peroxide as the positive control. Cells were treated with (●) or without (○) fpg. The data is presented as the LSM ± 95CI for n = 5 independent experiments, consisting of 2 replicates per independent from which 50 cells were scored per replicate. § indicates significant difference between both fpg treated and untreated cells and their respective controls, * indicates significant difference between fpg treated and untreated cells for a given exposure, ¥ indicates significant difference between fpg treated exposed and control cells ($p \leq 0.05$).

As demonstrated previously, hydrogen peroxide is generated in DMEM-F12 upon irradiation, which has been shown to generate 8-oxoG *in vitro* (30). Furthermore, HaCaT cells have been shown to constitutively express the human DNA glycosylase OGG1 in a cell cycle dependent manner under normal redox conditions (31). Thus, it is possible that the enhanced production of hydrogen peroxide induces excessive oxidative lesions such as 8-oxoG which may be excised by OGG1 leading to enhanced single strand breaks which if in close proximity to one another may be detected as double

strand breaks (32). In turn, this would increase the amount of damage detected in fpg untreated cells whilst simultaneously limiting the amount detected in fpg treated cells. The progressive decrease in the amount of damage detected between fpg treated and untreated cells with increasing exposure time is believed to be a dose dependent effect resulting from the increased generation of hydrogen peroxide with increasing exposure time. As the concentration of hydrogen peroxide generated increases, a corresponding increase in the yield of oxidative lesions such as 8-oxoG would also be expected, which through the actions of endogenous DNA glycosylase OGG1 may be increasingly detected as SSBs and / or DSBs. Although an intriguing conjecture, it necessitates that OGG1 is constitutively expressed in sufficient quantities to offset the efficacy of fpg treatment since the comet assay is initiated immediately post irradiation which negates the possibility of de novo protein synthesis. The results further suggest that the glycosylase activities of OGG1 requires a threshold level of oxidative damage to trigger its response since the amount of DNA damage measured in cells irradiated for 2 minutes was significantly increased when treated with fpg. This suggests that the OGG1 glycosylase endogenous to HaCaT cells does not reduce the efficacy of fpg treatment by excising 8-oxoG lesions formed by the concentration of hydrogen peroxide generated when DMEM-F12 is irradiated for 2 minutes. This is supported by reports that OGG1 relocates from the nucleoplasm to euchromatin (33), regions of lightly packed chromatin that are rich in gene content and are often under active transcription (34), in response to oxidative stress and not transcription blockage (35). Furthermore, human OGG1 has been reported to exhibit increased specificity for 8-oxoG than fpg (36).

Interestingly, fpg treated cells were also found to be not significantly different from their untreated counterparts at all concentrations in the hydrogen peroxide dose response

study. It can, however, be seen that the level of damage in fpg treated control cells and those treated with non-toxic concentrations of hydrogen peroxide is consistently elevated, albeit not significantly, with respect to their fpg untreated counterparts, an effect that is not maintained at concentrations ≥ 0.1 mM. Based on the similarities between the data elicited with non-toxic and toxic concentrations of hydrogen peroxide and that of the control and 10 minute DMEM-F12 exposures respectively, it is tempting to speculate that irradiation of DMEM-F12 for 10 minutes generates an extracellular concentration of at least 0.1 mM hydrogen peroxide. Following on from this, it could also be speculated that the 2 and 5 minute exposures generate hydrogen peroxide concentrations between 0.01 and 0.1 mM which according to the hydrogen peroxide dose response curve is the narrow range over which hydrogen peroxide becomes increasingly toxic to HaCaT cells.

Furthermore, the level of oxidative damage in DMEM-F12 irradiated cells can be seen to saturate when cells are irradiated for 5 minutes while the level of DNA damage in fpg untreated cells continues to increase with increasing exposure duration. It was previously demonstrated in chapter 3 that cells irradiated for 5 minutes in DMEM-F12 using the Q-sun solar simulator results in significantly but not maximally reduced survival. Together, these data concur with the results of Garg and Chang (37) who, as discussed in chapter 5, observed that the level of intracellular ROS generated saturated when cells were treated with a dose of 0.5 mM hydrogen peroxide although no cell death was observed unless a concentration of ≥ 1 mM was employed. Based on the above comparative speculations made between cells irradiated in DMEM-F12 and those treated with hydrogen peroxide, the concentration of hydrogen peroxide at which oxidative damage saturates in HaCaT cells appears to occur between 0.01 and 0.1 mM.

Although the median concentration of this range (0.055 mM) is approximately 10 fold less than the concentration at which Garg and Chang (37) found saturation effects to occur, the discrepancy in the concentration required to induce saturation effects is not unreasonable when the differences in endpoints and cell lines employed are considered. The saturation effects reported by Garg and Chang (37) were observed in terms of intracellular ROS generated in a human retinal pigment epithelial cell line (APRE-19) treated with a definite concentration of hydrogen peroxide. While the saturation effects presented here are in terms of oxidative lesions induced in a human keratinocyte cell line (HaCaT) exposed to an undefined concentration of hydrogen peroxide generated extracellularly in response to solar simulated irradiation. Although HaCaT cells may simply be more sensitive to hydrogen peroxide than APRE-19 cells, it is important to consider that solar simulated radiation may generate higher concentrations than those speculated to occur. Furthermore, although extracellular production of hydrogen peroxide is clearly the dominant effect when cells are directly irradiated in DMEM-F12, the effect of direct interactions between incident radiation and cells may significantly contribute to intracellular effects such as the induction of oxidative DNA lesions.

Figure 6.7 shows that cells irradiated in PBS also exhibit a dose dependent increase in DNA damage that, similar to cells irradiated in DMEM-F12, saturates in fpg treated cells at the 30 minute exposure which also corresponds to a significant but not maximal reduction in cell survival. In contrast to the DMEM-F12 results, however, the progressive decrease in the difference between fpg treated and untreated cells with increasing exposure is not as pronounced in PBS irradiated cells. In fact, fpg treated cells can be seen to display a clear and significant increase in the amount of tail DNA with respect to their fpg untreated counterparts for all exposure times. This suggests that

different oxidising agent(s) with reduced capabilities of generating 8-oxoG are formed in PBS irradiated cells and / or that the oxidising agent(s) are formed in significantly lower quantities despite being irradiated up to 6 times longer than DMEM-F12 exposures. The lack of photosensitising agents in unsupplemented PBS indicates that the oxidising agent(s) responsible are generated intracellularly. Furthermore, the results of Kvam and Tyrrell (38) indicate that singlet oxygen is the agent responsible for 8-oxoG induction in cells irradiated in PBS with UVA radiation.

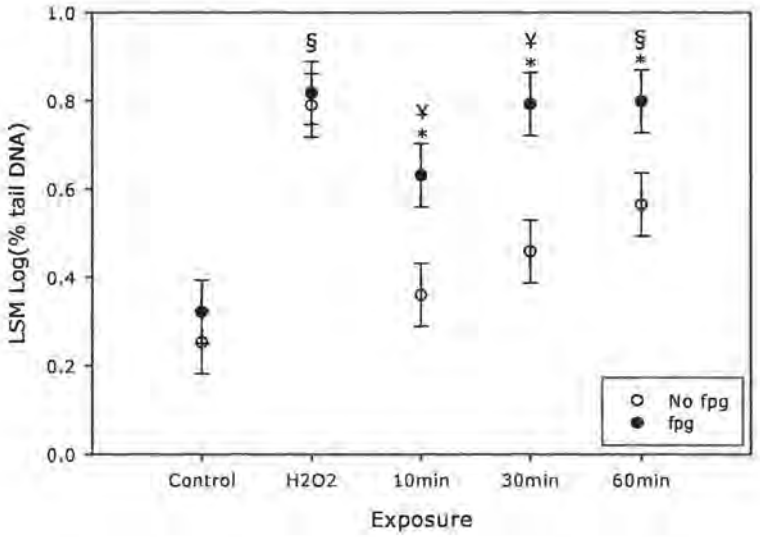

Figure 6.7 Comet assay results for HaCaT cells irradiated or sham irradiated in PBS using the Q-sun solar simulator and 0.1 mM hydrogen peroxide as the positive control. Cells were treated with (●) or without (○) fpg. The data is presented as the LSM ± 95CI for n = 5 independent experiments, consisting of 2 replicates per independent from which 50 cells were scored per replicate. § indicates significant difference between both fpg treated and untreated cells and their respective controls, * indicates significant difference between fpg treated and untreated cells for a given exposure, ¥ indicates significant difference between fpg treated exposed and control cells ($p \leq 0.05$).

6.4 Conclusions

If left unrepaired, 8-oxoG lesions produce in GC→TA transversions as shown in figure 6.8, and are considered the signature mutation of 8-oxoG (39).

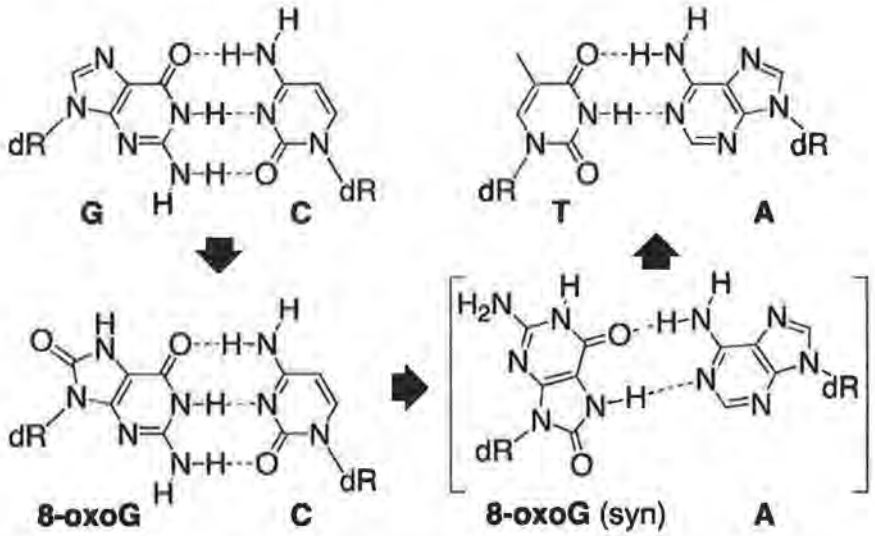

Figure 6.8 The base pairing pathway by which 8-oxoG causes GC→TA transversions using the A-rule (39).

However, reports in the literature regarding the mutagenic capacity of 8-oxoG lesions are somewhat conflicting. Kozmin et al (40) concluded UVA radiation is highly mutagenic in yeast cells incapable of repairing 8-oxoG and found that the mutagenic contribution of CPDs is trivial compared to 8-oxoG. In direct contrast with this, Courdavault et al (41) reported enhanced CPD induction compared to 8-oxoG induction in primary human fibroblasts and keratinocytes post UVA irradiation. This concurs with the work of Jiang et al (42) and Kappes and Rünger (43) who reported that UVA radiation is capable of directly generating CPDs in DNA plasmids and that 8-oxoG does not play a significant role in UVA mutagenesis in mouse embryonal fibroblasts respectively. Although the cell type and endogenous photosensitisers will play a role in the mutagenic capabilities of UVA radiation, the aforementioned studies employed

UVA irradiances of 800, 550, 450 and 300 Wm^{-2} respectively. If 60 Wm^{-2} is taken as a coarse guide for solar UVA irradiance at the terrestrial level, the UVA irradiances employed by these studies are 5-13 fold greater than that administered by solar radiation. Although mutagenic studies were not performed, it is clear from the work presented in the literature that mutagenic investigations using solar simulated radiation are urgently needed in biologically relevant cell lines since the initiating step in any cancer including skin carcinogenesis, is dependent on the ability of the damaging agent involved to induce mutations.

6.5 References

(1) R. Dahm (2005) Friedrich miescher and the discovery of DNA *Dev Biol* **278,** 274-88.

(2) M. Conese & J. Rejman (2006) Stem cells and cystic fibrosis *Journal of Cystic Fibrosis* **5,** 141-143.

(3) C. Booth, B. Inusa & S. K. Obaro (2010) Infection in sickle cell disease: A review *Int J Infect Dis* **14,** e2-e12.

(4) P. Richette, T. Bardin & C. Stheneur (2008) Achondroplasia: From genotype to phenotype *Joint Bone Spine* **75,** 125-30.

(5) N. Kobayashi, A. Nakagawa, T. Muramatsu, Y. Yamashina, T. Shirai, M. W. Hashimoto, Y. Ishigaki, T. Ohnishi & T. Mori (1998) Supranuclear melanin caps reduce ultraviolet induced DNA photoproducts in human epidermis *J Invest Dermatol* **110,** 806-10.

(6) O. Howe, K. O'Malley, M. Lavin, R. A. Gardner, C. Seymour, F. Lyng, D. Mulvin, D. M. Quinlan & C. Mothersill (2005) Cell death mechanisms associated with g2 radiosensitivity in patients with prostate cancer and benign prostatic hyperplasia *Radiat Res* **164,** 627-34.

(7) A. R. Collins, A. A. Oscoz, G. Brunborg, I. Gaivao, L. Giovannelli, M. Kruszewski, C. C. Smith & R. Stetina (2008) The comet assay: Topical issues *Mutagenesis* **23,** 143-151.

(8) D. Scott, A. R. Spreadborough & S. A. Roberts (2003) Less g(2) arrest in irradiated cells of breast cancer patients than in female controls: A contribution to their enhanced chromosomal radiosensitivity? *Int J Radiat Biol* **79,** 405-11.

(9) P. Boukamp, R. T. Petrussevska, D. Breitkreutz, J. Hornung, A. Markham & N. E. Fusenig (1988) Normal keratinization in a spontaneously immortalized aneuploid human keratinocyte cell line *Journal of Cell Biology* **106,** 761-71.

(10) J. T. Zilfou & S. W. Lowe (2009) Tumor suppressive functions of p53 *Cold Spring Harb Perspect Biol* **1,** a001883.

(11) A. M. Abukhdeir & B. H. Park (2008) P21 and p27: Roles in carcinogenesis and drug resistance *Expert Rev Mol Med* **10,** e19.

(12) T. A. Lehman, R. Modali, P. Boukamp, J. Stanek, W. P. Bennett, J. A. Welsh, R. A. Metcalf, M. R. Stampfer, N. Fusenig, E. M. Rogan & et al. (1993) P53 mutations in human immortalized epithelial cell lines *Carcinogenesis* **14,** 833-9.

(13) D. Parry, D. Mahony, K. Wills & E. Lees (1999) Cyclin d-cdk subunit arrangement is dependent on the availability of competing ink4 and p21 class inhibitors *Mol Cell Biol* **19,** 1775-83.

(14) J. R. Burke, A. J. Deshong, J. G. Pelton & S. M. Rubin (2010) Phosphorylation-induced conformational changes in the retinoblastoma protein inhibit e2f transactivation domain binding *J Biol Chem.*

(15) B. G. Gabrielli, B. Sarcevic, J. Sinnamon, G. Walker, M. Castellano, X. Q. Wang & K. A. Ellem (1999) A cyclin d-cdk4 activity required for g2 phase cell cycle progression is inhibited in ultraviolet radiation-induced g2 phase delay *J Biol Chem* **274,** 13961-9.

(16) S. Pavey, S. Conroy, T. Russell & B. Gabrielli (1999) Ultraviolet radiation induces p16cdkn2a expression in human skin *Cancer Res* **59,** 4185-9.

(17) W. Chen, J. Kang, J. Xia, Y. Li, B. Yang, B. Chen, W. Sun, X. Song, W. Xiang, X. Wang, F. Wang, Y. Wan & Z. Bi (2008) P53-related apoptosis resistance and tumor

suppression activity in uvb-induced premature senescent human skin fibroblasts *Int J Mol Med* **21,** 645-53.

(18) Y. Y. He, J. L. Huang, R. H. Sik, J. Liu, M. P. Waalkes & C. F. Chignell (2004) Expression profiling of human keratinocyte response to ultraviolet a: Implications in apoptosis *J Invest Dermatol* **122,** 533-43.

(19) B. A. Edgar & T. L. Orr-Weaver (2001) Endoreplication cell cycles: More for less *Cell* **105,** 297-306.

(20) J. Erenpreisa & M. S. Cragg (2001) Mitotic death: A mechanism of survival? A review *Cancer Cell Int,* 1-7.

(21) S. Mehrotra, S. B. Maqbool, A. Kolpakas, K. Murnen & B. R. Calvi (2008) Endocycling cells do not apoptose in response to DNA rereplication genotoxic stress *Genes Dev* **22,** 3158-71.

(22) K. Kino, N. Ito, K. Sugasawa, H. Sugiyama & F. Hanaoka (2004) Translesion synthesis by human DNA polymerase eta across oxidative products of guanine *Nucleic Acids Symp Ser (Oxf),* 171-2.

(23) X. Yang, X. B. Wang, E. R. Vorpagel & L. S. Wang (2004) Direct experimental observation of the low ionization potentials of guanine in free oligonucleotides by using photoelectron spectroscopy *Proc Natl Acad Sci U S A* **101,** 17588-92.

(24) G. B. Schuster (2009) One-electron oxidation of DNA: Mechanism and consequences *Nucleic Acids Symp Ser (Oxf),* 85-6.

(25) B. Tudek (2007) Base excision repair modulation as a risk factor for human cancers *Mol Aspects Med* **28,** 258-75.

(26) T. K. Hazra, A. Das, S. Das, S. Choudhury, Y. W. Kow & R. Roy (2007) Oxidative DNA damage repair in mammalian cells: A new perspective *DNA Repair (Amst)* **6,** 470-80.

(27) A. Bapat, M. L. Fishel & M. R. Kelley (2009) Going ape as an approach to cancer therapeutics *Antioxid Redox Signal* **11,** 651-68.

(28) J. H. Hoeijmakers (2001) Genome maintenance mechanisms for preventing cancer *Nature* **411,** 366-74.

(29) J. Dahle, G. Brunborg, D. H. Svendsrud, T. Stokke & E. Kvam (2008) Overexpression of human ogg1 in mammalian cells decreases ultraviolet a induced mutagenesis *Cancer Letters* **267,** 18-25.

(30) J. Wu, Z. Jiang, M. Liu, X. Gong, S. Wu, C. M. Burns & Z. Li (2009) Polynucleotide phosphorylase protects escherichia coli against oxidative stress *Biochemistry* **48,** 2012-20.

(31) L. Luna, V. Rolseth, G. A. Hildrestrand, M. Otterlei, F. Dantzer, M. Bjoras & E. Seeberg (2005) Dynamic relocalization of hogg1 during the cell cycle is disrupted in cells harbouring the hogg1-cys326 polymorphic variant *Nucl. Acids Res.* **33,** 1813-1824.

(32) L. J. Fell, N. D. Paul & T. J. McMillan (2002) Role for non-homologous end-joining in the repair of uva-induced DNA damage *Int J Radiat Biol* **78,** 1023-7.

(33) R. Amouroux, A. Campalans, B. Epe & J. P. Radicella (2010) Oxidative stress triggers the preferential assembly of base excision repair complexes on open chromatin regions *Nucleic Acids Res.*

(34) E. Bartova, J. Krejci, A. Harnicarova, G. Galiova & S. Kozubek (2008) Histone modifications and nuclear architecture: A review *J Histochem Cytochem* **56,** 711-21.

(35) A. Campalans, R. Amouroux, A. Bravard, B. Epe & J. P. Radicella (2007) Uva irradiation induces relocalisation of the DNA repair protein hogg1 to nuclear speckles *J Cell Sci* **120,** 23-32.

(36) C. C. Smith, M. R. O'Donovan & E. A. Martin (2006) Hogg1 recognizes oxidative damage using the comet assay with greater specificity than fpg or endoiii *Mutagenesis* **21,** 185-90.

(37) T. K. Garg & J. Y. Chang (2004) 15-deoxy-delta 12, 14-prostaglandin j2 prevents reactive oxygen species generation and mitochondrial membrane depolarization induced by oxidative stress *BMC Pharmacol* **4,** 6.

(38) E. Kvam & R. M. Tyrrell (1997) Induction of oxidative DNA base damage in human skin cells by uv and near visible radiation *Carcinogenesis* **18,** 2379-84.

(39) N. J. Greco, R. W. Sinkeldam & Y. Tor (2009) An emissive c analog distinguishes between g, 8-oxog, and t *Org Lett* **11,** 1115-8.

(40) S. Kozmin, G. Slezak, A. Reynaud-Angelin, C. Elie, Y. de Rycke, S. Boiteux & E. Sage (2005) Uva radiation is highly mutagenic in cells that are unable to repair 7,8-dihydro-8-oxoguanine in saccharomyces cerevisiae *Proc Natl Acad Sci U S A* **102,** 13538-43.

(41) S. Courdavault, C. Baudouin, M. Charveron, A. Favier, J. Cadet & T. Douki (2004) Larger yield of cyclobutane dimers than 8-oxo-7,8-dihydroguanine in the DNA of uva-irradiated human skin cells *Mutat Res* **556,** 135-42.

(42) Y. Jiang, M. Rabbi, M. Kim, C. Ke, W. Lee, R. L. Clark, P. A. Mieczkowski & P. E. Marszalek (2009) Uva generates pyrimidine dimers in DNA directly *Biophysical Journal* **96,** 1151-1158.

(43) U. P. Kappes & T. M. Runger (2005) No major role for 7,8-dihydro-8-oxoguanine in ultraviolet light-induced mutagenesis *Radiat Res* **164,** 440-5.

Chapter 7 Spectroscopic analysis of cell culture medium exposed to solar simulated radiation

7.1 Introduction

The results thus far have demonstrated that the response of cells is not only critically dependent on the irradiator (chapter 3) but also the exposure medium employed (chapter 3-6) where the extensive cell killing observed when cells were irradiated in DMEM-F12 was attributed to the extracellular production of hydrogen peroxide (chapter 4). Cell culture medium is a complex soup of nutrients and amino acids necessary for healthy cell growth where degradation and / or photosensitisation of one or more of these constituent ingredients may be the mechanism responsible for this excessive cell killing. There are reports in the literature that elements of cell culture media such as riboflavin and supplements such as HEPES (2-[4-(2-hydroxyethyl)piperazin-1-yl]ethanesulfonic acid) possess the ability to generate reactive species (1-5). However, only a few studies have examined the effects on cells and within that cohort of studies found, the cell lines employed were non skin related (6, 7). Thus not only is it desirable to determine the effects of solar simulated irradiation on DMEM-F12 medium and its components, their effects on relevant cell lines such as HaCaT keratinocyte skin cells is vital for studies attempting to elucidate the contributions of solar radiation in skin carcinogenesis. To further investigate the effects of solar-simulated radiation on DMEM-F12 medium, a more in-depth spectroscopic analysis was conducted, on both individual components of, and complete

DMEM-F12 medium, in order to identify the possible component(s) responsible for the increased cell killing observed when irradiated with solar simulated radiation.

7.2 Methods

7.2.1 Spectroscopic analysis

Absorption spectra were measured using a dual beam PerkinElmer Lambda 900 UV/Vis/NIR spectrometer with 1 cm optically matched quartz cuvettes where the reference cuvette contained deionised water. The emission spectra were measured using a LS 55 PerkinElmer Luminescence spectrometer and a 1 cm^2 quartz cuvette.

7.2.2 Cell culturing, seeding and the clonogenic assay

HaCaT cells were cultured, seeded and the clonogenic assay performed as outlined in chapter 3, sections 3.2.1 and 3.2.2. Briefly, HaCaT cells were cultured in DMEM-F12 cell culture medium containing 10% FBS, 1% penicillin-streptomycin and 1 μg/ml hydrocortisone. Cells were incubated under humid conditions at 37°C, with 5% CO_2 in air and subcultured when cells were 80-90% confluent. Cells for direct and indirect (unexposed recipient cell) exposures were seeded at a density of 400 cells in 3 ml DMEM-F12 per well 16 hours before irradiation or treatment. For the clonogenic assay, cells were exposed or treated and then incubated for 7 days after which they were stained using carbol fuchsin for 5 minutes and scored.

7.2.3 Direct exposures performed in DMEM-F12

Cells were seeded 16 hours prior to irradiation. The cells were directly irradiated in 3 ml DMEM-F12 without lids using the Q-sun and returned to the incubator immediately post exposure. For some experiments, medium changes were conducted immediately, 1, 2, 4, 6, 8 and 24 hours post exposure or not at all. The cells were returned to the incubator on receipt of fresh medium post exposure.

7.2.4 Direct exposures performed in L-15 or PBS with and without reagents

The cells were seeded 16 hours prior to irradiation. Immediately before irradiation, DMEM-F12 cell culture medium was harvested from the cells, filtered and stored in the incubator. Cells were washed once with 1 ml pre warmed (37°C) PBS and the wash discarded. Cells were covered in 3 ml fresh pre warmed exposure medium (PBS, phenol red in PBS (0.00863 g/l), riboflavin in PBS (0.00022 g/l), phenol red and riboflavin together in PBS (0.00863 g/l and 0.00022 g/l respectively), or L-15 riboflavin free cell culture medium (Sigma, Dorset, U.K.) containing 10% FBS, 2 mM L- glutamine, 1% penicillin-streptomycin and 1 μg/ml hydrocortisone) and then exposed. Post exposure, the exposure media was discarded and the stored DMEM-F12 replaced at 3 ml per well before the cells were returned to the incubator for 7 days. All medium changes were carried out immediately post exposure except for L-15 exposures which were changed 4 hours post exposure, the reasons for which are outlined in the results and discussion section.

7.2.5 Statistics

Results represent a minimum of 3 independent tests unless otherwise stated, with a minimum of 2 replicates per independent test. ANOVA was performed on the log transformed data and the pair-wise data were computed using the Bonferroni adjustment. Data are presented as the LSM ± 95CI. All analyses were done using statistical software package SAS 9.1 and SAS enterprise guide 3.0. Significance was taken at a level of $p \leq 0.05$.

7.3 Results and discussion

Fluorescence is the re-emission of photons at longer and less energetic wavelengths than the initiating photons absorbed which induce the electronic transition to an excited state required for fluorescence to occur. The absorption and emission wavelengths of a fluorophore are characteristic of the molecular structure of the absorbing species. It is on this premise that fluorescence spectroscopy was employed to determine if solar simulated irradiation of DMEM-F12 and select components of DMEM-F12 undergo structural changes at the molecular level that may in turn compromise their functionality and thus nutrient value. Prior to fluorescence analysis, knowledge of the wavelengths at which the substance under investigation absorbs is required in order to determine appropriate excitation wavelengths. Thus, absorption spectroscopy was employed first. In order to simplify presentation the absorption data are presented as transmittance spectra.

Both riboflavin and phenol red are constitutive components of DMEM-F12 and were examined. Riboflavin was examined because, as previously mentioned, it has been reported to possess photosensitising capabilities. Phenol red was chosen because some studies irradiate cells in phenol red free cell culture medium (8-10) where the reasons for its absence are not always given but assumed to be due to concerns regarding photosensitisation. Thus, individual solutions of riboflavin (0.00022 g/l) and phenol red (0.00863 g/l) in PBS at concentrations similar to those found in DMEM-F12 (11) were examined. However, there is also evidence in the literature showing that phenol red not only produces negligible amounts of reactive species but that the ability of riboflavin to

produce reactive species is diminished due to the presence of phenol red (12). It is for this reason that a composite solution of riboflavin and phenol red together in PBS was also examined alongside complete DMEM-F12, undiluted foetal bovine serum (FBS), phenol red free DMEM-F12 with and without 10% FBS and PBS.

Figure 7.1 shows the transmittance spectra for the aforementioned solutions. As seen in figure 2.33 and presented again in figure 7.1, DMEM-F12 absorbs significantly below 600 nm with transmission minima observed at 410 nm and 558 nm. Analysis of the components of DMEM-F12 reveals how the transmittance spectrum of DMEM-F12 is an amalgamation of the transmittance properties of its components, particularly phenol red and FBS. At the same concentration found in DMEM-F12, phenol red in PBS can be seen to have maximal absorption, observed as troughs in the transmittance spectrum, at 435 nm and 558 nm which coincides with the absorption troughs observed with DMEM-F12 but absent in phenol red free DMEM-F12 with and without 10% FBS. However, the maximal absorption of DMEM-F12 in the blue region occurs at 410 nm and not 435 nm as phenol red would suggest. This discrepancy in maximal absorption is due to the presence of 10% FBS in DMEM-F12, as verified by the transmittance spectra of undiluted FBS and phenol red free DMEM-F12 containing 10% FBS, both of which can be seen to possess absorption troughs at 410 nm as is the case for DMEM-F12. Interestingly the transmittance spectrum for riboflavin in PBS shows that at the same concentration to that found in DMEM-F12, riboflavin has minimal absorption but still retains absorption troughs at 370 nm and 440 nm as shown in the inset of figure 7.1, which concurs with values listed in the literature (13). The transmittance of phenol red and riboflavin together is identical in distribution to phenol

red alone but with increased losses in transmission with decreasing wavelength most probably due to the combined absorption of both reagents.

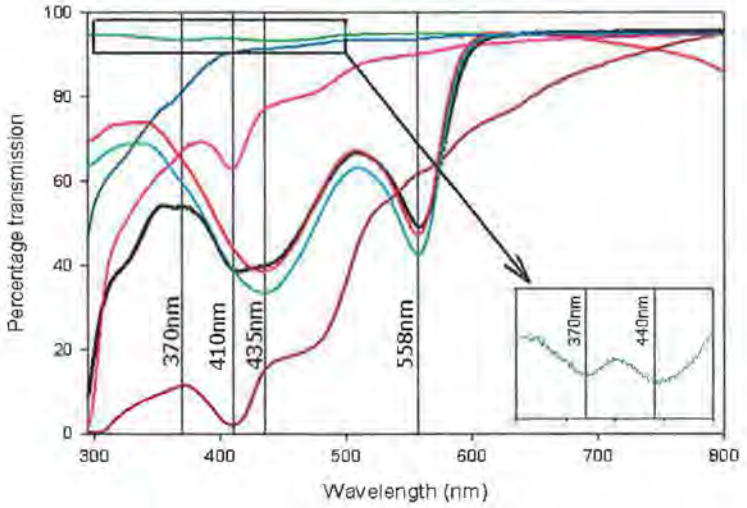

Figure 7.1 Transmittance spectra for DMEM-F12 (—), undiluted FBS (—), phenol red in PBS (—), phenol red and riboflavin in PBS (—), riboflavin in PBS (—), phenol free DMEM-F12 (—), and phenol free DMEM-F12 with 10% FBS (—) where the troughs indicate absorption maxima.

Based on the transmittance spectra shown in figure 7.1, excitation wavelengths of 370 nm, 410 nm, 440 nm and 558 nm were chosen to perform fluorescence spectroscopy on all eight solutions. Solutions were exposed for 10 minutes in the Q-sun solar simulator which as shown in chapter 3 was the exposure time that yielded the most cell death. Irradiated solutions were compared to unexposed solutions examined under identical conditions. Although fluorescence spectroscopy was performed using excitation wavelengths of 370 nm, 410 nm, 440 nm and 558 nm, the emission spectra obtained using an excitation wavelength of 370 nm was found to provide the most detailed account of changes incurred to irradiated media, hence only these emission spectra are presented and discussed.

Figure 7.2A shows the emission spectra of irradiated and unirradiated DMEM-F12 with 10% FBS. Similar to the transmittance spectrum of DMEM-F12, the emission spectrum for unexposed DMEM-F12 can be primarily attributed to the presence of FBS and phenol red. Peak emission wavelengths for DMEM-F12 were observed at 450 nm, 508 nm and 584 nm. Emission at 584 nm is attributed to the presence of phenol red where irradiation of DMEM-F12 yields a reduction in intensity at 584 nm similar to that observed for phenol red in PBS when irradiated as shown in figure 7.2C. The emission peaks at 450 nm and 508 nm are attributed to the presence of FBS. Irradiating DMEM-F12 yields a loss of the peak at 508 nm which is also observed when undiluted FBS is irradiated as shown in figure 7.2B. Figures 7.2A and 7.2B also show that the emission intensity of irradiated DMEM-F12 and irradiated undiluted FBS exceeds that of their respective controls. However, when undiluted FBS is irradiated the peak emission is redistributed from 448 nm to 458 nm, an effect that is not observed when DMEM-F12 is irradiated, and may be attributable to one or a combination of radiation induced structural changes and / or concentration dependent re-absorption processes (14, 15).

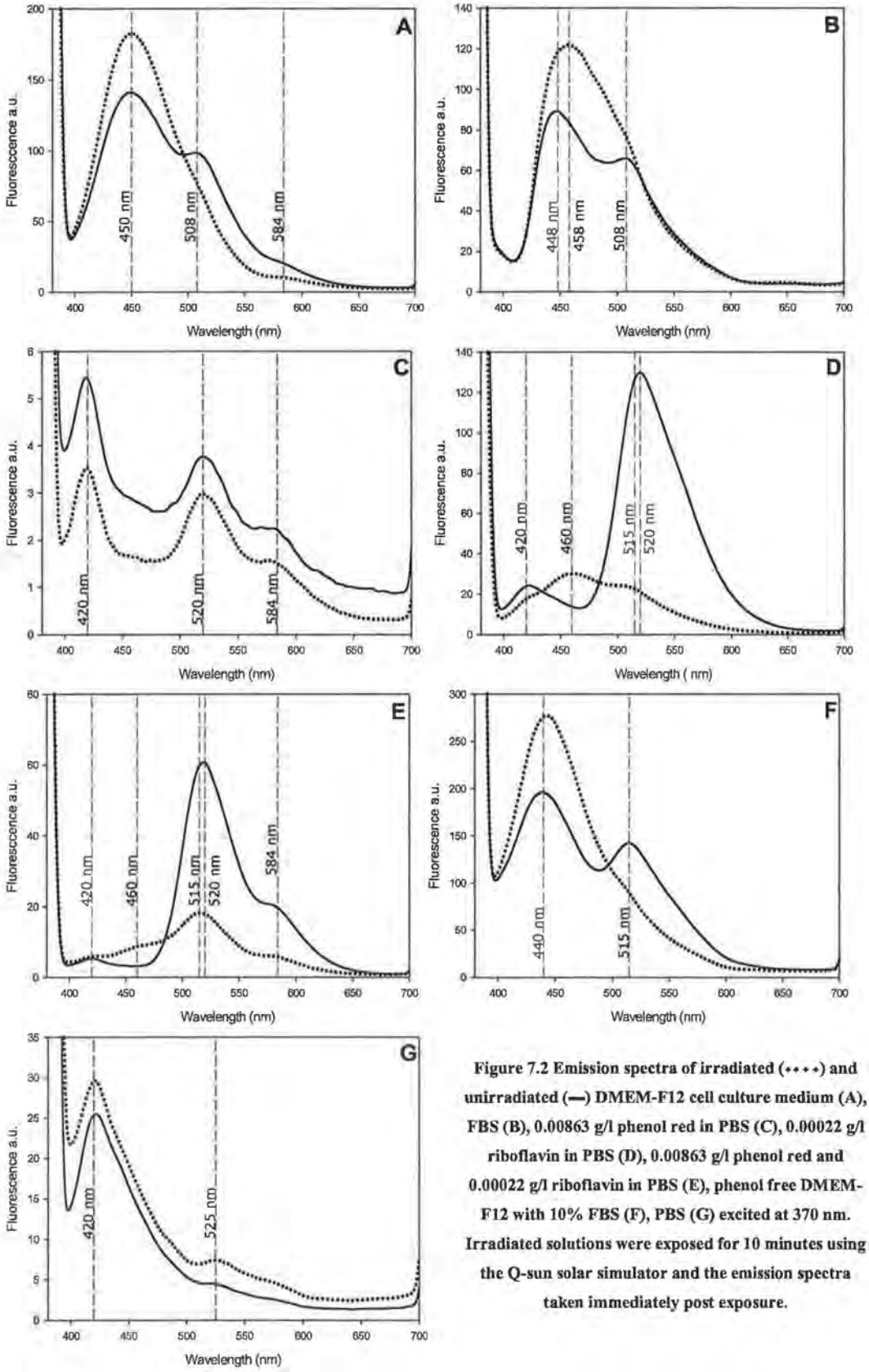

Figure 7.2 Emission spectra of irradiated (++++) and unirradiated (—) DMEM-F12 cell culture medium (A), FBS (B), 0.00863 g/l phenol red in PBS (C), 0.00022 g/l riboflavin in PBS (D), 0.00863 g/l phenol red and 0.00022 g/l riboflavin in PBS (E), phenol free DMEM-F12 with 10% FBS (F), PBS (G) excited at 370 nm. Irradiated solutions were exposed for 10 minutes using the Q-sun solar simulator and the emission spectra taken immediately post exposure.

As mentioned, absorption and emission wavelengths are dependent on the chemical structure of a fluorophore. Since UV radiation has been demonstrated in the literature to be capable of producing CPDS (16-18) and in chapter 6 solar simulated radiation was shown to produce 8-oxoG, it is not unreasonable to believe that solar simulated radiation can incur modifications to the chemical structure of a reagent. Thus, it is possible that solar simulated irradiation induced structural changes to the fluorophore(s) in FBS responsible for emissions at 508 nm, produce a blue shift (spectral movements toward shorter more energetic wavelengths) in the absorption and emission spectra of the fluorophore. The absorbing potential of this modified fluorophore may supersede that of the original fluorophore responsible for emissions at 448 nm when excited at 370 nm thus yielding an emission spectrum dominated by the structurally altered molecule. Alternatively, increases in fluorophore concentration via radiation induced evaporation may result in overlapping absorption and emission spectra (14, 15). These overlapping spectra may in turn, result in re-absorption of emitted photons that are re-emitted at an even lower wavelength thus producing an apparent red shift (spectral movements toward longer less energetic wavelengths) in the emission spectrum such as that observed for FBS (448 nm to 458 nm). The absence of such a red shift from the emission spectrum of DMEM-F12 may be due to the dilution of FBS in DMEM-F12 and / or the presence of phenol red.

Comparing the emission spectra of three unirradiated solutions with and without phenol red shows the presence of phenol red to reduce the fluorescence intensity of all three solutions. The emission spectra for unirradiated PBS with and without phenol red are shown in figures 7.2C and 7.2G. The fluorescence spectrum of PBS without phenol red (figure 7.2G)

shows PBS to have an emission peak at 420 nm despite PBS being minimally absorbing as shown in figure 2.33. In the presence of phenol red, the emission peak of unirradiated PBS is still visible at 420 nm (figure 7.2C). However, the intensity can be seen to be reduced by 75-80% due to the presence of phenol red. Similar for DMEM-F12, the unirradiated emission spectra of the cell culture medium with and without phenol red presented in figures 7.2A and 7.2F show the presence of phenol red to reduce the peak emission intensity by approximately 25%. The third solution examined was riboflavin in PBS with and without phenol red, shown in figures 7.2E and 7.2D respectively, where the peak emission can be seen to be reduced by more than 50% due to the presence of phenol red. It is clear from these results that phenol red reduces the fluorescence emission of different fluorophores excited at 370 nm. This suggests that phenol red acts as a quencher due to a combination of the facts that phenol red is a potent absorber of radiation below 600 nm (figure 7.1), and yet is minimally fluorescent (figure 7.2C). When a solution is irradiated, the ability of that solution to absorb incident radiation is dependent on the abilities of the absorbing species present in the solution to absorb at a given wavelength. Thus, it is reasonable to assume that the emission spectrum of a given solution is dependent on the absorbing potential of the different fluorophores present in the solution. Compared to PBS, phenol red free DMEM-F12 and riboflavin in PBS, the absorption potential of phenol red in PBS at 370 nm far exceeds that of the aforementioned solutions (figure 7.1). Although addition of 10% FBS to phenol red free DMEM-F12 results in an absorption potential indistinguishable from that of phenol red at 370 nm, it can be seen that phenol red complete DMEM-F12 supplemented with 10% FBS is more absorbing again. Hence inclusion of phenol red in DMEM-F12, PBS and riboflavin in PBS reduces the intensity of their

respective emission spectra since the number of incident photons available for absorption to initiate fluorescence is much reduced compared to the availability in the absence of phenol red.

Furthermore, since phenol red is minimally fluorescent, its presence in the emission spectrum of a solution can be poorly represented despite its ability to modify the optical properties of the solution. This is demonstrated by the visibility of riboflavin in the emission spectrum of DMEM-F12 in the presence (figure 7.2A) and absence (figure 7.2F) of phenol red. The peak emission of unirradiated riboflavin occurs at 515-520 nm as shown in both figures 7.2D and 7.2E where the presence of phenol red reduces the fluorescence intensity of this peak emission by approximately 50% (figure 7.2E). Thus, only in the absence of phenol red can the presence of riboflavin be detected in the emission spectrum of unirradiated DMEM-F12, peaking at 515 nm and over shadowing the emission of 10% FBS at 508 nm as shown in figure 7.2F. Moreover, irradiating riboflavin in the absence or presence of phenol red can be seen to reduce emissions at 515-520 nm and introduce a new emission peak at 460 nm. This new feature at 460 nm is attributed to radiation induced structural alterations of the riboflavin molecule leading to a blue shift in the absorption and emission spectra of the modified riboflavin molecule, thus reducing emissions at 515-520 nm. However, it can be seen that the emission at 515-520 nm is still the dominant emission in the presence of phenol red (figure 7.2E). This is attributed to the ability of phenol red to absorb incident radiation more effectively than riboflavin resulting in fewer alterations of the riboflavin molecule and thus less emission at 460 nm compared to the emission spectrum of irradiated riboflavin in the absence of phenol red.

Thus from the spectroscopic results presented it is clear that DMEM-F12 cell culture medium is optically dominated by the presence of FBS and phenol red. Although minimally absorbing, riboflavin has been shown to be a potent fluorophore which is poorly represented in the emission spectrum of DMEM-F12 due to the absorbing capabilities of phenol red and FBS. Moreover, irradiation of riboflavin has been shown to result in de novo emissions at 460 nm which were found to persist for at least 48 hours as shown in figure 7.3 where such spectral movements toward higher energy wavelengths, i.e. blue shifts, are indicative of structural changes in the form of conjugation losses (19).

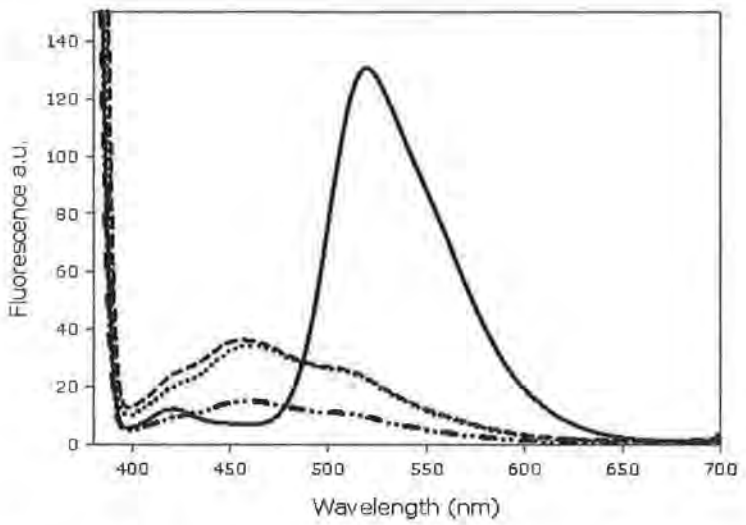

Figure 7.3 Emission spectra of 0.00022 g/l riboflavin in PBS irradiated for 10 minutes using the Q-sun solar simulator and analysed immediately (+ - + - +), 24 hours (- - - -) and 48 hours (▬·▬) post exposure and compared to unirradiated solutions (——) excited at 370 nm.

Based on the fluorescence results, the effects of phenol red and riboflavin on cell survival were investigated. Cells were irradiated in PBS containing phenol red (0.00863 g/l) and / or riboflavin (0.00022 g/l) and in L-15 riboflavin free cell culture medium as outlined in the

materials and methods section. Medium changes were carried out immediately post exposure for all variant PBS exposures to limit the length of time cells were without nutrients. To minimise differences between direct DMEM-F12 and L-15 exposures, cells irradiated in L-15 cell culture medium would ideally be maintained in L-15 for the 7 days prior to clonogenic staining with no medium change post exposure. However, HaCaT cells cultured in L-15 showed reduced proliferative abilities compared to cells cultured in DMEM-F12, thus eliminating the possibility of clonogenic expansion in L-15 medium. This concurs with the results of Werner et al (20) who observed decreased proliferative rates in HepG2 cells cultured in riboflavin deficient medium. Hence, it was necessary to find a time point to perform medium changes at which changing the medium of direct DMEM-F12 exposures would yield survival not significantly different from DMEM-F12 exposures with no medium change.

Cells were irradiated in DMEM-F12 for 10 minutes in the Q-sun solar simulator. The irradiated DMEM-F12 was then replaced, or not, with fresh unirradiated DMEM-F12 at different times post exposure and the cells incubated for the remainder of the 7 day clonogenic incubation period. The results in figure 7.4 show that cells irradiated in DMEM-F12 undergo two distinct cell death events. The first is a rapid event exacted within 1 hour of exposure followed by a slower event with maximal cell death observed after 24 hours exposure to the medium. In fact it was the 24 hour time point that was found to result in survival not significantly different from cells that did not receive a medium change post exposure ($p = 0.5071$). However, a medium change time point of 24 hours post irradiation was deemed unsuitable for L-15 exposures due to the reduced proliferative capacity of

HaCaT cells in L-15 medium. Although medium changes performed 1 to 8 hours post exposure were all significantly ($p < 0.05$) increased with respect to no medium change (figure 7.4), none were found to be significantly different to one another ($p = 1$) thus a median time point of 4 hours was employed for cells exposed in L-15 before the stored DMEM-F12 was re-introduced post exposure.

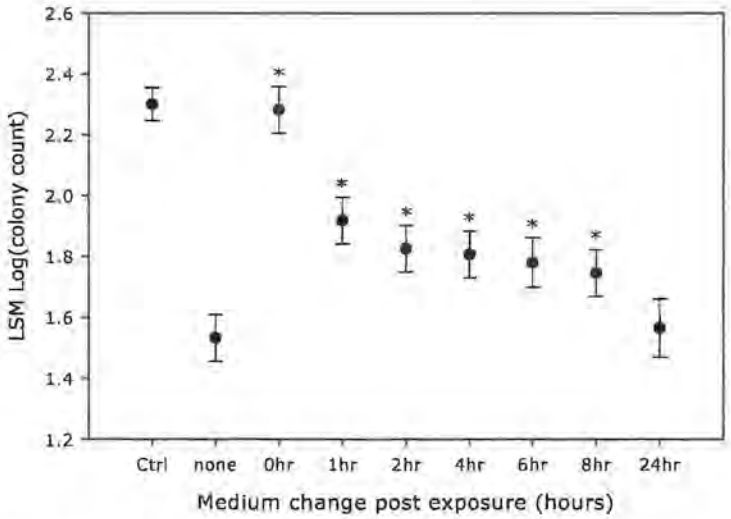

Figure 7.4 Survival of HaCaT cells irradiated for 10 minutes in DMEM-F12 and receiving a medium change post exposure or not (none). Data are presented as the LSM ± 95CI for n=3 independent experiments, * implies significant difference with respect to the 10 minute exposure that did not receive a medium change post exposure i.e. none ($p \leq 0.05$).

The survival curves for cells irradiated in the aforementioned solutions are shown in figure 7.5. The medium was changed immediately post exposure except for L15 medium which was changed 4 hours post exposure as described above. Exposure in all media resulted in survival not significantly different to their respective controls when irradiated for up to 10 minutes which concurs with the survival of cells irradiated in DMEM-F12 for 10 minutes and receiving a medium change immediately post exposure (figure 7.4). A 60 minute

exposure resulted in minimal survival irrespective of the exposure medium. It was the 30 minute exposures that showed the most intriguing results. Although all media elicited survival significantly different to their respective controls when irradiated for 30 minutes, the results clearly demonstrate a dependence on the exposure medium employed for irradiation.

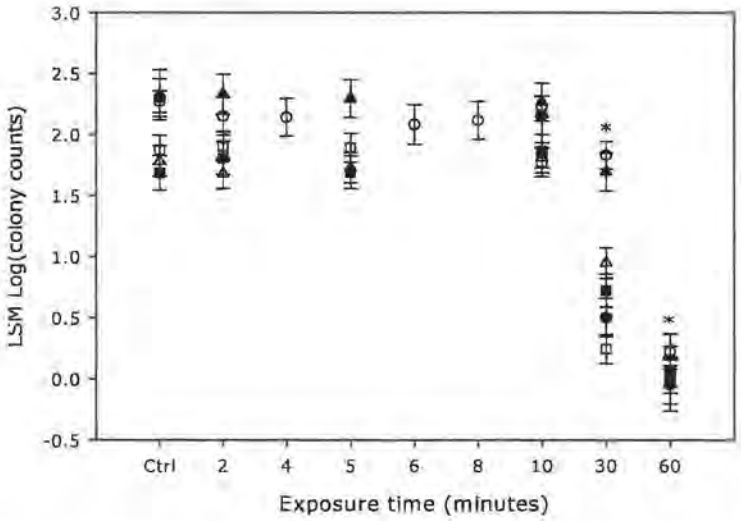

Figure 7.5 Direct exposure dose response curves for cells irradiated using the Q-sun solar simulator in PBS (n=3, O), L-15 riboflavin free cell culture medium (n=3, ▲), Phenol red in PBS (0.00863 g/l) (n=3, △), Phenol red (0.00863 g/l) & Riboflavin (0.00022 g/l) together in PBS (n=3, ■), riboflavin in PBS (0.00022 g/l) (n=3, □) and DMEM-F12 (n=2, ●). All medium changes were conducted immediately post exposure except for L-15 exposures which were carried out 4 hours post exposure. Data are presented as the LSM ± 95CI for n independent experiments, * implies all exposures irrespective of the exposure medium is significant difference to their respective to control ($p \leq 0.05$).

Figure 7.5 indicates that the most cytotoxic solution is riboflavin in PBS, which resulted in minimal survival after a 30 minute exposure and was found to be significantly different to all other 30 minute exposures ($p < 0.05$) in figure 7.5 except DMEM-F12. Although the

presence of phenol red in PBS was also found to significantly increase cell death above that observed with PBS alone ($p < 0.0001$), it was also found to significantly reduce the cytotoxic abilities of riboflavin ($p = 0.0001$). In fact, the survival of cells irradiated for 30 minutes in phenol red with and without riboflavin was found to be not significantly different to one another ($p = 1$). These results concur with the literature (12, 21) and the fluorescence results by showing phenol red to be a mild photosensitiser that possesses significant quenching abilities.

Based on the results presented in figure 7.5, it is believed that riboflavin is the most cytotoxic nutrient present in cell culture medium and is primarily responsible for the dramatic dose response curve observed in figure 3.2. This is supported by the fact that the survival of cells irradiated for 30 minutes in DMEM-F12 and receiving a medium change immediately post exposure were found to be not significantly different from the survival of cells irradiated for 30 minutes in riboflavin in PBS ($p = 1$) (figure 7.5). These results show that cells irradiated identically in PBS and DMEM-F12 containing the same concentration of riboflavin produces survival not significantly different from one another. The cytotoxic abilities of riboflavin are further demonstrated by the absence and presence of riboflavin in cell culture media during irradiation. Cells that received a medium change 4 hours post exposure when irradiated for 10 minutes in L-15 riboflavin free cell culture medium (figure 7.5) resulted in significantly increased survival compared to an identical exposure in DMEM-F12 ($p < 0.0001$) (figure 7.4).

Moreover, no significant difference was found between the survival of cells irradiated in PBS and L-15 ($p = 1$) for all exposure durations, irrespective of the difference in medium change time points (immediately and 4 hours post exposure respectively) or the presence of phenol red in L-15 which as shown augments the cytotoxicity of PBS (figure 7.5). The discrepancy between the L-15 and phenol red exposures could be the result of inefficient cellular functions due to the absence of nutrients during phenol red exposures compared to cells irradiated in L-15 culture medium. Concomitantly or alternatively, the discrepancy may be due to the absence of other reagents competing with phenol red in terms of radiation absorption in the PBS solution, which implies that absorption of incident radiation by phenol red in PBS is virtually uninhibited. And since phenol red is minimally fluorescent, it dissipates excess energy via non radiative energy transfers where the only substrates are the PBS solvent and cells. Thus, it is possible that the absence of other reagents may serve to increase the probability of direct non radiative energy transfer to cells. This may explain the increased cytotoxicity of phenol red in PBS compared to L-15 cell culture medium, particularly when it is known that the concentration of phenol red in L-15 (0.011 g/l (22)) is ~27% greater than that in DMEM-F12 which was the same concentration of phenol red used in PBS (0.00863 g/l).

If cells irradiated in L-15 received a medium change immediately post exposure like those irradiated in PBS, it would not be unreasonable to expect an increase in survival since it is unlikely that riboflavin and phenol red are the only photosensitisers present in cell culture media. However, any such increases in survival would not be expected to be significant since photosensitisers elicit their effects rapidly and thus will be accounted for in the L-15

results presented in figure 7.5. This suggests that any possible photosensitiser(s) present in L-15 are minimally effective compared to riboflavin. And is supported by the fact that cells irradiated in L-15 for 30 minutes and medium changed 4 hours post exposure resulted in survival significantly increased above that for cells irradiated for 30 minutes in DMEM-F12 and medium changed immediately post exposure (figure 7.5).

The evidence presented in this chapter strongly implicates riboflavin as the component responsible for the production of extracellular hydrogen peroxide in DMEM-F12 when irradiated with solar simulated radiation. This is supported by reports in the literature that riboflavin is capable of producing hydrogen peroxide when irradiated (21, 23). Furthermore, the two distinct cell death events observed in figure 7.4 when cells are irradiated in DMEM-F12 are attributed to riboflavin. The first event is believed to be propagated by hydrogen peroxide generated via the photosensitisation of riboflavin in DMEM-F12 which can be abrogated by the presence of catalase and GSH as shown in chapter 4. The second event is attributed to riboflavin deficiency resulting from radiation induced structural alteration and thus defunctionalisation of riboflavin as reflected in its emission spectrum (figure 7.2F) which was shown to persist for at least 48 hours (figure 7.3) and supported by the reduced proliferative capacity of HaCaT cells in L-15 riboflavin deficient medium.

7.4 Conclusions

Riboflavin is required for the culture of healthy cells and its absence has been demonstrated in the literature to lead to cellular stress events (20, 24, 25). It is the precursor to coenzymes flavin mononucleotide (FMN) and flavin adenine dinucleotide (FAD) (20, 26). FAD is involved with various metabolic processes such as protein folding in the endoplasmic reticulum (20, 27) and the redox cycle of glutathione where FAD is a coenzyme for glutathione reductase (20, 28, 29) which serves to reduce GSSG to GSH (30). In chapter 4 it was surmised that GSH supplementation during indirect exposures resulted in survival not significantly different to controls at all times of transfer (0-48 hours) due to the ability of GSH to permeate the cell membrane and increase the GSH:GSSG ratio. In light of the results supporting defunctionalisation of riboflavin, it is believed that GSH supplementation not only serves to increase the capacity of cells to process endogenous ROS but also enables the coenzymes formed from the remaining functional riboflavin to participate in metabolic processes other than the redox cycle of glutathione such as protein folding.

The objective of this chapter was to determine the agent responsible for the excessive cell death observed when cells are irradiated in DMEM-F12 compared to PBS. Although the results presented in this chapter show riboflavin to be a modest fluorophore, exposures performed in riboflavin supplemented PBS yielded results not significantly different from DMEM-F12 exposures while exposures performed in riboflavin free cell culture medium yielded results not significantly different to PBS exposures. From this, it is concluded that riboflavin is the photosensitising agent responsible for the dramatic dose response observed

when cells are irradiated in DMEM-F12. Thus, the cell death observed when cells are irradiated in DMEM F12 medium is more a reflection of riboflavin photosensitisation and degradation than of solar simulated radiation induced cell death.

7.5 References

(1) A. M. Edwards & E. Silva (2001) Effect of visible light on selected enzymes, vitamins and amino acids *Journal of Photochemistry and Photobiology B: Biology* **63,** 126-31.

(2) P. C. Joshi, C. Carraro & M. A. Pathak (1987) Involvement of reactive oxygen species in the oxidation of tyrosine and dopa to melanin and in skin tanning *Biochemical and Biophysical Research Communications* **142,** 265-74.

(3) A. Besaratinia, S. I. Kim, S. E. Bates & G. P. Pfeifer (2007) Riboflavin activated by ultraviolet a1 irradiation induces oxidative DNA damage-mediated mutations inhibited by vitamin c *Proceedings of the National academy of Sciences* **104,** 5953-8.

(4) R. G. Keynes, C. Griffiths & J. Garthwaite (2003) Superoxide-dependent consumption of nitric oxide in biological media may confound in vitro experiments *Biochemical Journal* **369,** 399-406.

(5) H. Kim, L. J. Kirschenbaum, I. Rosenthal & P. Riesz (1993) Photosensitized formation of ascorbate radicals by riboflavin: An esr study *Photochemistry and Photobiology* **57,** 777-84.

(6) J. D. Stoien & R. J. Wang (1974) Effect of near-ultraviolet and visible light on mammalian cells in culture ii. Formation of toxic photoproducts in tissue culture medium by blacklight *Proceedings of the National academy of Sciences* **71,** 3961-5.

(7) F. M. Griffin, G. Ashland & R. L. Capizzi (1981) Kinetics of phototoxicity of fischer's medium for l5178y leukemic cells *Cancer Research* **41,** 2241-8.

(8) M. Kwitniewski, A. Juzeniene, L.-W. Ma, R. Glosnicka, A. Graczyk & J. Moan (2009) Diamino acid derivatives of ppix as potential photosensitizers for photodynamic therapy of

squamous cell carcinoma and prostate cancer: In vitro studies *Journal of Photochemistry and Photobiology B: Biology* **94,** 214-222.

(9) T. J. Piva, K. G. Francis, D. R. Krause, G. M. Chojnowski & K. A. O. Ellem (1998) Effect of uv irradiation on cell surface protease activity and amino acid uptake *Mutation Research/Fundamental and Molecular Mechanisms of Mutagenesis* **422,** 55-67.

(10) S. D'Angelo, D. Ingrosso, V. Migliardi, A. Sorrentino, G. Donnarumma, A. Baroni, L. Masella, M. Antonietta Tufano, M. Zappia & P. Galletti (2005) Hydroxytyrosol, a natural antioxidant from olive oil, prevents protein damage induced by long-wave ultraviolet radiation in melanoma cells *Free Radical Biology and Medicine* **38,** 908-919.

(11) Sigma-Aldrich (2009) Dmem-f12 product information http://www.sigmaaldrich.com/etc/medialib/docs/Sigma/Formulation/d8062for.Par.0001.File.tmp/d8062for.pdf 2nd November 2009.

(12) A. Grzelak, B. Rychlik & G. Bartosz (2001) Light-dependent generation of reactive oxygen species in cell culture media *Free Radical Biology and Medicine* **30,** 1418-25.

(13) L. Ali & I. Naseem (2002) Hemolysis of human red blood cells by combination of riboflavin and aminophylline *Life Sciences* **70,** 2013-22.

(14) A. B. Dalton, J. N. Coleman, M. Panhuis, B. McCarthy, A. Drury, W. J. Blau, B. Paci, J. M. Nunzi & H. J. Byrne (2001) Controlling the optical properties of a conjugated co-polymer through variation of backbone isomerism and the introduction of carbon nanotubes *Journal of Photochemistry and Photobiology A: Chemistry* **144,** 31-41.

(15) K. Sakuma, N. Hirosaki & R.-J. Xie (2007) Red-shift of emission wavelength caused by reabsorption mechanism of europium activated ca-[alpha]-sialon ceramic phosphors *Journal of Luminescence* **126,** 843-852.

(16) C. G. C. van der Wees, M. P. G. Vreeswijk, M. Persoon, A. van der Laarse, A. A. van Zeeland & L. H. F. Mullenders (2003) Deficient global genome repair of uv-induced cyclobutane pyrimidine dimers in terminally differentiated myocytes and proliferating fibroblasts from the rat heart *DNA Repair* **2,** 1297-1308.

(17) S. Courdavault, C. Baudouin, M. Charveron, B. Canguilhem, A. Favier, J. Cadet & T. Douki (2005) Repair of the three main types of bipyrimidine DNA photoproducts in human keratinocytes exposed to uvb and uva radiations *DNA Repair* **4,** 836-844.

(18) P.-M. Girard, M. Pozzebon, F. Delacôte, T. Douki, V. Smirnova & E. Sage (2008) Inhibition of s-phase progression triggered by uva-induced ros does not require a functional DNA damage checkpoint response in mammalian cells *DNA Repair* **7,** 1500-1516.

(19) L. P. Candeias, G. Padmanaban & S. Ramakrishnan (2001) The effect of broken conjugation on the optical absorption spectra of the triplet states of isolated chains of poly(phenylene vinylene)s *Chemical Physics Letters* **349,** 394-398.

(20) R. Werner, K. C. Manthey, J. B. Griffin & J. Zempleni (2005) Hepg2 cells develop signs of riboflavin deficiency within 4 days of culture in riboflavin-deficient medium *Journal of Nutritional Biochemistry* **16,** 617-24.

(21) A. Grzelak, B. Rychlik & G. Bartosz (2000) Reactive oxygen species are formed in cell culture media *Acta Biochimica Polonica* **47,** 1197-8.

(22) Sigma-Aldrich (2009) L-15 product information http://www.sigmaaldrich.com/etc/medialib/docs/Sigma/Formulation/l5520for.Par.0001.File.tmp/l5520for.pdf 2nd November 2009.

(23) H. M. Jernigan (1985) Role of hydrogen peroxide in riboflavin-sensitized photodynamic damage to cultured rat lenses *Experimental Eye Research* **41,** 121-129.

(24) K. C. Manthey, Y. C. Chew & J. Zempleni (2005) Riboflavin deficiency impairs oxidative folding and secretion of apolipoprotein b-100 in hepg2 cells, triggering stress response systems *The Journal of Nutrition* **135,** 978-82.

(25) K. C. Manthey, R. Rodriguez-Melendez, J. T. Hoi & J. Zempleni (2006) Riboflavin deficiency causes protein and DNA damage in hepg2 cells, triggering arrest in g1 phase of the cell cycle *Journal of Nutritional Biochemistry* **17,** 250-6.

(26) Campbell (1996) *Biology* (The Benjamin/Cummings Publishing Company, California).

(27) E. Papp, G. Nardai, J. Mandl, G. Bánhegyi & P. Csermely (2005) Fad oxidizes the ero1-pdi electron transfer chain: The role of membrane integrity *Biochemical and Biophysical Research Communications* **338,** 938-945.

(28) G. E. Schulz, R. H. Schirmer & E. F. Pai (1982) Fad-binding site of glutathione reductase *Journal of Molecular Biology* **160,** 287-308.

(29) K. Becker, M. Leichsenring, L. Gana, H. J. Bremer & R. H. Schirmer (1995) Glutathione and association antioxidant systems in protein energy malnutrition: Results of a study in nigeria *Free Radical Biology and Medicine* **18,** 257-63.

(30) S. I. Baskin & H. Salem (1997) *Oxidants, antioxidants and free radicals* (Taylor & Francis, Washington DC).

Chapter 8 Solar radiation induced medium mediated bystander effects

8.1 Introduction

In chapter 4 direct irradiation of cells in DMEM-F12 or treatment of unirradiated recipient cells with blank (no cells) irradiated DMEM-F12 was shown to elicit significant decreases in cell survival. Increased cell death was observed when cells were directly exposed in the absence of antioxidants (figure 4.3) compared to recipient cell survival when treated with blank irradiated medium immediately post exposure (figure 4.4). The difference in survival may be the result of one or a combination of direct interaction of incident radiation with cells during exposure, the time taken to exact immediate medium transfers thus treating recipient cells with DMEM-F12 with reduced levels of reactive species compared to cells directly exposed and / or factors secreted by irradiated cells. Thus, this chapter investigates the possibility of cell secreted factors post solar simulated irradiation.

Traditionally, radiation biology is the study of biological mechanisms including cell death that occur in biological samples post exposure to ionising radiation or particles. Central to the field of radiation biology was the belief that in order to observe biological effects, damage must be incurred directly to the nucleus of the cell (1, 2). However, a new branch has budded in this field which conflicts with this paradigm, due to radiation effects occurring in unirradiated samples. This relatively new field, aptly titled bystander responses, stems from unexpected observations of irradiated effects in unirradiated cells due to their proximity to irradiated cells. In 1992 Nagasawa and Little (3) reported that the induction frequency of sister chromatid exchanges (SCEs) in cells

irradiated with low doses of α-particles was significantly increased above the population of cells actually traversed by an α-particle. Although the term 'Bystander' was not yet adopted in radiobiology this study has since been accredited with being the first report of bystander signalling (4), however abscopal effects or long distance bystander effects (5) were first described by Mole in 1953 (6). The majority of the work to date regarding bystander responses have been performed using low linear energy transfer (LET), x- and γ-radiation, and high LET, α-particle radiation, and include effects such as DNA damage, transformation, mutations, adaptive responses and cell death, see recent reviews (7-10). The scope of this field has expanded and now encompasses non-ionising UV radiation. In fact 8 years prior to the work of Nagasawa and Little (3), a study conducted by Schorpp et al (11) observed UVC bystander effects in skin fibroblasts where unirradiated recipient cells treated with medium harvested from directly irradiated cells 24 and 48 hours post exposure were found to have the same protein expression observed in directly irradiated cells. However, compared to ionising radiation, UV induced bystander investigations are still in their infancy which is reflected by the small volume of work in this field in the different UV wavebands; UVC (11-13), UVB (14-16), UVA (15-18), and solar simulated radiation (19).

In contrast to that observed by Mothersill et al (20), but in agreement with that reported by Lehnert's group (21, 22) for ionising radiation, it was demonstrated in chapter 4 that solar simulated radiation can elicit bystander responses when cell culture medium is irradiated in the absence of cells. This effect was found to be dependent both on dose and on the time of medium transfer. The bystander effects observed by Lehnert's group, however, were enhanced when cells were present during irradiation (22, 23) thus this

chapter investigates the possibility of solar simulated radiation induced bystander effects in human keratinocyte HaCaT cells.

8.2 Methods

8.2.1 Cell culturing, seeding and exposure

As described in sections 3.2.1 and 3.2.2 of chapter 3, HaCaT cells were cultured in DMEM-F12 cell culture medium containing 10 % FBS, 1 % penicillin-streptomycin and 1 μg/ml hydrocortisone. Cells were incubated under humid conditions at 37°C, with 5 % CO_2 in air and subcultured when cells were 80-90 % confluent. Cell counts were performed using a haemocytometer. Both donor cells and recipient cells were seeded 16 hours prior to irradiation and treatment respectively.

Donor cells were seeded, in 6 well plates, such that at the time of transfer post exposure densities of 1×10^5, 2×10^5, 5×10^5 and 1×10^6 cells would be expected in untreated samples. Donor cells were either sham irradiated or irradiated for 10 minutes without lids in 3 ml DMEM-F12 in the Q-sun solar simulator with an irradiance setting of 0.68 Wm^{-2} at 340 nm which as described in chapter 2 provides a UV spectral irradiance of ~64 Wm^{-2} at the level platform constructed in the chamber.

Post exposure, the irradiated donor cell medium was harvested, filtered and transferred to unirradiated recipient cells 0 (immediately), 1 hour, 24 and 48 hours post exposure. Donor cells designated for the late times of transfer were returned to the incubator post exposure until the appropriate time of transfer.

Recipient cells were seeded 16 hours before treatment with donor cell medium at a density of 400 cells per well in 6 well plates. The DMEM-F12 covering recipient cells

was discarded and the donor cell medium transferred. On receipt of the donor cell medium, recipient cells were returned to the incubator for 7 days prior to clonogenic staining.

8.2.2 Statistics

Results represent a minimum of 3 independent tests with a minimum of 2 replicates per independent test. The data was log transformed and ANOVA was performed on the linear regressions and pair-wise data were computed using the Bonferroni adjustment. Data are presented as the LSM of the Log(colony count) ± 95CI. All analyses were done using statistical software package SAS 9.1 and SAS enterprise guide 3.0. Significance was taken at a level of $p \leq 0.05$.

8.3 Results and discussion

To investigate the possibility of cell secreted factors, donor cell medium transfer experiments were performed. Such effects have been shown in response to ionising radiation exposures, i.e. radiation induced bystander effects, where the donor cell density has been shown to be important (20).

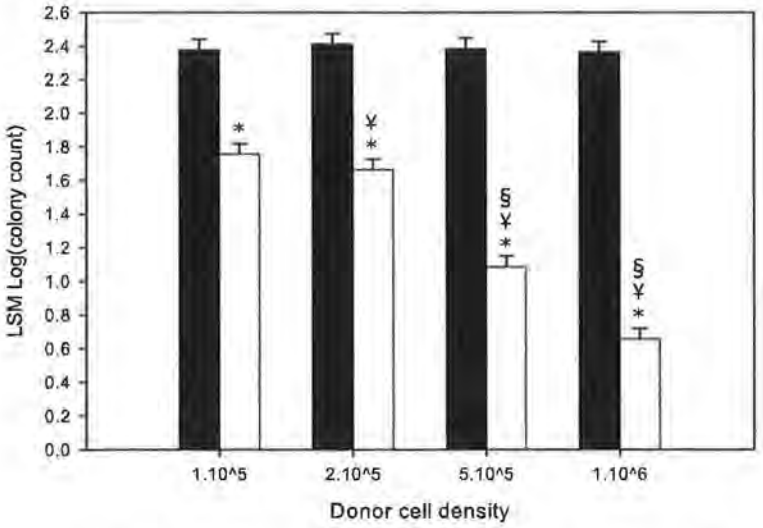

Figure 8.1 Recipient cell survival treated with donor cell medium harvested immediately post exposure. Donor cells seeded at a density of 1 x 10^5, 2 x 10^5, 5 x 10^5 or 1 x 10^6 cells per well were irradiated (□) or sham irradiated (■) using the Q-sun. Data presented as the LSM ± 95%CI; * indicates significant difference between irradiated and sham irradiated controls, all exposures tagged with ¥ are significantly different to one another; § indicates significant difference with respect to donor cell density 1x10^5, $p \leq 0.05$.

Figure 8.1 illustrates the survival of unexposed recipient cells treated with donor cell medium immediately post exposure. A clear and significant decrease in recipient cell survival with increasing donor cell density is observed. Statistical analysis showed no significant difference between control recipient cells despite receiving sham irradiated DMEM-F12 from differing donor cell densities thus eliminating reservations regarding

nutrient consumption. All 10 minute exposures were found to be significantly different from their respective controls. Furthermore, all recipient cells treated with exposed donor cell DMEM-F12 transfers were found to be significantly different from one another except for 1 x 10^5 and 2 x 10^5 donor cell densities which were not significantly different from one another.

These results show that the presence of cells during irradiation accentuates medium mediated cell killing effects of unirradiated recipient cells in a donor cell density dependent manner, supporting the conjecture that cells present during solar simulated irradiation release factor(s) into the medium. However this effect was found to be transient, lasting less than 1 hour, since donor cell medium transfers carried out 1, 24 and 48 hours post exposure were found to elicit survival not significantly different from controls at all times of transfer, (figures 8.2 – 8.4).

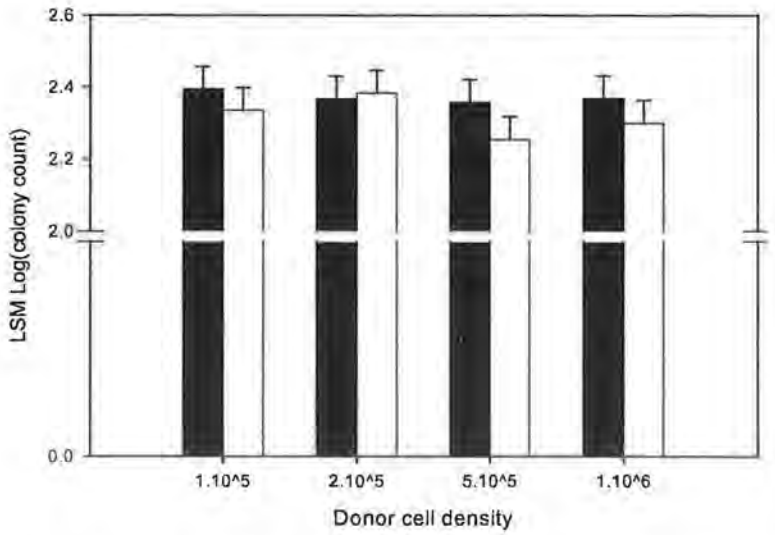

Figure 8.2 Recipient cell survival treated with donor cell medium harvested 1 hour post exposure. Donor cells seeded at a density of 1 x 10^5, 2 x 10^5, 5 x 10^5 or 1 x 10^6 cells per well were irradiated (□) or sham irradiated (■) using the Q-sun. Data presented as the LSM ± 95%CI;

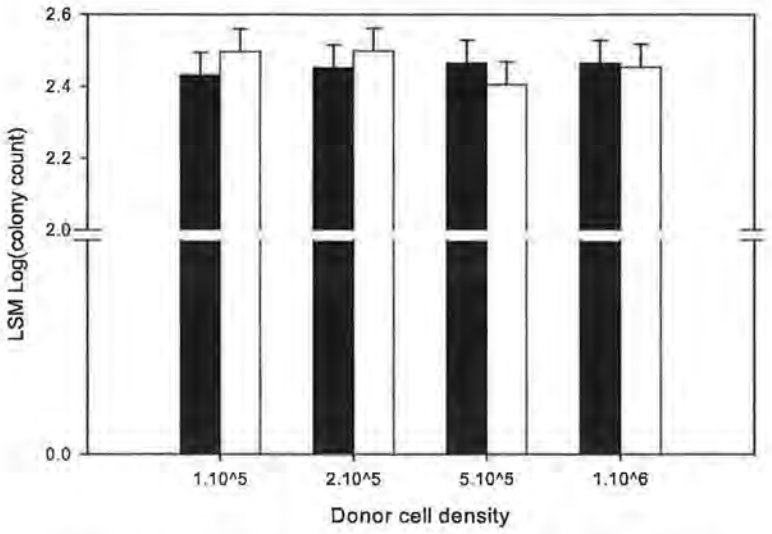

Figure 8.3 Recipient cell survival treated with donor cell medium harvested 24 hours post exposure. Donor cells seeded at a density of 1 x 10^5, 2 x 10^5, 5 x 10^5 or 1 x 10^6 cells per well were irradiated (□) or sham irradiated (■) using the Q-sun. Data presented as the LSM ± 95%CI;

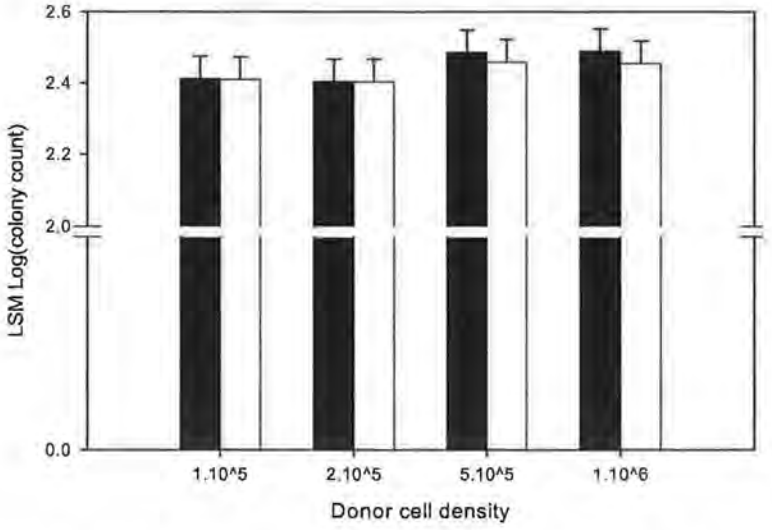

Figure 8.4 Recipient cell survival treated with donor cell medium harvested 48 hours post exposure. Donor cells seeded at a density of 1 x 10^5, 2 x 10^5, 5 x 10^5 or 1 x 10^6 cells per well were irradiated (□) or sham irradiated (■) using the Q-sun. Data presented as the LSM ± 95%CI;

These results conflict with the work of Banerjee et al (14) who found that apoptosis was initiated in unexposed recipient HaCaT cells treated with UVB irradiated donor cell medium when the medium transfers were performed ≥ 12 hours post exposure of the

donor cells but not before. However Banerjee et al (14) assayed cell survival using the method of transcriptional and translational (MTT) assay, which measures the reduction of tetrazolium salts by viable cells with active mitochondrial dehydrogenases to a blue formazan end product that is then measured spectrophotometrically (24). Although the chemosensitivity of the MTT assay has been found to yield a high level of correlation with the clonogenic assay (25), a study investigating the radiosensitivities of the clonogenic and MTT assays found the clonogenic assay to be most sensitive while the MTT assay was reported to be relatively insensitive especially at lower radiation levels (26). Thus the temporal differences observed between this and the study performed by Banerjee et al (14) may be due to radiosensitivity differences in the assays employed.

However, a further discrepancy regarding apoptotic induction at the late times of transfer also exists between the two studies. In chapter four, it was demonstrated that blank (no cells) DMEM-F12 irradiated for 10 minutes produced a significant decrease in unirradiated recipient cell survival compared to their respective controls at all transfer times; immediately, 1 hour, 24 and 48 hours post exposure (see figure 4.4). The results presented in this chapter show that the induction of cell death is transient, lasting less than 1 hour, which implies that the presence of cells during solar simulated irradiation incurs a 'protective' effect that overcomes the detrimental effects observed with blank irradiated DMEM-F12 at the later times of transfer. In contrast to this, Banerjee et al (14) observed decreasing cell viability with increasing time of transfer of the donor cell medium post exposure as measured by the MTT assay.

In addition to the MTT data, Banerjee et al (14) also reported an increase in mRNA levels of pro-apoptotic Bcl-2 family member Bax and the cell surface death receptor Fas

in bystander cells. Although both are indicative of apoptotic induction, their expression together is somewhat incongruous since Bax and Fas are involved in the intrinsic and extrinsic apoptotic pathways respectively. However, it is possible that these bystander cells fall under the heading of type II extrinsically apoptotic cells, which are cells in which the extrinsic apoptotic signalling is insufficient to activate the necessary caspase cascade required and thus induce the intrinsic apoptotic pathway (27, 28). This could explain not only the expression of Bax and Fas together but also the temporal differences in their expression where the expression of Bax was found to lag that of Fas. Activation of Bax and/or Bak is required for mitochondrial pore formation (29, 30) where mitochondrial outer membrane permeablisation is generally considered as the point of no return regarding apoptosis (31). However the reduced viability of UVB irradiated HaCaT cells has been shown to be abrogated by 5 μM of a ginseng derivative, ginsenoside, as measured using the MTT assay with no corresponding reduction in Bax mRNA expression (32). Furthermore, evidence has been presented that extrinsically apoptotic cells partially committed to apoptosis can recover and survive (33). This combined with the potentially pro-survival disposition of HaCaT cells due to their p53 homozygous mutant genotype (34) suggests that the discrepancy between the results presented by Banerjee et al (14) and this study may not be differences in bystander effect(s) but more reflective of experimental procedures and time points.

The proliferative response incurred in bystander cells, and shown in figures 8.2 – 8.4, that overcome the detrimental effects of solar simulated irradiated blank medium may be related to the findings of Lehnert and colleagues (21-23), Dissanayake et al (35, 36) and McMillan et al (37).

Over the course of several publications investigating the bystander response incurred by low dose α–particle irradiation, Lehnert and colleagues (21-23) found elevated intracellular ROS and a time of transfer dependent induction of SCEs in bystander cells not only treated with medium harvested from irradiated donor cells but also irradiated blank cell culture medium. Interestingly though, only cell conditioned medium modulated protein expression in a manner that favoured a pro-mitogenic state which concurred with the enhanced proliferation of bystander cells. No such effects were observed in bystander cells treated with blank fresh irradiated medium thus indicating that the factor(s) involved were cell derived. Based on their experimental observations, they postulated that this radiation induced transmissible factor was a cytokine, specifically, transforming growth factor beta (TGF-β1) which was found to be secreted into the supernatant of irradiated cells. Further investigation found TGF-β1 capable of inducing enhanced intracellular ROS, the same protein expression and the enhanced proliferative state observed in bystander cells when untreated cells were supplemented with concentrations of TGF-β1 similar to that secreted into the supernatant of irradiated cells. Moreover, effects that are observed in bystander cells such as enhanced intracellular ROS and reduced p53 protein levels could be abrogated by addition of a TGF-β1 neutralising antibody. Collectively, the work by Lehnert's group presents strong evidence that TGF-β1, at least in part, mediates α–particle induced bystander effects. In a study examining the effects of UVA and UVB radiation on primary human keratinocytes derived from neonatal foreskin, Dissanayake et al (35, 36) showed that both UVA alone or UVA and UVB combined induced enhanced secretion of TGF-β1 into the cell culture medium. In contrast to the results presented in this chapter, when this medium was harvested from directly irradiated cells and transferred to unirradiated primary keratinocytes 24 hours post exposure, the unirradiated recipient bystander cells

were found to exhibit decreased proliferation but increased cornification (epidermal thickening) with respect to sham irradiated donor cell medium transfers. However, Dissanayake et al (36) do state that cornification is not only the result of increases in the stratum corneum but also increased keratinocyte proliferation. There are some differences in methodology between the work presented here and that of Dissanayake et al (35, 36) that may significantly contribute to the different proliferative effects observed. In the work by Dissanayake et al (35, 36), cells were irradiated in PBS with UVA and UVB irradiances of 2 Wm^{-2} and 0.8 Wm^{-2} or 3.7 Wm^{-2} and 0.02 Wm^{-2} respectively but no distribution spectra were provided. Pre and post exposure cells were maintained in DMEM cell culture medium supplemented with 10 mM HEPES, a potent photosensitiser that is sensitised even by fluorescent room lighting in the presence of riboflavin (38). There was no mention of donor cell medium filtration prior to medium transfer thus it is possible that directly irradiated keratinocytes were unintentionally transferred and co-incubated with the unirradiated recipients which may potentially confound results. The irradiated donor cell medium was diluted in unirradiated DMEM at a ratio of 3:7 when immediately before transfer to unirradiated recipient cells. Genotypic differences between primary and immortalised keratinocytes may potentially provide growth advantages in the latter. Furthermore, proliferation was determined via cell counts just 36 hours post medium transfer when the primary keratinocytes could potentially be arrested to facilitate repair and thus may not reflect actual cell death but merely a transient lull in proliferative capacity.

Thus, from the results presented by both Lehnert's group (21-23) and Dissanayake et al (35, 36), it is postulated that TGF-β1 may have a role in solar simulated bystander responses that results in the enhanced proliferation observed in HaCaT bystander cells

(figures 8.2-8.4). Further support stems from the fact that TGF-β1 activates reduced nicotinamide adenine dinucleotide phosphate (NADPH) (39) which when inhibited was found to attenuate UVA radiation induced bystander effects (37). Furthermore, extracellular ROS can activate latent TGF-β1, thus establishing a positive feedback mechanism for the activation of TGF-β1 (39) which through its ability to elevate intracellular production of ROS (23, 39) may actively participate in sustaining oxidative stress which has been linked to UV induced genomic instability (40, 41).

In fact, increased oxidative stress was observed in UVA and UVB irradiated V79 hamster fibroblasts (41) which were found to possess both early and delayed mutations in the hypoxanthine-guanine phosphoribosyltransferase (hprt) gene (15). The induction of hprt mutations was attributed to bystander effects via gap junction intercellular communication (GJIC) and also extracellular factors secreted into the medium (unpublished preliminary results) (15). Furthermore, the occurrence of such mutations was found to be inhibited with antioxidants (16). However, this work conflicts with that presented by Whiteside and McMillan (17) who observed bystander effects with UVA but not UVB radiation in human keratinocyte and fibroblast cell lines. Although these discrepancies may be the result of differing cell models, it must be noted that the bystander effects reported by Dahle et al (15, 16) were in fact observed in directly irradiated cell populations which may in itself impair the ability of a study to observe bystander effects without direct effects confounding the observations. A non contact co incubation technique similar to that employed by Whiteside and McMillan (17) was used by Müller et al (19) who reported UVB induced bystander effects in unirradiated marine aquatic 3D cell cultures. However, the irradiator employed was a solar simulator with outputs in the UVA, visible and infrared regions as well as UVB. Thus, it cannot

be conclusively drawn that the effects observed were specific to UVB radiation. Although UVC radiation is not an environmentally relevant waveband, bystander signalling has been report with UVC radiation (11-13), thus it would be reasonable to believe that UVB radiation can elicit bystander responses since both UVA and UVC radiation effects have been demonstrated.

Table 8.1 Principle exposure parameters of known UVB bystander investigations in literature

Author	Cell line	Expo medium	Irradiance (Wm^{-2})	Waveband (nm)	Bystander effect
Whiteside and McMillan (17)	HaCaT	PBS	2-4	280-380	No
Whiteside and McMillan (17)	MRC5	PBS	2-4	280-380	No
Dahle et al (15)	V79	PBS	23.3	290-320	Yes
Banerjee et al (14)	HaCaT	PBS	n/a	UVA + B	Yes
Müller et al (19)	Demosponge	Seawater	n/a	UVA/B vis & IR	Yes

The discrepancies between studies reporting UVB bystander effects might be attributable to the irradiance employed. Table 8.1 illustrates some of the principal parameters of the different UVB bystander investigations cited in this chapter. As discussed in chapter 2, a UVB irradiance greater than 3 Wm^{-2} would not be expected at the terrestrial level. Although their irradiator emits radiation below the lowest terrestrial wavelength of 295 nm (42), Whiteside and McMillan (17) is the only study that can be confirmed to employ an irradiance reflective of that found at the terrestrial level, nor do their results appear to be cell line specific. And since it is not possible, in the absence of optical filtering, to discern which waveband predominantly contributes to full spectrum solar simulated bystander responses, it could well be that at environmentally relevant irradiances, UVA radiation is the dominant waveband regarding bystander effects.

Despite the variability of UV bystander effects from different groups, the results presented by Whiteside and McMillian (17) demonstrate an intriguing effect. They showed that irradiated HaCaT cells, which have been likened to suprabasal layer epidermal cells (43), can not only elicit autocrine bystander responses in unirradiated identical cell types but also paracrine bystander responses in unirradiated dermal fibroblasts via non contact co-incubation of the two cell populations (irradiated and unirradiated) (17). It is known that the capacity of radiation to penetrate the skin decreases with decreasing wavelength (44, 45). Using ex vivo full thickness epidermal samples, it has been shown that UV radiation is predominantly absorbed in the epidermal layer of the skin with less than 20 % of the incident radiation at 365 nm exiting the basal layer (46). In addition, epidermal keratinocytes obtain nutrients via diffusion across the basal membrane (47) since the dermal but not the epidermal layer is vascularised (44, 47). Thus, it is not unreasonable to believe that signals produced by epidermal keratinocytes in response to UV radiation could be transmitted to dermal fibroblasts which due to epidermal absorption of radiation remain relatively unexposed to UV radiation. Such bystander responses could potentially increase the senescence of dermal fibroblasts.

Using primary human keratinocytes, Kuhn et al (48) showed that cells irradiated with UVB radiation in medium devoid of exogenous growth factors that activate IGF-IR (insulin like growth factor I receptor) were significantly more apoptotic than those irradiated in the presence of IGF-IR activators. The pro-survival response of IGF-IR activation was found to result in post mitotic cells (incapable of replicating) whereas IGF-IR inactivated cells that survived irradiation were fully capable of proliferating with potentially mutagenic genomes. Physiological concentrations of both insulin and

IGF-I (insulin like growth factor I) were found to activate IGF-IR, however insulin provided only partial protection while IGF-I fully protected keratinocytes from UVB induced apoptosis. Dermal fibroblasts but not epidermal keratinocytes, unless involved in foetal growth or wound healing, produce and secrete IGF-I (49). Furthermore the production of IGF-I has been shown to be depleted in senescent human fibroblasts *in vitro* (50). Thus based on their results, Kuhn et al (48) speculated that the response of epidermal keratinocytes to UVB radiation is tightly linked to the health of dermal fibroblasts and their ability to secrete IGF-I *in vivo*. This conjecture was recently confirmed by the same group who observed reduced expression of both IGF-I mRNA transcripts and IGF-I protein in *in vivo* geriatric dermal fibroblasts (volunteers ≥ 65 years old) compared to *in vivo* young adult dermal fibroblasts (volunteers age 20-28 years old) (51). The reduced IGF-I expression in geriatric dermal fibroblasts was found to promote proliferating DNA damaged epidermal keratinocytes *in vivo* post UVB irradiation, an effect that was not observed when IGF-I proficient young adult skin was irradiated and was abrogated when geriatric skin was supplemented via intradermal injection with recombinant human IGF-I prior to UVB irradiation (51).

8.4 Conclusions

The results presented here and in the literature clearly demonstrate that human skin cells are capable of both autocrine and paracrine bystander signalling in response to UV radiation. The biological relevance may be highly significant in light of the recent work by Lewis et al (51) whose results suggest a new paradigm for the induction of skin carcinogenesis via dermal fibroblast senescence in vivo. Furthermore, Lewis et al (51) also showed that IGF-I expression silencing could be equally induced in primary

cultured normal human fibroblasts via continuous replication and oxidative stress. UVA radiation, the predominant solar UV waveband, is believed to elicit its effects primarily through oxidative processes (52). Thus, the hypothesis presented here is that solar UVA radiation contributes to and / or accelerates the senescence of dermal fibroblasts via TGF-β1 sustained oxidative paracrine bystander signalling which may ultimately undermine the capability of epidermal keratinocytes to execute the appropriate response to solar UVB radiation induced damage due to reduced secretion of IGF-1 by the now senescent dermal fibroblasts. This hypothesis needs to be tested, but the potential of solar radiation induced bystander signalling and its relevance to the *in vivo* situation clearly exists and warrants further investigation.

8.5 References

(1) W. F. Morgan (2003) Non-targeted and delayed effects of exposure to ionizing radiation: I. Radiation-induced genomic instability and bystander effects in vitro *Radiat Res* **159,** 567-80.

(2) K. M. Prise, G. Schettino, M. Folkard & K. D. Held (2005) New insights on cell death from radiation exposure *Lancet Oncol* **6,** 520-8.

(3) H. Nagasawa & J. B. Little (1992) Induction of sister chromatid exchanges by extremely low doses of alpha-particles *Cancer Res* **52,** 6394-6.

(4) H. Matsumoto, A. Takahashi & T. Ohnishi (2004) Radiation-induced adaptive responses and bystander effects *Biol Sci Space* **18,** 247-54.

(5) J. M. Kaminski, E. Shinohara, J. B. Summers, K. J. Niermann, A. Morimoto & J. Brousal (2005) The controversial abscopal effect *Cancer Treatment Reviews* **31,** 159-172.

(6) R. H. Mole (1953) Whole body irradiation--radiobiology or medicine? *Br J Radiol* **26,** 234-241.

(7) W. F. Morgan & M. B. Sowa (2007) Non-targeted bystander effects induced by ionizing radiation *Mutat Res* **616,** 159-64.

(8) K. M. Prise & J. M. O'Sullivan (2009) Radiation-induced bystander signalling in cancer therapy *Nat Rev Cancer* **9,** 351-60.

(9) D. Averbeck (2010) Non-targeted effects as a paradigm breaking evidence *Mutation Research/Fundamental and Molecular Mechanisms of Mutagenesis* **In Press, Accepted Manuscript.**

(10) D. T. Goodhead (2010) New radiobiological; radiation risk and radiation protection paradigms *Mutation Research/Fundamental and Molecular Mechanisms of Mutagenesis* **In Press, Accepted Manuscript**.

(11) M. Schorpp, U. Mallick, H. J. Rahmsdorf & P. Herrlich (1984) Uv-induced extracellular factor from human fibroblasts communicates the uv response to nonirradiated cells *Cell* **37,** 861-8.

(12) R. Ghosh & G. Bhaumik (1995) Supernatant medium from uv-irradiated cells influences the cytotoxicity and mutagenicity of v79 cells *Mutat Res* **335,** 129-35.

(13) L. C. DeVeaux, L. S. Durtschi, J. G. Case & D. P. Wells (2006) Bystander effects in unicellular organisms *Mutation Research/Fundamental and Molecular Mechanisms of Mutagenesis* **597,** 78-86.

(14) G. Banerjee, N. Gupta, A. Kapoor & G. Raman (2005) Uv induced bystander signaling leading to apoptosis *Cancer Letters* **223,** 275-84.

(15) J. Dahle, O. Kaalhus, T. Stokke & E. Kvam (2005) Bystander effects may modulate ultraviolet a and b radiation-induced delayed mutagenesis *Radiat Res* **163,** 289-95.

(16) J. Dahle, E. Kvam & T. Stokke (2005) Bystander effects in uv-induced genomic instability: Antioxidants inhibit delayed mutagenesis induced by ultraviolet a and b radiation *Journal of Carcinogenesis* **4,** 11.

(17) J. R. Whiteside & T. J. McMillan (2009) A bystander effect is induced in human cells treated with uva radiation but not uvb radiation *Radiat Res* **171,** 204-11.

(18) J. Dahle, S. Bagdonas, O. Kaalhus, G. Olsen, H. B. Steen & J. Moan (2000) The bystander effect in photodynamic inactivation of cells *Biochimica et Biophysica Acta (BBA) - General Subjects* **1475,** 273-280.

(19) W. E. G. Müller, H. Ushijima, R. Batel, A. Krasko, A. Borejko, I. M. Müller & H.-C. Schröder (2006) Novel mechanism for the radiation-induced bystander effect: Nitric oxide and ethylene determine the response in sponge cells *Mutation Research/Fundamental and Molecular Mechanisms of Mutagenesis* **597,** 62-72.

(20) C. Mothersill & C. Seymour (1997) Medium from irradiated human epithelial cells but not human fibroblasts reduces the clonogenic survival of unirradiated cells *Int J Radiat Biol* **71,** 421-7.

(21) B. E. Lehnert, E. H. Goodwin & A. Deshpande (1997) Extracellular factor(s) following exposure to alpha particles can cause sister chromatid exchanges in normal human cells *Cancer Res* **57,** 2164-71.

(22) P. K. Narayanan, E. H. Goodwin & B. E. Lehnert (1997) Alpha particles initiate biological production of superoxide anions and hydrogen peroxide in human cells *Cancer Res* **57,** 3963-71.

(23) R. Iyer, B. E. Lehnert & R. Svensson (2000) Factors underlying the cell growth-related bystander responses to alpha particles *Cancer Res* **60,** 1290-8.

(24) P. Lemieux, M. Michaud & M. Pagé (1993) A new formazan amplified clonogenic assay for cytotoxicity testing *Biotechnology Techniques* **7,** 1573-6784.

(25) K. Kawada, T. Yonei, H. Ueoka, K. Kiura, M. Tabata, N. Takigawa, M. Harada & M. Tanimoto (2002) Comparison of chemosensitivity tests: Clonogenic assay versus mtt assay *Acta Med Okayama* **56,** 129-34.

(26) D. Banasiak, A. Barnetson, R. , R. Odell, A., H. Mameghan & P. Russell, J. (1999) Comparison between the clonogenic, mtt, and srb assays for determining radiosensitivity in a panel of human bladder cancer cell lines and a ureteral cell line *Radiation Oncology Investigations* **7,** 77-85.

(27) Z. Assefa, A. Van Laethem, M. Garmyn & P. Agostinis (2005) Ultraviolet radiation-induced apoptosis in keratinocytes: On the role of cytosolic factors *Biochimica et Biophysica Acta - Reviews on Cancer* **1755,** 90-106.

(28) C. Sheridan & S. J. Martin (2008) Commitment in apoptosis: Slightly dead but mostly alive *Trends in Cell Biology* **18,** 353-357.

(29) M. C. Wei, W.-X. Zong, E. H. Y. Cheng, T. Lindsten, V. Panoutsakopoulou, A. J. Ross, K. A. Roth, G. R. MacGregor, C. B. Thompson & S. J. Korsmeyer (2001) Proapoptotic bax and bak: A requisite gateway to mitochondrial dysfunction and death *Science* **292,** 727-730.

(30) W. X. Zong, T. Lindsten, A. J. Ross, G. R. MacGregor & C. B. Thompson (2001) Bh3-only proteins that bind pro-survival bcl-2 family members fail to induce apoptosis in the absence of bax and bak *Genes Dev* **15,** 1481-6.

(31) D. R. Green & G. Kroemer (2005) Pharmacological manipulation of cell death: Clinical applications in sight? *The Journal of Clinical Investigation* **115,** 2610-2617.

(32) E. H. Lee, S. Y. Cho, S. J. Kim, E. S. Shin, H. K. Chang, D. H. Kim, M. H. Yeom, K. S. Woe, J. Lee, Y. C. Sim & T. R. Lee (2003) Ginsenoside f1 protects human hacat keratinocytes from ultraviolet-b-induced apoptosis by maintaining constant levels of bcl-2 *J Investig Dermatol* **121,** 607-613.

(33) J. G. Albeck, J. M. Burke, B. B. Aldridge, M. Zhang, D. A. Lauffenburger & P. K. Sorger (2008) Quantitative analysis of pathways controlling extrinsic apoptosis in single cells *Mol Cell* **30,** 11-25.

(34) T. A. Lehman, R. Modali, P. Boukamp, J. Stanek, W. P. Bennett, J. A. Welsh, R. A. Metcalf, M. R. Stampfer, N. Fusenig, E. M. Rogan & et al. (1993) P53 mutations in human immortalized epithelial cell lines *Carcinogenesis* **14,** 833-9.

(35) N. S. Dissanayake, G. E. Greenoak & R. S. Mason (1993) Effects of ultraviolet irradiation on human skin-derived epidermal cells in vitro *J Cell Physiol* **157,** 119-27.

(36) N. S. Dissanayake & R. S. Mason (1998) Modulation of skin cell functions by transforming growth factor-beta1 and acth after ultraviolet irradiation *J Endocrinol* **159,** 153-163.

(37) T. J. McMillan, E. Leatherman, A. Ridley, J. Shorrocks, S. E. Tobi & J. R. Whiteside (2008) Cellular effects of long wavelength uv light (uva) in mammalian cells *J Pharm Pharmacol* **60,** 969-76.

(38) R. G. Keynes, C. Griffiths & J. Garthwaite (2003) Superoxide-dependent consumption of nitric oxide in biological media may confound in vitro experiments *Biochemical Journal* **369,** 399-406.

(39) A. Sánchez-Capelo (2005) Dual role for tgf-[beta]1 in apoptosis *Cytokine & Growth Factor Reviews* **16,** 15-34.

(40) R. P. Phillipson, S. E. Tobi, J. A. Morris & T. J. McMillan (2002) Uv-a induces persistent genomic instability in human keratinocytes through an oxidative stress mechanism *Free Radic Biol Med* **32,** 474-80.

(41) J. Dahle & E. Kvam (2004) Increased level of oxidative stress in genomically unstable cell clones *Journal of Photochemistry and Photobiology B: Biology* **74,** 23-28.

(42) D. B. Brown, A. E. Peritz, D. L. Mitchell, S. Chiarello, J. Uitto & F. P. Gasparro (2000) Common fluorescent sunlamps are an inappropriate substitute for sunlight *Photochemistry and Photobiology* **72,** 340-4.

(43) K. M. Lee, J. G. Lee, E. Y. Seo, W. H. Lee, Y. H. Nam, J. M. Yang, S. H. Kee, Y. J. Seo, J. K. Park, C. D. Kim & J. H. Lee (2005) Analysis of genes responding to ultraviolet b irradiation of hacat keratinocytes using a cdna microarray *Br J Dermatol* **152,** 52-9.

(44) F. R. de Gruijl (1997) Health effects from solar uv radiation *Radiat Prot Dosimetry* **72,** 177-196.

(45) S. E. Freeman, H. Hacham, R. W. Gange, D. J. Maytum, J. C. Sutherland & B. M. Sutherland (1989) Wavelength dependence of pyrimidine dimer formation in DNA of human skin irradiated in situ with ultraviolet light *Proc Natl Acad Sci U S A* **86,** 5605-9.

(46) W. A. Bruls, H. Slaper, J. C. van der Leun & L. Berrens (1984) Transmission of human epidermis and stratum corneum as a function of thickness in the ultraviolet and visible wavelengths *Photochem Photobiol* **40,** 485-94.

(47) K. U. Schallreuter & J. M. Wood (1995) The human epidermis *Proc Nutr Soc* **54,** 191-5.

(48) C. Kuhn, S. A. Hurwitz, M. G. Kumar, J. Cotton & D. F. Spandau (1999) Activation of the insulin-like growth factor-1 receptor promotes the survival of human keratinocytes following ultraviolet b irradiation *Int J Cancer* **80,** 431-8.

(49) S. R. Edmondson, S. P. Thumiger, G. A. Werther & C. J. Wraight (2003) Epidermal homeostasis: The role of the growth hormone and insulin-like growth factor systems *Endocr Rev* **24,** 737-764.

(50) A. Ferber, C. Chang, C. Sell, A. Ptasznik, V. J. Cristofalo, K. Hubbard, H. L. Ozer, M. Adamo, C. T. Roberts & D. LeRoith (1993) Failure of senescent human fibroblasts to express the insulin-like growth factor-1 gene *Journal of Biological Chemistry* **268,** 17883-17888.

(51) D. A. Lewis, J. B. Travers, A. K. Somani & D. F. Spandau (2009) The igf-1/igf-1r signaling axis in the skin: A new role for the dermis in aging-associated skin cancer *Oncogene.*

(52) M. Schauen, H.-T. Hornig-Do, S. Schomberg, G. Herrmann & R. J. Wiesner (2007) Mitochondrial electron transport chain activity is not involved in ultraviolet a (uva)-induced cell death *Free Radical Biology and Medicine* **42,** 499-509.

Chapter 9 Conclusions and future work

As outlined in the chapter 1, the purpose of this study was to address some of the key issues that are potentially hindering the progress of skin carcinogenesis investigations. The results presented in this thesis clearly emphasise the importance of both the irradiator and exposure medium employed in *in vitro* investigations.

Although dosimetry is rarely the endpoint of a given study, it is however, one of the founding parameters of radiobiological investigations. From the literature, it is evident that the provision of dosimetric measurements in UV investigations is justly gaining momentum. However, the environmental irrelevance and / or inadequate dosimetry in some studies suggest that there is still much confusion in this area. While the importance of dosimetry is undisputed, the dose administered is not the only aspect of an irradiator that necessitates analysis. Both spectral distribution and output delivery are also highly important when determining the relevance of an irradiator. Furthermore, analysing and measuring the characteristics of an irradiator alone is not enough, a frame of reference is required. For skin carcinogenesis investigations, this reference is solar radiation where a reference spectrum that reflects solar radiation at mid to near tropic latitudes is reasonable in light of studies that have found that the rates of melanoma and non melanoma skin cancers increase with decreasing latitude in America, Norway and New Zealand (1-3). Utilising a reference spectrum of solar radiation enables investigators to better identify the environmental relevance of an irradiator in terms of irradiance, spectral distribution and output delivery. This is effectively demonstrated in the recently published work presented

in chapters 2 and 3 (4), see appendix four for cited publication. While this work was intended to demonstrate the vastly different capabilities of different irradiators to elicit cell death due to differences in their spectral distribution, irradiance and nature, it clearly demonstrates how competent dosimetry and reference to solar radiation can aid investigations. Based on the distribution spectra presented in figure 2.24, it was speculated that the UVB lamp was the most detrimental irradiator under investigation which was later confirmed by radiobiological experimentation. These pre-experimental observations re-affirm spectroradiometry as the superior technique to calibrate irradiators since radiometers, although advantageous in their own right, do not provide any information regarding the spectral distribution of a source. Furthermore the ability of spectroradiometric data to unambiguously communicate the spectral irradiance of an irradiator not only permits visual inter comparison of sources including solar radiation but also confirms the credibility, or lack thereof, of manufacturer data thus reiterating the above points.

In addition to the spectral distribution and irradiance, the output delivery is another aspect of an irradiator that has the potential to confound investigations. The environmental relevance of the Q-sun solar simulator was found to be reciprocity law compliant despite delivering an exaggerated irradiance per pulse. This was based on the increased cell survival observed when cells were irradiated using the Q-sun compared to a similar exposure using the Oriel solar simulator and was attributed to the increased irradiance in the UVB waveband of the Oriel. However, a threshold pulse frequency is suspected at which cells would begin to deviate significantly from the response expected when an equivalent dose is administered using a continuous source since a decrease in pulse

frequency would require an increase in radiant intensity delivered per pulse in order to achieve the same integral exposure. However, the pulse frequency of the Q-sun is fixed, thus preventing further investigation into frequency mediated reciprocity effects. The possibility, however, that the Q-sun would result in enhanced cell death compared to the Oriel for equivalent effective doses remains to be elucidated. Furthermore, it is possible that intracellular death effector pathways activated in response to equivalent effective doses delivered in a pulsed and continuous manner are significantly different to one another. In addition, reciprocity studies examining the effects of energy delivered per second i.e. irradiance based reciprocity effects, are feasible using the Oriel solar simulator. As demonstrated in chapter 2, the Oriel is a continuous source and the spectral irradiance is variable by means of its current settings. Thus, irradiance based reciprocity studies are possible by (a) employing a fixed exposure distance and varying the spectral irradiance via the current settings, (b) employing a fixed exposure distance and a fixed current setting in conjunction with a series of neutral density filters and / or (c) by making use of the inverse square law and employing a fixed current setting but varying the exposure distance. In order to determine the required exposures needed to deliver equivalent effective doses the spectral irradiance of the Q-sun and the Oriel would need to be spectrally weighted prior to further radiobiological investigation into these reciprocity effects. However, due to the rapidly increasing efficacy of action spectra with decreasing wavelength particularly in the UVB, weighting requires rigorous stray light rejection to minimise erroneous overestimations in irradiance particularly at biologically effective wavelengths such as those in the UVB. Stray light rejection is determined by the bandpass and hence optical resolution of a spectroradiometer (5), which are nominally achieved with double

monochromator spectroradiometers (6). Thus, despite stray light corrections outlined in chapter 2, the precision of data collected using a USB2000 spectrometer is not believed to be of a level at which weighting irradiance spectra would be appropriate. Thus, in the absence of a bench top double monochromator spectroradiometer, further reciprocity studies were not feasible for this current body of research. However, while it is important to acknowledge instrumental limitations, it is important to emphasise that data collected using the USB2000 spectrometer effectively served its intended purpose which was to obtain reasonable approximations on the irradiance spectra of the irradiators under investigation.

Another founding parameter that appears to be given little attention in the literature is the exposure medium employed during non-ionising investigations which varies widely from cell culture medium to water, seawater, saline solutions, phenol red free media and PBS (7-12). The primary exposure media appear to be cell culture medium and PBS, thus exposures in this study were performed in both DMEM-F12 cell culture medium and PBS. It was during the radiobiological investigations examining the differential effects of different irradiators on cell survival that the disparate effects of irradiation in DMEM-F12 and PBS were observed.

Although further investigation is required to clarify the pathways by which cell death is incurred in the different exposure media, all endpoints examined here demonstrated significant differences between the response of cells irradiated in PBS and DMEM-F12. Although the absence of proapoptotic events in cells irradiated in PBS may be due to the induction of non intrinsic apoptotic pathways(s) or merely temporal discrepancies between

measurement and induction of intrinsic apoptotic events, the inability of cells to arrest at the G_2 checkpoint suggests that cells irradiated in PBS for extended durations become endocyclic. Furthermore, the inclusion of fpg in the comet assay of PBS irradiated cells demonstrates a similar pattern to that observed in cells irradiated in DMEM-F12 in terms of oxidative damage saturation. However, in contrast to DMEM-F12 irradiated cells, fpg treated and untreated cells irradiated in PBS were found to be significantly different at all exposure durations. Although this may be indicative of lower levels of oxidative damage, the fact that DNA damage is the trigger for endocycle entry (13), which does not occur in DMEM-F12 irradiated cells, implies that a sufficient level of damage does occur and / or that the distribution of DNA damage induced in PBS irradiated cells is different to that induced in DMEM-F12 irradiated cells. Since the dose has been reported to play a significant role in the distribution of UVB induced mutations (14), it would not be unreasonable to expect differences due to the exposure media if only due to differences in their transmittance spectra. The possibility that this effect may be cell specific cannot be overlooked since HaCaT cells are p53 deficient which provides a susceptibility to endocycle entry (13). However, working with primary human keratinocytes is not always feasible and immortalisation of human keratinocyte cell lines commonly employs deregulation of at least one tumour suppressor such as Rb and / or p53 (15, 16). Thus, the induction of endocycles in cells may pose a significant obstacle for solar simulated irradiation investigations if exposures are performed in PBS.

In contrast to cells irradiated in PBS, cells irradiated in DMEM-F12 are mitotically inhibited post irradiation and undergo apoptosis where caspase-3 activation is observed 2

hours post irradiation. However, the ability of DMEM-F12 to augment cell death above that observed when cells were irradiated in PBS was greatly perplexing in light of their transmittance properties. Further investigation revealed that this extensive cell killing in DMEM-F12 was due to the extracellular production of hydrogen peroxide attributed to the photosensitisation of riboflavin which is most probably enhanced by the radiation induced degradation of riboflavin in DMEM-F12 demonstrated by its emission spectrum. Riboflavin photosensitisation in DMEM-F12 when irradiated with solar simulated radiation is supported by exposures performed using the UVB irradiator. As shown in chapter 3, cells irradiated in DMEM-F12 and PBS with the UVB lamp yielded cell survival curves that concur with their transmittance properties such that increased cell death was observed when cells were irradiated in PBS. This was suggested to occur due to the omission of hypothetically photosensitising wavelengths in the output of the UVB irradiator. Riboflavin was demonstrated to absorb at 370 nm and 440 nm which are not present in the spectral distribution of the UVB irradiator. However, it is well documented in the literature that riboflavin is a photosensitiser (17-21) that absorbs at 365 nm and 440 nm (22). In fact, it is for this reason that Mahns et al (23) recommend using PBS during UVA irradiation. Although this may effectively overcome the photosensitising effects observed when cells are UVA irradiated in the presence of riboflavin, performing UVB exposures in PBS does not appear to be beneficial in light of the results presented by both Kuhn et al (24) and Lewis et al (25). Whose results suggest that UVB irradiation in the absence of extracellular growth factors facilitates the survival of potentially mutagenic keratinocytes, albeit at low levels.

Such discrepancies highlight the need to identify a suitable exposure medium that can be employed in UVA, UVB and solar simulated radiation investigations with minimal modifications, in order to aid not only the biological relevance of an investigation but also inter lab comparison. Although PBS clearly possesses superior transmittance properties compared to DMEM-F12 as shown in chapter 2, the capacity of radiation to penetrate the skin is known to decrease with decreasing wavelength (26, 27), where less than 20% of the incident radiation at 365 nm was found to exit the basal layer of *ex vivo* full thickness epidermal samples (28). Thus, PBS does not simulate *in vivo* conditions by permitting increased transmission of short wavelengths to proliferating cells which are found predominantly in the basal layer, which would not occur *in vivo* due to absorption in suprabasal layers. The biological relevance of PBS is further questioned by the absence of nutrients in the extracellular environment during irradiation since keratinocytes in the non vascularised epidermal layer obtain nutrients that diffuse across the basal membrane into the extracellular space (29). Thus under 'normal' conditions, *in vivo* epidermal keratinocytes are not devoid of nutrients in their extracellular environment during solar irradiation. The importance of this has been demonstrated *in vitro* (24) and *in vivo* (25).

Whilst it is recognised that *in vitro* experimentation will never truly mimic the *in vivo* situation, it is important that *in vitro* studies attempt to bridge the gap separating them in order for progress to be made in skin carcinogenesis investigations. Thus, based on evidence in the literature and the results presented here, it is recommended that serum supplemented riboflavin free cell culture media is employed as the exposure medium

during non-ionising radiation investigations. Furthermore, the ability of phenol red to quench riboflavin photosensitisation suggests that phenol red free cell culture media are substantially more phototoxic not only because of uninhibited photosensitisation of riboflavin but also because amino acids such as tryptophan and tyrosine have been demonstrated to augment the oxidising potential of riboflavin (30). Thus, it is further recommended that phenol red free cell culture media are not used during non-ionising radiation investigations.

Despite the above recommendations, a final point to contemplate is the biological relevance of riboflavin's presence during irradiation. Riboflavin is necessary for healthy growth and its absence has been demonstrated to lead to cellular stress events (31-33). Thus, it is possible that riboflavin is maintained in the extracellular environment of proliferating epidermal cells. Since molecules move down their concentration gradient it would be reasonable to assume that if riboflavin is maintained in the epidermis, it would be found at concentrations less than that found in blood plasma levels which have been reported to occur between 12.7-53.4 nM and 8.2-57.8 nM for infants and adolescents respectively (34). Notably the concentration of riboflavin found in DMEM-F12 (0.58 μM) is approximately 10 fold higher than the maximum blood plasma concentration of riboflavin reported by Capo-chichi et al (34). Thus, although excessive photosensitisation is undesirable, if it is confirmed that riboflavin is maintained in the epidermis at some threshold level, the presence of riboflavin in the exposure medium during *in vitro* solar radiation investigations may need to be re-addressed.

However, in the absence of such evidence, investigations into the effects of solar simulated radiation on human skin cells are planned using riboflavin free cell culture medium as the exposure medium. Further investigations into the different apoptotic pathways activated when cells are irradiated in DMEM-F12, PBS and L-15 in order to highlight their differential effects, if any, and to determine whether or not cells irradiated in PBS do in fact become endocyclic or whether the absence of apoptotic markers in PBS irradiated cells are merely temporal issues. The proliferative bystander effect observed in chapter 8 will be further investigated in order to determine if human keratinocytes do secrete factors in response to solar simulated radiation and if this factor is indeed the cytokine TGF-β1 or if some other transmissible factor(s) are responsible. In addition, the abilities of both UVA and UVB radiation to influence these effects will also be performed using optical filters.

References

(1) M. J. Eide & M. A. Weinstock (2005) Association of uv index, latitude, and melanoma incidence in nonwhite populations--us surveillance, epidemiology, and end results (seer) program, 1992 to 2001 *Arch Dermatol* **141,** 477-81.

(2) J. Moan, A. Dahlback, Z. Lagunova, E. Cicarma & A. C. Porojnicu (2009) Solar radiation, vitamin d and cancer incidence and mortality in norway *Anticancer Res* **29,** 3501-9.

(3) J. L. Bulliard, B. Cox & J. M. Elwood (1994) Latitude gradients in melanoma incidence and mortality in the non-maori population of new zealand *Cancer Causes Control* **5,** 234-40.

(4) A. Maguire, F. M. Lyng & J. E. Walsh (2010) Solar simulated radiation induced cell death depends on spectral distribution and irradiance but not output delivery *Radiation Protection Dosimetry*, 1-11.

(5) E. C. Weatherhead & A. R. Webb (1997) International response to the challenge of measuring solar ultra-violet radiation *Radiat Prot Dosimetry* **72,** 223-229.

(6) C. R. Roy, H. P. Gies, D. J. Lugg, S. Toomey & D. W. Tomlinson (1998) The measurement of solar ultraviolet radiation *Mutation Research/Fundamental and Molecular Mechanisms of Mutagenesis* **422,** 7-14.

(7) Y.-T. Han, Z.-W. Han, G.-Y. Yu, Y.-J. Wang, R.-Y. Cui & C.-B. Wang (2004) Inhibitory effect of polypeptide from chlamys farreri on ultraviolet a-induced oxidative damage on human skin fibroblasts in vitro *Pharmacological Research* **49,** 265-274.

(8) S. Kozmin, G. Slezak, A. Reynaud-Angelin, C. Elie, Y. de Rycke, S. Boiteux & E. Sage (2005) Uva radiation is highly mutagenic in cells that are unable to repair 7,8-dihydro-8-oxoguanine in saccharomyces cerevisiae *Proc Natl Acad Sci U S A* **102,** 13538-43.

(9) W. E. G. Müller, H. Ushijima, R. Batel, A. Krasko, A. Borejko, I. M. Müller & H.-C. Schröder (2006) Novel mechanism for the radiation-induced bystander effect: Nitric oxide and ethylene determine the response in sponge cells *Mutation Research/Fundamental and Molecular Mechanisms of Mutagenesis* **597,** 62-72.

(10) C. A. Koch-Paiz, S. A. Amundson, M. L. Bittner, P. S. Meltzer & A. J. Fornace, Jr. (2004) Functional genomics of uv radiation responses in human cells *Mutat Res* **549,** 65-78.

(11) M. Kwitniewski, A. Juzeniene, L.-W. Ma, R. Glosnicka, A. Graczyk & J. Moan (2009) Diamino acid derivatives of ppix as potential photosensitizers for photodynamic therapy of squamous cell carcinoma and prostate cancer: In vitro studies *Journal of Photochemistry and Photobiology B: Biology* **94,** 214-222.

(12) G. Banerjee, N. Gupta, A. Kapoor & G. Raman (2005) Uv induced bystander signaling leading to apoptosis *Cancer Letters* **223,** 275-84.

(13) J. Erenpreisa & M. S. Cragg (2001) Mitotic death: A mechanism of survival? A review *Cancer Cell Int,* 1-7.

(14) J.-L. Ravanat, T. Douki & J. Cadet (2001) Direct and indirect effects of uv radiation on DNA and its components *Journal of Photochemistry and Photobiology B: Biology* **63,** 88-102.

(15) P. Boukamp, R. T. Petrussevska, D. Breitkreutz, J. Hornung, A. Markham & N. E. Fusenig (1988) Normal keratinization in a spontaneously immortalized aneuploid human keratinocyte cell line *Journal of Cell Biology* **106,** 761-71.

(16) K. Münger & P. M. Howley (2002) Human papillomavirus immortalization and transformation functions *Virus Research* **89,** 213-228.

(17) A. M. Edwards & E. Silva (2001) Effect of visible light on selected enzymes, vitamins and amino acids *Journal of Photochemistry and Photobiology B: Biology* **63,** 126-31.

(18) P. C. Joshi, C. Carraro & M. A. Pathak (1987) Involvement of reactive oxygen species in the oxidation of tyrosine and dopa to melanin and in skin tanning *Biochemical and Biophysical Research Communications* **142,** 265-74.

(19) A. Besaratinia, S. I. Kim, S. E. Bates & G. P. Pfeifer (2007) Riboflavin activated by ultraviolet a1 irradiation induces oxidative DNA damage-mediated mutations inhibited by vitamin c *Proceedings of the National academy of Sciences* **104,** 5953-8.

(20) R. G. Keynes, C. Griffiths & J. Garthwaite (2003) Superoxide-dependent consumption of nitric oxide in biological media may confound in vitro experiments *Biochemical Journal* **369,** 399-406.

(21) H. Kim, L. J. Kirschenbaum, I. Rosenthal & P. Riesz (1993) Photosensitized formation of ascorbate radicals by riboflavin: An esr study *Photochemistry and Photobiology* **57,** 777-84.

(22) L. Ali & I. Naseem (2002) Hemolysis of human red blood cells by combination of riboflavin and aminophylline *Life Sciences* **70,** 2013-22.

(23) A. Mahns, I. Melchheier, C. V. Suschek, H. Sies & L. O. Klotz (2003) Irradiation of cells with ultraviolet-a (320-400 nm) in the presence of cell culture medium elicits biological effects due to extracellular generation of hydrogen peroxide *Free Radic Res* **37,** 391-7.

(24) C. Kuhn, S. A. Hurwitz, M. G. Kumar, J. Cotton & D. F. Spandau (1999) Activation of the insulin-like growth factor-1 receptor promotes the survival of human keratinocytes following ultraviolet b irradiation *Int J Cancer* **80,** 431-8.

(25) D. A. Lewis, J. B. Travers, A. K. Somani & D. F. Spandau (2009) The igf-1/igf-1r signaling axis in the skin: A new role for the dermis in aging-associated skin cancer *Oncogene.*

(26) F. R. de Gruijl (1997) Health effects from solar uv radiation *Radiat Prot Dosimetry* **72,** 177-196.

(27) S. E. Freeman, H. Hacham, R. W. Gange, D. J. Maytum, J. C. Sutherland & B. M. Sutherland (1989) Wavelength dependence of pyrimidine dimer formation in DNA of human skin irradiated in situ with ultraviolet light *Proc Natl Acad Sci U S A* **86,** 5605-9.

(28) W. A. Bruls, H. Slaper, J. C. van der Leun & L. Berrens (1984) Transmission of human epidermis and stratum corneum as a function of thickness in the ultraviolet and visible wavelengths *Photochem Photobiol* **40,** 485-94.

(29) K. U. Schallreuter & J. M. Wood (1995) The human epidermis *Proc Nutr Soc* **54,** 191-5.

(30) A. Grzelak, B. Rychlik & G. Bartosz (2001) Light-dependent generation of reactive oxygen species in cell culture media *Free Radical Biology and Medicine* **30,** 1418-25.

(31) R. Werner, K. C. Manthey, J. B. Griffin & J. Zempleni (2005) Hepg2 cells develop signs of riboflavin deficiency within 4 days of culture in riboflavin-deficient medium *Journal of Nutritional Biochemistry* **16,** 617-24.

(32) K. C. Manthey, Y. C. Chew & J. Zempleni (2005) Riboflavin deficiency impairs oxidative folding and secretion of apolipoprotein b-100 in hepg2 cells, triggering stress response systems *The Journal of Nutrition* **135,** 978-82.

(33) K. C. Manthey, R. Rodriguez-Melendez, J. T. Hoi & J. Zempleni (2006) Riboflavin deficiency causes protein and DNA damage in hepg2 cells, triggering arrest in g1 phase of the cell cycle *Journal of Nutritional Biochemistry* **17,** 250-6.

(34) C. D. Capo-chichi, J. L. Gueant, F. Feillet, F. Namour & M. Vidailhet (2000) Analysis of riboflavin and riboflavin cofactor levels in plasma by high-performance liquid chromatography *J Chromatogr B Biomed Sci Appl* **739,** 219-24.

Appendix 1

Protocol for making Agar dishes for sterility assessments

17.5 g of plate count Agar (Oxoid, tryptone 5g/L, yeast extract 2.5 g/L, glucose 1 g/L and Agar 9 g/L) was suspended in 1 litre deionised water and autoclaved at 121 °C for 15 minutes. Once sterilised, 15 ml agar was decanted into 90 mm Petri dishes and allowed to cool. Prior to use, the agar dishes were stored in the refrigerator. Agar dishes were used to determine the sterility of the exposure field for both the Q-sun and Oriel solar simulators. The solar simulators were ignited and allowed to initialise for at least 15 minutes. The exposure field of each irradiator was cleaned and sterilised using Virkon and 100% methanol as would be used prior to irradiation experiments. The maximum exposure employed in this study was 60 minutes, thus, agar dishes were also irradiated for 60 minutes. After irradiation the dark cycle employed to sham irradiate controls was initiated and a further set of agar dishes were sham irradiated for 30 seconds as was every sham irradiated control. Agar dishes were handled identically to cell cultures during both the irradiation and sham irradiation procedures. Once the agar dishes were irradiated or sham irradiated, the agar dishes were incubated for 7 days as would be the case for the clonogenic assays. The agar dishes were monitored over the 7 day incubation but no growth was observed in either the irradiated or sham irradiated agar plates.

Cell counts using a Haemocytometer

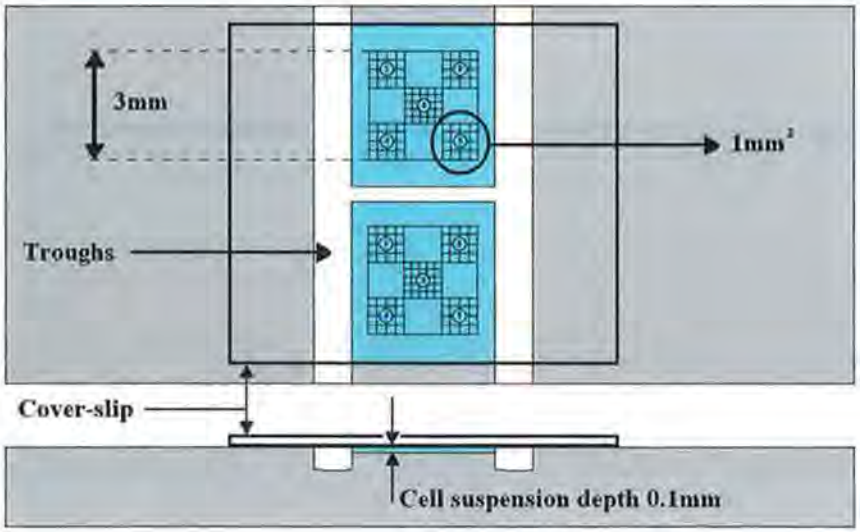

Figure A1.1 Ariel and side view of a haemocytometer with coverslip.

The haemocytometer is a microscope slide on which two counting chambers are etched as shown in figure A1.1. Each counting chamber consists of a grid divided into 9 chambers (figures A1.1 and A1.2A). A cover slip is mounted on the haemocytometer and the cell suspension is taken up by capillary action where the volume of fluid held between the haemocytometer grid and the cover slip is known (0.1 cm x 0.1 cm x 0.01 cm = $10^{-4}cm^3 = 10^{-4}ml$).

Under the microscope, a detailed view of the grid can be seen along with any cells in the suspension. Cells present in chambers 1-5 (figure A1.2A) are counted in both the top and bottom grids and the mean cell count of the 10 chambers obtained. Counts in the top and bottom grids should be within 10% of one another. Cells located on the perimeter lines of the chambers are counted or ignored depending on where they are situated. Figure A1.2B shows a sample chamber that contains 20 cells. Of the 20 cells, 11 are located on the perimeter. Cells located on the left and upper perimeter are

counted whilst cells located on the right and lower perimeter are not. Thus for this particular chamber only the green cells are counted, yielding a final cell count of 15. The concentration of cells per millilitre is determined using equation A1.1 where n is the mean number of cells counted in all 10 chambers and d is the dilution factor. If the cell suspension was not diluted then d =1.

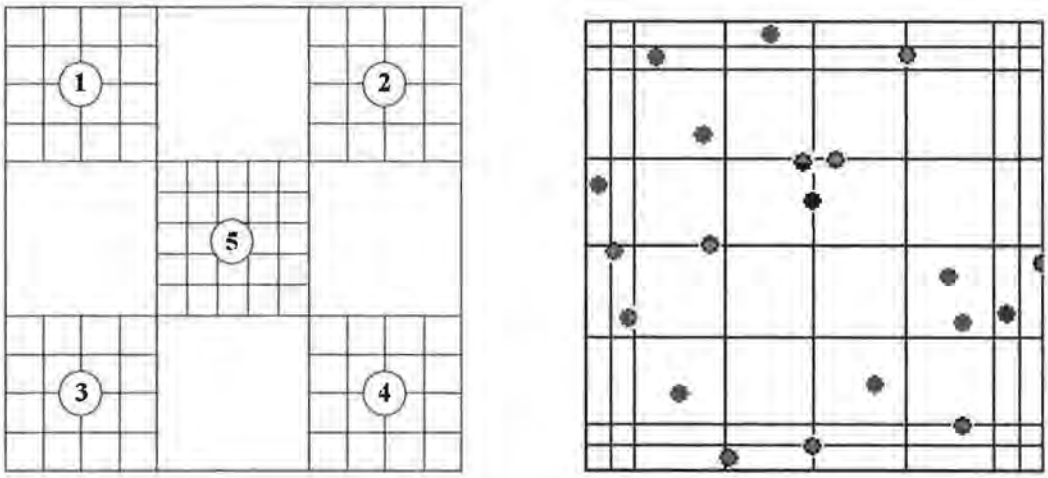

(A) *(B)*

Figure A1.2 (A) Schematic of the haemocytometer grid and the 5 chambers in a given grid that are used when determining the concentration of cells in a solution and (B) an example showing a counting chamber with the cells that should be counted (green) and not counted (red).

$$Cells/ml = \frac{n \times 10^4}{d} \qquad \textit{EquationA1.1}$$

Cell viability assay using the Trypan Blue exclusion method

The percentage viability of cells can be obtained using the haemocytometer in conjunction with Trypan Blue stain. A 1/10 dilution (d=1/10) of the cell stock in Trypan blue is used as the cell suspension. Non-viable cells take up the dye and appear blue whereas viable cells do not and appear white. The percentage viability is ascertained using equation A1.2.

$$\textit{EquationA1. 2}\quad \text{Percentage viability} = \frac{(\text{number of white cells})*100}{(\text{number of blue + white cells})}$$

Appendix 2

Protocol to make 100 ml phenol free DMEM-F12 cell culture medium

1.56g DMEM-F12 powdered medium (Sigma, Dorset, U.K), 0.12g Sodium bicarbonate (Sigma) and 90ml deionised water are mixed together to give 90 % of the final volume. Stir the solution until and the powdered medium and sodium bicarbonate have gone into solution and then measure the pH, adjusting if necessary using HCl or NaOH to achieve pH 6.9 ± 0.3. Once the solution is at the desired pH the final 10 ml deionised water is added to the solution and is then filter-sterilised using a 0.22 μm filter.

Protocol to make MgCaPBS

The below reagents at the concentrations listed generates the stock solution of Mg Ca PBS, which is subsequently diluted to 1 % in PBS to achieve the working stock.

Reagent	Fomula weight	Concentration	Making 100ml
NaCl (Sigma)	(FW 58.44g/l)	want 130mM	759.72mg
KCl (Sigma)	(FW 74.55g/l)	want 5mM	37.275mg
Na_2NPO_4 (Sigma)	(FW 141.96g/l)	want 1mM	14.196mg
$MgCl_2$ (Sigma)	(FW 203.31g/l)	want 1mM	20.331mg
$CaCl_2$ (Sigma)	(FW 147.01g/l)	want 1mM	14.701mg
PBS (Sigma)			100ml

Appendix 3

1% Normal agarose (50ml)

Add 0.5g normal agarose to 50ml PBS; heat until clear.

Use this solution to coat slides. Submerge sample-end of slide into solution, remove and wipe one side. Lie on tissue paper over night at room temperature to allow dry. Coat slides quickly before solution sets in beaker/container.

0.8% Low Melting Point (LMP) agarose (25ml);

Add 0.2g normal agarose to 25ml PBS; heat until clear. Use this to re-suspend cells. Make on same day as assay.

For H_2O_2 dose response or H_2O_2 positive control;

Solution A 9ml PBS + 1ml H_2O_2 = $10^6\mu M$

Solution B 9ml PBS + 1ml soluA = $10^5\mu M$

Solution C 9ml PBS + 1ml soluB = $10^4\mu M$

Solution D 9ml PBS + 1ml soluC = $10^3\mu M$

Solution E 9ml PBS + 1ml soluD = $10^2\mu M$*

Solution F 9ml PBS + 1ml soluE = $10^1\mu M$

Solution G 9ml PBS + 1ml soluF = $10^0\mu M$

Solution H 9ml PBS + 1ml soluG = $10^{-1}\mu M$

*Concentration used for positive controls

Lysis solution (200ml);

2.5M Sodium Chloride (NaCl) 29.2g,

1mM EDTA 0.07g,

10mM Tris base 0.2g

Dissolve in 178mls distilled water.

Bring to pH10 with sodium hydroxide (NaOH)

Immediately before use add…

10% dimethyl sulphoxide (DMSO) – 17.8ml

1% Triton X-100 – 1.78ml

Enzyme Buffer (500ml);

40mM Hepes 4.8g

0.1M potassium chloride (KCl) 3.7g

0.5mM EDTA 0.09g

0.2mg/ml Albumin from Bovine Serum (BSA)

Dissolve in 500ml distilled water

Bring to pH8 with potassium hydroxide (KOH)

Electrophoresis Buffer (2L);

0.3M Sodium hydroxide (NaOH) 24g

1mM EDTA 0.7g

Dissolve in 2000ml distilled water

Ensure pH>13

Neutralisation Buffer (1L);

0.4M Tris base 48.5g

Dissolve in 900ml distilled water

Bring to pH7.5 with conc. HCl

Add 100ml distilled water to make up 1L

Fpg aliquots for freezing;

Using fresh enzyme buffer as described above make a 20ml aliquot of enzyme buffer containing 10% glycerol (EG buffer) and vortex to obtain uniform solution. 10µg fpg enzyme is diluted in 10ml of the EG buffer giving a concentration of 1µg/ml. Dispense the fpg containing EG buffer into 100x100µl aliquots and store at -80°C. Each stock aliquot is 100µl at a concentration of 1µg/ml. Dilute the stock aliquot with 500ml fresh enzyme buffer to obtain working concentration of 0.16µg/ml on day of assay.

Appendix 4 Awards, publications and conferences

Awards

Awarded an Oncology Scholars Travel Award 2005 from Cancer Research Ireland in order to attend the American Association of Cancer Research (AACR) annual meeting in held in Washington DC April 2006.

Awarded the Marie Curie training fellowship 2006 which facilitated 3 months training in the comet assay at the LIGHT laboratories in Leeds University from June – September 2006.

Publications

Maguire, A. Lyng, F. M. Walsh, J. E. (2010) Solar simulated radiation induced cell death depends on spectral distribution and irradiance but not output delivery. Radiat Prot Dosimetry. 2010 Jul;140(2):147-57. Epub 2010 Mar 4.

Maguire, A. Walsh, J. E. Lyng, F. M. (2011) Medium mediated effects increase cell killing in a human keratinocyte cell line exposed to solar simulated radiation. Int J Radiat Biol. 2011 Jan;87(1):98-111. Epub 2010 Oct 25.

Conferences

Oral presentation at the Association for Radiation Research (ARR), Manchester UK, March 2008

Oral presentation at the Association for Radiation Research (ARR), Belfast NI, April 2007

Poster presentation at the 11th World Congress on Cancers of the Skin, Amsterdam, The Netherlands. June 2007

Poster presentation at the Microscopical Society Ireland (MSI) annual meeting 2006 in NUI Galway, Ireland, August 2006

Poster presentation at the American Association for Cancer Research (AACR) annual meeting 2006 in Washington DC, USA, April 2006

Poster presentation at the Irish Association for Cancer Research (IACR) annual meeting 2006 in Galway, Ireland, March 2006

Poster presentation at the European Radiation Research (ERR) annual meeting 2005 Leicester, UK, September 2005

Poster presentation at the Irish Association for Cancer Research (IACR) annual meeting 2005 in Kilkenny, Galway, Ireland, March 2005